VILNIUS UNIVERSITY
CENTER FOR PHYSICAL SCIENCES AND TECHNOLOGY

Algimantas
ČERNIAUSKAS

Chemical and kinematical properties of Galactic globular cluster 47 Tucanae

DOCTORAL DISSERTATION

Physical sciences,
Physics (02 P)

VILNIUS 2018

Doctoral Dissertation was completed during doctorate studies at Vilnius University, Institute of Theoretical Physics and Astronomy, in 2012-2016 and is defended in extern.

Scientific supervisor – dr. Arūnas Kučinskas (Vilnius University, Physical sciences, Physics – 02 P). From 2012 10 01 until 2016 09 30

Scientific adviser – dr. Arūnas Kučinskas (Vilnius University, Physical sciences, Physics – 02 P). From 2018 06 13 until 2018 09 14

Council of the doctoral dissertation defense:
Chairman – prof. dr. Vladas Vansevičius (Vilnius University, Physical sciences, Physics – 02 P).

Members:
Dr. Šarūnas Mikolaitis (Vilnius university, Faculty of Physics, Physical sciences, Physics – 02 P)
Prof. dr. Tamara Mishenina (Odesa Mechnikov National University, Astronomical Observatory, Physical sciences, Physics – 02 P)
Dr. Donatas Narbutis (Vilnius university, Faculty of Physics, Physical sciences, Physics – 02 P)
Dr. Julius Sperauskas (Vilnius university, Faculty of Physics, Physical sciences, Physics – 02 P)

Doctoral dissertation will be defended at the public meeting at the National Centre of Physical and Technological Sciences (room D401) at 3:00 p.m. on 14th September, 2018.
Adress: Saulėtekio al. 3, LT–10257, Vilnius, Lithuania
Contact Tel.: (+370–5) 223 4636; Fax.: (+370–5) 223 4637

The dissertation is available at the Vilnius University internet site:
www.vu.lt/lt/naujienos/ivykiu-kalendorius

VILNIAUS UNIVERSITETAS
FIZINIŲ IR TECHNOLOGIJOS MOKSLŲ CENTRAS

Algimantas
ČERNIAUSKAS

Galaktikos kamuolinio žvaigždžių spiečiaus Tukano 47 cheminės ir kinematinės savybės

DAKTARO DISERTACIJA

Fiziniai mokslai,
fizika (02 P)

VILNIUS 2018

Disertacija rengta 2012–2016 metais Vilniaus universitete, Teorinės fizikos ir astronomijos institute, studijuojant doktorantūroje ir ginama eksternu.

Mokslinis vadovas – dr. Arūnas Kučinskas (Vilniaus universitetas, fiziniai mokslai, fizika – 02 P). Nuo 2012 10 01 iki 2016 09 30.

Mokslinis konsultantas – dr. Arūnas Kučinskas (Vilniaus universitetas, fiziniai mokslai, fizika – 02 P). Nuo 2018 06 13 iki 2018 09 14.

Gynimo taryba:
Pirmininkas – prof. dr. Vladas Vansevičius (Vilniaus universitetas, Fizikos fakultetas, fiziniai mokslai, fizika – 02 P)

Nariai:
Dr. Šarūnas Mikolaitis (Vilniaus universitetas, Fizikos fakultetas, fiziniai mokslai, fizika – 02 P)
Prof. dr. Tamara Mishenina (Odesos nacionalinis I. I. Mečnikovo vardo universitetas, Astronomijos observatorija, fiziniai mokslai, fizika – 02 P)
Dr. Donatas Narbutis (Vilniaus universitetas, Fizikos fakultetas, fiziniai mokslai, fizika – 02 P)
Dr. Julius Sperauskas Vilniaus universitetas, Fizikos fakultetas, fiziniai mokslai, fizika – 02 P)

Disertacija ginama viešame posėdyje, 2018 m. rugsėjo mėn. 14 d. 15:00 val. Nacionaliniame fizinių ir technologijos mokslų centre, D401 auditorijoje.
Adresas: Saulėtekio al. 3, LT–10257, Vilnius, Lietuva
Kontaktinis telefonas: (+370–5) 223 4636; Faksas: (+370–5) 223 4637

Disertaciją galima peržiūrėti Vilniaus universiteto bibliotekoje ir Vilniaus universiteto interneto svetainėje adresu: www.vu.lt/lt/naujienos/ivykiu-kalendorius

Abstract

Galactic globular clusters (GGCs) are old, metal-poor objects located in the Galactic halo and bulge. For many years GGCs were thought to be good examples of simple stellar populations. However, recent spectroscopic and photometric observations seem to provide evidence that their stellar populations originated during more than one star formation episode. Unfortunately, it is not clear how this could have happened. In order to obtain new insights on the possible evolutionary scenarios of the GGCs, we studied abundances of a few chemical elements (Na, Mg, K and Zn) in the Galactic globular cluster 47 Tucanae (47 Tuc). Based on this new information, we investigated relationships between the abundances of these chemical elements and kinematical properties of the cluster stars.

With these goals in mind, we determined abundances of Na, Mg, K, and Zn in the atmospheres of red giant branch stars (RGB) and abundances of Mg and K in the main sequence turn-off (TO) stars. This was done by using publicly available high-resolution archival 2dF/HERMES and FLAMES/GIRAFFE spectra, and applying 1D NLTE and LTE abundance analysis tools. 1D NLTE abundances of Na, Mg, and K were determined using the MULTI code and 1D hydrostatic ATLAS9 stellar model atmospheres. In the case of Zn, 1D LTE abundances were determined using the SYNTHE package which operates together with the 1D hydrostatic ATLAS9 stellar model atmospheres. The effects of convection on the formation of all spectral lines used in this study were analyzed using 3D hydrodynamical CO^{5}BOLD and 1D hydrostatic LHD stellar model atmospheres.

The average 1D NLTE [Na/Fe], [Mg/Fe], and [K/Fe] abundance ratios determined in the atmospheres of 32 RGB stars were 0.42 ± 0.13, 0.41 ± 0.11, and 0.05 ± 0.14, respectively. The maximum-likelihood (ML) test of the obtained data suggests the existence of a small intrinsic abundance variation in case of Mg, $\sigma^{\rm int}([{\rm Mg/Fe}]) = 0.08 \pm 0.02$ dex. No evidence for the intrinsic abundance spread was found for [K/Fe], $\sigma^{\rm int}([{\rm K/Fe}]) = 0.00 \pm 0.05$. For all spectral lines used in this work the 3D–1D LTE abundance corrections were small (≤ 0.07 dex), which suggests only a minor influence of convection on the formation of these lines in the atmospheres of RGB stars. At the same time, the 1D NLTE–LTE abundance corrections for the same elements were found to be significantly larger (e.g., up to –0.55 dex in the case of K), negative, and increasing towards the lower effective temperatures. Our analysis did not reveal statistically significant relationship between the abundances of Na, Mg, and K in the atmospheres of RGB stars, or between the abundance or abundance-abundance ratios and projected distance from the cluster center. Similarly, we found no evidence for statistically significant relationships between

the radial velocities of individual RGB stars and abundances of Na, Mg, and K in their atmospheres.

The average 1D NLTE abundance ratios of [Mg/Fe] and [K/Fe] determined in the atmospheres of 75 TO stars were 0.47 ± 0.12 and 0.39 ± 0.09. In the case of [Mg/Fe] we detected a small but statistically significant intrinsic abundance variation, $\sigma^{\rm int}([{\rm Mg/Fe}]) = 0.09 \pm 0.01$, which agrees well with the intrinsic abundance spread obtained by us in the case of RGB stars. No evidence for the intrinsic abundance spread was found for [K/Fe], $\sigma^{\rm int}([{\rm K/Fe}]) = 0.00 \pm 0.03$. The 3D–1D LTE abundance corrections calculated for the Mg I and K I lines were always <0.1 dex, therefore suggesting only a minor influence of convection on the formation of these spectral lines in the atmospheres of TO stars. For TO stars, the average 1D NLTE–LTE abundance corrections of Mg and K were −0.03 dex and −0.50 dex, respectively. Our data do not show any statistically significant relations between the [Mg/Fe] and [K/Fe] abundance ratios and projected distance from the cluster center. As for RGB stars, we found no relationships between the radial velocities of individual TO stars and abundances of [Mg/Fe] and [K/Fe] in their atmospheres.

Finally, we determined abundance ratios in 27 RGB stars, with the average 1D LTE value of 0.11 ± 0.09 dex. For this element, we found no statistically significant intrinsic abundance variation, $\sigma^{\rm int}([{\rm Zn/Fe}]) = 0.00 \pm 0.04$. The 3D–1D LTE abundance corrections for the both Zn I line which were used in this study, were less than 0.05 dex. Our results suggest no statistically significant relationship between the abundance of Zn and Na, Mg, K, as well as between the [Zn/Fe] and kinematical properties of the cluster stars.

The results obtained in this Thesis therefore suggest that nucleosynthesis of K and Zn in 47 Tuc has proceeded differently from that of O and Na. The obtained [K/Fe] and [Zn/Fe] abundance ratios are well comparable to those observed in the Galactic field stars at the same metallicity. This, together with the non-detection of intrinsic abundance variations in the case of the [K/Fe] and [Zn/Fe] abundance ratios suggests that there were no additional enrichment of K or Zn in the second-generation stars of 47 Tuc.

Abbreviations

1D – one-dimensional
3D – three-dimensional
47 Tuc – 47 Tucanae (NGC 104)
AAO – Australian Astronomical Observatory
AAT – Anglo-Australian Telescope
AGB – asymptotic giant branch
CMD – color-magnitude diagram
FRMS – fast rotating massive stars
GGC – Galactic globular cluster
IAS – intrinsic abundance spread
IR – infrared
LTE – local thermodynamic equilibrium
ML – maximum-likelihood
MS – main sequence
NLTE – non-local thermodynamic equilibrium
RGB – red giant branch
RTE – radiative transfer equation
SGB – subgiant branch
TO – main sequence turn-off point

Contents

Introduction

Galactic globular clusters (hereafter, GGCs) are massive, 10^4-$10^6\,M_\odot$, and compact (half-light radius 1-17 pc) stellar systems (see, e.g., van den Bergh 2010). There are ~150 GGCs in our Galaxy (Harris 1996), with a few clusters possibly still undiscovered (see, eg., Ivanov & Borissova 2002). Although metallicities of the GGCs span over a wide range ($-2.37 \leq$ [Fe/H] ≤ 0.00, Harris 1996), it was long thought that chemical composition of the cluster member stars is identical (Elmegreen & Efremov 1997). Nevertheless, research done over the last two decades has shown that stars of almost all GGCs studied differ in the abundances of light elements and, possibly, the age, too (see Gratton et al. 2012; Bastian & Lardo 2017, for a detailed review). The first observational evidence that GGCs may be significantly more complex systems than it was assumed earlier relied on CNO determined abundances in the atmospheres of individual stars in different GGCs (Osborn 1971; Bell & Dickens 1980; Kraft 1994). These studies have shown that spreads in CNO abundances up to 1 dex are typical to all GGCs studied. Detailed spectroscopic studies of past two decades (Gratton et al. 2004, 2012) revealed that stars in a given GGC may be different also in the abundances of other light chemical elements, such as Li, Na, and Al. In addition, abundances of these elements show correlations (such as, Na–Al, Carretta et al. 2011) or anti-correlations (Na–O, Carretta et al. 2009a). Subsequent investigations have shown that cluster stars with either low or high light element abundances may also differ in their kinematical properties, such that stars with higher Na abundance appear to be more centrally concentrated and have larger absolute radial velocities (e.g., Richer et al. 2013; Kučinskas et al. 2014). No such correlations have been detected in the case of heavy chemical elements. Almost all investigated GGCs (with the exception of ω Cen, M54, M22) show very small scatter in the abundances of iron-group elements and *s*- and *r*-process elements, typically < 0.1 dex (Carretta et al. 2009a). Photometric investigations of the GGCs have also shown that slightly broadened sequences in the color-magnitude diagrams (CMDs) are typical to almost all studied clusters, while in some cases these sequences even split into several well-defined subsequences (Hartwick & McClure 1972; Lardo et al. 2011; Piotto et al. 2015). The current consensus is that the split is caused by the different helium abundance in the atmospheres of cluster stars (Salaris et al. 2006). All these studies therefore indicate that GGCs consist of several stellar populations (or even generations) of stars which differ in their abundances of light chemical elements and kinematical properties. It is worth emphasizing that correlations between the abundances of light elements mentioned above have been observed so far only in the GGCs, while they are not detected in the open clusters and/or Galactic field stars.

Several scenarios of the GGC evolution have been proposed so far in the attempt to explain the anomalies in chemical composition and kinematical properties of the cluster stars mentioned above. Since these are the properties that are inherent to almost all GGCs, scenarios of the cluster evolution must be quite universal in this sense, i.e., they should be able to explain the observed abundance scatter and correlations over a wide range in cluster mases and metallicities. For example, one of the proposed scenarios invokes massive (7-9 $M_{\odot}$) asymptotic giant branch (AGB) stars which start to lose their envelopes during the late AGB evolution, thereby enriching the intra-cluster medium with the elements produced in the earlier stages of their evolution. Second generation stars that form later in the same cluster should therefore be enriched in elements synthesized in the first generation stars (e.g., Ventura et al. 2001; D'Ercole et al. 2012). In an alternative scenario, second generation stars are enriched in elements produced in the fast-rotating massive stars (FRMS). The FRMS loose significant fraction of their massive envelopes due to centrifugal force while still on the main sequence, thus enriching intra-cluster medium with various chemical elements synthesized in their hot cores (Decressin et al. 2007; Maeder & Meynet 2006). Other evolutionary scenarios have been suggested as well, such as chemical enrichment in massive binary systems (de Mink et al. 2009), early disk accretion (Bastian et al. 2013).

Nevertheless, none of the proposed evolutionary scenarios is capable of explaining all observed chemical and kinematical properties of the GGCs. It is important to stress here, however, that only relatively small star samples were used to study abundances of chemical elements in the GGCs so far. In addition, nearly all earlier studies were limited to the abundance analysis and only in a few cases attempts were made to study the connections between the chemical and kinematical properties of the member stars (e.g., Bellazzini et al. 2012; Richer et al. 2013; Kučinskas et al. 2014). Finally, additional information is needed to put further observational constraints on the evolutionary scenarios of the GGCs, such as about abundances of other elements and their possible connections with the abundances of light elements and kinematical properties of cluster stars.

With these goals in mind, we therefore focused on the investigation of the abundances of Na and Mg in the atmospheres of the TO and RGB stars in the GGC 47 Tuc (Fig. 1). In addition, abundances of two other elements that until now were little investigated in the context of cluster evolution - K and Zn - were determined in the atmospheres of cluster RGB stars. Our study was motivated by the following:

- spectroscopic and photometric investigations of 47 Tuc of the last two decades have shown that this cluster contains several stellar populations which are different in their light element and helium abundances (Milone et al. 2012; Carretta et al. 2009a). The investigation of possible relations between the chemical and

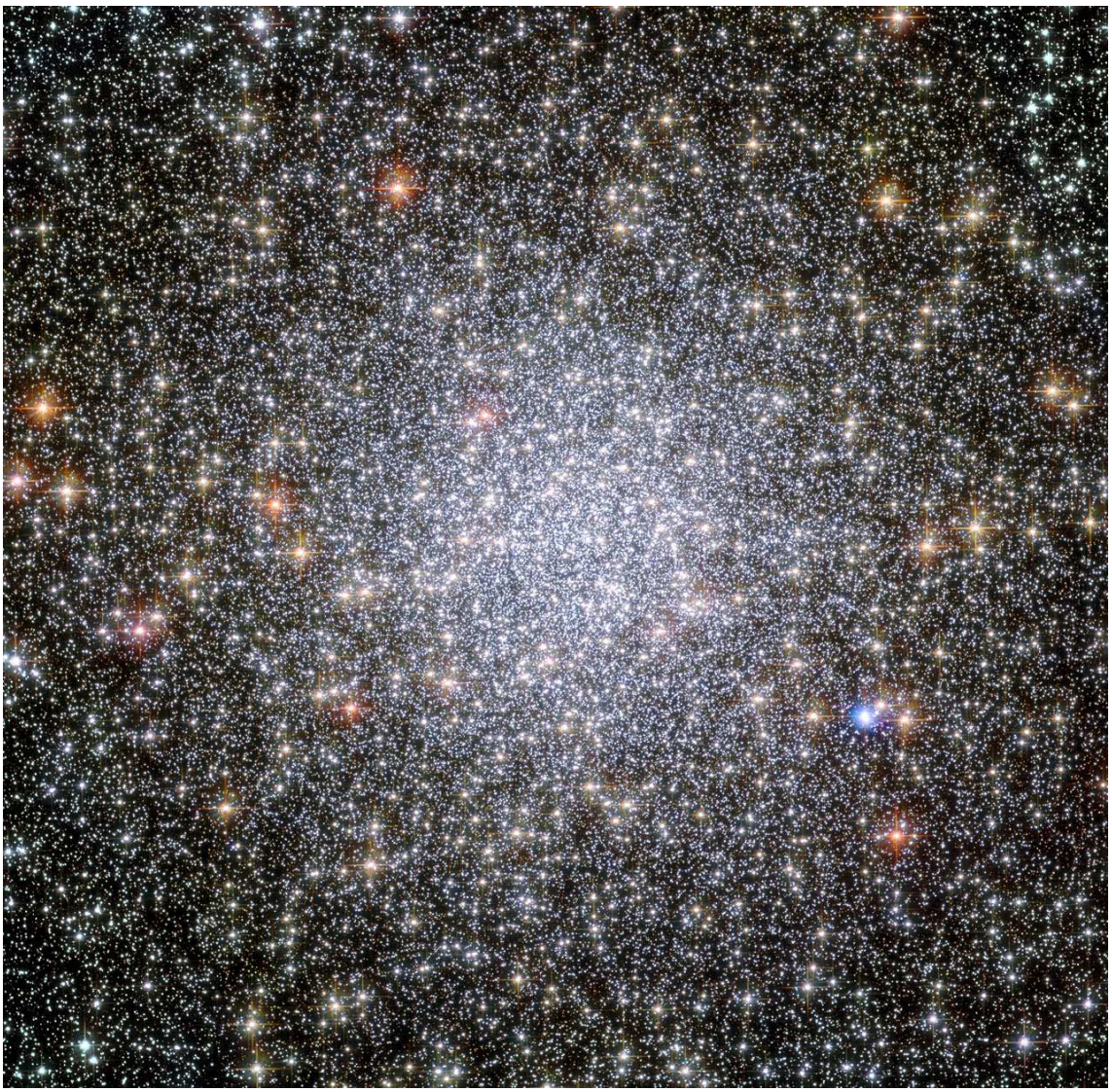

Figure 1. Galactic globular cluster 47 Tucanae (47 Tuc). Image credit: NASA, ESA, and the Hubble Heritage (STScI/AURA)-ESA/Hubble Collaboration Acknowledgment: J. Mack (STScI) and G. Piotto (University of Padova, Italy).

kinematical properties of 47 Tuc has shown that stars with different O and Na abundance are characterized by different kinematical properties, such as projected radial velocities (Kučinskas et al. 2014);

- 47 Tuc is one of the closest GGCs (d = 4.5 kpc, McDonald et al. 2011), therefore it is one of a few clusters where determination of reliable elemental abundances based on the analysis of high-resolution spectra is possible both in the TO and RGB stars. Investigation of TO stars is especially important because their atmospheres should not be enriched in the chemical elements synthesized in their interiors. Therefore, chemical composition of the atmospheres of TO stars and that of the matter from which these stars have formed should be identical. The knowledge of elemental abundances in the TO and RGB stars may therefore pro-

vide valuable additional information and may aid in identifying the most likely scenario(s) of the GGC evolution;

- 47 Tuc is one of the most massive GGCs ($M \approx 7 \times 10^5\,M_\odot$, Baumgardt 2017). Given its relatively long dynamical relaxation time, t_{rh} = 3.0 Gyr (Harris 1996), it is conceivable that its member stars that are characterized by different chemical composition may be still not well kinematically mixed (Vesperini et al. 2013). Therefore, one may expect to detect various relations between the chemical composition and kinematical properties of stars in this particular cluster. Such information could provide additional constraints on the evolutionary scenarios of the GGCs;

- investigation of the abundances of K and Zn may provide additional information in this context, especially, in the light of recent claims of Mucciarelli et al. (2012) and Mucciarelli et al. (2017) regarding the discovery of K–O correlation and K–Na anti-correlation in 47 Tuc. Nucleosynthesis of K and Zn, as well as Na and Mg, takes place at very different temperatures (Karakas et al. 2009; Ventura et al. 2012). Therefore, new facts about the possible correlations between the abundances of K, Zn, Na, and Mg, as well as possible connections between the chemical and kinematical properties of cluster stars, may help to identify the polluters that enriched atmospheres of the second generation stars with the products synthesized during the earlier stages of cluster evolution.

Aim of the study

The goal of this study is to determine the abundances of Na, Mg, K, and Zn in the Galactic globular cluster 47 Tuc, and to investigate possible relations between the chemical and kinematical properties of the cluster stars.

Main tasks

1. Determine abundances of Na, Mg, K, and Zn in the atmospheres of TO and RGB stars in the Galactic globular cluster 47 Tuc using 1D/3D hydrostatic/hydrodynamic stellar model atmospheres and 1D NLTE/LTE spectral synthesis methodology.

2. Determine intrinsic astrophysical spreads in the abundances of Mg and K in TO stars, and Na, Mg, K, and Zn in RGB stars of 47 Tuc.

3. Compute the 1D NLTE–LTE abundance corrections for Na, Mg, and K, and investigate the influence of NLTE effects on the formation of the Na I, Mg I, and K I spectral lines in the atmospheres of TO and RGB stars in 47 Tuc.

4. Study the possible connections between the abundances of Na, Mg, K, and Zn in the 47 Tuc stars, as well as possible relations between the chemical and kinematical properties of the cluster stars.

Results and statements to defend

1. 1D NLTE abundances of Na, Mg, and K and 1D LTE abundance of Zn have been determined in the atmospheres of RGB stars in the 47 Tuc. The average obtained abundance ratios in the investigated star samples are [Na/Fe] = 0.42 ± 0.13 (30 stars), [Mg/Fe] = 0.41 ± 0.11 (25 stars), [K/Fe] = 0.05 ± 0.14 (28 stars), and [Zn/Fe] = 0.11 ± 0.09 (27 stars).

2. 1D NLTE abundances of Mg and K have been determined in the atmospheres of TO stars in the 47 Tuc. The average obtained abundance ratios are [Mg/Fe] = 0.47 ± 0.12 (53 stars) and [K/Fe] = 0.39 ± 0.09 (75 stars).

3. The 1D NLTE–LTE abundance corrections for the Na I (λ = 568.3 nm and λ = 568.8 nm), Mg I (λ = 769.2 nm), and K I (λ = 769.9 nm) lines observed in the spectra of RGB stars of 47 Tuc are negative and increase with the decreasing of $T_{\rm eff}$ and $\log g$: at $T_{\rm eff}$ = 4720 K and $\log g$ = 2.3 [cgs] the corrections are −0.19 dex for Na, −0.01 dex for Mg, and −0.40 dex for K; at $T_{\rm eff}$ = 4390 K and $\log g$ = 1.6 [cgs] the corrections increase to −0.28 dex for Na, −0.08 dex for Mg, and −0.55 dex for K.

4. The 1D NLTE–LTE abundance corrections for the Mg I (λ = 769.2 nm) and K I (λ = 769.9 nm) lines observed in the spectra of TO stars of 47 Tuc remain essentially constant throughout the investigated atmospheric parameter range: at $T_{\rm eff}$ = 5690 K and $\log g$ = 4.0 [cgs] the abundance corrections are −0.03 dex for Mg and −0.48 dex for K while at $T_{\rm eff}$ = 5940 K and $\log g$ = 4.1 [cgs] the corrections are −0.02 dex for Mg and −0.50 dex for K.

5. The determined intrinsic astrophysical abundance spread of Mg in the studied sample of RGB stars of 47 Tuc is $\sigma^{\rm int}$([Mg/Fe]) = 0.08 ± 0.02 dex. No intrinsic astrophysical spread was found for K, $\sigma^{\rm int}$([K/Fe]) = 0.00 ± 0.05, thus the observed scatter in K abundance is caused by errors in the abundance determination.

6. The determined intrinsic astrophysical abundance spread of Mg in the studied sample of TO stars of 47 Tuc is $\sigma^{\rm int}$([Mg/Fe]) = 0.09 ± 0.01 dex. There is no intrinsic astrophysical spread in the case of K, $\sigma^{\rm int}$([K/Fe]) = 0.00 ± 0.03 dex, which indicates that the observed scatter in K abundance is caused solely by the errors in the abundance determination.

7. The determined average zinc-to-iron abundance ratio in the atmospheres of RGB stars in 47 Tuc, [Zn/Fe] = 0.11 ± 0.09 (27 objects), does not differ significantly from the average abundance ratio determined in the Galactic field stars of the same metallicity, [Zn/Fe] = 0.15 ± 0.14 (19 objects).

Novelty

The novelty of the results presented in the Thesis are:

1. Systematic and homogeneous analysis of the abundances of K and Mg was performed using 1D NLTE methodology in the largest sample of TO stars to date in the Galactic globular cluster 47 Tuc. The abundance of K and Mg was investigated using the same methodology both for TO and RGB stars. We determined that there is no statistically significant relation between the abundances of K and Mg.

2. Abundance of Zn was determined in the atmospheres of 27 RGB stars which is the largest sample investigated in 47 Tuc so far. The average Zn abundance determined in RGB stars of 47 Tuc is very similar (within 0.04 dex) to the average value of the Galactic field stars. This means that Zn in 47 Tuc has been produced via the same nucleosynthesis channels as in the Galactic field stars.

3. For the first time, abundance(s) of K (and Mg) was/were determined in the atmospheres of TO stars in 47 Tuc and relations between this/these and other chemical elements and kinematical properties of cluster stars were investigated. The results of the analysis show that there is no statistically significant relation between the abundance(s) of K (and Mg) and kinematical properties of TO stars.

4. The new grid of 1D NLTE–LTE K abundance corrections was computed for TO and RGB stars using an updated model atom of K, ATLAS9 hydrostatic model atmospheres and MULTI code.

Publications on the Thesis topic in the Clarivate Analytics WoS journals

1. **Černiauskas, A.**, Kučinskas, A., Klevas, J., Prakapavičius, D., Korotin, S. A., Bonifacio, P., Ludwig, H.-G., Caffau, E., Steffen, M. 2017, *Abundances of Na, Mg, and K in the atmospheres of red giant branch stars of Galactic globular cluster 47 Tucanae* // Astronomy and Astrophysics, 604, A35.

2. **Černiauskas, A.**, Kučinskas, A., Klevas, J., Dobrovolskas, V., Korotin, S. A., Bonifacio, P., Ludwig, H.-G., Caffau, E., Steffen, M. 2018, *Abundances of Mg and K in the atmospheres of turn-off stars in Galactic globular cluster 47 Tucanae* // Astronomy and Astrophysics, in press (DOI: https://doi.org/10.1051/0004-6361/201731659).

3. **Černiauskas, A.**, Kučinskas, A., Klevas, J., Bonifacio, P., Ludwig, H.-G., Caffau, E., Steffen, M. 2018, *Abundance of zinc in the atmospheres of red giant*

branch stars of Galactic globular cluster 47 Tucanae // Astronomy and Astrophysics, in press (DOI: https://doi.org/10.1051/0004-6361/201833255).

Other publications in the Clarivate Analytics WoS journals

1. Kučinskas, A., Dobrovolskas, V., **Černiauskas, A.**, Tanabé, T. 2008, *Properties of Red Giant Branches of Star Clusters in the Magellanic Clouds and Their Relation with Cluster Metallicity* // Baltic Astronomy, 17, 363–372.

Presentations at the conferences

1. **Černiauskas, A.**, Kučinskas, A., Klevas, J., Prakapavičius, D., Korotin, S. A., Bonifacio, P., Ludwig, H.-G., Caffau, E., Steffen, M. 2018, *Abundance of K in the Galactic globular cluster 47 Tuc: current status and future challenges* // COST ChETEC WG3 workshop, Vilnius, 14–16 March, 2018 (oral presentation).

2. **Černiauskas**, A. and Kučinskas, A., Bonifacio, P., Andrievsky, S. M., Korotin, S. A., Dobrovolskas, V. 2014 *Light element abundances in the Galactic globular cluster 47 Tuc* // International conference "Metal Production and Distribution in a Hierarchical Universe", 21–25 October, 2013, Paris (France). MmSAI, 85, 291 (poster presentation).

3. **Černiauskas, A.**, Kučinskas, A., Bonifacio, P., Andrievsky, S., Korotin, S., Dobrovolskas, V., 2013 *Chemical evolution of light elements in the Galactic globular cluster 47 Tuc* // "40th Lithuanian National Physics Conference", 10–12 June, 2013, Vilnius, (poster presentation; published in the abstracts book, Vilnius University, p. 226).

Personal contribution

The author performed data reduction of the raw archival spectra obtained using the 2dF/HERMES spectrograph and determined atmospheric parameters of 32 RGB stars, computed 1D hydrostatic model atmospheres, performed 1D NLTE spectral synthesis, determined abundances of Na, Mg, K, and Zn in the atmospheres of RGB stars in 47 Tuc, and estimated abundance errors. The author also performed 1D NLTE spectral synthesis computations and determination abundances of Mg and K in the atmospheres of 75 TO stars in 47 Tuc, estimated abundance determination errors. The author, together with the co-authors, estimated intrinsic astrophysical abundance spreads in the atmospheres of TO and RGB stars and analyzed possible relations between the abundances in the atmospheres of these stars and their kinematical properties (the co-authors formulated research goals and tasks, developed the tools for the 1D NLTE abundance analysis and computation of the intrinsic astrophysical abundance spread, computed 3D hydrodynamical stellar model atmospheres and 3D–1D LTE abundance corrections for the spectral lines of Na I, Mg I, K I, and Zn I). The obtained results were published in Černiauskas et al. (2017), Černiauskas et al. (2018a), Černiauskas et al. (2018b), which are listed in Section "Publications on the Thesis topic in the Clarivate Analytics WoS journals".

The author developed a number of Python routines which allow to determine stellar effective temperature and microturbulence velocities in a semi-automatic way, using ATLAS9 and SYNTHE packages and equivalent widths of Fe I spectral lines. The author also developed a number of Python routines which allow to use the MULTI package in a semi-automatic way, by specifying the input parameters in a single input file.

Thesis outline

The Thesis consists of Introduction, four Chapters, Conclusions and two Appendices.

In Chapter 1 we provide a description of stellar spectroscopic data used in the analysis, outline/present the methodology used in the determination of stellar atmospheric parameters and the computation of stellar model atmospheres and synthetic spectra, as well as describe the different computer codes and software packages used in the abundance analysis.

In Chapter 2 we present the results of Na, Mg, and K abundance determination in the atmospheres of RGB stars in 47 Tuc. Here we also summarize the results of the influence of 3D hydrodynamical and NLTE effects on the formation of spectral lines of Na, Mg, and K in the atmospheres of RGB stars in 47 Tuc. The Chapter also summarizes the findings of the analysis of possible relations between the abundances of chemical elements and kinematic properties of cluster RGB stars.

In Chapter 3 we outline the results of the study of Mg and K abundances in the atmospheres of 75 TO stars. Here we also summarize the results of the influence of 3D hydrodynamical and NLTE effects on the formation spectral lines of Mg and K in the atmospheres of TO stars. In this Chapter we also study the possible relations between the abundances of chemical elements and kinematic properties of TO stars.

In Chapter 4 we describe the results obtained in a study of Zn abundance in the atmospheres of RGB stars in the 47 Tuc. Here we also discuss the results of the influence of 3D hydrodynamical effects on the formation spectral lines of Zn in the atmospheres of RGB stars in 47 Tuc. We also present the results obtained in the analysis of possible connections between the abundances of different chemical elements, as well as possible relations between the abundances and kinematical properties of stars in 47 Tuc.

In Conclusions we summarize the main results obtained in this work and provide recommendations for possible future studies in this field of research.

In Appendix A we provide a list of target RGB stars, their atmospheric parameters, and the 1D NLTE abundances of Na, Mg, and K, together with the 1D LTE abundances of Zn determined in their atmospheres.

In Appendix B we provide a list of target TO stars, their atmospheric parameters, and the 1D NLTE Mg and K abundances.

1 Abundance determination of chemical elements: methodology

Spectroscopic abundance analysis is a powerful tool that allows to determine chemical composition of stars. For this, besides of the observational material in the form of good-quality stellar spectra, one also needs realistic theoretical model atmospheres and tools for modeling radiative transfer, constructed either under the assumption of local thermodynamic equilibrium (LTE) or non-local thermodynamic equilibrium (NLTE). In the Chapter we summarize the approaches used in this Thesis to determine abundances of chemical elements in the atmospheres of TO and RGB stars in the GGC 47 Tuc. We also describe the tools that were utilized in the investigation of the influence of convection and NLTE effects on the spectral lines formation in the atmospheres of the cluster stars.

1.1. Spectroscopic data

Throughout this Thesis we used spectroscopic observations obtained with two spectrographs: 2dF/HERMES at the Australian Astronomical Observatory (Siding Springs Observatory, Australia), and FLAMES/GIRAFFE at the Very Large Telescope (VLT, European Southern Observatory, Chile). Both of them are fibre-fed multi-object spectrographs that allow to observe more than one hundred objects simultaneously. More details about these two instruments and the data reduction procedures are provided in the next two Subsections below.

1.1.1. 2dF/HERMES spectroscopic observations

2dF/HERMES is a four-channel fibre-fed echelle high resolution multi-object spectrograph (de Silva et al. 2012). It is designed primarily for the Galactic Archaeology Survey carried out with the AAT telescope (see Freeman & Bland-Hawthorn 2002, for details). 2dF/HERMES provides simultaneous observations in the following fixed passbands: blue - 483.3 nm, green - 578.8 nm, red - 664.2 nm, IR - 777.8 nm. The 2dF/HERMES system is built upon the AAT's existing Two-Degree Field (2dF) optical fibre positioner. The spectrograph designed to allow the acquisition of up to 392 simultaneous spectra of objects anywhere within a two degree field on the sky. The total efficiency of the 2dF/HERMES system from the telescope to the detector is approximately 10%, such that a 1 hour integration time results in a signal-to-noise ratio of 100 per resolution element for a V=14 mag star.

All spectroscopic observations obtained with 2dF/HERMES are archived and made accessible through the AAO data archive. This database contains only raw spectra and can be reached via a request form provided at the archive webpage[1].

In this Thesis we used spectroscopic observations of RGB stars in 47 Tuc obtained with the 2dF/HERMES spectrograph and the main results obtained in the analysis of these spectroscopic data are presented in Chapters 2 and 4. The spectra were obtained during the science validation period of GALAH survey (de Silva et al. 2015) and were retrieved from the AAO raw data archive. We used 2dF/HERMES spectra obtained in the following wavelength regions: 471.5-490.0 nm (blue), 564.9-587.3 nm (green), and 758.5-788.7 nm (IR). Spectra obtained in all regions have the same spectral resolution of $R \sim 28000$. The exposure time was 1200 s and typical signal-to-noise ratio in the vicinity of Na, Mg, and K lines was $S/N \approx 50$. All 2dF/HERMES spectra were registered during the period of 2013/10/22 - 2013/12/19. The raw spectra were reduced using the 2dfdr data reduction software (see Sect. 1.2), sky subtraction was done using sky spectra obtained with 25 sky fibres during each observing night.

1.1.2. FLAMES/GIRAFFE spectroscopic observations

FLAMES/GIRAFFE spectrograph (R=5500-38000) covers the visual and near-IR range (370-900 nm) and is mounted on the Nasmyth A platform of the Very Large Telescope (VLT UT2). FLAMES/GIRAFFE spectrograph has 32 predefined setups, 24 at high (R=18000-38000) and 8 at low (R=5500-8500) resolution. Observations used in this Thesis were made in the "Medusa" mode which has the spatial scale of 0.3 arcsec/pixel. Up to 132 separate objects (including sky fibres) can be observed simultaneously in this mode, with each fibre having an aperture of 1.2 arcseconds on the sky.

In this Thesis we used archival FLAMES/GIRAFFE observations. Those observations that were taken after February 21, 2003 are available in FITS format via the raw data query form[2]. In addition, all observations obtained with FLAMES/GIRAFFE since 2015 are automatically reduced at ESO and are available in another query form[3].

In the abundance analysis of TO stars in 47 Tuc (Chapter 3) we utilized FLAMES/GIRAFFE spectra of 110 stars that were also used in Dobrovolskas et al. (2014, programme ID: 081.D-0287A). These observations were obtained during the period 2008/08/18-20 in the "Medusa" mode using HR 18 setup (λ =746.8 - 788.9 nm, R=18400). The typical signal-to-noise ratio (per pixel) in the vicinity of Na and Mg lines was $S/N \approx 80$. During these observations, 16 fibers were used for registering sky spectra.

[1] http://site.aao.gov.au/arc-bin/wdb/aat_database/observation_log/make

[2] http://archive.eso.org/wdb/wdb/eso/giraffe/form

[3] http://archive.eso.org/wdb/wdb/adp/phase3_spectral/form?collection_name=GIRAFFE

1.2. Reduction of spectroscopic data

1.2.1. Data reduction procedure

In case of 2dF/HERMES data, the reduction procedure was carried out using 2dfdr[4] package. The 2dfdr package was also utilized by us to reduce the spectra of RGB stars in 47 Tuc observed with the AAT and used in this Thesis. In this procedure, 2dfdr uses several additional calibration files such as bias frame, flat field frame, and arc lamp frame.

Modern CCD detectors have very low dark current thus dark frame subtraction is skipped in the FLAMES/GIRAFFE and 2dF/HERMES spectra reduction pipelines. The following steps are involved in the 2dF/HERMES data reduction procedure:

- generate a master bias frame which was done by finding and using the median bias frame from several available bias frames;
- subtract the master bias frame. The master bias frame was subtracted from each arc frame, object frame, and flat-field frame;
- generate master flat-field frame(s). Again, this done by finding the median frame of several flat-field frames and the master flat-field frame was subtracted from all object and sky frames;
- generate a dispersion solution using the arc-lamp frame;
- extract science spectra of each object (star) using calibration data obtained in the previous steps.

Bias frame is required to remove "background" voltage which is applied to every CCD pixel before exposure to light. It is acquired with exposure of zero seconds and closed spectrograph shutter and later is removed from flat, thorium-argon, and science frames.

Flat fielding is the process of dividing object frame by an uniformly illuminated image (flat field) to remove the pixel sensitivity variations across the CCD.

For wavelength calibration of the 2dF/HERMES data, thorium-argon lamp is used. To obtain a good calibration, it is necessary to have at least three or four identifiable spectral lines per echelle order, preferably with one line close to each end of the wavelength range and one or more located near the middle. The main task of the reduction pipeline during the wavelength calibration is to determine centers of the calibration

[4]https://www.aao.gov.au/science/software/2dfdr

lamp lines and derive a function to map the pixel scale to the wavelength scale (dispersion solution). After this, the 2dfdr pipeline applies the dispersion solution to obtain a wavelength-calibrated spectrum of each science object (star).

Once wavelength-calibrated spectrum was ready, the next step was continuum normalization of the individual star spectra. For this, we used IRAF (Tody 1986) *continuum* task.

1.2.2. Telluric spectral lines

Telluric features in the observed stellar spectra are atmospheric absorption lines that originate in the Earth's atmosphere. These features are located in the visual and near-IR region of the spectrum and are mainly the result of absorption by O_3, O_2, H_2O, and CO_2. The most problematic are H_2O lines which vary on short time scales not only with air mass but also with the changing humidity levels within the atmosphere. Earth atmosphere is not static, therefore, the telluric features will not be identical in each spectrum of the object if several different exposures were obtained over prolonged periods of time.

We used two diagnostic tools to identify possible telluric features around the stellar lines which later were used in the abundance analysis. For the initial quick-look analysis we used spectra of fast rotating O- and B-type stars as the telluric templates (Vacca et al. 2003). The spectra of O- and B-type stars do not contain many detectable spectral features because of high temperatures in their photospheres and because of their high rotational velocities which smooth out weaker absorption lines in their spectra. The biggest advantage of this method, if the telluric star spectrum was observed right before or after target stars, is that the atmospheric conditions when the spectrum of telluric star was taken (i.e., the air mass, water vapor content, Doppler broadening due to movements of the atmospheric air masses) will be essentially identical to those when the target stars were observed. However, if the spectrum of telluric star has been taken with a large time difference with respect to the observation of the target stars, the obtained telluric spectrum may differ substantially from the one that would be taken at the time of target star observations.

Since there were no telluric star spectra taken close to the dates when our target stars were observed, for the analysis of telluric features we also used the online TAPAS service[5]. The TAPAS allows to compute a simulated atmospheric transmission for the specific observing conditions at a given observing site (see Bertaux et al. 2014, for details). For this, the code computes atmospheric transmittance from the top of the atmosphere down to the surface using the data from the HITRAN molecular database. The output from this simulation is a telluric spectrum in a wavelength range that can be

[5]http://www.pole-ether.fr/tapas/

chosen anywhere between 350 and 2500 nm. The telluric spectra used in our analysis were computed using the same resolving power as in observations of the target stars.

By applying both methods we found that no telluric features blends with the spectral lines of target elements Na, Mg, K, Zn abundances of which were determined in this Thesis (see Sect. 2.2.3; B1).

1.3. Stellar atmospheric parameters

It is impossible to do analysis of chemical composition of stars without the knowledge of accurate stellar atmospheric parameters. These are: effective temperature, $T_{\rm eff}$, surface gravity, $\log g$, microturbulance velocity, $\xi_{\rm mic}$, rotational velocity, $v\sin i$, and macroturbulence velocity, $\xi_{\rm mac}$.

Atmospheric parameters of stars can be determined using direct and indirect methods. Direct determination is usually impractical for most stars because it requires accurate measurements of the angular diameter and bolometric flux of a target star which are only possible to obtain for the most nearby stars. Indirect methods, such as photometric color-effective temperature calibrations, spectrophotometric flux fitting, fitting of the Balmer line profiles, derivation of $T_{\rm eff}$ and $\log g$ using the assumption of excitation and ionization balance, are more suitable for analyzing more distant and/or larger samples of stars.

In this Thesis effective temperatures were determined using effective temperature - photometric color calibration in case of RGB stars and Hα profile fitting in case of TO stars. The main reason why we did not apply excitation and ionization balance analysis or spectrum synthesis techniques was the absence of sufficient number of good quality Fe I and Fe II lines in 2dF/HERMES and in FLAMES/GIRAFFE spectra, due to low signal-to-noise ratio of the observed spectra.

Photometric data of the RGB stars were taken from the catalog of Bergbusch & Stetson (2009) which is the largest and deepest compilation of photometric data of 47 Tuc that were obtained using ground- and space-based facilities. Photometric observations of TO and RGB stars used in our analysis were made with the 1.5 m telescope at the Cerro Tololo Inter-American Observatory in 2000 (Stetson 2000). This is the largest CCD-based $UBVR_{\rm c}I_{\rm c}$ study of $\sim 200\,000$ objects in 47 Tuc. The CMD of the target RGB stars is shown in Fig. 2.1 (Sect. 2.1).

In case of RGB stars, effective temperatures were estimated by applying the $T_{\rm eff} - (V-I)$ calibration from Ramírez & Meléndez (2005). Before doing this, we dereddened the original photometric data from Bergbusch & Stetson (2009) assuming $E(B-V) = 0.04$ and the color excess ratio $E(V-I)/E(B-V) = 1.33$ taken from Berg-

busch & Stetson (2009). The estimates of stellar surface gravities, $\log g$, were obtained using the following relation

$$\log(g/g_{\odot}) = \log(\mathrm{M/M}_{\odot}) + 4 \times \log(T_{\mathrm{eff}}/T_{\mathrm{eff}\odot}) - \log(L/L_{\odot}) \tag{1.1}$$

For each individual star, we determined luminosities and masses using Yonsei-Yale isochrones of 12 Gyr and [Fe/H] = −0.75 (Yi et al. 2001). Their absolute V magnitudes were estimated assuming the distance modulus of $V - M_V = 13.37$ (Harris 1996).

For TO stars, we used atmospheric parameters determined in Dobrovolskas et al. (2014). In this case, the effective temperatures were obtained by fitting the wings of Hα line profiles, while the gravities were estimated using Eq. (1.1) above.

We used fixed microturbulence velocities of 1.0 km s^{-1} and 1.5 km s^{-1} for the TO and RGB stars, respectively (see Sect. 1.7.1 for details). The macroturbulence velocity was varied during each iteration as a free parameter, to obtain the best match of the synthetic to the observed spectral line profile. The determined macroturbulence velocities of all the TO and RGB stars covered the range of 1 to 8 km s^{-1}.

The final adopted atmospheric parameters of TO and RGB stars are provided in Appendix B (Table B1) and Appendix A (Table A1), respectively.

1.4. Stellar model atmospheres

The analysis carried out in this Thesis is based on two types of model atmospheres: classical hydrostatic one-dimensional (1D) model atmospheres; and state-of-the-art three-dimensional (3D) hydrodynamical model atmospheres.

Examples of some widely-used 1D hydrostatic atmosphere codes are ATLAS9 (Kurucz 1993), PHOENIX (Hauschildt et al. 1999), and MARCS (Gustafsson et al. 2008). The ATLAS9 model atmosphere package was widely used in our study; its detailed description is presented in Sect. 1.4.1. One of the major limitations of the 1D hydrostatic codes is that convection is modeled in a very simplified way, using a number free parameters which are usually poorly known (such as the mixing-length parameter). On the contrary, 3D hydrodynamical models are significantly more complex. The model atmosphere in this case is obtained as a solution of the time-dependent equations of hydrodynamics and radiative transfer. While not being free from various simplifications, these models are certainly state-of-the-art and are capable of providing very realistic models of stellar atmospheres of different types of stars. However, at the same time, they demand large computational resources. Currently, there are several computer packages that are used to compute 3D hydrodynamical model atmospheres (though none of them is publicly available yet): STAGGER (Nordlund & Galsgaard 1992), CO^{5}BOLD

(Freytag et al. 2012), and MURaM (VSS05). CO^{5}BOLD model atmospheres were used in this Thesis; detailed description of this package is presented in Sect. 1.4.3.

1.4.1. 1D hydrostatic ATLAS9 model atmospheres

To compute a 1D hydrostatic stellar model atmosphere, amongst other things one needs to solve radiation transfer equation (RTE). In order to solve the RTE, a source function S_λ must be known. The latter is defined as the ratio between emission and absorption coefficients at a given wavelength and is a function of optical depth in the atmosphere. Moreover, the distribution of temperature, T, pressure, P, electron density, n_e, and other quantities as functions of the optical depth must be known (i.e., computed), too.

Calculation of a 1D model atmosphere is a straightforward process once several assumption and approximations have been made. In these classical 1D model atmospheres the solution of physical and computational problems is simplified by making the following assumptions:

- the atmosphere of the star is in a steady state;
- the radiative energy flux is constant throughout the atmosphere since the energy source lies far below the atmosphere and there is no incoming radiative flux from above the atmosphere. Radiative flux emerging at the top of the atmosphere, $F_{\rm tot}$, is specified only by the effective temperature, $F_{\rm tot} = \sigma T_{\rm eff}^4$, were σ is the Stefan-Boltzmann constant;
- the atmosphere is homogeneous and features like granules, spicules, cells, spots, magnetic field are ignored;
- there is no relative motion of the atmospheric layers;
- the chemical composition (i.e., abundances of chemical elements) is pre-defined and constant throughout the atmosphere.

Sometimes, additional assumption is made that the atmosphere is thin relative to the radius of the star, therefore plane-parallel structure is assumed in the computations instead of concentric spherical shells.

ATLAS is the code developed by Robert Kurucz in the 1970s which was subsequently updated/improved by him and colleagues. Currently, the most widely used versions are ATLAS9 in which the model atmosphere is computed using opacity distribution functions (ODF), and ATLAS12 where opacity sampling (OS) method is used. Tests made with the ATLAS9 and ATLAS12 show that differences between the models computed using the two methods are minor and can be ignored in all practical cases (Sbordone et al. 2004). Therefore, the option to use ATLAS9 or ATLAS12 is mostly a

matter of convenience: if one needs to compute a large number of models with the same chemical composition, then ATLAS9 is the obvious choice.

ATLAS9 model atmosphere is specified by three main stellar parameters: $T_{\rm eff}$, $\log g$ and metallicity. Other important input option is chemical composition which is provided in a form of a table containing information about 99 chemical elements. By default, chemical composition of a model atmosphere is set to solar. Additionally, model atmospheres may be computed using solar-scaled or α-element (O, Ne, Mg, Si, S, Ca, and Ti) enhanced chemical composition, with the constant enhancement factor of +0.4 dex for all α-elements. In the computation of ATLAS9 model atmospheres used in this Thesis we used solar-scaled abundances from Grevesse & Sauval (1998).

In the abundance analysis of all elements we used 1D hydrostatic ATLAS9 model atmospheres (Kurucz 1993) that were computed using the Linux port of the ATLAS9 code (Sbordone et al. 2004; Sbordone 2005). In the model calculations, we used ODFNEW opacity tables for [M/H] = −1.0 (Castelli & Kurucz 2003). The $\alpha-$element enhancement was set to [α/Fe] =+0.4, mixing length parameter to $\alpha_{\rm MLT}$ = 1.25. Overshooting was switched off during all model computations.

1.4.2. 1D hydrostatic LHD model atmospheres

LHD is a classical 1D hydrostatic model atmosphere code which is set up in a plane-parallel geometry (Caffau & Ludwig 2007). Similarly to ATLAS9, any given LHD model atmosphere is defined by its $T_{\rm eff}$, $\log g$, and chemical composition. Mixing length theory in the formulation of Mihalas (1978) is used with the LHD models to compute convective flux, thus the mixing-length parameter, $\alpha_{\rm MLT}$, is one of the input parameters that has to be specified beforehand. The latter parameter was set to $\alpha_{\rm MLT}$ = 1 when computing LHD models that were used in our study. Let us stress that LHD uses the same equation of state (EOS) and opacity tables as utilized with the CO^{5}BOLD code (see Section 1.4.3). This allows, for example, to make a differential comparison of synthetic spectral lines computed with the CO^{5}BOLD and LHD model atmospheres, and, therefore, to assess the influence of convection on the spectral line formation (see Chapter 2). We did not make differential 3D–1D comparisons comparisons using the ATLAS9 model atmospheres because ATLAS9 models use different opacities and EOS compared to those utilized with either LHD or CO^{5}BOLD.

The 1D hydrostatic LHD model atmospheres were used to assess the influence of convection on the formation of Na I, Mg I, K I and Zn I lines in the atmospheres of stars in 47 Tuc (see Sect. 1.6). As it was already mentioned above, their atmospheric parameters were identical to those of the CO^{5}BOLD models.

1.4.3. 3D hydrodynamical CO^{5}BOLD model atmospheres

Standard 1D model atmospheres are calculated assuming of hydrostatic equilibrium thus, are time-independent. Obviously, this is not the case in real nature. For example, from the observations of the Sun we know that solar surface is not static and changes with time. Granulation, which is a direct consequence of convection, is yet another proof of it. Therefore, 3D hydrodynamical model atmospheres are used to overcome the deficiencies of 1D model atmospheres for modeling convection.

The main goal for using the CO^{5}BOLD model atmospheres in our work was to study the influence of convection on the formation of Na I, Mg I, and K I lines in the atmospheres of the target TO and RGB stars in 47 Tuc (see Sect. 1.6). The CO^{5}BOLD stands for COnservative COde for the COmputation of COmpressible COnvection in a BOx of L Dimensions with L = 2 or 3. The CO^{5}BOLD package was developed by B. Freytag and M. Steffen, with contributions from H.-G. Ludwig, W. Schaffenberger, O. Steiner, and S. Wedemeyer-Böhm (Freytag et al. 2012). It is capable of operating in two modes: 1) the "box-in-a-star" mode, in which the computational domain covers a small portion of the stellar surface; and 2) the "star-in-a-box" mode, in which the computational domain includes the entire star. During the model computations, the code solves time-dependent equations of conservation of mass, momentum, and energy, as well as the equation of radiative transfer.

The large amount of information provided by the 3D hydrodynamical models comes at a larger computational cost and thus the treatment of certain physical effects needs to be simplified. For example, in the computation of a hydrodynamical model, the opacities are grouped into a small number of opacity bins, usually less than 14 (Nordlund 1982; Ludwig et al. 1994; Vögler et al. 2004).

We used MARCS opacities (Gustafsson et al. 2008) that were grouped into six opacity bins (see, e.g., Ludwig 1992; Ludwig et al. 1994) in order to compute the CO^{5}BOLD models used throughout this study. Solar-scaled abundances were taken from Grevesse & Sauval (1998) except that for CNO we used the following values: A(C) = 8.41, A(N) = 7.80, A(O) = 8.67. The latter values were taken from Caffau et al. (2008). All CO^{5}BOLD models were computed using α-element enhancement of [α/Fe] = +0.4. They were all calculated using a "box-in-a-star" setup. The Cartesian grids used in these computations had different number of numerical grid points (and spatial dimensions) in the case of TO and RGB stars (see Sect. 2.2.4, 3.2.4, 4.2.3 for details). LTE was assumed when computing radiative opacities and source function. Typical CO^{5}BOLD simulation sequence usually covered the interval of $\approx$ 10 convective turnover times (see Ludwig & Kučinskas 2012, for details).

Performing spectral line synthesis using the entire simulation run would lead to prohibitively high computational costs. Therefore, we selected a subset of twenty 3D hydro-

dynamical model structures computed at different time instants (snapshots) and spaced over the entire span of the model simulation run (see Kučinskas et al. 2013, for details on snapshot selection procedure). These subsets of snapshots were then used to perform spectral line synthesis calculations.

1.5. Determination of abundances of chemical elements

One of the most important things to learn from stellar spectra is their chemical composition. The latter is characterized in terms of chemical abundances, where abundance of an element X, A(X), is defined as $A(\mathrm{X})=\log_{10}(N_\mathrm{X}/N_\mathrm{H})+12.00$, where N_X and N_H are concentrations of the element X and hydrogen, respectively. In astrophysics, element-to-hydrogen abundance ratio, [X/H], is defined as the ratio of concentrations of the two elements with those observed in the Sun and is expressed as

$$[\mathrm{X/H}] = \log_{10}\left(\frac{N_\mathrm{X}}{N_\mathrm{H}}\right)_\mathrm{star} - \log_{10}\left(\frac{N_\mathrm{X}}{N_\mathrm{H}}\right)_\odot \tag{1.2}$$

One way to obtain abundance of a given chemical element in the atmosphere of a target star is using the curve-of-growth analysis. In this approach, one measures equivalent width of a given spectral line of interest (or several lines of the same element) and, by finding theoretically computed equivalent width that equals to the observed one, determines abundance of this element in the atmosphere of the target star.

One of the major drawbacks of this method is that it is not always possible to measure the equivalent width of a given spectral line reliably, especially in the case of poor continuum definition, blends with lines of other elements, and so on. Also, in case of strong(er) lines the major contribution to the equivalent width occurs due to growing absorption in the line wings. These, again, are difficult to measure reliably as they will be normally be blended with the profiles of other lines. Despite these limitations, we used the curve-of-growth approach to compute the 3D-1D abundance corrections for the spectral lines of Na I, Mg I, and K I used in our analysis. This was done because in this particular case we only had to deal with theoretical line profiles and, thus, the measurement of the equivalent widths was done easily by simply integrating over the line profiles (see Sect.1.6).

In another approach, synthetic spectrum is fitted to the observed one in a wavelength range centered around the spectral line(s) of interest. By adjusting abundances of the target element, one computes a set of synthetic spectra and determines the abundance of the target element by finding the best-fitting theoretical spectrum to the observed one. This method is very useful when blended spectral lines are used for abundance determination. In principle, this method can be applied fully automatically or manually by

finding (iteratively) best match between the observed and theoretical spectral line profiles. Star spectrum needs to be normalized and the main stellar parameters ($T_{\rm eff}$, $\log g$, $\xi_{\rm mic}$, $\xi_{\rm mac}$, $v\sin i$) should be determined before this method can be applied. Alternatively, some of these parameters, i.e. $\xi_{\rm mac}$, $v\sin i$ may be considered as a free-parameters and can be determined iteratively during the fitting procedure.

In this Thesis we applied synthetic spectrum method for the determination of 1D LTE/NLTE abundances of Na I, Mg I, and K I in the TO and RGB stars of 47 Tuc. For 1D LTE abundance determinations, spectral line profiles were computed with the SYNTHE code (Sect. 1.5.1), while the 1D NLTE line profiles were calculated with the MULTI code (Sect. 1.5.2).

1.5.1. 1D LTE spectral synthesis code SYNTHE

The only element for which we determined 1D LTE abundances (i.e., not 1D NLTE) was Zn; the detailed description of the analysis procedure is provided in Chapter 4. In this part of the study, the 1D LTE synthesis of Zn I lines was performed with the SYNTHE package (Kurucz & Furenlid 1979). SYNTHE allows to compute synthetic spectrum in a chosen wavelength range using the given LTE model atmosphere.

Several simplifications are made in the computation of 1D LTE synthetic spectra with the SYNTHE code:

- the local thermodynamic equilibrium, LTE, is valid throughout the atmosphere;
- the radiation field at any given point in the atmosphere is characterized by the local temperature, T;
- particle velocities follow the local Maxwellian velocity distribution;
- atomic level populations are described by the Boltzmann equation;
- population ratios between the atomic levels of successive ionization stages of a given element are described by the Saha equation.

Together with the input script, one needs to provide a chosen model atmosphere and a parameter list for the atomic and molecular lines the profiles of which need to be computed (line wavelengths, line excitation potentials, oscillator strengths, line broadening parameters). SYNTHE allows to use different model atmospheres, such as MARCS, PHOENIX, not only ATLAS9 or ATLAS12.

1.5.2. 1D NLTE MULTI software package

Non-local thermodynamic equilibrium is a relatively loose term which implies that the assumption of LTE fails. This approximation is usually called non-LTE or NLTE, which may be perceived as a negation of local equilibrium. This is evidently not true, since in

this "non-equilibrium" there are still particle velocities in equilibrium. The basic difference between LTE and NLTE is the behavior of atomic level populations. The approximation of LTE allows relatively simple and fast computation of the level populations using the Saha-Boltzmann equation. The NLTE approximation takes into account the fact that the level populations are influenced by the radiation field arising far from a given point in the atmosphere where these populations are calculated. In this case, the level populations of each atom are determined by the equations of kinetic equilibrium

$$n_i \sum_{j \neq i}^{L} (R_{ij} + C_{ij}) - \sum_{j \neq i}^{L} n_j (R_{ij} + C_{ij}) = 0 \tag{1.3}$$

where i = 1,..., L and L is the total number of atomic energy levels considered. $R_{\rm ij}$ and $C_{\rm ij}$ are radiative transition rates and collision transition rates, respectively. When level population numbers are known, NLTE–LTE departure coefficients can be computed for each atomic level of interest (defined as $b_i = \dfrac{n_i}{n_i^*}$, where n_i is the non-LTE population and n_i^* the LTE population of level i). These departure coefficients may be further fed into the equation of radiative transfer and, by solving it, one may obtain NLTE line profiles of the target spectral lines. It is important to stress though that it is only when the NLTE level populations are known, the NLTE spectral line profiles can be computed. To compute the NLTE level populations, we used the 1D NLTE code MULTI.

First version of the MULTI code was developed by Mats Carlsson (Carlsson 1986). This code can be used to solve non-LTE radiative transfer problems in semi-infinite, plane-parallel one-dimensional atmospheres with a prescribed macroscopic velocity field. One of the main input files of this code is that of a model atom. This model atom may contain many atomic levels distributed across several ionization stages. The synthetic spectral lines are assumed to be formed in a complete frequency redistribution over the line profile function which is assumed to be a Voigt function. Obviously, for each chemical element of interest one should provide a realistic model atom containing information about the atomic level energies, probabilities for collisional and radiative excitation and ionization, and so forth.

One of the biggest disadvantages of the MULTI code from the user point of view is the absence of one single input file/script. First, one should provide an input model atmosphere. Then, there are two other main input files used with MULTI, "ATOM" and "ATOM2". The preferred values of chemical element abundance must be duplicated in both files. In the MULTI code there is no external atomic line list, only the internal line list of pre-selected atomic lines. This information about the atomic line parameters is provided in the "ATOM2" file. The "ATOM2" file is also dedicated to provide input

for the spectral line synthesis computations, such as spectral resolution, line broadening parameters, and so on. The information about the atomic levels and their energies is stored in the "ATOM" file. In this Thesis we developed a number of Python routines which allow to use the MULTI package in a semi-automatic way, by specifying the input parameters in a single input file.

Throughout this study, we used a version of MULTI which was modified by S. Korotin (Korotin et al. 1999). We note that the LTE spectral line profiles computed with MULTI perfectly match those calculated with SYNTHE. We used several model atoms in our work. The model atom of Na used in the abundance analysis was presented and tested in Dobrovolskas et al. (2014). It was constructed using 20 levels of Na I and the ground level of Na II. To compute level populations, 46 bound-bound radiative transitions were taken into account. For the lowest 9 levels, we used collisional cross-sections that were obtained in quantum mechanical computations (Barklem et al. 2010). For other levels, we used the classical formula of Drawin (Steenbock & Holweger 1984). The correction factor for the collisions with hydrogen was set to $S_{\rm H} = 1/3$.

The model atom of Mg was taken from Mishenina et al. (2004). Three ionization levels were taken into account, with 84 atomic levels for Mg I, 12 levels of Mg II, and a ground state of Mg III. The departure coefficients were computed by taking into account radiative transitions between the first 59 levels of Mg I and ground level of Mg II. Quantum mechanical collision cross-sections obtained by using quantum mechanical computations by Barklem et al. (2012) were used in case of the lowest 7 atomic levels of Mg I. For other levels, we used the formula of Steenbock & Holweger (1984) with the correction factor $S_{\rm H} = 0.15$.

Finally, we used the model of K from Andrievsky et al. (2010) that comprised 20 levels of K I and the ground level of K II. In total, 62 bound-bound radiative transitions were included when computing atomic level populations (see Andrievsky et al. 2010, for further details). The formula of Steenbock & Holweger (1984) was used to take into account collisions with hydrogen using the correction factor $S_{\rm H} = 0.05$ (Andrievsky et al. 2010).

1.5.3. 3D LTE/NLTE spectral synthesis code Linfor3D

Spectral synthesis codes like SYNTHE and MULTI may be used only with the 1D model atmospheres. To perform spectral line synthesis computations with the 3D hydrodynamical model atmospheres we used Linfor3D spectral synthesis package[6].

Linfor3D is a spectrum synthesis code which works with the 3D hydrodynamical model atmospheres and is specifically tailored to those computed with the CO^{5}BOLD code (Section 1.4.3). The Linfor3D code solves the RTE under the assumption of ei-

[6]http://www.aip.de/Members/msteffen/linfor3d

ther LTE or NLTE. The RTE should be solved over the range of geometrical and optical depths where a non-negligible contribution to the spectral line formation can be expected. Our spectral synthesis computations were therefore performed in the optical depth range extending from $\log \tau_{\rm Ross} = 2.0$ at the inner boundary to $\log \tau_{\rm Ross} = -6.0$ at the outer boundary, with a step of $\Delta \log \tau_{\rm Ross} = 0.08$. The RTE was solved along one vertical and two inclined directions, in each case at four azimuthal angles.

For each selected CO^{5}BOLD snapshot, Linfor3D also computes an average 3D model structure, $\langle$3D$\rangle$, by averaging hydrodynamical and thermodynamic quantities (such as gas velocity, temperature, pressure, internal energy, etc.) on surfaces of equal optical depth. Then, spectral line synthesis calculations are performed using the average $\langle$3D$\rangle$ model. Since the average $\langle$3D$\rangle$ model is a 1D model atmosphere, it may be used to assess the impact of horizontal inhomogeneities of thermodynamic and dynamical properties on the spectral line formation, by comparing the predictions of 3D hydrodynamical and $\langle$3D$\rangle$ model atmospheres (see Chapter 2). Linfor3D is also capable of reading in a reference 1D model atmosphere (in our case computed with the LHD code) for which the spectral line synthesis is done as well, providing a possibility to differentially compare the predictions of full 3D, average $\langle$3D$\rangle$, and 1D model atmospheres.

1.6. 3D–1D abundance corrections

Since the 1D hydrostatic model atmospheres may only account for convection in a rather approximate way, we used 3D hydrodynamical model atmospheres to asses the possible impact of convection on the formation of spectral lines used in our study. To do this in a strictly differential way, we used 3D hydrodynamical CO^{5}BOLD (Sect.1.4.3) and 1D hydrostatic LHD (Sect.1.4.2) model atmospheres (see Freytag et al. 2012; Caffau et al. 2008, respectively).

The influence of convection on the line strengths was assessed using 3D–1D LTE abundance corrections, $\Delta_{\rm 3D-1D\ LTE}$. This quantity, i.e., the abundance correction, allows to measure the difference in the abundance of a given chemical element that would be obtained using 3D hydrodynamical and 1D hydrostatic model atmospheres from the given observed spectral line (e.g., Kučinskas et al. 2013; Dobrovolskas et al. 2013). First, synthetic curves-of-growth were calculated using the CO^{5}BOLD and LHD model atmospheres. Then, we chose the lowest and highest values of equivalent line widths which were measured for a given line in a real stellar spectrum. Finally, we then computed the difference in the abundance as indicated by the difference in the 3D and 1D curves of growth at these particular equivalent widths, $\Delta_{\rm 3D-1D\ LTE}$. Using this procedure we therefore obtained the 3D–1D LTE abundance corrections for several values of W and for each spectral line that we used in our study (for the line list used in the abundance analysis of TO and RGB stars see Sect. 3.2.2 and 2.1, respectively). The

value of microturbulence velocity, $\xi_{\rm mic}$, which is needed to compute synthetic spectral lines using the 1D LHD model atmospheres, was determined using 3D hydrodynamical model atmospheres (see Steffen et al. 2013, Method 1, for details). In this way one may expect to minimize the influence of the limitations of 3D hydrodynamical models on the computation of line profiles and their strengths (see Prakapavičius et al. 2017, for a discussion). In computations of $\xi_{\rm mic}$, we therefore ignored the original velocity field of the 3D hydrodynamical model and used a set of microturbulence velocities instead for computing the corresponding curves of growth. The latter were then used to interpolate between the equivalent widths of the synthetic 1D spectral lines in order to find the value of $\xi_{\rm mic}$ at which the equivalent width of the line profile computed using 3D model and given value of depth independent $\xi_{\rm mic}$ was equal to that calculated using full 3D hydrodynamical model atmosphere (i.e., with hydrodynamical velocity field taken into account). We then utilized the obtained value of $\xi_{\rm mic}$ to compute 1D spectral line profiles and to subsequently construct the corresponding curves-of-growth. The latter, along with the curves-of-growth obtained utilizing the 3D hydrodynamical model, were finally used to compute the 3D–1D LTE abundance corrections, $\Delta_{\rm 3D-1D\ LTE}$.

The results of 3D–1D LTE abundance corrections for the lines of Na I, Mg I, and K I observed in the spectra of RGB stars are presented in Sect. 2.2.4 (Table 2.4). The corrections for Mg I and K I lines seen in the spectra of TO and those of Zn I observable in RGB stars are provided in Sect. 3.2.4 (Table 3.4) and Sect. 4.2.3 (Table 4.3), respectively.

1.7. Statistical analysis of abundance determination uncertainties and intrinsic abundance spreads

As it will be shown in Sect. 2.3, 3.3, 4.3, there is a non-negligible star-to-star variation in the abundances of light elements, both in the TO and RGB stars in 47 Tuc. One may wonder whether this variation could be caused by real cosmic scatter in the elemental abundances (i.e., intrinsic abundance variation), or whether it could be due to the observational errors alone. To answer this question, we performed a maximum-likelihood test with which we aimed to determine the possible extent of the intrinsic star-to-star abundance variations. For this, one first needs to obtain realistic estimates of the abundance errors. The main sources of the latter are: (1) errors in the determined atmospheric parameters ($T_{\rm eff}$, $\log g$, and $\xi_{\rm mic}$); and (2) errors in the fitting of the spectral line profiles due to uncertainties in the choice of continuum level and inaccurate fits of the spectral line profiles. There are also two important notes: (1) uncertainties in the atomic line parameters and sources of various systematic errors were ignored; (2) the determined uncertainties therefore provide only a lower limit to the abundance errors.

1.7.1. Uncertainties in the determined abundances

Errors in the effective temperatures of RGB stars were estimated by using $V-I$ color indices that were increased and decreased by the amount given by their observational errors. For the latter, we used a conservative estimate of $\sigma(V) = \sigma(I) = 0.03$ mag which led to the uncertainty in the effective temperature of ±65 K. To estimate the influence of this errors on the elemental abundance, we re-determined abundances of the light elements using the effective temperatures increased or decreased by ±65 K. For the TO star sample we assumed $T_{\rm eff}$ ±100 K as a conservative error in the effective temperatures (we remind that Teff of TO stars were determined by fitting their Hα line profiles in Dobrovolskas et al. (2014)). Just as in the case of RGB stars, we used this value to estimate the effect of uncertainty in the determined effective temperatures on the light element abundances in TO stars.

We then used the determined errors in the effective temperature, luminosity, ±0.03 $L_{\odot}$, (estimated from the photometric error in M_V), and stellar mass, ±0.01 $M_{\odot}$ (obtained from theoretical isochrones), to obtain the error in $\log g$, ±0.04 dex. In our view, however, the latter value is unrealistically low, thus we used a slightly higher (and, in our view, more realistic) value of ±0.1 dex to estimate the uncertainty in the light element abundances, $\sigma(\log g)$. Identical values of $\sigma(\log g)$ were adopted for both TO and RGB stars. It is important to stress, however, that these errors are very small. Therefore, their contribution to the final abundance uncertainty is negligible.

The errors arising due uncertainty in the determined microtubulence velocities were estimated in a slightly different way for the TO and RGB stars. In case of the latter, we used 58 RGB stars from Carretta et al. (2009a) and 81 RGB stars from Cordero et al. (2014) which had $\xi_{\rm t}$ determined spectroscopically from Fe I lines. We computed RMS variation of $\xi_{\rm t}$ in the combined sample of 139 RGB stars and used this value to estimate the errors in the resulting light element abundances, $\sigma(\xi_{\rm t})$. It is worthwhile noting that the mean value of $\xi_{\rm t}$ and its RMS in this combined sample of RGB stars, $\xi_{\rm t} = 1.48 \pm 0.18$ km/s, is nearly identical to $\xi_{\rm t} = 1.5$ km/s used in our study.

In case of TO stars, we estimated the microturbulence velocity by evaluating the slope uncertainty in the [Fe/H] $-$ W plane. For this, we determined iron abundance from individual Fe I lines in six TO stars from our sample (as it was already mentioned earlier in Sect. 1.3, iron abundance determination was not possible for a larger number of stars because of the small number of usable Fe I lines and poor S/N of the observed spectra). The average determined slope error was ±0.001 dex/pm which corresponds to the error in $\xi_{\rm t}$ of ±0.29 km/s. The latter value was used to estimate uncertainty due to

microturbulence velocity in the light element abundances determined in TO stars. The error in the continuum determination was estimated using the following expression

$$err(\text{cont}) = \frac{\sigma_{\text{cont}}}{\sqrt{N}} \tag{1.4}$$

where σ_{cont} is dispersion in the variation of continuum level computed using data from all wavelength windows where the continuum determination was possible for a given spectral line, while N is the total number of wavelength points in these wavelength windows. The influence of this uncertainty on the abundance errors was estimated by fitting the line profiles with the continuum level shifted by *err(*cont).

For estimating errors in the line profile fitting, we compute RMS deviation between the observed and best-fitted line profiles. These uncertainties were further converted into errors in the line equivalent widths which were used to estimate errors in the elemental abundances due to uncertainties in the line fitting, σ_{fit}.

For RGB star sample uncertainties in the abundances of Na, Mg, and K due to T_{eff}, $\log g$, and ξ_{t} are presented in Sect. 2.2.3, Table 2.3, columns 4, 5, 6, respectively. For Zn, the corresponding uncertainties are provided in Sect. 4.2.3, Table 4.3. In the case of TO star sample, uncertainties in the abundances of Li, O, Na, Mg, and K are presented in Sect. 3.2.2 Table 3.3. The abundance errors due to uncertainties in the continuum variation and line profile fitting are listed in Table 2.3, columns 7 and 8, respectively.

The individual contributions due to uncertainties in the atmospheric parameters, continuum determination, and spectral line profile fitting were added in quadratures to obtain the total error in the abundances of Na, Mg, K, and Zn. These errors are provided in Sect. 2.2.3, Table 2.3 (for RGB target stars), Sect. 3.2.2, Table 3.3 (for TO target stars). In the case of Zn abundance, the errors are provided in Sect. 4.2.2, Table 4.2.

1.7.2. Analysis of intrinsic abundance spreads

In order to search for possible intrinsic spreads[7] in the abundances of Na, Mg, K, and Zn determined in our sample stars we followed a prescription provided in Mucciarelli et al. (2012, 2015). This method uses maximum-likelihood (ML) technique to determine both the mean abundance ratio, $\langle$[A/B]$\rangle$, of elements A and B, and the intrinsic spread of this abundance ratio, σ_{int}. It should be noted that this test is based on assumption that the distributions of the determined abundances and their errors are Gaussian (Eq. 1.6).

In this test, one assumes that the spread in the observed abundances is caused by two factors: (a) errors in the determined abundances; and (b) intrinsic abundance spread. In

[7]Intrinsic abundance spread is defined as variation in the abundance of a given element that is observed in the sample of target stars that is caused by real start-to-star abundance differences, i.e., after the spread due to abundance determination errors is removed.

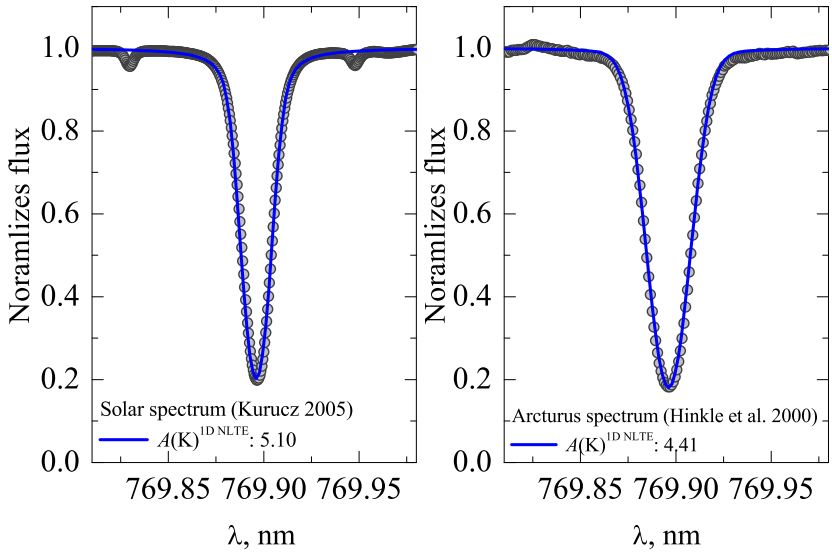

Figure 1.1. K I line in the spectra of the Sun (left) and Arcturus (right). The observed spectra are ploted as gray filled circles, synthetic 1D NLTE line profiles computed using the MULTI code are shown as blue solid lines.

case when the observed spread can be accounted for by the abundance determination errors alone, no intrinsic spread is detected. However, when the latter is detected it is then possible to estimate the size and error of the intrinsic abundance spread. The likelihood function is defined as

$$L(\langle[\mathrm{A/B}]\rangle, \sigma_{\mathrm{int}}) = \prod_{\mathrm{i}=1}^{N} p_{\mathrm{i}}(\langle[\mathrm{A/B}]\rangle, \sigma_{\mathrm{int}}), \tag{1.5}$$

where N is anumber of stars in a given sample and p_{i} is a Gaussian probability function defined as

$$p_{\mathrm{i}}(\langle[\mathrm{A/B}]\rangle, \sigma_{\mathrm{int}}) = \frac{1}{\sqrt{\sigma_{\mathrm{int}}^2+\sigma_{\mathrm{i}}^2}} \exp\left[-\frac{1}{2}\left(\frac{\langle[\mathrm{A/B}]\rangle - \langle[\mathrm{A/B}]\rangle_{\mathrm{i}}}{\sqrt{\sigma_{\mathrm{int}}^2+\sigma_{\mathrm{i}}^2}}\right)^2\right] \tag{1.6}$$

here $\langle[\mathrm{A/B}]\rangle_{\mathrm{i}}$ and σ_{i} is the abundance ratio and its error for the i-th star in the sample.

The likelihood values were computed on a 2D grid that extended over all possible combinations of $\langle[\mathrm{A/B}]\rangle$, σ_{int}. The given mean abundance ratio and its intrinsic spread were then determined by maximizing the likelihood in this 2D grid. The errors in all determined quantities were computed following Pryor & Meylan (1993, see their Eq. (5)-(10)).

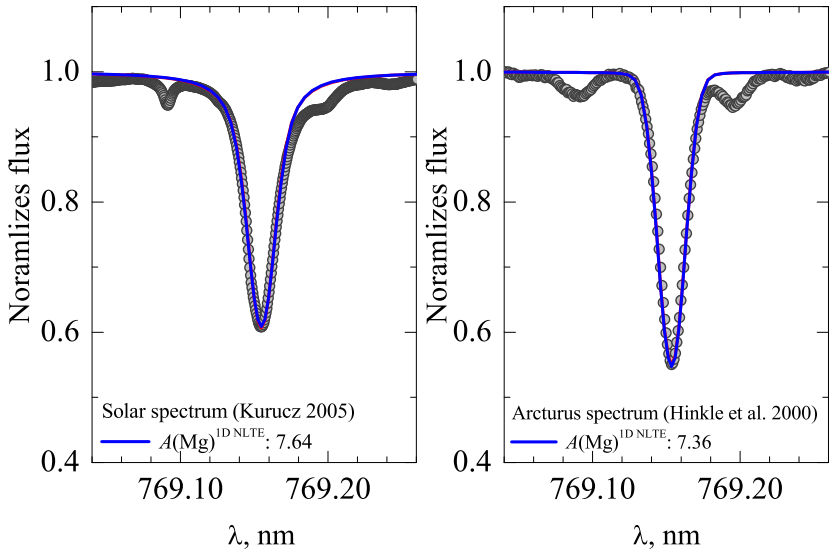

Figure 1.2. Mg I line profiles in the spectra of the Sun (left) and Arcturus (right). Observed spectra are are plotted as gray circles, synthetic 1D NLTE lines profiles computed using MULTI code are shown as the blue solid lines.

The obtained mean abundance ratios, $\langle[X_i/\mathrm{Fe}]\rangle$, and its uncertainties, as well as the total variations, $\sigma[X_i/\mathrm{Fe}]$ ($=\sqrt{\sigma^2_{\mathrm{int}}+\sigma^2_i}$), and the determined intrinsic abundance spreads, $\sigma_{\mathrm{int}}[X_i/\mathrm{Fe}]$, are provided in Sect. 2.3, Table 2.5 for RGB sample stars, and in Sect. 3.3.1, Table 3.5 for TO sample stars. The results for [Zn/Fe] are presented in Sect 4.3.

1.8. Mg, K, and Zn abundance in the reference stars

In this study we present differential analysis of chemical elements, which means that all abundances of chemical elements are provided relative to the solar abundance scale (see Sect.1.5). To define "zero-points" in our abundance scale we need to determine abundance of the same elements using solar spectrum and the same methodology as used in our determination of abundances in 47 Tuc. Sometimes, depending on what the target star is, Sun may not be the best reference star. For example, if target stars are red giant stars, a better choice could be Arcturus. Therefore, we verified the adopted model atoms of Mg and K, as well as the atomic parameters of Na , Mg I, K I, and Zn I lines used in our study by determining abundances of these elements in the Sun and Arcturus. The solar abundances of these elements obtained in our study were further used to compute element-to-iron abundance ratios in the studied TO and RGB stars (Sect. 2.2.3, Sect. 3.2.2, Sect. 4.2). Let us note that similar analysis for Na has been already performed by Dobrovolskas et al. (2014) thus in this Thesis (Sect. 3.2.2) we used solar abundance of Na determined in the latter study.

Table 1.1. Errors in the abundances of Mg, K, and Zn determined in the atmospheres of the Sun and Arcturus, $\sigma(A)_{\rm tot}$, obtained by changing various atmospheric parameters by the size of their errors. The sign ± or ∓ reflects the change in the elemental abundance which occurs due to increase (top sign) or decrease (bottom sign) in a given atmospheric parameter.

Element	Line	$\sigma(T_{\rm eff})$	$\sigma(\log g)$	$\sigma(\xi_{\rm t})$	σ(cont)	σ(fit)	$\sigma(A)_{\rm tot}$
	λ, nm	dex	dex	dex	dex	dex	dex
Sun							
Mg I	769.16	±0.004	∓0.001	∓0.001	±0.009	±0.025	0.026
K I	769.16	±0.009	∓0.005	∓0.009	±0.008	±0.055	0.057
Zn I	472.21	±0.005	∓0.001	∓0.023	±0.015	±0.017	0.032
Zn I	481.05	±0.011	∓0.005	∓0.032	±0.016	±0.019	0.042
Arcturus							
Mg I	769.16	±0.009	∓0.012	∓0.015	±0.022	±0.045	0.054
K I	769.89	±0.033	∓0.001	∓0.088	±0.028	±0.059	0.114

To determine the 1D NLTE abundances of Mg and K in the Sun we used the re-reduced Kitt Peak Solar Flux atlas from Kurucz (2006). This solar spectrum was obtained at the resolution of $R = 523\,000$ and $S/N \sim 4000$ (near-IR) and spans the wavelength range of of 300-1000 nm. Abundances of Mg and K were determined using solar model atmosphere computed with the ATLAS9 code. Values of the effective temperature and surface gravity used for the computation of the model atmosphere were $T_{\rm eff} = 5777 \pm 10$ K and $\log g = 4.43 \pm 0.02$ (Andreasen et al. 2015). The value of solar microturbulence velocity, $\xi_{\rm t} = 1.01 \pm 0.06$ km/s, was also taken from Andreasen et al. (2015).

For Arcturus, we used a high-resolution ($R = 150\,000$) spectrum from Hinkle et al. (2000). This spectrum spans a wavelength range from 372.7 nm to 930.0 nm and has $S/N \sim 1000$ in the near-infrared part of the spectrum. The ATLAS9 model atmosphere that was used in the abundance determination was computed using $T_{\rm eff} = 4286 \pm 30$ K and $\log g = 1.66 \pm 0.05$ as recommended in Ramírez & Allende Prieto (2011). The value of microturbulence velocity, $\xi_{\rm t} = 1.58 \pm 0.12$ km/s, was taken from Jofré et al. (2015).

The solar 1D NLTE abundance of K obtained in our analysis was $A({\rm K})_{\odot}^{\rm 1D\ NLTE} = 5.10 \pm 0.06$, with only a slightly higher value determined in 1D LTE, $A({\rm K})_{\odot}^{\rm 1D\ LTE} = 5.20 \pm 0.06$. The latter value is comparable to that determined by Ramirez Ramírez & Allende Prieto (2011), $A({\rm K})_{\odot}^{\rm 1D\ LTE} = 5.31 \pm 0.02$. The corresponding values determined by us for Mg were $A({\rm Mg})_{\odot}^{\rm 1D\ NLTE} = 7.64 \pm 0.03$ and $A({\rm Mg})_{\odot}^{\rm 1D\ LTE} = 7.67 \pm 0.03$. The value obtained by us in 1D LTE only slightly exceeds $A({\rm Mg})_{\odot}^{\rm 1D\ LTE} = 7.59 \pm 0.02$ determined by Ramírez & Allende Prieto (2011).

In case of Arcturus, the determined K abundance was $A({\rm K})^{\rm 1D\ NLTE} = 4.41 \pm 0.11$ Similarly to what we obtained in the case of the Sun, the 1D LTE K abundance, $A({\rm K})^{\rm 1D\ LTE} = 5.01 \pm 0.11$, agrees well with $A({\rm K})^{\rm 1D\ LTE} = 4.99 \pm 0.07$ determined by Ramírez & Allende Prieto (2011). In case of Mg, we determined $A({\rm Mg})^{\rm 1D\ NLTE} =$

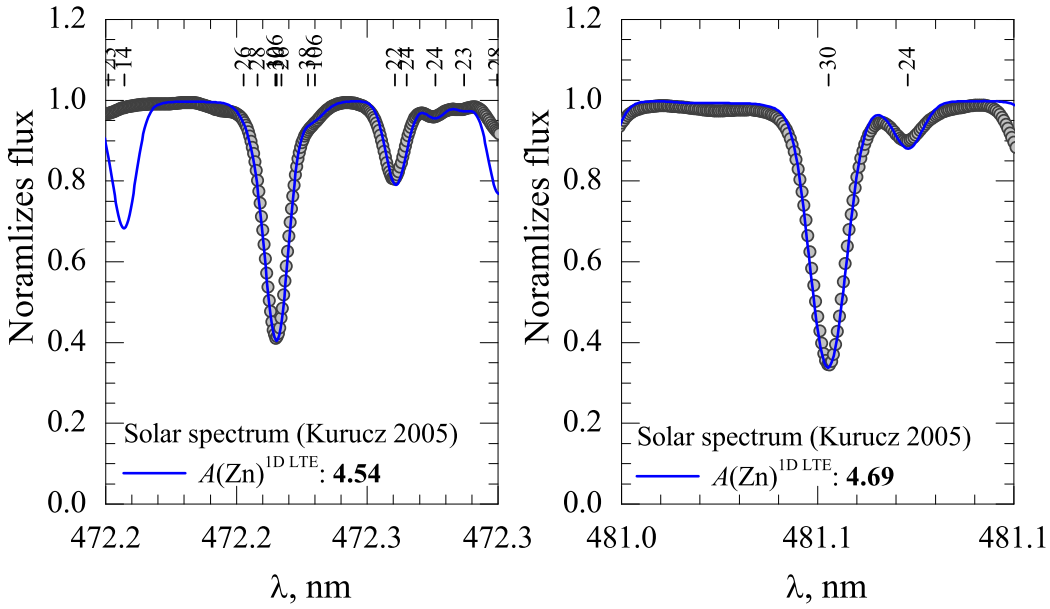

Figure 1.3. Zn I lines (λ=472.2, 481.0 nm) in the spectrum of the Sun, shwon as gray filled circles. Blue solid line shows synthetic spectrum of the Sun. Vertical ticks mark the spectral lines of various chemical elements indicated by their atomic numbers.

7.36 ± 0.05. There is a good agreement between the 1D LTE abundance determined in our study, $A(\mathrm{Mg})^{\mathrm{1D\ LTE}} = 7.46 \pm 0.05$, and $A(\mathrm{Mg}) = 7.47 \pm 0.03$ obtained by Ramírez & Allende Prieto (2011).

Observed spectra of the Sun and Arcturus, together with best-fitted syntheticMg I and K I line profiles, are shown in Fig. 1.1 and Fig. 1.2. Errors in the determined abundances of Mg and K in the Sun and Arcturus were estimated by utilizing the same methodology that was used to determine abundance errors for the TO and RGB stars (Sect. 1.7.1). The obtained abundance errors are listed in Table 1.1.

For obtaining the estimate of the solar Zn abundance, we used the same Zn I lines that were utilized in our analysis of Zn abundance in the RGB stars in 47 Tuc (see Sect. 4.2.2). Atomic line parameters were identical to those used in the analysis of RGB stars and were taken from the VALD-3 atomic database (Piskunov et al. 1995; Kupka et al. 2011). SYNTHE spectral line synthesis package and ATLAS9 model atmospheres ($T_{\mathrm{eff}} = 5777 \pm 10$ K and $\log g = 4.43 \pm 0.02$, as recommended by Andreasen et al. 2015) were used for computing synthetic line profiles (see Fig. 1.3). Just as in the case of Mg and K, the Kitt Peak Solar Flux Atlas (Kurucz 2006) was used for measuring solar Zn abundance. Abundances of Zn obtained from the two spectral lines (λ=472.2, 481.0 nm) were $A(\mathrm{Zn})_{\odot}^{\mathrm{1D\ LTE}} = 4.54$ and $A(\mathrm{Zn})_{\odot}^{\mathrm{1D\ LTE}} = 4.65$, respectively, with the mean value of $A(\mathrm{Zn})_{\odot}^{\mathrm{1D\ LTE}} = 4.60 \pm 0.08$. The obtained value agrees well with the solar Zn abundance determined in other studies, for example, e.g., $A(\mathrm{Zn})_{\odot}^{\mathrm{1D\ LTE}} = 4.58$ (Takeda et al. 2005),

$A(\mathrm{Zn})_{\odot}^{\mathrm{1D\ LTE}} = 4.62$ (Lodders et al. 2009), and $A(\mathrm{Zn})_{\odot}^{\mathrm{1D\ LTE}} = 4.56 \pm 0.05$ (Asplund et al. 2009).

Errors in the obtained solar Zn abundance were estimated using the same procedure and uncertainties in the atmospheric parameters of the Sun as in the case of Mg and K (see this Section above). These errors are provided in Table 1.1. The final determined value of Zn abundance in the Sun obtained from the two Zn I lines is $A(\mathrm{Zn})_{\odot}^{\mathrm{1D\ LTE}} = 4.60 \pm 0.04$.

2 Abundances of Na, Mg, and K in the atmospheres of RGB stars in 47 Tuc

In this Chapter, we present 32 RGB stars in 47 Tuc, aimed to study the possible Na–K and Mg–K relations, similar to those that were recently claimed to exist in two other GGCs, NGC 2419 (Mucciarelli et al. 2012) and NGC 2808 (Mucciarelli et al. 2015). In this study the abundances of K, Na, and Mg were determined using high-resolution 2dF/HERMES spectra collected with the AAT. In our study we applied the 1D NLTE abundance analysis techniques, with the spectral line profiles synthesized using the MULTI code and 1D ATLAS9 model atmospheres (Sect. 1.5).

2.1. Introduction

First evidence suggesting the existence of several stellar populations in the GGCs came with the detection of star-to-star light element abundance variations, and later, with a discovery of various correlations/anti-correlations between their abundances (see, e.g., Kraft 1994; Gratton et al. 2004, for a review). Photometric studies of the GGCs have revealed the existence of multiple sub-sequences across their color-magnitude diagrams, such as on the MS, SGB, and RGB (Piotto et al. 2007; Milone et al. 2012). Further spectroscopic observations have confirmed that stars on these sub-sequences are different in their light element abundances (Carretta et al. 2009a; Marino et al. 2008; Gratton et al. 2012). At around the same time, it also became clear that stars with different light element abundances tend to concentrate in different parts of the cluster (Bellazzini et al. 2012; Cordero et al. 2014). All this evidence clearly pointed to the existence of several distinct populations in nearly all GGCs studied which was in stark contrast with the classical notion which held that the GGCs were nearly perfect examples of simple stellar populations.

It is generally agreed today that first generation (1G) stars in the GCCs must have enriched the second-generation (2G) objects in certain light elements, such as Na, and depleted them in others, such as O. Such scenario would be able to explain the existence of various correlations/anti-correlations between the abundances of light chemical elements observed in the GGCs, such as Na–O anti-correlation (Carretta et al. 2006, 2009a; Marino et al. 2011), Mg–Al anti-correlation (Carretta et al. 2009a), Li–O correlation (Pasquini et al. 2005; Shen et al. 2010). Recent theoretical scenarios also predict that stars belonging to different generations may have retained different spatial distributions and dynamical properties, which, in certain GGCs, may still be possible to detect (Bekki 2011; Hénault-Brunet et al. 2015). This is also supported by recent observa-

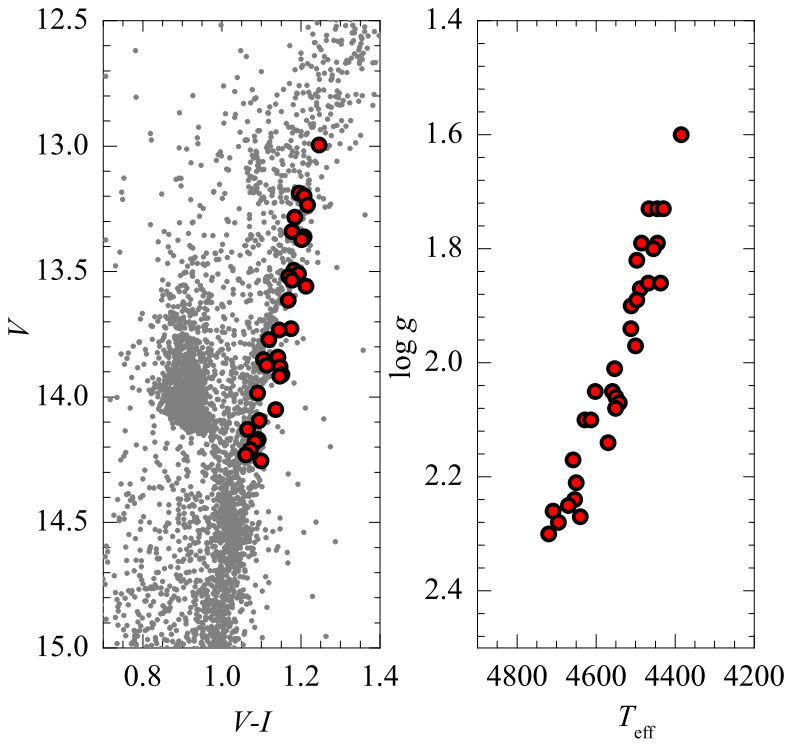

Figure 2.1. Left: upper part of the of $V-(V-I)$ color-magnitude diagram of 47 Tuc (photometric observations from Bergbusch & Stetson 2009). Stars used in this study are marked as filled red circles. Right: a sample of RGB stars used our study, plotted in the $T_{\rm eff}-\log g$ plane.

tional studies (Richer et al. 2013; Kučinskas et al. 2014). However, none of the proposed evolutionary scenarios of the GGCs is able to meet *all* available constraints simultaneously yet (see, e.g., Bastian et al. 2013; Renzini et al. 2015). Further evidence that may help to discriminate between the proposed evolutionary scenarios may come from still undiscovered relations between the abundances of other chemical elements.

In this context, the recently discovered Mg–K anti-correlation may help to better understand the nucleosynthetic networks that have taken place in the GGC stars. So far, this anti-correlation has been observed in two clusters only, NGC 2419 (Mucciarelli et al. 2012) and NGC 2808 (Mucciarelli et al. 2015). The authors have also claimed a detection of statistically significant correlations of [K/Fe] with [Na/Fe] and [Al/Fe], and anti–correlation with [O/Fe] ratios. It is important to note, however, that these clusters have extreme He enrichment: NGC 2808 Y=0.34 (Marino et al. 2014), NGC 2419 Y=0.42 (di Criscienzo et al. 2011). These helium abundances are significantly higher than those determined in other globular clusters (see, e.g., Milone et al. 2014). The question is, therefore, whether such correlations/anti-correlations are typical to other GGCs as well. Indeed, it is possible that NGC 2419 and 2808 are not typical examples of genuine GGCs: NGC 2419 may be a remnant of an accreted dwarf galaxy (Mackey & van den Berg 2005), while NGC 2808 shows a very extended O–Na anti-correlation

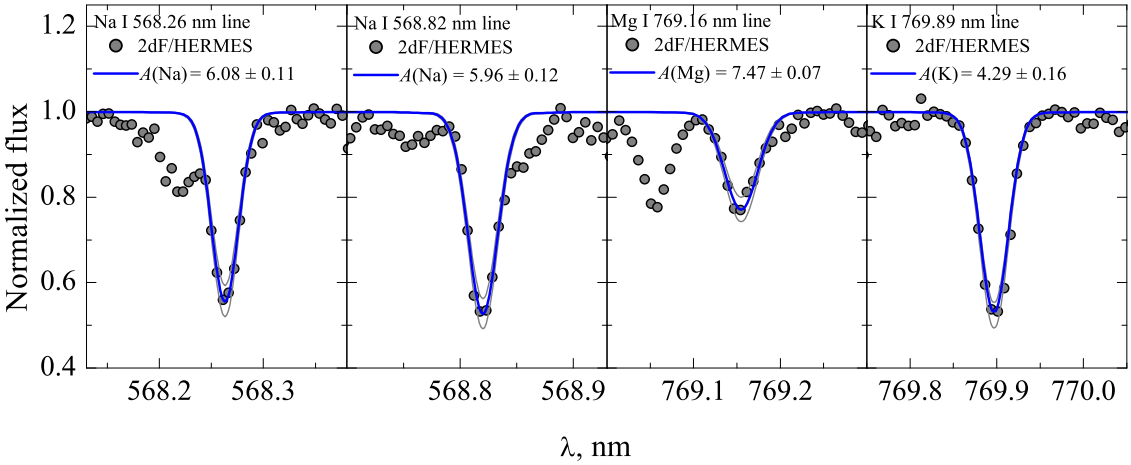

Figure 2.2. Best-fitted theoretical and observed Na I, Mg I, and K I line profiles in the spectrum of target RGB star 47TucS2220 ($T_{\rm eff}$ = 4490 K, $\log g$ = 1.8). Abundances and their errors determined using each individual spectral line are provided in each panel. Thin gray lines show synthetic profiles computed with the abundances altered by ±0.2 dex.

(e.g., Carretta et al. 2009a) and harbors four Mg-poor ([Mg/Fe] < 0) stars (e.g., Carretta et al. 2009b; Carretta 2014). Such properties are not common amongst other GGCs. In addition, Carretta et al. (2013) have studied K abundances in seven "classical" GGCs and have detected no intrinsic scatter in K abundance. However, in their more recent study Mucciarelli et al. (2017) claimed a detection of K–Na correlations and K–O anti-correlations NGC 6752, NGC 6809 and 47 Tuc. Nevertheless, it is still not clear whether such relations between the abundance of K and those of light elements may be common in other GGCs too. To answer this question, analysis based on larger stellar samples in other clusters is needed.

In this part of the Thesis we therefore determined abundances of Na, Mg, and K in a sample of 32 RGB stars in 47 Tuc and used this new information to search for the possible Mg–K anti-correlation and Na–K correlation. This cluster shows interesting connections between chemical abundances and kinematical properties of stars belonging to different generations (e.g., Richer et al. 2013; Kučinskas et al. 2014). Such connections have not been observed in many other GGCs yet. Therefore, this offers a possibility to investigate whether or not stars characterized with different K abundance do also differ in their kinematical properties.

2.2. Methodology

Our analysis was performed in two steps. First, we determined 1D NLTE abundances of Na, Mg, and K which was done using the MULTI package and 1D ATLAS9 model atmospheres. We then used the obtained abundances to search for possible relations

Table 2.1. Atomic parameters of Na I, Mg I, and K I lines used in the abundance determination.

Element	λ, nm	χ, eV	loggf	log γ_{rad}	log$\frac{\gamma_4}{N_e}$	log$\frac{\gamma_6}{N_H}$
Na I	568.26	2.102	−0.70	7.84	−4.22	−6.85
Na I	568.82	2.104	−0.45	7.84	−4.22	−6.85
Mg I	769.16	5.753	−0.78	7.57	−3.25	−6.83
K I	769.89	0.000	−0.17	7.56	−5.44	−7.45

between the abundances of the three elements, as well as between their abundances and kinematical properties of cluster stars.

2.2.1. Spectroscopic data

In this study we used a sample of 32 RGB stars in 47 Tuc which were observed with the 2dF optical fibre positioner and HERMES spectrograph mounted on the Anglo-Australian Telescope (AAT). Continuum normalization of the observed spectra was done with the IRAF *continuum* task (Tody 1986). Radial velocities of the cluster stars were measured using the IRAF *fxcorr* task, to make sure that all stars are cluster members. The CMD of 47 Tuc with the target RGB stars marked is shown in Fig. 2.1. For more specific information about these observations see Sect. 1.1.1.

2.2.2. Atmospheric parameters of the target stars

Atmospheric parameters of target RGB stars were determined using methodology discussed in Sect. 1.3. To recall briefly, effective temperatures were obtained using photometric data from Bergbusch & Stetson (2009) and the $T_{\rm eff} - (V - I)$ calibration from Ramírez & Meléndez (2005). Surface gravities were estimated using the classical relation between the surface gravity, mass, effective temperature, and luminosity (Eq. 1.1).

2.2.3. 1D NLTE abundances of Na, Mg, and K

To determine abundances of Na, we used two spectral lines of Na I doublet at 568.26 and 568.82 nm (GREEN region in the 2dF/HERMES spectra). In the case of Mg, we used one line located at 769.16 nm (IR region in the 2dF/HERMES spectra). For K, two lines of K I resonance doublet located at 766.49 nm and 769.89 nm were available in the observed 2dF/HERMES spectra (IR region). Unfortunately, the weaker line (λ = 766.49 nm) was strongly blended with telluric O_2 feature which made this K line unusable.Therefore, to determine K abundance we used the remaining clean line located at 769.89 nm. The two Na I lines and Mg I line were not affected by telluric lines.

For all spectral lines, the atomic data were taken from the VALD-3 database (Piskunov et al. 1995; Kupka et al. 2011). In case of K, we used oscillator strengths from Morton (1991) and the line broadening constants from the VALD-3 database. All atomic data are summarized in Table 2.1 where the line wavelengths, excitation po-

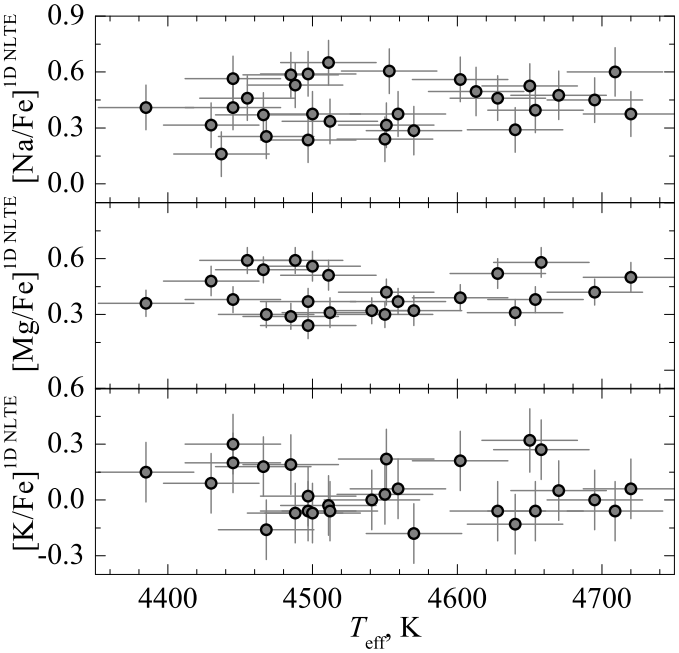

Figure 2.3. [Na/Fe] (top), [Mg/Fe] (middle), and [K/Fe] (bottom) abundance ratios determined in 32 RGB stars in 47 Tuc, as a function of effective temperature.

tentials, and oscillator strengths are provided in columns 2-4, and the line broadening constants (natural, Stark, and van der Waals) are given in columns 5-7.

The 1D NLTE abundances of all three elements were determined using the synthetic spectrum fitting technique (see Sect. 1.5). Since the atmospheric parameters of our sample stars were very similar, we used identical microturbulence velocity for all stars, $\xi_{\rm mic} = 1.5\,{\rm km\,s^{-1}}$. For choosing this value, we used the mean microturbulence velocity that was determined in a sample of 139 RGB stars in 47 Tuc using the data from Carretta et al. (2009a, 58 objects) and Cordero et al. (2014, 81 objects); we refer to Sect. 1.7.1 for details. For all sample stars, we also assumed identical rotational velocity of $2\,{\rm km\,s^{-1}}$. Typical $\xi_{\rm mac}$ values were in the range of 3-5 $\rm km\,s^{-1}$. To check the validity of this assumption, we determined iron abundance for three RGB stars with the best-quality spectra in our sample (S167, S1490, and S1563; $T_{\rm eff} = 4385, 4560, 4695\,{\rm K}$ and $\log g = 1.60, 2.05, 2.30$, respectively). For each star, we could identify six Fe I lines suitable for the abundance analysis. The determined iron-to-hydrogen ratios were $[{\rm Fe/H}]^{\rm 1D\ LTE} = -0.77, -0.73$, and –0.76, respectively, with the mean value of, $\langle[{\rm Fe/H}]^{\rm 1D\ LTE}\rangle = -0.75$, which nearly coincides with $[{\rm Fe/H}]^{\rm 1D\ LTE} = -0.76 \pm 0.03$ from (Carretta et al. 2009a) which was used in our study. However, determination of iron abundances for all stars in our sample was not feasible.

Synthetic profiles of Na I, Mg I, and K I lines were computed with the MULTI code (Carlsson 1986) modified by Korotin et al. (1999). This code and the model atoms of Na, Mg, and K are described in Sect. 1.5.2.

Table 2.2. 1D NLTE–LTE abundance corrections, $\Delta_{\text{1D NLTE–LTE}}$, computed for the spectral lines of Na I, Mg I, and K I used in this study.

Element	λ, nm	$T_{\rm eff}$=4385, $\log g$=1.6		$T_{\rm eff}$=4720, $\log g$=2.3	
		W, pm	$\Delta_{\text{1D NLTE–LTE}}$	W, pm	$\Delta_{\text{1D NLTE–LTE}}$
Na I	568.26	12.3	−0.25	10.6	−0.19
		16.4	−0.28	15.1	−0.23
Na I	568.82	13.3	−0.26	11.7	−0.20
		16.7	−0.26	15.5	−0.22
Mg I	769.16	8.5	−0.05	7.6	−0.01
		11.0	−0.08	10.1	−0.01
K I	769.89	19.8	−0.48	17.3	−0.55
		24.0	−0.40	21.6	−0.49

Typical fits of the synthetic 1D NLTE line profiles to those observed in the 2dF/HERMES spectrum are shown in Fig. 2.2. The determined abundances of all three elements are provided in Table A1 (Appendix A). We verified that for all elements studied there is no dependence of the determined abundances on the effective temperature (Fig. 2.3).

To investigate the influence of NLTE effects on the formation of spectral lines, we also computed 1D NLTE–LTE abundance corrections for the spectral lines used in our study. The corrections were computed using two ATLAS9 model atmospheres with values of $T_{\rm eff}$ and $\log g$ similar to those of stars at the extreme ends of our RGB star sample, for two line equivalent widths for each spectral line used (the values of equivalent width, W, represented the minimum and maximum values measured in the RGB star spectra). The obtained abundance corrections are provided in Table 2.2. Clearly, they are large for the lines of Na and K which shows that NLTE effects play an important role in their formation and that NLTE analysis is necessary in order to measure reliable elemental abundances using these spectral lines. This is in line with the findings of earlier studies (e.g., Takeda et al. 2009, Lind et al. (2011).

The total errors in the determined abundances of Na, Mg, and K, as well as individual contributions to the total error entering during different steps of the abundance analysis, are provided in Table 2.3; the total error, $\sigma(A)_{\rm tot}$, is a sum of individual contributions in quadratures). The details related to the error determination procedure are provided in Sect. 1.7.1.

2.2.4. 3D–1D LTE abundance corrections

The influence of convection on the formation of Na I, Mg I, and K I lines in the atmospheres of the target RGB stars was investigated using 3D hydrodynamical CO^{5}BOLD (Sect.1.4.3) and 1D hydrostatic LHD (Sect.1.4.2) model atmospheres. The procedure

Table 2.3. Errors of the determined abundances of Na, Mg, and K.

Element	λ, nm	$\sigma(T_{\rm eff})$	$\sigma(\log g)$	$\sigma(\xi_{\rm t})$	σ(cont)	σ(fit)	$\sigma(A)_{\rm tot}$
		dex	dex	dex	dex	dex	dex
Na I	568.26	±0.07	∓0.01	∓0.08	0.03	0.04	0.12
Na I	568.82	±0.07	∓0.01	∓0.08	0.04	0.06	0.13
Mg I	769.16	±0.03	∓0.01	∓0.05	0.03	0.04	0.08
K I	769.89	±0.07	∓0.00	∓0.14	0.04	0.05	0.17

The sign ± or ∓ reflects the change in the elemental abundance which occurs due to increase (top sign) or decrease (bottom sign) in a given atmospheric parameter. For example, an increase in the effective temperature leads to an increase in the abundance (±) while increasing microturbulence velocity results in decreasing abundance (∓).

used to compute the 3D–1D LTE abundance corrections, $\Delta_{\rm 3D-1D\ LTE}$, is described in Section1.6.

For computing 3D-1D abundance corrections we used 3D hydrodynamical and 1D hydrostatic model atmospheres with the atmospheric parameters similar to those of the median object in our RGB star sample (median star: $T_{\rm eff} \approx 4545$ K and $\log g = 2.02$; model: $T_{\rm eff} \approx 4490$ K and $\log g = 2.0$). Since we did not have models at the metallicity of 47 Tuc, we used those computed at [M/H] = −1.0. We expect, however, that this difference in metallicity should have a negligible effect on the determined abundance corrections (see Dobrovolskas et al. 2013, for discussion).

The obtained 3D–1D LTE abundance corrections are provided in Table 2.4. The abundance corrections were computed for two values of line equivalent width (i.e., "weak" and "strong" lines) that bracketed those measured in the spectra of RGB stars. We used the following values of W in our computations: 8.5, 5, and 20 pm, for the weakest, and 14, 9, and 22 pm, for the strongest lines in case of Na, Mg, and K. In column 3 of Table 2.4 we provide microturbulence velocities determined for each spectral line using 3D hydrodynamical CO^{5}BOLD model atmosphere (see Sect. 1.6 for details).

For all lines, the abundance corrections are small, < 0.07 dex which indicates that the role of convection in the formation of these spectral lines in the atmospheres of RGB stars is minor. This is in line with our earlier findings which have shown that at the metallicity of 47 Tuc the $\Delta_{\rm 3D-1D\ LTE}$ corrections expected for lines of Na I, Mg I, and K I should be small, typically, < 0.10 dex (Dobrovolskas et al. 2013; see also Collet et al. 2007). Obviously, NLTE effects may play their part in, for example, changing the concentration of neutral atoms in atmospheres of RGB stars due to overionization. However, it was not possible in our case to evaluate the size of these effects for Na, Mg, and K in 3D NLTE.

One may therefore conclude that $\Delta_{\rm 3D-1D\ LTE}$ abundance corrections were found to be small and it is likely that they will not be dramatically different if obtained in 3D NLTE. Nevertheless, we refrain from adding the obtained 3D–1D LTE corrections

Table 2.4. The 3D–1D abundance corrections, $\Delta_{\text{3D−1D LTE}}$, computed for different strengths of spectral lines of Na I, Mg I, K I used in this work (see text for the details).

Element	λ, nm	ξ_{micro} km s^{-1}	$\Delta_{\text{3D−1D LTE}}$, dex	
			weak	strong
Na I	568.26	1.11 ± 0.02	+0.05	+0.06
Na I	568.82	1.11 ± 0.02	+0.06	+0.07
Mg I	769.16	1.03 ± 0.01	+0.06	+0.07
K I	769.89	1.06 ± 0.002	+0.05	+0.05

to our 1D NLTE abundances. As it was shown in Klevas et al. (2016), such procedure is generally incorrect since it may predict abundances that are significantly different from those that would be obtained using the full 3D NLTE approach, especially at sub-solar metallicities. In any case, given their size, the 3D–1D abundance corrections are not very important in the context of the present study because, if applied, they would only lead to a small uniform shift in the abundance zero-points.

2.3. Results and discussion

Abundances of potassium in 47 Tuc were investigated by Carretta et al. (2013). The authors used three TO and nine SGB stars and obtained the average 1D NLTE element-to-iron abundance ratios $\langle[\text{K/Fe}]\rangle_{\text{TO}}^{\text{1D NLTE}} = 0.19 \pm 0.07$ and $\langle[\text{K/Fe}]\rangle_{\text{SGB}}^{\text{1D NLTE}} = 0.12 \pm 0.12$, respectively (numbers after the ± sign are standard deviation due to star-to-star variation in the measured abundance ratios). These values are comparable with those obtained in this work using RGB stars, $\langle[\text{K/Fe}]\rangle^{\text{1D NLTE}} = 0.05 \pm 0.14$, although the star-to-star variation is slightly larger in our case. In case of Na and Mg, the average values obtained by us are $\langle[\text{Na/Fe}]\rangle^{\text{1D NLTE}} = 0.42 \pm 0.13$ and $\langle[\text{Mg/Fe}]\rangle^{\text{1D NLTE}} = 0.41 \pm 0.11$, respectively. Again, these values are comparable with those obtained in 1D NLTE by Carretta et al. (2009b), $\langle[\text{Na/Fe}]\rangle^{\text{1D NLTE}} = 0.53 \pm 0.15$ and $\langle[\text{Mg/Fe}]\rangle^{\text{1D NLTE}} = 0.52 \pm 0.03$ though scatter in the case of Mg is significantly larger in our case (also see below).

Recently, Mucciarelli et al. (2017) measured 1D NLTE abundance of K in 144 RGB stars and obtained the average element-to-iron abundance ratio $\langle[\text{K/Fe}]\rangle_{\text{RGB}} = -0.12 \pm 0.01$. This value is 0.17 dex lower than the one obtained in our study. Nevertheless, this difference between the two abundance estimates and can be explained by differences in the analysis techniques, for example, different approaches for evaluating microturbulence velocities in the two studies. It is important to stress, however, Mucciarelli et al. (2017) find no intrinsic spread of potassium abundance in 47 Tuc, just as we found in our study (see below).

The 1D NLTE element-to-iron abundance ratios obtained in our study are plotted in Fig. 2.4 (abundance ratios shown in this plot were computed using a fixed value of $[\text{Fe/H}]^{\text{1D LTE}} = -0.76 \pm 0.03$, see Sect. 2.2.3). There is a significant star-to-star variation

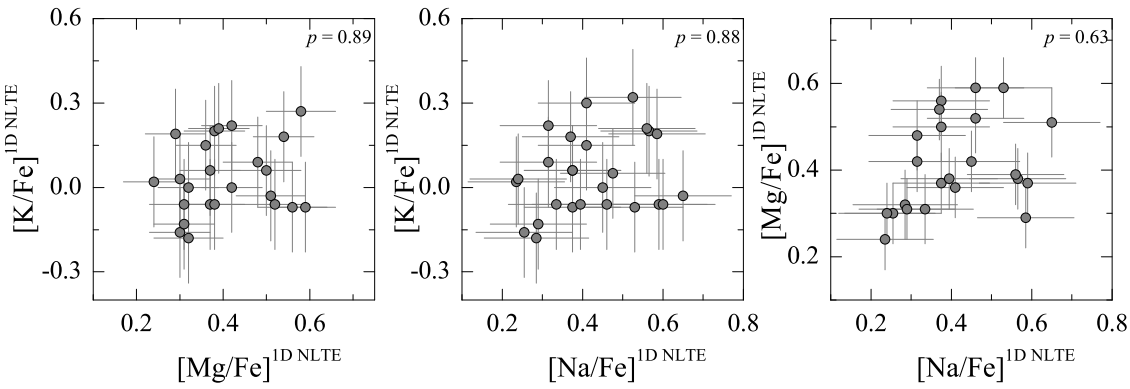

Figure 2.4. [Na/Fe], [Mg/Fe], and [K/Fe] abundance ratios determined in the sample of RGB stars and shown in various abundance-abundance planes. Student's *t*-test probability *p*-values are marked in the corresponding panels.

in the case of all three elements. Obviously, it is very important to understand whether this variation could be cause by the intrinsic spread in elemental abundances. To answer this question, we used the maximum-likelihood (ML) technique identical to the one applied by Mucciarelli et al. (2012, 2015) to study K abundance spreads in NGC 2419 and NGC 2808 (see Sect. 1.7.2 for details). The results of the ML test suggest that there may exist small intrinsic abundance spreads in the case of Na and Mg, 0.04 ± 0.05 dex and 0.08 ± 0.02 dex, respectively (Table 2.5). However, in the case of Mg the abundance determination errors may be larger than those provided in Table 2.5 (see Sect. 1.7.1). This may be also indirectly supported by the larger total star-to-star RMS abundance variation seen in our sample, for example, in comparison to that determined in other studies (e.g., Carretta et al. 2009b). Therefore, the existence of intrinsic abundance spread in the case of Mg still needs to be confirmed. However, we detected no intrinsic spread in the abundance of K, $\sigma^{\rm int}([{\rm K/Fe}]) = 0.00 \pm 0.03$.

We find no statistically significant correlations between [Na/Fe], [Mg/Fe], and [K/Fe] abundance ratios (Fig. 2.4). For this, we verified whether or not the null hypothesis (i.e., that the slope in the given *x*-*y* plane is zero) can be rejected based on the two-tailed probability *p* that was determined from our data using Student's *t*-test (with smaller *p* meaning higher evidence against the null hypothesis). In all planes the obtained *p* values indicate that the rejection of the null hypothesis is unwarranted. Similarly, no statistically significant relations were found between either the various abundance ratios in a given star and its distance from the cluster center (Fig. 2.5). In the case of the [Na/Fe] ratio, non-detection agrees with our earlier result obtained using 110 TO stars in 47 Tuc where no correlation between Na abundance and distance from the cluster center was found (cf. Kučinskas et al. 2014).

Following Kučinskas et al. (2014), we also computed absolute radial velocities of the target RGB stars, $|\Delta v_{\rm r}| \equiv \left| v_{\rm rad} - \langle v_{\rm rad} \rangle^{\rm clust} \right|$, where $v_{\rm rad}$ is radial velocity of the individual

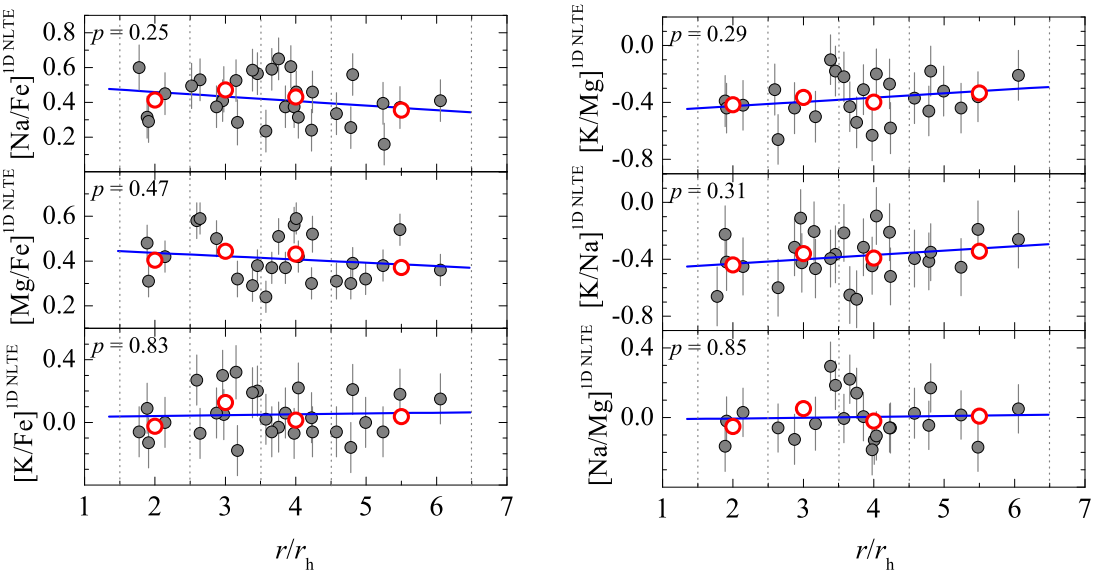

Figure 2.5. [Na/Fe], [Mg/Fe], and [K/Fe] abundance ratios determined in the sample of 27 RGB stars in 47 Tuc and plotted versus the projected radial distance of individual stars (small filled symbols). Large red open circles are averages obtained in non-overlapping $\Delta r/r_h = 1$ bins.

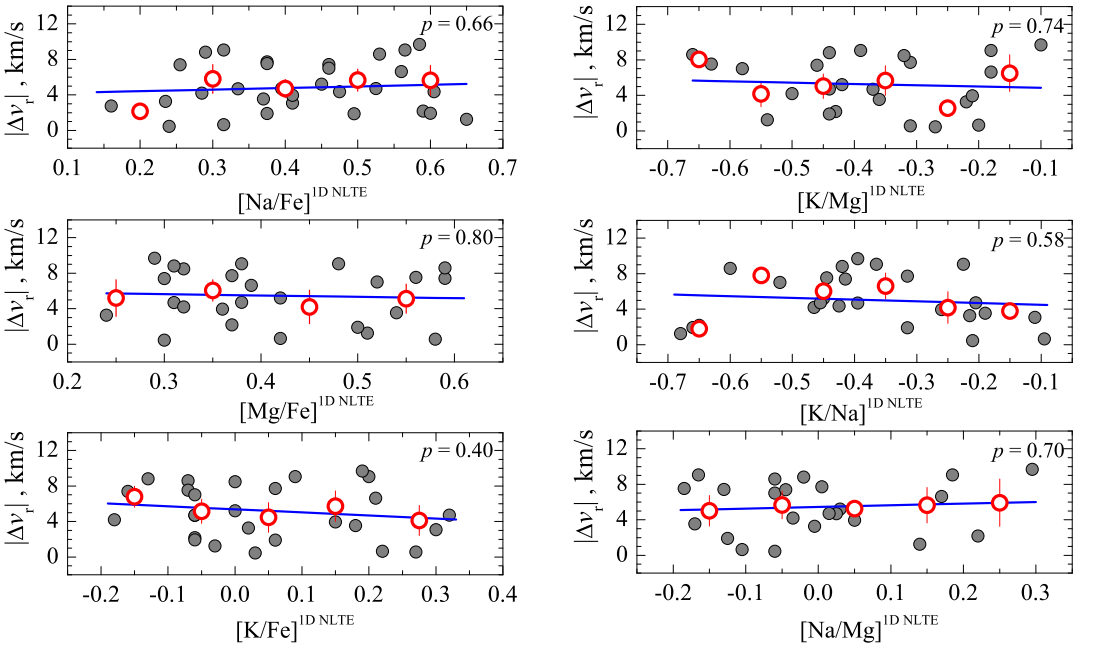

Figure 2.6. Absolute radial velocities determined for the sample of RGB stars in 47 Tuc and plotted versus [Na/Fe], [Mg/Fe], and [K/Fe] abundance ratios of individual stars.

star and $\langle v_{\rm rad}\rangle^{\rm clust} = -18.6$ km/s is the mean radial velocity of the RGB star sample used in this study. The obtained absolute radial velocities of individual stars are plotted versus abundance ratios in Fig. 2.6 (in this figure we also show the average absolute velocities which were computed in 0.1 dex-wide bins). No statistically significant relation have been found in this case, too.

Table 2.5. Results of the maximum-likelihood (ML) testing of the intrinsic spread in the abundances of Na, Mg, and K.

Element	$\langle[X_i/Fe]\rangle$	$\sigma[X_i/Fe]$	$\sigma^{int}([X_i/Fe])$
X_i	dex	dex	dex
Na	0.49 ± 0.02	0.13	0.04 ± 0.05
Mg	0.48 ± 0.02	0.11	0.08 ± 0.02
K	0.10 ± 0.03	0.14	0.00 ± 0.05

Taken together, these results suggest that RGB stars belonging to different stellar generations in 47 Tuc (as indicated, e.g., by their Na abundance) do not show statistically significant differences in the abundances of Mg and/or K. Similarly, it seems that stars in different stellar generations do not differ in their mean absolute radial velocities, too. The latter finding contradicts our results obtained using 110 TO stars in 47 Tuc which suggested that kinematical properties of stars in primordial (1G) and extreme generations (3G) may be different (Kučinskas et al. 2014). In this context, it is important to stress that the sample of RGB stars used in this Thesis is kinematically cooler than that of TO stars used in (Kučinskas et al. 2014). For example, the fraction of stars with $|\Delta v_r| \leq 8.0$ km/s is larger in our sample than that in the sample of TO stars, $\approx 83\%$ versus $\approx 70\%$, respectively. Also, in our sample there are no stars with $|\Delta v_r| > 10.0$ km/s while the fraction of such objects in the TO sample is $\approx 18\%$. Therefore, it is possible that the disagreement may be due to the fact that in our RGB star sample we lack some of primordial generation stars with largest absolute velocities.

3 Abundances of Mg and K in the atmospheres of TO stars in 47 Tuc

In this Chapter we study the abundances of Mg and K in the atmospheres of 53 (Mg) and 75 (K) TO stars of the Galactic globular cluster 47 Tuc. The obtained abundances, together with those of Li, O, and Na that were determined earlier in the same sample of stars, were used to search for possible relations between the abundances of K and those of light elements. We also studied the possible connections between the elemental abundances in TO stars and kinematical properties of the host stars. Elemental abundances were determined using archival high-resolution VLT FLAMES/GIRAFFE spectra and 1D NLTE abundance analysis techniques. Synthetic spectral line profiles were calculated with the MULTI package (see Sect. 1.5.2 for details). As in the previous Chapter, to assess the influence of convection on the spectral line formation we used 3D hydrodynamical CO^{5}BOLD and 1D hydrostatic LHD model atmospheres for computing 3D–1D LTE abundance corrections for the spectral lines of Mg, and K. In what follows below we provide a short description of all steps involved in our analysis and discuss the obtained results.

3.1. Introduction

As it was already noted in Chapter 2 (Sect. 2.1), it is currently thought that the majority of the GGCs harbour stars that belong to several (multiple) generations. The first strong evidence in favor of this paradigm came from spectroscopic observations, which revealed a large star-to-star in the light element abundances within a given GGC (Kraft 1994; Gratton et al. 2004), and, then, various (anti-)correlations between the abundances of these elements (Carretta et al. 2009a; Pasquini et al. 2005; Shen et al. 2010; Bonifacio et al. 2007). Further evidence came from photometric observations which uncovered the existence of multiple subsequences in the cluster CMDs, that consisted of stars characterized by different light element abundances (Piotto et al. 2007; Milone et al. 2012).

Theoretical evolutionary scenarios of the GGCs that were proposed to explain these observational trends are that either massive AGB stars (e.g., Ventura et al. 2001) or fast-rotating massive stars (e.g., Decressin et al. 2007) enriched the second-generation stars in elements such as Na, Al, and depleted them in, for example, O and Mg. Other scenarios, such as enrichment by binary stars (de Mink et al. 2009) and early disc accretion (Bastian et al. 2013) have been discussed, too. However, as it was already discussed

in the previous Chapter, none of them is capable of explaining all observational facts simultaneously (see discussion in, e.g., Bastian et al. 2015).

Potentially, new clues may possibly come from the investigations of K abundance. Since K is synthesized mainly in high-mass stars, it is unlikely that the atmospheric K abundance would undergo any appreciable changes during the course of the stellar evolution of the low-mass stars in the GGCs. In their recent study Mucciarelli et al. (2017) argued the detection of statistically significant correlations K–Na, K–O anticorrelations in several GGCs, including 47 Tuc. To explain these finding, they suggested a self-enrichment model proposed by D'Ercole et al. (2012). In this scenario, Mg-poor/K-rich (extreme population) stars must have formed from the ejecta of AGB and super-AGB stars. However, this scenario still requires some fine tuning in the nuclear reaction cross-sections and burning temperatures to explain the observed trends satisfactorily.

It is interesting to note that the findings of Mucciarelli et al. (2017) are in contrast of our recent study of Na, Mg, and K abundances in the RGB stars in 47 Tuc. Our results have revealed no statistically significant between the abundance of K and those of light elements, as well as between the abundance of K and kinematical properties of RGB stars (Černiauskas et al. 2017, see Sect. 2.3 for details). It is conceivable, however, that non-detection in our case could be due to a smaller sample of RGB stars studied, 32 in our work versus 144 in the study of Mucciarelli et al. (2017).

As far as studies of K abundance in TO stars in 47 Tuc are concerned, the only investigation performed so far was the one of Carretta et al. (2013) who determined K abundances in 3 TO stars. Obviously, the size of their stellar sample was too small to study any possible relations between the abundances of K and those of other elements.

Given this somewhat ambiguous situation, investigation of K abundances in the atmospheres of TO stars in 47 Tuc could be very desirable, especially if based on a larger sample of stars than that used by Carretta et al. (2013). It is well know that the cores of unevolved low-mass stars do not reach temperatures high enough for Ne – Na and/or Mg – Al cycles to operate. Moreover, their convective envelopes are not sufficiently deep so that the products of proton-proton cycles could be brought to the stellar surface. Therefore, chemical composition of TO star atmospheres should be identical to that of the primordial cloud from which the GGC have formed - unless their atmospheres have been contaminated by accreted chemical elements synthesized in other stars.In this part of the Thesis we therefore determine abundances of Mg and K in the atmospheres of TO stars in 47 Tuc, and then use this information to study the possible relations between the abundances of Mg and K, and those of other light elements.

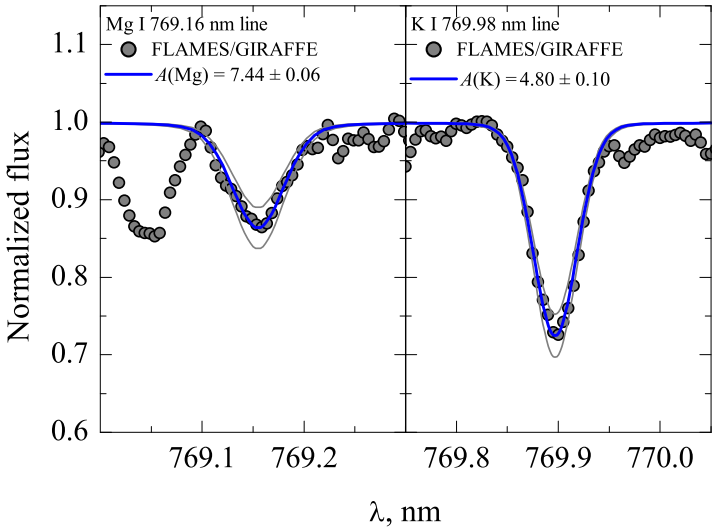

Figure 3.1. Observed (gray dots) and best-fitted theoretical profiles (blue lines) of the K I and Mg I lines used in this study, in the spectra of the target TO star 47Tuc−45982 ($T_{\rm eff}$ = 5707 K, $\log g$ = 4.00). We also provide the abundances determined from each observed line, A(X), together with their errors.

3.2. Methodology

Abundances of Mg and K were determined using 1D hydrostatic ATLAS9 model atmospheres and 1D NLTE abundance analysis methodology. In addition, we also used 3D hydrodynamical CO^{5}BOLD and 1D hydrostatic LHD model atmospheres for assessing the influence of convection on the formation of Mg I and K I lines used in our study. A brief description of all steps involved in the abundance analysis is provided below.

3.2.1. Spectroscopic data

In this study we used the same sample of TO stars of 47 Tuc as in Dobrovolskas et al. (2014). It is important to note that in the latter study abundances of Mg and K in these TO stars were not determined. A detailed description of the data acquisition and reduction procedures is provided in Sect. 1.1.2.

3.2.2. Determination of 1D NLTE abundances of Mg and K

In our analysis several types of model atmospheres were used:

– ATLAS9: for the atmospheric parameters of each individual sample star we computed a 1D hydrostatic model atmosphere using the ATLAS9 code (see Sect. 1.4.1). These model atmospheres were used in the 1D NLTE abundance analysis of Mg and K, i.e., for synthesizing their spectral line profiles with the MULTI code (see Sect. 1.5.2);

Table 3.1. Parameters of the 3D hydrodynamical CO^{5}BOLD model atmospheres used in our study.

$T_{\rm eff}$, K	$\log g$	[M/H]	Grid dimension, Mm x × y × z	Grid resolution x × y × z
5470	4.0	0.0	20.3 × 20.3 × 10.6	140 × 140 × 150
5530	4.0	-1.0	19.9 × 19.9 × 10.6	140 × 140 × 150
5930	4.0	0.0	25.8 × 25.8 × 12.5	140 × 140 × 150
5850	4.0	-1.0	25.8 × 25.8 × 12.5	140 × 140 × 150

– LHD: these 1D hydrostatic models were computed using the LHD model atmospheres code (see Sect. 1.4.2) which utilizes chemical composition, equation of state, and opacities identical to those used with the 3D hydrodynamical CO^{5}BOLD model atmospheres (see below). In order to compute the 3D–1D abundance corrections for Mg and K (Sect. 3.2.4), atmospheric parameters of the LHD models were selected to match those to those of the CO^{5}BOLD model atmospheres (Table 3.1);

– CO^{5}BOLD: Similarly to what was done in Dobrovolskas et al. (2014), we used four 3D hydrodynamical model atmospheres CO^{5}BOLD (see Sect. 1.4.3) from the CIFIST grid (Ludwig et al. 2009). These models were utilized for computing the 3D–1D abundance corrections. Their atmospheric parameters are provided in Table 3.1.

The 1D NLTE abundances of Mg and K were determined using the MULTI code (Sect.1.5.2). Atomic parameters of the spectral lines that were used in our study were taken from the VALD-3 atomic database (Piskunov et al. 1995; Kupka et al. 2011) and are provided in Table 3.2. For K I line, $\log gf$ value was taken from Morton (1991). We stress that in the case of K, the NLTE approach in the abundance analysis is critical since for this element 1D NLTE–LTE abundance corrections in TO stars are typically very large and range from −0.5 to −0.7 dex (Takeda et al. 2002). Besides, the corrections tend to become larger at lower effective temperatures and increase with decreasing metallicity (Andrievsky et al. 2010).

Abundances of each element were determined by fitting theoretical line profiles to those observed in the spectrum of a given TO star. A typical example of the obtained best fits are shown in Fig. 3.1. A fixed value of $[{\rm Fe/H}]^{\rm 1D\ LTE} = -0.76 \pm 0.03$ taken from Carretta et al. (2009a) was used throughout this study. The model atoms of Mg and K that were used in our study are briefly described in Sect. 1.5.2 (see also references therein).

Before the determination of Mg and K abundances, Mg I and K I lines in the spectra of all stars studied were carefully inspected for blends and/or possible contamination

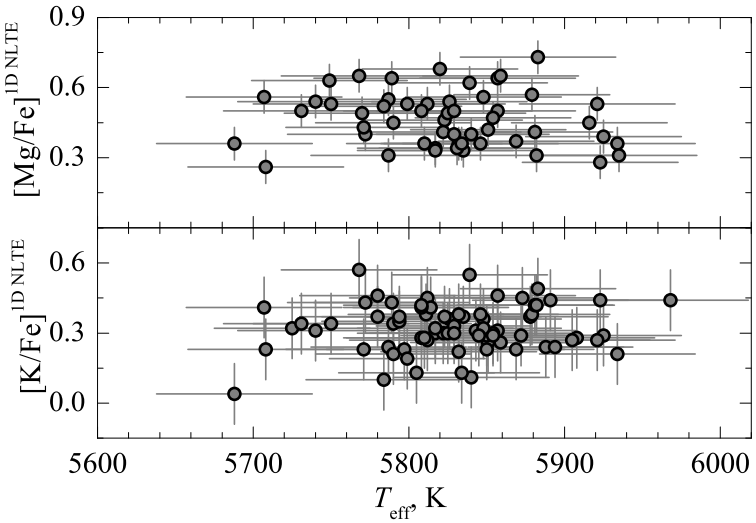

Figure 3.2. [Mg/Fe] (top) and [K/Fe] (bottom) abundance ratios determined in the sample of TO stars in 47 Tuc and plotted versus the effective temperature of individual stars. Error bars show uncertainties that were computed as described in Sect.3.2.3.

by telluric lines (we had only one spectral line per element available for the abundance determination in the spectrum of each TO star). This inspection revealed significant star-to-star variation in terms of the line quality. It is for this reason why both Mg and K could not be determined in all the stars, because for some stars only one of the two lines was suitable for abundance determination.

To verify that the spectral lines used in our study were not seriously affected by telluric lines, such as telluric A band in the vicinity of the K I 769.89 nm line, we used (a) telluric lines identified in the spectrum of fast-rotating O6.5 III spectral type star HD94963 which was taken from the UVES POP spectral library (Bagnulo et al. 2003); and (b) a synthetic spectrum of the atmospheric transmission computed with the TAPAS tool (Bertaux et al. 2014) for the dates when the observations were done. This analysis has revealed that Mg I and K I lines were not seriously contaminated with telluric lines.

The 1D NLTE abundances of Mg and K were then determined by fitting synthetic spectral line profiles to those observed in the spectra of TO stars. We verified that the determined abundances show no dependence on the effective temperature (Fig. 3.2).

Because reliable determination of Fe abundances for individual TO stars was not possible, mainly due to poor quality of Fe I lines available in the VLT FLAMES/GIRAFFE spectra, for computing element-to-iron abundance ratios we used a fixed value of iron abundance $[\mathrm{Fe/H}]^{\mathrm{1D\ LTE}} = -0.76 \pm 0.03$ taken from Carretta et al. (2009a). Judging from the literature data, the star-to-star spread of iron abundance in 47 Tuc is very small and well within the errors of individual Fe abundance measurements. Such minor star-to-star differences in [Fe/H] ratio should not have any detectable influence on the possible relations between the light element abundances.

Table 3.2. Atomic parameters of the spectral lines used in the abundance determinations of Mg and K. Natural ($\gamma_{\rm rad}$), Stark ($\frac{\gamma_4}{N_{\rm e}}$), and van der Waals ($\frac{\gamma_6}{N_{\rm H}}$) broadening constants computed using classical prescription are provided in the last three columns.

Element	λ, nm	χ, eV	loggf	log$\gamma_{\rm rad}$	log$\frac{\gamma_4}{N_{\rm e}}$	log$\frac{\gamma_6}{N_{\rm H}}$
Mg I	769.16	5.753	−0.78	7.57	−3.25	−6.83
K I	769.89	0.000	−0.17	7.56	−5.44	−7.45

For the solar values of Mg and K abundances, we used $A({\rm Mg})_{\odot}^{\rm 1D\ NLTE} = 7.64 \pm 0.05$ and $A({\rm K})_{\odot}^{\rm 1D\ NLTE} = 5.10 \pm 0.07$ determined in this work (see Sect. 1.8). The 1D NLTE abundance ratios of [Li/Fe], [O/Fe], and [Na/Fe] were taken from Dobrovolskas et al. (2014) where they were obtained using the same [Fe/H] value as utilized in the present study (see Dobrovolskas et al. (2014) for details).

The determined average element-to-iron abundance ratios in the sample of TO stars are $\langle$[Mg/Fe]$\rangle^{\rm 1D\ NLTE} = 0.47 \pm 0.12$ (53 objects) and $\langle$[K/Fe]$\rangle^{\rm 1D\ NLTE} = 0.39 \pm 0.09$ (75 objects; numbers after the ± sign are standard deviation). In Fig.3.3 we show [K/Fe], [Mg/Fe], [Na/Fe], [O/Fe], and [Li/Fe] abundance ratios plotted in various abundance-abundance planes.

3.2.3. Uncertainties in the determined abundances of Li, O, Na, Mg, and K

Individual contributions arising from the different error sources to the total uncertainty in the determined abundances of O, Na, Mg, and K were estimated following the prescription provided in Sect.1.7.1. The determination of errors arising due to uncertainties in the atmospheric parameters ($T_{\rm eff}$ log$g$, $\xi_{\rm t}$) is described in Sect.1.3. The error in continuum determination was estimated in the same way as it was done in Sect. 2.2.3, i.e., by measuring the dispersion at the continuum level in the spectral regions expected to be free of spectral lines, both of stellar and telluric origin. The continuum was then shifted by the amount of this uncertainty to obtain the resulting error in the determined abundance. To estimate the errors in the line profile fitting, we computed RMS deviation between the observed and synthetic line profiles which were converted into the uncertainties in the line equivalent width, W, and, finally, the resulting errors in the determined abundances (see Sect.1.7.1 for details).

Individual errors were added in quadratures to obtain the total error in the determined abundances of O, Na, Mg, and K (col. 9 in Table 3.3). The obtained total errors were further used for analyzing possible intrinsic spreads in the obtained elemental abundances (Sect. 3.3). We stress that the obtained errors only provide a lower limit for the uncertainties in the determined abundances since they do not account for various systematic uncertainties that are unavoidable in the determination of stellar abundances.

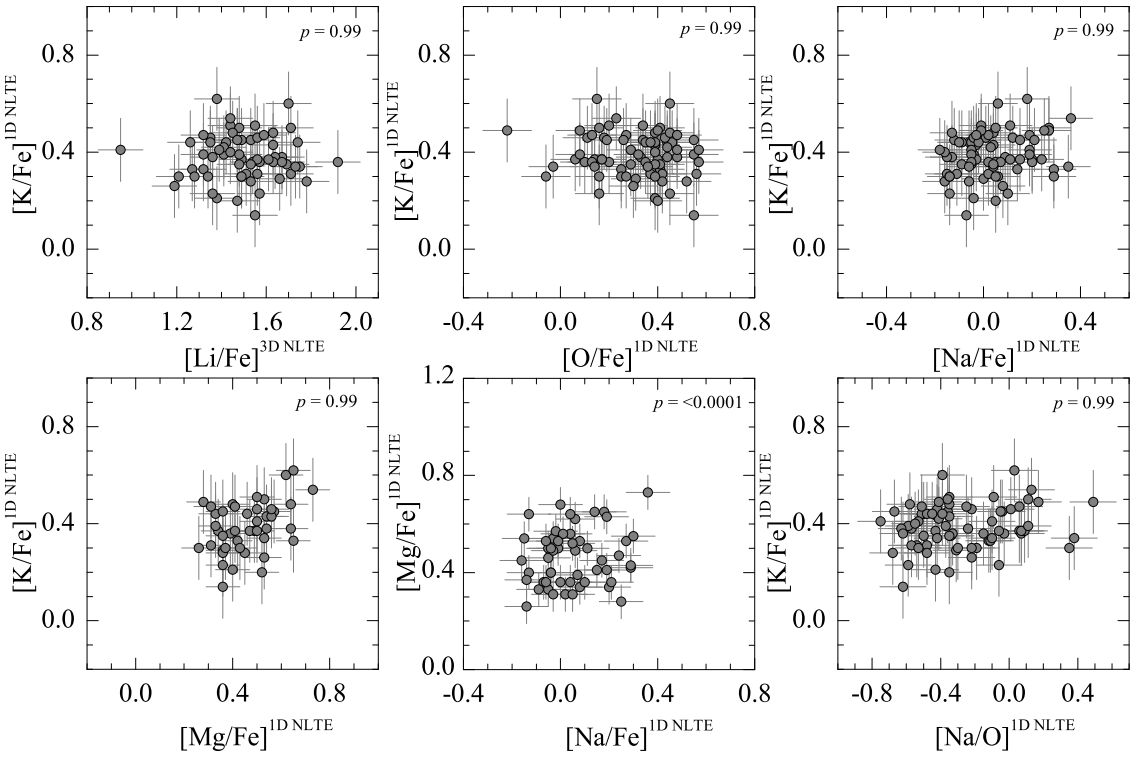

Figure 3.3. Element-to-iron abundance rations in the sample of TO stars. The two-tailed probability p-values are marked in the corresponding panels (see Sect. 3.3.2).

In case of Li, the procedure was similar except for the following two points:

– Li abundances in Dobrovolskas et al. (2014) were estimated by using the A(Li)-W interpolation formula from Sbordone et al. (2010) and W was determined by fitting synthetic line profiles. Therefore, we estimated the line profile fitting errors by measuring standard deviation between the observed and best-fit Gaussian profiles;

– an error in the determined Li abundance that arrises from the use of the interpolation formula was taken into account by using an estimated uncertainty of ±0.01 dex (Sbordone et al. 2010).

The determined uncertainties in Li abundance are provided in Table 3.3, together with those determined for other elements.

3.2.4. 3D–1D abundance corrections for Mg and K in TO stars

As in Sect.2.2.4, we used 3D hydrodynamical CO^{5}BOLD (Sect.1.4.3) and 1D hydrostatic LHD (Sect.1.4.2) model atmospheres to study the influence of convection on the formation of Mg I and K I in TO stars. The 3D–1D LTE abundance corrections for for the lines of O I and Na I were taken from Dobrovolskas et al. (2014).

The procedure used to compute the 3D–1D LTE abundance corrections, $\Delta_{\text{3D-1D LTE}}$, is described in Sect. 1.6. In case of each element they were computed for two values

Table 3.3. Errors in the determined abundance of Li, O, Na, Mg, and K. The sign ± or ∓ reflects the change in the elemental abundance which occurs due to the increase (top sign) or decrease (bottom sign) in the size of a given error source. For example, increase in the effective temperature leads to increasing abundance (±), while increasing $\xi_{\rm mic}$ results in decreasing abundance (∓).

Element	Line	$\sigma(T_{\rm eff})$	$\sigma(\log g)$	$\sigma(\xi_{\rm t})$	σ(cont)	σ(fit)	$\sigma(A)_{\rm tot}$
	λ, nm	dex	dex	dex	dex	dex	dex
Li I	670.80	±0.09	∓0.01	∓0.00	0.03	0.03	0.10
O I	777.19	±0.09	∓0.03	∓0.01	0.02	0.03	0.10
O I	777.53	±0.09	∓0.03	∓0.01	0.02	0.04	0.10
Na I	818.32	±0.06	∓0.02	∓0.03	0.02	0.03	0.08
Na I	819.48	±0.06	∓0.02	∓0.03	0.03	0.03	0.08
Mg I	769.16	±0.04	∓0.03	∓0.02	0.03	0.02	0.06
K I	769.89	±0.08	∓0.02	∓0.05	0.02	0.03	0.10

of line equivalent width, W (corresponding to "weak" and "strong" spectral lines) that bracketed the range measured in the observed spectra of the sample TO stars. Equivalent widths used for the weakest lines were 4 pm and 15 pm, while for the strongest lines we used 7 pm and 18 pm, in the case of Mg, and K, respectively. Microturbulence velocity in the 3D model atmosphere was determined by applying Method 1 described in Steffen et al. (2013) and was subsequently used in the spectral line synthesis with the LHD model atmospheres (see Sect.1.6 for details). The obtained 3D–1D LTE abundance corrections, $\Delta_{\rm 3D-1D\ LTE}$, are provided in Table 3.4. In all cases (i.e., both for the "weak" and "strong" spectral lines that bracket the values of line equivalent widths observed in the spectra of TO stars), they do not exceed 0.09 dex. This gives clear indication that the influence of convection on the formation of Mg I and K I lines in the atmospheres of TO stars is minor.

We note that the obtained abundance corrections were not used for obtaining 3D-corrected abundances which, in principle, could be done by adding the 3D–1D LTE corrections to the determined 1D NLTE abundances of Mg and K. Such a procedure was avoided for two reasons. First, abundances obtained in this way would be generally different from those that would be obtained using the full 3D NLTE approach (see, e.g., Klevas et al. 2016, for details). Second, the determined 3D–1D abundance corrections are small, therefore applying them would result in a small and nearly uniform shift of the abundances determined in all our sample stars. Nevertheless, our tests have shown that if these (small) 3D–1D abundance corrections are taken into account, our conclusions regarding the intrinsic abundance spreads and possible existence of different relations between, for example the abundance of K and those of other light elements, remain unaltered (see Sect. 3.3).

Table 3.4. The 3D–1D abundance corrections, $\Delta_{\text{3D−1D LTE}}$, computed for different strengths of Mg I and K I lines used in this work.

Element	λ_{central}	$\Delta_{\text{3D−1D LTE}}$, dex	
	nm	weak	strong
Mg I	769.16 nm	+0.04	+0.05
K I	769.89 nm	−0.09	−0.03

3.3. Results and discussion

3.3.1. Average abundances and intrinsic abundance spreads in 47 Tuc

As it was already mentioned earlier, the only studies of K abundance in 47 Tuc that have been carried out until now are those by Carretta et al. (2013) and Mucciarelli et al. (2017). The average 1D NLTE potassium-to-iron abundance ratios obtained by Carretta et al. (2013) in three TO and nine SGB stars were $\langle[\text{K/Fe}]\rangle_{\text{TO}} = 0.19 \pm 0.07$ and $\langle[\text{K/Fe}]\rangle_{\text{SGB}} = 0.12 \pm 0.12$, respectively (the error is standard deviation due to star-to-star abundance variation). These values are compatible with the average 1D NLTE abundance ratios obtained using RGB stars in Sect. 2.2.3, $\langle[\text{K/Fe}]\rangle_{\text{RGB}} = 0.05 \pm 0.13$. However, the average potassium-to-iron abundance ratio determined by us using TO stars, $\langle[\text{K/Fe}]\rangle_{\text{TO}} = 0.39 \pm 0.09$, is 0.2 dex higher than that obtained using three TO stars by Carretta et al. (2013). We found that two stars are common to both samples. For them, the average abundance ratios obtained by Carretta et al. (2013) and determined in our study are $\langle[\text{K/Fe}]\rangle_{\text{TO}} = 0.18$ and $\langle[\text{K/Fe}]\rangle_{\text{TO}} = 0.32$ (note that the 1D NLTE–LTE abundance corrections and microturbulence velocities used for these stars in the two studies are nearly identical). When corrected for the difference in iron abundance used by Carretta et al. (2013, [Fe/H] = −0.65) and us ($[\text{Fe/H}]^{\text{1D LTE}} = -0.76 \pm 0.03$), the two values become nearly identical, with our [K/Fe] ratio being only 0.03 dex higher. We therefore conclude that the difference in [K/Fe] ratios obtained in the TO samples by Carretta et al. (2013) and us is most likely due the different [Fe/H] values used to compute [K/Fe] ratios.

The sample-averaged K abundance obtained in the study of 144 RGB stars in 47 Tuc by Mucciarelli et al. (2017), $\langle[\text{K/Fe}]\rangle^{\text{1D NLTE}} = -0.12 \pm 0.08$, is somewhat lower than that determined in Sect. 2.2.3, $\langle[\text{K/Fe}]\rangle_{\text{RGB}} = 0.05 \pm 0.13$. This difference may be caused by the different microturbulent velocities used in the two studies: the sample-averaged value in Mucciarelli et al. (2017) is $\xi_{\text{t}} = 1.66$ km/s while in our analysis we used 1.5 km/s. Our tests show that this difference in ξ_{t} would lead to an ~ 0.13 dex decrease in the average [K/Fe] ratio determined in Sect. 2.2.3 using RGB stars. With this taken into account, abundances obtained in the two studies would become very similar.

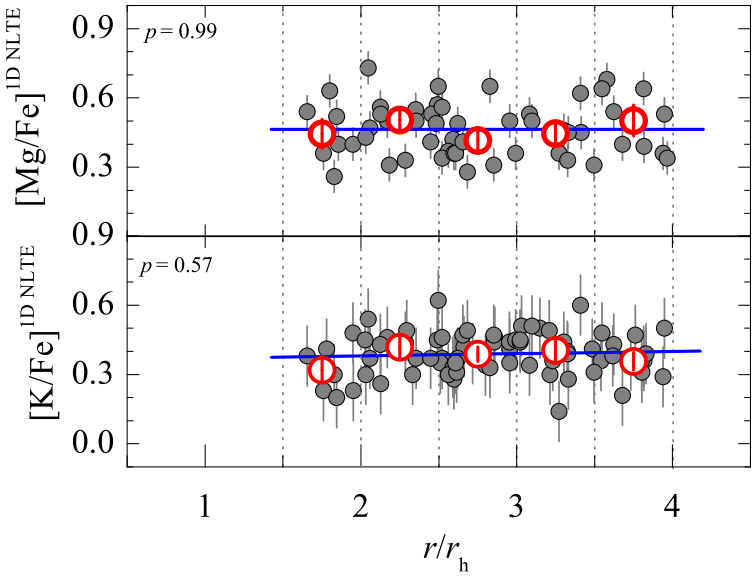

Figure 3.4. [Mg/Fe] (top) and [K/Fe] (bottom) abundance ratios determined in the sample of TO stars in 47 Tuc and plotted versus the projected radial distance of individual stars (small filled symbols). Large red open circles are averages obtained in non-overlapping $\Delta r/r_h = 1$ bins.

The origin of the significant difference between the average [K/Fe] ratios obtained by us in the TO and RGB stars, 0.34 dex, is not entirely clear, however. One possibility is that the value of microturbulent velocity used in our analysis of TO stars was in fact too low. We checked this using the six TO stars mentioned in Sect. 1.7.1 where we determined their iron abundances and microturbulence velocities using individual Fe I lines. The average microturbulence velocity obtained in this way was $\xi_t = 1.22 \pm 0.07$ km/s. This value is significantly higher than the one used in the present study, 1.0 km/s. With the higher value of ξ_t, the average abundance obtained in our sample of TO stars would become ≈ 0.1 dex lower. Still, this would still leave a difference of ≈ 0.25 dex between the values obtained using TO and RGB stars. On the other hand, it is also possible that the microturbulence velocity used in our analysis of RGB stars, 1.5 km/s, was slightly too low. For example, the $\xi_t - \log g$ calibration of Kirby et al. (2009) utilized by Mucciarelli et al. (2017) predicts the average microturbulence velocity of 1.66 km/s for our RGB stars. Unfortunately, we could not obtain a reliable constraint on ξ_t in our RGB stars using spectroscopic means, due to an insufficient number of iron lines available in their spectra (see Černiauskas et al. 2017). In any case, the increase in ξ_t in both TO and RGB star samples would reduce the average abundance but the difference between two samples would remain almost the same.

These differences notwithstanding, it is important to stress that analysis of the six TO stars mentioned above revealed that star-to-star scatter in the determined microturbulence velocities was $\approx \pm 0.07$ km/s. In terms of the determined K abundances, this would lead to a scatter of ≈ 0.03 dex. Such star-to-star variation should have no detectable ef-

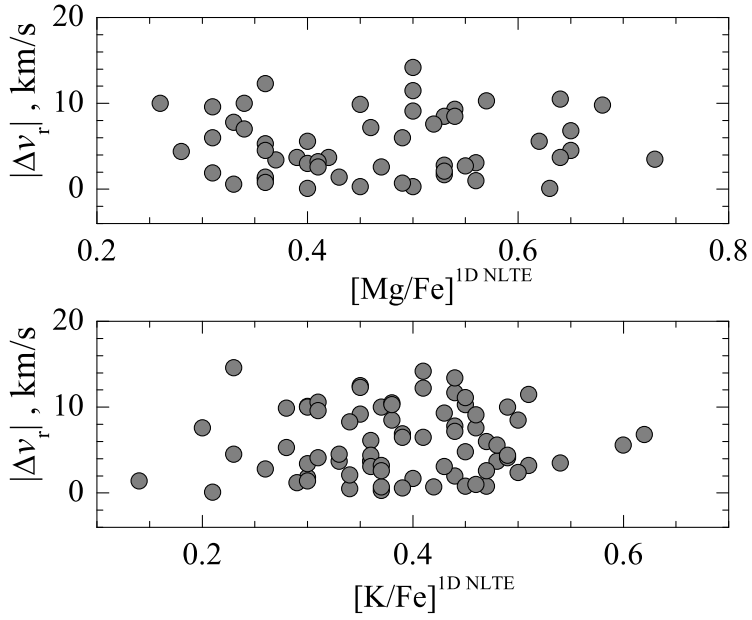

Figure 3.5. Absolute radial velocities determined for the sample of TO stars in 47 Tuc and plotted versus [Mg/Fe] (top) and [K/Fe] (bottom) ratios of individual stars.

fect on the possible relations between the light element abundances. Therefore, our conclusions obtained in Sect. 3.3.2 below should remain unaffected.

The intrinsic abundance spreads of Li, O, Na, Mg, and K determined in our analysis are provided in Table 3.5. In the case of K, we find zero intrinsic spread, $\sigma^{\rm int}$([K/Fe]) = 0.00 ± 0.03, identical to what was determined in Sect. 2.3 using RGB stars, $\sigma^{\rm int}$([K/Fe]) = 0.00 ± 0.05, and obtained by Mucciarelli et al. (2017), $\sigma^{\rm int}$([K/Fe]) = 0.00 ± 0.02. While the intrinsic spread of [Mg/Fe] in TO stars is similar to that determined by us in RGB stars, $\sigma^{\rm int}$([Mg/Fe]) = 0.08 ± 0.02 (Sect. 2.3), in the present work we obtain considerably larger intrinsic spread in [Na/Fe], $\sigma^{\rm int}$([Na/Fe]) = 0.12 ± 0.01 (TO) versus $\sigma^{\rm int}$([Na/Fe]) = 0.04 ± 0.05 (RGB, Sect. 2.3). The latter difference may be due to the lower quality of the RGB spectra which led to larger abundance errors obtained using RGB stars and, thus, smaller intrinsic abundance spread. An intrinsic scatter of similar size was obtained in the case of Li and O for TO stars, $\sigma^{\rm int}$([Li/Fe]) = 0.14 ± 0.02 and $\sigma^{\rm int}$([O/Fe]) = 0.10 ± 0.02.

3.3.2. Relations between the abundances of light elements and evolutionary properties of TO stars in 47 Tuc

As in our study of RGB stars the results of which are summarized in Sect. 2.3, in case of TO we also used Student's *t*-test to study the existence of possible relations between elemental abundances, as well as relations between the abundances and kinematical properties of the cluster stars. For this, using each $x - y$ dataset shown in the panels of Fig. 3.3, we computed the two-tailed probability, p, that the t-value in the given dataset

Table 3.5. Results of the ML determination of the intrinsic spread in the abundances of Li, O, Na, Mg, and K.

Element, $X_{\rm i}$	$\langle[X_{\rm i}/{\rm Fe}]\rangle$	$\sigma^{[X_{\rm i}/{\rm Fe}]}$	$\sigma^{\rm int}([X_{\rm i}/{\rm Fe}])$
	dex	dex	dex
Li	1.49 ± 0.02	0.18	0.15 ± 0.02
O	0.33 ± 0.01	0.16	0.12 ± 0.01
Na	0.03 ± 0.01	0.14	0.12 ± 0.01
Mg	0.47 ± 0.02	0.12	0.10 ± 0.01
K	0.39 ± 0.01	0.09	0.00 ± 0.03

could be equal or higher than its attained value when there is no correlation in the given $x - y$ plane. In all cases Pearson's correlation coefficients were computed by taking errors on both x and y axes into account.

Our results suggest that there is no statistically significant relations in the [K/Fe]–[O/Fe] and [K/Fe]–[Na/Fe] planes. Similarly, we find no evidence for statistically significant relations in the [K/Fe]–[Li/Fe], [K/Fe]–[O/Fe], [K/Fe]–[Mg/Fe], and [K/Fe]–[Na/O] planes. Only in the [Mg/Fe]–[Na/Fe] plane $p < 0.0001$, which may suggest that the null hypothesis can be formally rejected on a high significance level (see below, however)[1].

In Fig. 3.4 we show the determined [Mg/Fe] and [K/Fe] abundance ratios plotted versus the normalized distance from the cluster center, $r/r_{\rm h}$ (r is the projected distance from the cluster center and $r_{\rm h}$ is the half-light radius of 47 Tuc taken from Trager et al. 1993, $r_{\rm h} = 174''$). In both planes we detect no statistically significant relations between the two abundance ratios and the projected distance from the cluster center.

Following Kučinskas et al. (2014) and analysis presented in Sect. 2.3, we also investigated whether there are any significant relations between the kinematical properties of TO stars and the abundances of Mg and K in their atmospheres. For this we used absolute radial velocities of TO stars computed in Kučinskas et al. (2014), $|\Delta v_{\rm r}| \equiv \left|v_{\rm rad} - \langle v_{\rm rad}\rangle^{\rm clust}\right|$, where $v_{\rm rad}$ is the radial velocity of the individual star and $\langle v_{\rm rad}\rangle^{\rm clust} = -18.6\,{\rm km/s}$ is the mean radial velocity of the sample (Fig. 3.4). No statistically significant relations were found in this case either.

These findings support our earlier results obtained in the analysis of Na, Mg and K in 32 RGB stars obtained in Sect. 2.2.3, where we found no statistically significant relations in the abundance-abundance, abundance-distance or abundance-absolute radial velocity planes. In two planes, [K/Fe]–[Mg/Fe] and [K/Fe]–[Na/Fe], the obtained p-values are

[1]To test whether adding 3D–1D abundance corrections may change our conclusions regarding the possible relations in different abundance-abundance planes, we also computed Student's t-values using 3D+NLTE abundances instead of those determined in 1D NLTE. In all planes involving different abundance ratios the obtained p-values were only slightly different from those determined earlier, thereby confirming the findings obtained in the 1D NLTE case.

sufficiently small to indicate the possible existence of weak correlations. In the [K/Fe]–[Mg/Fe plane, however, the result may be rather strongly influenced by the three stars for which we determined the highest K abundances (for one of them K abundance and for two of them Na abundances were poorly determined as they were obtained from lines). Therefore, despite the relatively small p-values obtained in this plane using all data, we cannot reject with certainty the possibility that these small values are in fact a spurious result. In the [Mg/Fe]–[Na/Fe] plane, our results indicate that the very small p-value obtained by us in the analysis when errors on both the x and y axes were taken into account was spurious. Therefore, we conclude that also in this case the null hypothesis cannot be rejected. Finally, no statistically significant relations were detected between abundances (see Fig. 3.4-3.5).

The possible existence of the weak correlation in the [K/Fe]–[Na/Fe] plane may be seen as being compatible with the result obtained by Mucciarelli et al. (2017) who detected a correlation in the [K/Fe]–[Na/Fe] plane with Spearman's $p = 0.017$. Although our Pearson's p-values are larger than those computed by Mucciarelli et al. (2017), the difference at least in part may be due to different sample sizes used in the two studies. Nevertheless, the null hypothesis, i.e., that there is no correlation between the two abundance ratios, cannot be rejected with confidence based alone on the p-values obtained in our Pearson's test.

4 Abundance of Zn in the atmospheres of RGB stars in 47 Tuc

In this Chapter we investigated possible relations between the abundance of Zn and those of Na, Mg, and K in the atmospheres of RGB stars of the GGC 47 Tuc (with the abundances of the latter three elements determined in Chapter 2 of this Thesis). We used this new data to study the connections between the chemical composition and kinematical properties of the cluster stars. For this, we determined abundance of Zn in 27 RGB stars using 2dF/HERMES spectra obtained with the AAT (see Sect.1.1.1). While abundances of all other elements studied in this Thesis so far were obtained using 1D NLTE techniques, in the case of Zn we used standard 1D LTE methodology: synthetic spectra were computed with the SYNTHE code and 1D ATLAS9 model atmospheres. The main reason for this was that 1D NLTE–LTE abundance corrections for Zn I lines are small (< 0.1). Hence, ignoring NLTE effects in the abundance analysis should not affect the results and conclusions obtained in this Chapter.

4.1. Introduction

Observational and theoretical studies of Zn in the Galaxy have shown that Zn can be considered as a transition element between the iron-peak and *s*-process species, and it can be produced via a variety of channels. This includes explosive nucleosynthesis in type Ia and II supernovae, main component of the *s*-process in the intermediate-mass AGB stars and weak *s*-process component in M≥ 10 $M_{\odot}$ stars (see, e.g. Sneden et al. 1991; Matteucci et al. 1993; Mishenina et al. 2002; Kobayashi et al. 2006). Observational studies of Zn in different Galactic populations have revealed that Zn in the halo stars may reach [Zn/Fe]≈ +0.5 (at [Fe/H] < −3.0 Cayrel et al. 2004), while in the thin and thick disk stars the [Zn/Fe] ratio decreases with increasing metallicity and becomes lower than solar at [Fe/H] ≈ 0.0 (see, e.g. Duffau et al. 2017). In the solar neighborhood stars, the low and high α-element abundances seem to trace correspondingly low and high [Zn/Fe] ratios. Duffau et al. (2017) have shown that stars located at galactocentric distances < 7 kpc seem be to be depleted in Zn, down to [Zn/Fe] ≈ −0.3, which agrees with the [Zn/Fe] ratios determined in the Galactic bulge stars (Barbuy et al. 2015; da Silveira et al. 2018). All this observational evidence seems to suggest a related origin of Zn and α-elements (e.g. da Silveira et al. 2018). However, explanation the observed [Zn/Fe] trends at low metallicities may require Zn production in high-energy core-collapse supernovae or hypernovae (Kobayashi et al. 2006).

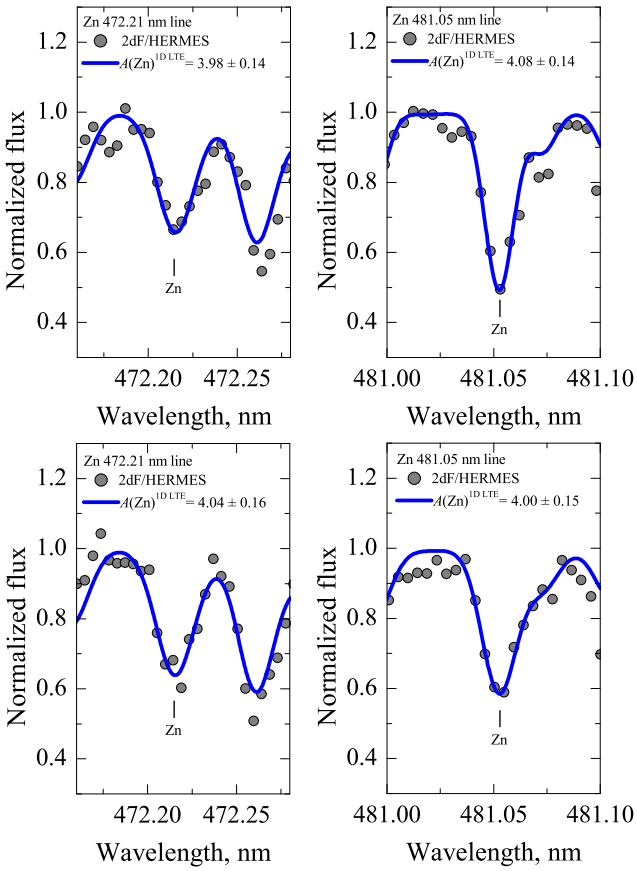

Figure 4.1. Observed (gray dots) and best-fitted theoretical profiles (blue lines) of the two Zn I lines used in this study, in the spectra of two RGB stars (top row: S1800, $T_{\rm eff}$ = 4510 K, $\log g$ = 1.90; bottom row: S167, $T_{\rm eff}$ = 4390 K, $\log g$ = 1.60). The Zn abundances, A(Zn), determined from each Zn I line are indicated in the corresponding panels.

In fact, Zn may be an interesting tracer also for studying chemical evolution of the GGCs. One of the proposed evolutionary scenarios of the GGCs implies that second-generation cluster stars could have been polluted with light chemical elements synthesized in AGB stars (Ventura et al. 2001). As it was mentioned above, Zn may be synthesized during the *s*-process in intermediate mass (3-6 $M_{\odot}$, e.g., Karakas et al. 2009). On the other hand, light chemical elements such as Na may be produced in AGB stars of slightly higher mass, 5-9 $M_{\odot}$ (D'Ercole et al. 2010; Ventura et al. 2012). Consequently, there may be a slight overlap in stellar masses (5-6 $M_{\odot}$) where both Zn and Na may be synthesized. Therefore, relations between the Zn abundance and those of light elements (e.g., O, Na) may point to AGB stars as possible polluters. In this context, 47 Tuc may be an interesting target because it shows: (a) relations between the abundances of light elements, e.g., Li, O, Na, Mg, and Al (Carretta et al. 2009a; D'Orazi et al. 2010; Dobrovolskas et al. 2014); and (b) relations between light element abundances and kinematical properties of cluster stars (see e.g. Kučinskas et al. 2014)

Table 4.1. Atomic parameters of Zn I lines used in this study. Broadening constants computed using classical prescription are provided in the last three columns (Natural ($\gamma_{\rm rad}$), Stark ($\frac{\gamma_4}{N_{\rm e}}$), and van der Waals ($\frac{\gamma_6}{N_{\rm H}}$, respectively).

Element	λ, nm	χ, eV	loggf	log$\gamma_{\rm rad}$	log$\frac{\gamma_4}{N_{\rm e}}$	log$\frac{\gamma_6}{N_{\rm H}}$
Zn I	472.21	4.02	−0.33	0.00	0.00	0.00
Zn I	481.05	4.07	−0.13	0.00	0.00	0.00

Let us also stress that available Zn abundance determinations in 47 Tuc are few. Moreover, such measurements were made using relatively small samples of stars. Thygesen et al. (2014), for example, investigated Zn abundances in 13 RGB stars in 47 Tuc and determined a median value of $[\mathrm{Zn/Fe}]^{\rm 1D\ LTE} = 0.26 \pm 0.13$. Duffau et al. (2017) have targeted 19 RGB stars and obtained the mean value of $\langle[\mathrm{Zn/Fe}]\rangle^{\rm 1D\ NLTE} = 0.17 \pm 0.10$. This is rather unfortunate because the two Zn I lines that are typically used for the abundance determinations (λ = 472.2 nm and 481.0 nm) are sufficiently strong in the RGB stars at the metallicity of 47 Tuc. Hence, RGB stars should be reliable tracers of Zn abundance in this and other GGCs.

Following these considerations, we aimed to determine Zn abundance in a larger sample of RGB in 47 Tuc. The main goal of this study was to search for possible relations between the abundance of Zn and those of light elements, as well as for relations between Zn abundance and kinematical properties of cluster RGB stars.

4.2. Methodology

The abundance of Zn was determined using standard 1D LTE abundance analysis methodology. A brief description of all steps involved in the abundance analysis is provided below.

4.2.1. Spectroscopic data and atmospheric parameters of the sample stars

To study Zn abundance, we used the same sample of RGB stars of 47 Tuc as utilized in Chapter 2, and the same high-resolution 2dF/HERMES spectra spectra acquired with the AAT. The reduction and continuum normalization procedures are described in detail in Chapter 1 (Sect. 1.1.1).

The target sample contained 27 RGB stars. Their effective temperatures were determined using photometric data from Bergbusch & Stetson (2009) and $T_{\rm eff} - (V - I)$ calibration of Ramírez & Meléndez (2005), while surface gravities were estimated using Eq. 1.1 (Sect. 1.3).

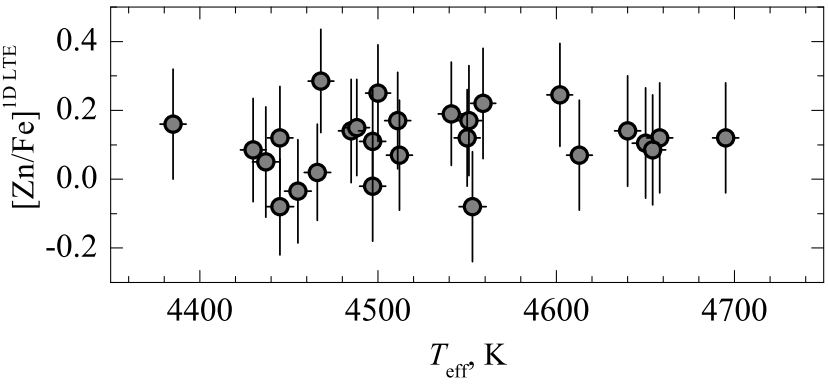

Figure 4.2. [Zn/Fe] abundance ratios determined in the sample of 27 RGB stars in 47 Tuc shown as a function of the effective temperature.

4.2.2. Determination of the 1D LTE Zn abundance

Abundances of Zn were measured using two Zn I lines at 472.21 nm and 481.05 nm. Their atomic parameters were taken from the VALD-3 database (Piskunov et al. 1995; Kupka et al. 2011) and are listed in Table 4.1. We checked that the two Zn I lines were not contaminated with blends, either of stellar or telluric origin.

Abundances of Zn were determined by fitting synthetic 1D LTE spectra to the observed Zn I line profiles. The former were computed with the SYNTHE package, using the 1D ATLAS9 model atmospheres (both the SYNTHE and ATLAS9 codes were utilized in the form of the Linux port by Sbordone et al. 2004 and Sbordone (2005)). Examples of the synthetic spectra fits are shown in Fig. 4.1. We used a fixed value of the microturbulence velocity, $\xi = 1.5$ km/s, while the macroturbulence velocity was determined as a free-fit parameter and had its values in the range of 1 to 6 km s^{-1}. The obtained abundances show no dependence on the effective temperature (Fig. 4.2).

For computing [Zn/Fe] abundance ratios, we used $A(\mathrm{Zn})_{\odot}^{\mathrm{1D\ LTE}} = 4.60 \pm 0.04$ determined in Sect. 1.8. To remind, this value was obtained using the same Zn I lines as used to determine abundances in the RGB stars (Table 4.1). We did not attempt to measure the iron abundance in the target RGB stars because, as it was already discussed in Sect. 1.3, the number of available Fe I lines was too small to warrant reliable abundance determination. Therefore, we used a single fixed value of $[\mathrm{Fe/H}]^{\mathrm{1D\ LTE}} = -0.76 \pm 0.03$ taken from Carretta et al. (2009a); see also discussion in Sect. 2.2.3).

The obtained Zn abundances were not corrected for NLTE effects. In fact, the only published 1D NLTE-LTE abundance corrections for the two Zn I lines are those computed by Takeda et al. (2005). However, the authors do not provide corrections at the effective temperatures and gravities of our sample stars. However, by extrapolating their data we estimate that corrections of the order of $\Delta_{\mathrm{1D\ NLTE-LTE}} \approx -0.05$ dex could be ex-

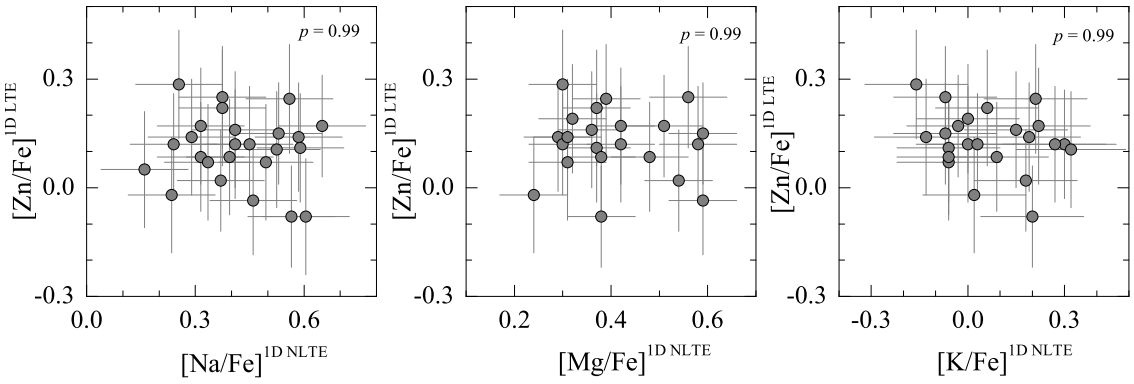

Figure 4.3. [Zn/Fe] abundance ratios determined in the sample of 27 RGB stars in 47 Tuc and plotted versus their [Na/Fe], [Mg/Fe], and [K/Fe] ratios (the latter were obtained in Sect. 2.2.3). The two-tailed probabilities, p, computed using Pearson's parametric correlation coefficients and by taking abundance determination errors into account are shown in the corresponding panels.

pected for our RGB stars. Obviously, they are too small to have an influence in the context of our investigation.

The errors in the determined Zn abundances that result from different uncertainty sources are provided in Table 4.2. The final uncertainty in the determined Zn abundance (obtained by adding individual components in quadratures) are shown in Fig.4.2, 4.3, and 4.4, as well as in Table 4.2. These errors were also used in the maximum-likelihood analysis (see Sect. 1.7.2) aimed to determine the average value of Zn abundance and its intrinsic spread in the sample RGB stars.

We stress that in this procedure we ignored errors in the uncertainties in the atomic line parameters. The total abundance uncertainties listed in Table 4.2 are therefore only the lower limits on the abundance errors because they do not account for the various systematic uncertainties that are unavoidable in the abundance analysis.

4.2.3. 3D–1D LTE abundance corrections

Until now, the role of 3D hydrodynamical effects in the formation of Zn I lines has been investigated in a single study for dwarf and subgiant stars (see Nissen et al. 2004). Although the authors concluded that the effect was small, the influence of convection on the spectral line formation in the atmospheres of RGB stars has not been studied yet.

To answer this question, we used 3D hydrodynamical CO^{5}BOLD (Freytag et al. 2012) and 1D hydrostatic LHD (Caffau et al. 2008) model atmospheres for studying the role of convection in the atmospheres of RGB stars of 47 Tuc. As it was done in Sect. 1.6, in this case we also used models with the atmospheric parameters similar to those of the median object in our RGB star sample, $T_{\rm eff} \approx 4490$ K, $\log g = 2.0$, and [M/H] = −1.0. Since the range covered by the atmospheric parameters of the sample stars was small

Table 4.2. Errors in the determined abundance of Zn. The ± or ∓ sign reflects the change in elemental abundance which occurs due to the increase (top sign) or decrease (bottom sign) in the size of a given error source. For example, increase in the $T_{\rm eff}$ leads to the increase in the abundance of Zn (±), while increasing $\xi_{\rm mic}$ results in results in its decrease (∓).

Element	Line	$\sigma(T_{\rm eff})$	$\sigma(\log g)$	$\sigma(\xi_{\rm t})$	σ(cont)	σ(fit)	$\sigma(A)_{\rm tot}$
	λ, nm	dex	dex	dex	dex	dex	dex
Zn I	472.21	±0.03	∓0.04	∓0.11	0.04	0.09	0.16
Zn I	481.05	±0.03	∓0.03	∓0.11	0.05	0.08	0.15

($\Delta T_{\rm eff} \approx 300$ K, $\Delta \log g \approx 0.3$), their variation acros the entire parameter range should be small. Thus, the obtained 3D–1D abundance corrections should be representative for all studied RGB stars. We remind that the CO^{5}BOLD and LHD models used in this test shared identical chemical composition, opacities, and equation of state (see Sect. 2.2.4 for details). Spectral line synthesis was done with the Linfor3D spectral synthesis package (see Sect. 1.5.3).

Since the equivalent widths, W, of Zn I lines observed in the spectra of individual RGB stars were different, we computed the abundance corrections for two values of W which bracketed the extreme values observed in the spectra of real stars. These were 8.5 pm and 8 pm, in case of the weakest lines, 10.5 pm and 10 pm, for strong lines (for Zn 472.21, and Zn 481.05, respectively). The microturbulence velocity used in this test, 1km s^{-1}, was determined using the 3D hydrodynamical model atmosphere, following the prescription provided in Steffen et al. (2013, Method 1; see also Sect 1.6). This value was used with the LHD model atmospheres in order to obtain 1D curves-of-growth and, ultimately, the 3D–1D abundance corrections.

The obtained 3D–1D LTE abundance corrections are provided in Table 4.3. For both lines, they do not exceed 0.05 dex and vary little with the line strength, suggesting that the influence of convection on the formation of these Zn I lines is minor.

It is important to stress that we did not use the obtained abundance corrections to correct the 1D abundances for the 3D effects. Since the abundance corrections were small and essentially independent of the line strength, applying them would have no effect on the possible relations between, e.g., the abundances and kinematical properties of the cluster stars.

4.3. Results and discussion

Our analysis yielded the mean value of [Zn/Fe] ratio in 27 RGB stars that is just slightly above solar, $[{\rm Zn/Fe}]^{\rm 1D\ LTE} = 0.11 \pm 0.09$ (the number after the ± sign is standard abundance deviation in this stellar sample). One may question whether this variation may be caused, at least in part, by the intrinsic star-to-star abundance scatter. For answering this question we applied the ML technique described in Sect. 1.7.2. The average

Table 4.3. The 3D–1D abundance corrections, $\Delta_{\mathrm{3D-1D\ LTE}}$, for different strengths of Zn I lines used in this work.

Element	$\lambda_{\mathrm{central}}$	$\Delta_{\mathrm{3D-1D\ LTE}}$, dex	
	nm	weak	strong
Zn I	472.21 nm	0.039	0.047
Zn I	481.05 nm	0.039	0.052

[Zn/Fe] ratio obtained in this test was [Zn/Fe] = 0.11 ± 0.03 (in this case the value after the ± sign is the error of the mean and thus it is smaller than the standard deviation determined in the same sample). The determined intrinsic abundance variation was $\sigma^{\mathrm{int}}([\mathrm{Zn/Fe}]) = 0.00 \pm 0.04$ which points to zero intrinsic Zn abundance variation in the RGB stars.

The obtained Zn abundances were used to study possible relations between the chemical and kinematical properties of RGB stars in 47 Tuc. For this, we used abundances of Na, Mg, and K obtained in Sect. 2.2.3. While abundances of the light elements were all determined in 1D NLTE, the 1D NLTE–LTE corrections for Zn are expected to be small. Thus, we directly compared 1D NLTE abundances of the light elements and 1D LTE abundances of Zn. Our comparison of Zn abundances and those of light elements was motivated by the fact that, e.g., Na shows significant star-to-star abundance variation in near all clusters studied so far. Some clusters also exhibit Mg–Al correlation which points to Mg–Al cycle that occurs at higher temperatures than Na synthesis does. Thus, the detection of a relation between the abundances of Zn and those of, e.g., Na and Mg, may indicate that all these elements were synthesized in the same polluters. In fact, as it was already mentioned in the introduction to this Chapter, there may be a slight overlap in stellar masses of AGB stars where both Zn and light elements could be synthesized. In such a situation, one would expect to see relations between the abundances of these elements.

It is also interesting to note in this context that, recently, Mucciarelli et al. (2017) suggested the existence of K–Na correlation and K–O anti-correlation in 144 RGB stars in 47 Tuc. Our own analysis of K abundance in TO and RGB stars of 47 Tuc, however, does not support this claim (see Chapters 2 and 3 for details). In addition, relations between the abundance of K and other light elements would be very difficult to explain from the theoretical point of view because K is synthesized at temperatures $\approx 2 \times 10^8$ K at which all Na should be fully destroyed (e.g., Prantzos et al. 2017). In this sense, the existence of relations between K and other light elements, as well as those between K and Zn, would add another interesting puzzle to already complicated picture of GGC evolution.

The obtained [Zn/Fe] ratios are plotted versus the light element element-to-iron ratios in Fig. 4.3. As in Chapters 2 and 3 above, here we also used Student's Student's *t*-test to verify the validity of the null hypothesis, i.e., that there is no correlation in the

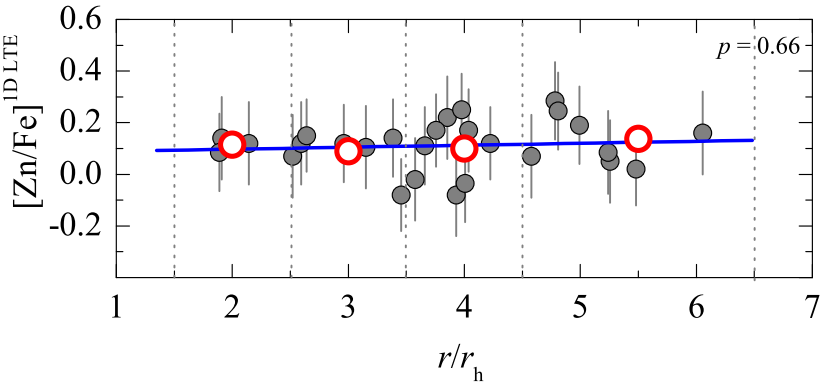

Figure 4.4. [Zn/Fe] abundance ratios determined in the sample of 27 RGB stars in 47 Tuc and plotted versus the projected radial distance of individual stars (small filled symbols). Large red open circles are averages obtained in non-overlapping $\Delta r/r_h = 1$ bins.

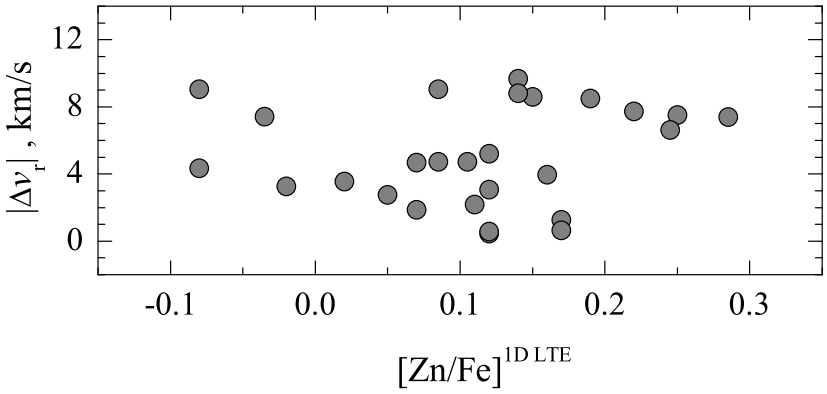

Figure 4.5. Absolute radial velocities determined for the sample of 27 RGB stars in 47 Tuc and plotted versus $[\mathrm{Zn/Fe}]^{\mathrm{1D\ LTE}}$ ratios of individual stars.

different panels of Fig. 4.3. For this, we computed the two-tailed probability, p, that the t-value in the given dataset could attain the determined value when the Pearson's correlation coefficient, r, in the given x-y plane is $r = 0$ (all r values were computed by taking errors on both x and y axes into account). These tests were also performed using the data shown in Fig. 4.4–4.6 (see discussion below), with the obtained p-values provided in the corresponding panels of Fig. 4.3–4.6.

The results of these tests do not suggest the existence of statistically significant relations between the abundances of Zn and the other light elements shown in Fig. 4.3. Similarly, there is no statistically significant relation between the determined [Zn/Fe] ratios and the distance from the cluster center, r/r_{h} (Fig. 4.4) (here, r is the projected distance from the cluster center and r_{h} is the half-light radius of 47 Tuc taken from Trager et al. 1993, $r_{\mathrm{h}} = 174''$). Further, we find no statistically significant relation between the [Zn/Fe] ratios and absolute radial velocities of RGB stars, $|\Delta v_{\mathrm{r}}| \equiv \left|v_{\mathrm{rad}} - \langle v_{\mathrm{rad}} \rangle^{\mathrm{clust}}\right|$, where

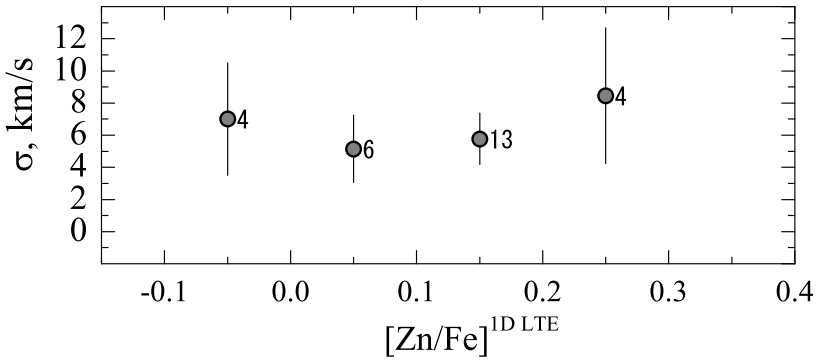

Figure 4.6. Radial velocity dispersion of RGB stars in 47 Tuc plotted versus the [Zn/Fe]ratio.

$v_{\rm rad}$ is radial velocity of the individual star and $\langle v_{\rm rad}\rangle^{\rm clust} = -18.6$ km/s is the mean radial velocity of the sample (Fig. 4.5). And finally, there seem to be no relation between the radial velocity dispersion of individual stars (computed in non-overlapping 0.1 dex wide bins of [Zn/Fe] ratios) and [Zn/Fe] ratios determined in their atmosphere.

Our results therefore indicate that nucleosynthesis of Zn and that of light elements in 47 Tuc was unrelated and proceeded in different types of stars. The obtained zinc-to-iron abundance ratio, $\langle$[Zn/Fe]$\rangle^{\rm 1D\ LTE} = 0.11 \pm 0.09$, agrees to within less than one sigma to those obtained by Thygesen et al. (2014), [Zn/Fe]$^{\rm 1D\ LTE} = 0.26 \pm 0.13$ (13 RGB stars), and Duffau et al. (2017), $\langle$[Zn/Fe]$\rangle^{\rm 1D\ NLTE} = 0.17 \pm 0.10$ (19 RGB stars).

It is also important to note that the value obtained in this work is nearly identical to the average [Zn/Fe] ratio observed in the Galactic field stars at the metallicity of 47 Tuc (e.g. Mishenina et al. 2002; Barbuy et al. 2015; Duffau et al. 2017; da Silveira et al. 2018). To directly compare these values, we selected 10 Galactic field stars from Bensby et al. (2014), 2 stars from Allende Prieto et al. (2004), and 7 stars from Mishenina et al. (2011) whose metallicity falls within the three-sigma interval of the metallicity of 47 Tuc, [Fe/H] $= 0.76 \pm 0.1$ dex (Taken from (Carretta et al. 2009a)). We then computed a mean [Zn/Fe] ratio in this sample of 19 Galactic field stars. This yielded 0.15 ± 0.14 dex which is in good agreement with the value determined in our work, $\langle$[Zn/Fe]$\rangle^{\rm 1D\ LTE} = 0.11 \pm 0.09$. The average [Zn/Fe] value determined by us in 47 Tuc also agrees well with the [Zn/Fe] ratio that is observed at this galactocentric distance in the Galactic red giants of similar metallicity (Duffau et al. 2017; Ernandes et al. 2018).

All this evidence suggests that production of Zn in 47 Tuc most likely followed along the same pathways as in the Galactic field stars of the same metallicity, possibly, through α-element nucleosynthesis. We find no evidence that Zn could have been synthesized in 47 Tuc during the *s*-process nucleosynthesis.

Summary and conclusions

In this Thesis we investigated possible connections between the chemical and kinematical properties of the main-sequence turn-off (TO) and red giant branch (RGB) stars in the Galactic globular cluster (GGC) 47 Tuc. For this, we determined 1D NLTE abundances of Na, Mg, and K, and 1D LTE abundances of Zn in the atmospheres of RGB stars, as well as 1D NLTE abundances of Na, Mg, and K in TO stars. All abundances were determined utilizing high-resolution spectra that were obtained with the 2dF/HERMES (Australian Astronomical Observatory) and FLAMES/GIRAFFE (European Southern Observatory) spectrographs.

Spectroscopic data were analyzed using 1D ATLAS9 model atmospheres and 1D LTE/NLTE abundance analysis tools. In the case of Na, Mg and K, 1D NLTE spectral line synthesis was performed with the MULTI package, while the SYNTHE code was used for the 1D LTE line synthesis in case of Zn. We also used 3D hydrodynamical CO^{5}BOLD and 1D hydrostatic LHD model atmospheres to compute 3D–1D abundance corrections for the spectral lines of all four chemical elements which were used in this study, in order to assess the influence of convection on the formation of these lines.

The obtained sample-averaged abundances in 32 RGB stars in 47 Tuc were $[\mathrm{Na/Fe}]^{\mathrm{1D\ NLTE}} = 0.42 \pm 0.13$, $[\mathrm{Mg/Fe}]^{\mathrm{1D\ NLTE}} = 0.41 \pm 0.11$ (30 stars), $[\mathrm{K/Fe}]^{\mathrm{1D\ NLTE}} = 0.05 \pm 0.14$ (28 stars), and $[\mathrm{Zn/Fe}]^{\mathrm{1D\ LTE}} = 0.11 \pm 0.09$ (27 stars; numbers after the ± sign are standard deviation). There were no statistically significant relations between the abundances of Na, Mg, K, and Zn. We also detected no significant correlations/anti-correlations between the abundance/abundance-abundance ratios and distance from the cluster center. Finally, no relations between the absolute radial velocities of individual stars and abundances of the light elements in their atmospheres were found. While in case of Mg we found evidence for a small intrinsic star-to-star abundance variation (spread), with its value being equal to $\sigma^{\mathrm{int}}([\mathrm{Mg/Fe}]) = 0.08 \pm 0.02$ dex, no such spread was detected in the case of K and Zn, with $\sigma^{\mathrm{int}}([\mathrm{K/Fe}]) = 0.00 \pm 0.05$ and $\sigma^{\mathrm{int}}([\mathrm{Zn/Fe}]) = 0.00 \pm 0.04$, respectively. The sample-averaged $[\mathrm{Zn/Fe}]^{\mathrm{1D\ LTE}}$ ratio coincides with the mean [Zn/Fe] ratio obtained in the Galactic field stars at the metallicity of 47 Tuc. All these facts indicate that the nucleosynthesis of K and Zn, and that of light elements, in particular, Na and Mg, has proceeded separately in 47 Tuc. The obtained average $[\mathrm{Zn/Fe}]^{\mathrm{1D\ LTE}}$ ratio suggests that Zn in this GGC most likely originated during the α-element nucleosynthesis.

The sample-averaged abundance determined in this Thesis in a sample of TO stars are $[\mathrm{Mg/Fe}]^{\mathrm{1D\ NLTE}} = 0.47 \pm 0.12$ (53 stars) and $[\mathrm{K/Fe}]^{\mathrm{1D\ NLTE}} = 0.39 \pm 0.09$ (75 stars). In case of Mg we find small but significant intrinsic star-to-star scatter in [Mg/Fe]

abundance ratio, $\sigma^{\rm int}([{\rm Mg/Fe}]) = 0.09 \pm 0.01$. No such variation was found for K, $\sigma^{\rm int}([{\rm K/Fe}]) = 0.00 \pm 0.03$. Our analysis does not support earlier claims published in the literature regarding the possible relations between the abundance of K and that of light elements O and Na. We also detected no statistically significant correlations/anti-correlations between the [Mg/Fe] and [K/Fe] abundance ratios and projected distance from the cluster center. Finally, we found no relations between the absolute radial velocities of individual stars and abundances of Mg and K in their atmospheres.

The results obtained in this Thesis also indicate that NLTE effects play a significant role in the formation of Mg I and K I lines in the atmospheres of TO stars and Na I and K I lines in the atmospheres of RGB stars. The 1D NLTE–LTE abundance corrections for Mg are small and do not exceed −0.03 and −0.08 dex in TO and RGB stars, respectively. In case of Na, they do not become larger than −0.28 dex in RGB stars. For K, in both cases they are large and may reach to −0.5 dex.

The influence of convection on the formation of spectral lines is generally small in case of all elements studied in this Thesis, both in TO and RGB stars. This is indicated by the size of 3D-1D LTE abundance corrections which in case of RGB stars do not exceed 0.07 dex for Na I, Mg I, K I, and Zn I lines. For Mg I and K I in TO stars, they are 0.05 and –0.06 dex, respectively.

The results obtained in this Thesis therefore suggest that K and Zn have been synthesized through different and, possibly, unrelated pathways from those in which the light elements Na and Mg were produced in 47 Tuc. It still needs to be verified, however, whether this conclusion may also hold true in the case of stars characterized by the largest absolute radial velocities, as well as for stellar populations in other GGCs. This is a task that will need to be performed in the future studies, both in 47 Tuc and other Galactic globular clusters.

Bibliography

Allende Prieto, C., Barklem, P. S., Lambert, D. L., et al. 2004, A&A, 420, 183

Andreasen, D.T., Sousa, S.G., Delgado Mena, E. et al. 2016, A&A, 585, A143

Andrievsky, S. M., Spite, M., Korotin, S. A., et al. 2010, A&A, 509, A88

Asplund, M., Grevesse, N., Sauval, A. J., et al. 2009, ARA&A, 47, 481

Bagnulo, S., Jehin, E., Ledoux, C., et al. 2003, The Messenger, 114, 10

Barbuy, B., Friaça, A. C. S., da Silveira, C. R., et al. 2015, A&A, 580, A40

Barklem, P. S., Belyaev, A. K., Dickinson, A. S., et al. 2010, A&A, 519, A20

Barklem, P. S., Belyaev, A. K., Spielfiedel, A., et al. 2012, A&A, 541, A80

Bastian, N., Lamers, H. M., de Mink, S. E., et al. 2013, MNRAS, 436, 2398

Bastian, N., Cabrera-Ziri, I., & Salaris, M. 2015, MNRAS, 449, 3333

Bastian, N., & Lardo, C. 2017, arXiv:1712.01286

Baumgardt, H. 2017, MNRAS, 464, 2174

Bekki, K. 2011, MNRAS, 412, 2241

Bell, R. A., & Dickens, R. J. 1980, ApJ, 242, 657

Bellazzini, M., Bragaglia, A., Carretta, E., et al. 2012, A&A, 538, A18

Bensby, T., Feltzing, S., & Oey, M. S. 2014, A&A, 562, A71

Bergbusch, P. A., & Stetson, P. B. 2009, AJ, 138, 1455

Bertaux, J.L., Lallement, R., Ferron, S. et al. 2014, A&A, 564, A46

Bonifacio, P., Pasquini, L., Molaro, P., et al. 2007, A&A, 470, 153

Caffau, E., & Ludwig, H.-G. 2007, A&A, 467, L11

Caffau, E., Ludwig, H.-G., Steffen, M., et al. 2008, A&A, 488, 1031

Carlsson, M. 1986, Uppsala Astronomical Observatory Reports, 33

Carretta, E., Gratton, R. G., Bragaglia, A., et al. 2004, A&A, 416, 925

Carretta, E., Bragaglia, A., Gratton, R. G., et al. 2006, A&A, 450, 523

Carretta, E., Bragaglia, A., Gratton, R., et al. 2009a, A&A, 505, 117

Carretta, E., Bragaglia, A., Gratton, R., et al. 2009b, A&A, 505, 139

Carretta, E., Lucatello, S., Gratton, R. G., et al. 2011, A&A, 533, A69

Carretta, E., Gratton, R., Bragaglia, A., et al. 2013, ApJ, 769, 40

Carretta, E. 2014, ApJ, 795, L28

Castelli, F., & Kurucz, R. L. 2003, in Modeling of Stellar Atmospheres, eds. N. E. Piskunov, W. W. Weiss, & D. F. Gray, Proc. IAU Symp. 210, poster, A20 (CD-ROM)

Cayrel, R., Depagne, E., Spite, M., et al. 2004, A&A, 416, 1117

Černiauskas, A., Kučinskas, A., Klevas, J., et al. 2017, A&A, 604, A35

Černiauskas, A., Kučinskas, A., Klevas, J., et al. 2018, in press (https://doi.org/10.1051/0004-6361/201731659)

Černiauskas, A., Kučinskas, A., Klevas, J., et al. 2018, in press (https://doi.org/10.1051/0004-6361/201833255)

Collet, R., Asplund, M., & Trampedach, R. 2007, A&A, 469, 687

Cordero, M. J., Pilachowski, C. A., Johnson, C. I., et al. 2014, ApJ, 780, 94

da Silveira, C. R., Barbuy, B., Friaça, A. C. S., et al. 2018, A&A, 614, 149

de Mink, S. E., Pols, O. R., Langer, N., et al. 2009, A&A, 507, L1

de Silva, G. M., Heijmans, J., Gers, L., Zucker, D., & Aao Hermes Team 2012, Galactic Archaeology: Near-Field Cosmology and the Formation of the Milky Way, 458, 415

De Silva, G. M., Freeman, K. C., Bland-Hawthorn, J., et al. 2015, MNRAS, 449, 2604

Decressin, T., Meynet, G., Charbonnel, C., et al. 2007, A&A, 464, 1029

D'Ercole, A., D'Antona, F., Ventura, P., et al. 2010, MNRAS, 407, 854

D'Ercole, A., D'Antona, F., Carini, R., et al. 2012, MNRAS, 423, 1521

di Criscienzo, M., D'Antona, F., Milone, A. P., et al. 2011, MNRAS, 414, 3381

Dobrovolskas, V., Kučinskas, A., Steffen, M., et al. 2013, A&A, 559, A102

Dobrovolskas, V., Kučinskas, A., Bonifacio, P., et al. 2014, A&A, 565, A121

D'Orazi, V., Lucatello, S., Gratton, R., et al. 2010, ApJ, 713L, 1

Duffau, S., Caffau, E., Sbordone, L., et al. 2017, A&A, 604, 128

Elmegreen, B. G., & Efremov, Y. N. 1997, ApJ, 480, 235

Ernandes, H., Barbuy, B., Alves-Brito, A., et al. 2018, arXiv:1801.06157

Freeman, K., & Bland-Hawthorn, J. 2002, ARA&A, 40, 487

Freytag, B., Steffen, M., & Dorch, B. 2002, AN, 323, 213

Freytag, B., Steffen, M., Ludwig, H.-G., et al. 2012, J. Comp. Phys., 231, 919

Gillingham, P., Smoker, J., Colless, M., et al. 2004, Proc. SPIE, 5492, 643

Gratton, R., Sneden, C., & Carretta, E. 2004, ARA&A, 42, 385

Gratton, R. G., Villanova, S., Lucatello, S., et al. 2012, A&A, 544, A12

Grevesse, N., & Sauval, A. J. 1998, Space Sci. Rev., 85, 161

Gustafsson, B., Edvardsson, B., Eriksson, K., et al. 2008, A&A, 486, 951

Harris, W. E. 1996, AJ, 112, 1487; online version:
http://physwww.mcmaster.ca/~harris/mwgc.dat (December 2010 revision)

Hartwick, F. D. A., & McClure, R. D. 1972, ApJ, 176, L57

Hauschildt, P. H., Allard, F., & Baron, E. 1999, ApJ, 512, 377

Hénault-Brunet, V., Gieles, M., Agertz, O., et al. 2015, MNRAS, 450, 1164

Hinkle, K., Wallace, L., Valenti, J., & Harmer, D. 2000, Visible and Near Infrared Atlas of the Arcturus Spectrum 3727-9300 A ed. Kenneth Hinkle, Lloyd Wallace, Jeff Valenti, and Dianne Harmer. (San Francisco: ASP) ISBN: 1-58381-037-4, 2000.

Ivanov, V. D., & Borissova, J. 2002, A&A, 390, 937

Jofré, P. Heiter, U, Soubiran, C. et al. 2015, A&A, 582, A81

Karakas, A. I., van Raai, M. A., Lugaro, M., et al. 2009, ApJ, 690, 1130

Kirby, E. N., Guhathakurta, P., Bolte, M., et al. 2009, ApJ, 705, 328

Klevas, J., Kučinskas, A., Steffen, M. et al. 2016, A&A, 586, A156

Kobayashi, C., Umeda, H., Nomoto, K., et al. 2006, ApJ, 653, 1145

Korotin, S. A., Andrievsky, S. M., & Luck, R. E. 1999, A&A, 351, 168

Kraft, R. P. 1994, PASP, 106, 553

Kučinskas, A., Steffen, M., Ludwig, H.-G., et al. 2013, A&A, 549, A14

Kučinskas, A., Dobrovolskas, V., & Bonifacio, P. 2014, A&A, 568, L4

Kupka, F., Dubernet, M.-L., & VAMDC Collaboration 2011, Baltic Astronomy, 20, 503

Kurucz, R. L., & Furenlid, I. 1979, SAO Special Report, 387, 387

Kurucz, R. L., Furenlid, I., Brault, J., & Testerman, L. 1984, National Solar Observatory Atlas, Sunspot, New Mexico: National Solar Observatory

Kurucz, R. L. 1993, ATLAS9 Stellar Atmosphere Programs and 2 km s^{-1} Grid, CD-ROM No. 13 (Cambridge, Mass)

Kurucz, R. L. 2006, arXiv:astro-ph/0605029

Lardo, C., Bellazzini, M., Pancino, E., et al. 2011, A&A, 525, A114

Lind, K., Asplund, M., Barklem, P. S., et al. 2011, A&A, 528, A103

Lodders, K., Palme, H., & Gail, H.-P. 2009, Abundances of the elements in the solar system. In Landolt Börnstein, New Series, Vol. VI/4B, Chap. 4.4, J.E. Trümper (ed.), Berlin, Heidelberg, New York: Springer-Verlag, p. 560-630.

Ludwig, H.G. 1992, Ph.D. Thesis, Univ. Kiel

Ludwig, H.-G., Jordan, S., & Steffen, M. 1994, A&A, 284, 105

Ludwig, H.-G., Caffau, E., Steffen, M., et al. 2009, Memorie della Societa Astronomica Italiana, 80, 711

Ludwig, H.-G., & Kučinskas, A. 2012, A&A, 547, A118

Mackey, A.D., & van den Berg, S. 2005, MNRAS, 360, 631

Maeder, A., & Meynet, G. 2006, A&A, 448, L37

Marino, A. F., Villanova, S., Piotto, G., et al. 2008, A&A, 490, 625

Marino, A. F., Villanova, S., Milone, A. P., et al. 2011, ApJL, 730, L16

Marino, A. F., Milone, A. P., Przybilla, N., et al. 2014, MNRAS, 437, 1609

Matteucci, F., Raiteri, C. M., Busso, M., et al. 1993, A&A, 272, 421

McDonald, I., Boyer, M. L., van Loon, J. T., et al. 2011, ApJS, 193, 23

Mihalas, D. 1978, Stellar Atmospheres, Freeman and Company, p.186

Milone, A. P., Piotto, G., Bedin, L. R., et al. 2012, ApJ, 744, 58

Milone, A. P., Marino, A. F., Dotter, A., et al. 2014, ApJ, 785, 21

Mishenina, T. V., Kovtyukh, V. V., Soubiran, et al. 2002, A&A, 396, 189

Mishenina, T. V., Soubiran, C., Kovtyukh, V. V., et al. 2004, A&A, 418, 551

Mishenina, T. V., Gorbaneva, T. I., Basak, N. Y., et al. 2011, Astronomy Reports, 55, 689

Morton, D.C. 1991, ApJS, 77, 119

Mucciarelli, A., Bellazzini, M., Ibata, R., et al. 2012, MNRAS, 426, 2889

Mucciarelli, A., Bellazzini, M., Merle, T., et al. 2015, ApJ, 801, 68

Mucciarelli, A., Merle, T., & Bellazzini, M. 2017, arXiv:1702.02953

Nissen, P. E., Chen, Y. Q., Asplund, M., et al. 2004, A&A, 415, 993

Nordlund, A., & Galsgaard, K. 1992, Electromechanical Coupling of the Solar Atmosphere, 267, 13

Nordlund, A. 1982, A&A, 107, 1

Osborn, W. 1971, The Observatory, 91, 223

Pasquini, L., Bonifacio, P., Molaro, P., et al. 2005, A&A, 441, 549

Piotto, G., Bedin, L. R., Anderson, J., et al. 2007, ApJL, 661, 53

Piotto, G., Milone, A. P., Bedin, L. R., et al. 2015, AJ, 149, 91

Piskunov, N. E., Kupka, F., Ryabchikova, T. A., et al. 1995, A&AS, 112, 525

Prakapavičius, D., Kučinskas, A., Dobrovolskas, V., et al. 2017, A&A, 599, A128

Prantzos, N., Charbonnel, C., & Iliadis, C. 2017, A&A, 608, A28

Pryor, C. & Meylan, G. 1993, ASP Conf. Ser., 50, 357

Ramírez, I., Meléndez, J. 2005, ApJ, 626, 465

Ramírez, I., & Allende Prieto, C. 2011, ApJ, 743, 135

Renzini, A., D'Antona, F., Cassisi, S., et al. 2015, MRRAS, 454, 4197

Richer, H.B., Heyl, J., Anderson, J., et al. 2013, ApJ, 771, L15

Salaris, M., Weiss, A., Ferguson, J. W., et al. 2006, ApJ, 645, 1131

Sbordone, L., Bonifacio, P., Castelli, F., et al. 2004, Memorie della Societa Astronomica Italiana Supplementi, 5, 93

Sbordone, L. 2005, Memorie della Societa Astronomica Italiana, 8, 61

Sbordone, L., Bonifacio, P., Caffau, E., et al. 2010, A&A, 522, A26

Shen, Z.-X., Bonifacio, P., Pasquini, L., et al. 2010, A&A, 524, L2

Sneden, C., Gratton, R. G., & Crocker, D. A. 1991, A&A, 246, 354

Steenbock, W., & Holweger, H. 1984, A&A, 130, 319

Steffen, M., Caffau, E., & Ludwig, H.-G. 2013, Memorie della Societa Astronomica Italiana Supplementi, 24, 37

Stetson, P. B. 2000, PASP, 112, 925

Takeda, Y., Zhao, G., Chen, Y.-Q., et al. 2002, PASP, 54, 275

Takeda, Y., Hashimoto, O., Taguchi, H., et al. 2005, PASJ, 57, 751

Takeda, Y., Kaneko, H., Matsumoto, N., et al. 2009, PASP, 61, 563

Thygesen, A. O., Sbordone, L., Andrievsky, S., et al. 2014, A&A, 572, A108

Tody, D. 1986, Proc. SPIE, 627, 733

Trager, S.C., Djorgovski, S.G., & King, I.R. 1993, ASP Conf. Ser., 50, 347

Vacca, W. D., Cushing, M. C., & Rayner, J. T. 2003, PASP, 115, 389

van den Bergh, S. 2010, AJ, 140, 1043

Ventura, P., D'Antona, F., Mazzitelli, I., et al. 2001, ApJ, 550, L65

Ventura, P., D'Antona, F., Di Criscienzo, M., et al. 2012, ApJ, 761, L30

Vesperini, E., McMillan, S. L. W., D'Antona, F., et al. 2013, MNRAS, 429, 1913

Vögler, A., Bruls, J. H. M. J., et al. 2004, A&A, 421, 741

Vögler, A., Shelyag, S., Schüssler, M., et al. 2005, A&A, 429, 335

Yi, S., Demarque, P., Kim, Y.-C., et al. 2001, ApJS, 136, 417

Appendix A. 1D NLTE abundances of Na, Mg, and K, and 1D LTE abundances of Zn determined in RGB stars of 47 Tuc

In this Section we provide a list of target RGB stars (32 objects), their atmospheric parameters (determined in Sect. 1.3), and abundances of Na, Mg, K, and Zn (Sect. 2.2.3, 2.2.4, and 4.2.2). This information is summarized in Table A1 the contents of which are as follows:

- column 1: object name;
- column 2: right ascension;
- column 3: declination;
- column 4: V magnitude;
- column 5: I magnitude;
- column 6: effective temperature;
- column 7: surface gravity;
- column 8: radial velocity;
- column 9: 1D NLTE abundance of Na and its error;
- column 10: 1D NLTE abundance of Mg and its error;
- column 11: 1D NLTE abundance of K and its error.
- column 11: 1D LTE abundance of Zn and its error.

Table A1. Target RGB stars in 47 Tuc, their atmospheric parameters, and determined abundances of Na, Mg, K, and Zn.

Star	RA	Dec.	V	I	$T_{\rm eff}$	$\log g$	$v_{\rm rad}$	[Na/Fe]	[Mg/Fe]	[K/Fe]	[Zn/Fe]
name	(2000)	(2000)	mag	mag	K	[cgs]	km/s	1D NLTE	1D NLTE	1D NLTE	1D NLTE
N104-S1667	6.40433	–72.20061	13.19	11.99	4450	1.73	–9.5	0.56 ±0.12	0.38 ±0.07	0.20 ±0.16	–0.08 ±0.14
N104-S2214	6.31979	–72.07552	13.23	12.01	4430	1.73	–27.6	0.31 ±0.12	0.48 ±0.08	0.09 ±0.16	0.08 ±0.15
N104-S1213	5.79479	–71.93364	13.28	12.09	4490	1.79	–8.9	0.58 ±0.12	0.29 ±0.07	0.19 ±0.16	0.14 ±0.15
N104-S1430	5.98271	–71.90491	13.34	12.16	4500	1.82	–16.4	0.59 ±0.12	0.37 ±0.07	–0.06 ±0.16	0.11 ±0.15
N104-S1625	6.35437	–71.98103	13.36	12.15	4450	1.79	–21.6	0.41 ±0.12	...	0.30 ±0.16	0.12 ±0.15
N104-S2499	6.64554	–72.11236	13.37	12.17	4460	1.80	–11.2	0.46 ±0.12	0.59 ±0.07	...	–0.04 ±0.15
N104-S2220	6.36883	–72.01095	13.49	12.31	4490	1.87	–27.2	0.53 ±0.12	0.59 ±0.07	–0.07 ±0.16	0.15 ±0.14
N104-S1800	6.55300	–72.00191	13.52	12.35	4510	1.90	–17.3	0.65 ±0.12	0.51 ±0.08	–0.03 ±0.16	0.17 ±0.14
N104-S1481	6.09350	–72.25283	13.53	12.35	4500	1.89	–21.8	0.23 ±0.12	0.24 ±0.07	0.02 ±0.16	–0.02 ±0.16
N104-S1849	6.60921	–72.01517	13.72	12.55	4500	1.97	–26.1	0.38 ±0.12	0.56 ±0.08	–0.07 ±0.16	0.25 ±0.14
N104-S1779	6.53142	–71.97400	13.73	12.58	4550	2.01	–22.9	0.61 ±0.12	...	...	–0.08 ±0.16
N104-S1490	6.13163	–72.26456	13.84	12.69	4560	2.05	–10.8	0.38 ±0.12	0.37 ±0.07	0.06 ±0.16	0.22 ±0.16
N104-S2328	5.39333	–72.14819	13.85	12.74	4630	2.10	–11.5	0.46 ±0.12	0.52 ±0.08	–0.06 ±0.16	...
N104-S1636	6.36917	–72.02222	13.87	12.76	4610	2.10	–16.7	0.49 ±0.13	...	...	0.07 ±0.16
N104-S1751	6.51550	–72.20506	13.91	12.77	4550	2.08	–19.2	0.31 ±0.12	0.42 ±0.07	0.22 ±0.16	0.17 ±0.16
N104-S1657	6.39483	–72.13347	13.98	12.89	4660	2.17	–18.0	...	0.58 ±0.08	0.27 ±0.16	0.12 ±0.16
N104-S1750	6.51125	–72.05508	14.09	13.00	4650	2.21	–23.3	0.53 ±0.12	...	0.32 ±0.17	0.10 ±0.16
N104-S1543	6.23467	–72.13755	14.12	13.06	4710	2.26	–16.6	0.60 ±0.13	...	–0.06 ±0.16	...
N104-S1732	6.49112	–72.08711	14.17	13.09	4670	2.25	–22.9	0.47 ±0.13	...	0.05 ±0.16	...
N104-S1563	6.27129	–72.15166	14.21	13.13	4700	2.28	–13.4	0.45 ±0.12	0.42 ±0.07	0.00 ±0.16	0.12 ±0.16
N104-S167	5.09500	–72.02045	12.99	11.75	4390	1.60	–22.5	0.41 ±0.12	0.36 ±0.07	0.15 ±0.16	0.16 ±0.16
N104-S292	5.17163	–72.04539	13.18	11.99	4470	1.73	–15.0	0.37 ±0.12	0.54 ±0.07	0.18 ±0.16	0.02 ±0.14
N104-S1084	5.60667	–71.88953	13.50	12.31	4470	1.86	–11.2	0.25 ±0.12	0.30 ±0.07	–0.16 ±0.16	0.28 ±0.15
N104-S2474	6.47350	–71.86870	13.55	12.34	4440	1.86	–15.8	0.16 ±0.12	...	...	0.05 ±0.16
N104-S1844	6.60458	–71.95181	13.61	12.44	4510	1.94	–23.2	0.33 ±0.12	0.31 ±0.08	–0.06 ±0.16	0.07 ±0.16
N104-S2333	5.40721	–72.21652	13.77	12.65	4600	2.05	–25.2	0.56 ±0.12	0.39 ±0.07	0.21 ±0.16	0.24 ±0.15
N104-S1070	5.58192	–72.23414	13.87	12.73	4550	2.06	–18.1	0.24 ±0.12	0.30 ±0.07	0.03 ±0.16	0.12 ±0.14
N104-S2494	6.62525	–72.23708	13.91	12.75	4540	2.07	–10.1	...	0.32 ±0.07	0.00 ±0.16	0.19 ±0.15
N104-S1692	6.43354	–71.99447	14.05	12.91	4570	2.14	–22.8	0.29 ±0.13	0.32 ±0.08	–0.18 ±0.16	...
N104-S2439	6.24533	–71.83745	14.17	13.07	4650	2.24	–23.3	0.39 ±0.12	0.38 ±0.07	–0.06 ±0.16	0.08 ±0.16
N104-S1524	6.19971	–72.20933	14.23	13.17	4720	2.30	–16.7	0.38 ±0.12	0.50 ±0.08	0.06 ±0.16	...
N104-S2176	6.21292	–72.00975	14.25	13.15	4640	2.27	–27.4	0.29 ±0.12	0.31 ±0.07	–0.13 ±0.16	0.14 ±0.16
mean								0.42	0.41	0.05	0.11
σ								0.13	0.11	0.14	0.09

Appendix B. 1D NLTE abundances of Mg and K determined in the TO stars of 47 Tuc

The 1D NLTE [Mg/Fe] and [K/Fe] abundance ratios determined in the sample of TO stars in 47 Tuc are provided in Table B1. A detailed description of the methodology used to determine elemental abundances is given in Sect. 3.2.2. The contents of Table B1 are:

- column 1: object ID;
- column 2: right ascension;
- column 3: declination;
- column 4: effective temperature;
- column 5: surface gravity;
- column 6: radial velocity;
- column 7: 1D NLTE magnesium abundance and its error;
- column 8: 1D NLTE potassium abundance and its error.

The sample-averaged values of the determined abundance ratios and their standard deviation values are provided in the last two lines of Table B1.

Table B1. Target TO stars in 47 Tuc, their atmospheric parameters, and determined [Mg/Fe] and [K/Fe] abundance ratios.

Star ID	RA (2000)	Dec. (2000)	B mag	I mag	$T_{\rm eff}$ K	$\log g$ [cgs]	$v_{\rm rad}$ km/s	[Mg/Fe] 1D NLTE	[K/Fe] 1D NLTE
00006129	6.15846	–71.96322	17.93	17.37	5851	4.06	–21.1	0.42 ±0.06	0.33 ±0.10
00006340	5.96746	–71.96075	17.86	17.30	5817	4.02	–7.4	0.34 ±0.06	0.37 ±0.10
00007619	6.33533	–71.94289	17.95	17.39	5790	4.05	–10.9	...	0.41 ±0.10
00007969	6.11763	–71.93814	17.97	17.40	5811	4.06	–28.5	...	0.45 ±0.10
00008359	6.24488	–71.93133	17.94	17.36	5839	4.06	–23.0	0.62 ±0.06	0.60 ±0.10
00008881	6.16508	–71.92217	17.97	17.40	5916	4.10	–17.1	0.45 ±0.06	...
00009191	6.21133	–71.91592	17.96	17.40	5826	4.07	–26.7	0.54 ±0.06	0.43 ±0.10
00009243	6.27892	–71.91464	17.97	17.42	5857	4.08	–27.9	0.64 ±0.06	0.38 ±0.10
00009434	6.24204	–71.91056	17.95	17.39	5872	4.08	–21.8	...	0.36 ±0.10
00009540	6.11050	–71.90853	17.93	17.36	5843	4.06	–7.1	...	0.38 ±0.10
00014912	5.80258	–71.96294	17.94	17.39	5859	4.08	–12.9	0.65 ±0.06	0.33 ±0.10
00015086	5.76054	–71.96000	17.95	17.38	5878	4.07	–30.8	...	0.44 ±0.10
00015174	5.82779	–71.95847	17.93	17.37	5788	4.04	–24.3	...	...
00015346	5.58437	–71.95531	17.96	17.38	5725	4.03	–10.5	...	0.39 ±0.10
00016131	5.77725	–71.94094	18.00	17.42	5823	4.07	–10.2	0.46 ±0.06	0.44 ±0.10
00016631	5.75729	–71.92917	18.01	17.44	5820	4.08	–27.2	0.68 ±0.06	...
00017628	5.87896	–71.90236	17.99	17.43	5925	4.11	–21.1	0.39 ±0.06	0.36 ±0.10
00017767	5.84779	–71.89828	17.95	17.38	5812	4.06	–25.9	0.53 ±0.06	0.50 ±0.10
00031830	5.41504	–72.04769	17.92	17.35	5832	4.05	–18.6	0.36 ±0.06	0.29 ±0.10
00036086	5.70875	–72.20400	17.91	17.35	5850	4.05	–14.3	...	0.36 ±0.10
00036747	5.77333	–72.19608	18.00	17.46	5814	4.09	–9.8	...	0.46 ±0.10
00038656	5.62004	–72.17497	17.95	17.40	5850	4.08	–19.2	...	0.30 ±0.10
00040049	5.74092	–72.16181	17.94	17.40	5822	4.07	–14.2	0.41 ±0.06	0.37 ±0.10
00040087	5.53888	–72.16119	17.92	17.34	5787	4.03	–27.0	0.31 ±0.06	0.31 ±0.10
00040355	5.72492	–72.15906	17.93	17.35	5879	4.06	–7.1	0.57 ±0.06	0.45 ±0.10
00043095	5.67775	–72.13700	17.97	17.40	5770	4.05	–23.4	0.49 ±0.06	...
00043108	5.57883	–72.13678	17.89	17.33	5797	4.03	–19.5	...	...
00044983	5.71950	–72.12375	17.89	17.33	5848	4.04	–14.3	0.56 ±0.06	0.43 ±0.10
00045982	5.64500	–72.11706	17.90	17.32	5707	4.00	–16.4	0.56 ±0.06	0.46 ±0.10
00046498	5.51050	–72.11339	17.92	17.35	5790	4.04	–7.5	0.45 ±0.06	0.28 ±0.10
00049829	5.76571	–72.09175	17.87	17.29	5740	3.99	–25.9	0.54 ±0.06	0.38 ±0.10
00051341	5.55921	–72.08197	17.93	17.33	5731	4.01	–3.2	0.50 ±0.06	0.41 ±0.10
00051740	5.53704	–72.07939	17.95	17.38	5857	4.07	–28.9	0.50 ±0.06	0.51 ±0.10

Star ID	RA (2000)	Dec. (2000)	B mag	I mag	$T_{\rm eff}$ K	$\log g$ [cgs]	$v_{\rm rad}$ km/s	[Mg/Fe] 1D NLTE	[K/Fe] 1D NLTE
00052108	5.50988	–72.07694	17.90	17.32	5688	3.99	–16.0	0.36 ±0.06	0.14 ±0.10
00054596	5.61767	–72.06100	17.93	17.37	5825	4.05	–16.7	0.49 ±0.06	0.37 ±0.10
00058492	5.68208	–72.03306	17.94	17.36	5728	4.02	–11.1	...	...
00059579	5.66825	–72.02414	17.89	17.32	5660	3.98	–7.9	...	...
00061639	5.69313	–72.00528	17.89	17.34	5779	4.03	–20.0	...	...
00062314	5.56467	–71.99794	18.00	17.38	5740	4.03	1.3	...	...
00062737	5.58004	–71.99319	17.94	17.35	5691	4.01	–20.4	...	...
00062773	5.87338	–71.99317	17.88	17.33	5854	4.05	–20.0	0.47 ±0.06	0.37 ±0.10
00063201	5.60025	–71.98767	17.92	17.33	5759	4.02	–13.8	...	...
00063954	5.77167	–71.97908	17.90	17.30	5801	4.02	–13.2	...	...
00063973	5.70850	–71.97875	17.89	17.31	5780	4.02	–8.1	...	...
00065981	6.05225	–72.22219	17.97	17.42	5814	4.07	–26.2	...	...
00066603	6.05375	–72.21225	17.97	17.42	5848	4.08	–10.9	...	0.39 ±0.10
00066813	6.34237	–72.20903	17.96	17.40	5817	4.07	–16.8	0.33 ±0.06	0.39 ±0.10
00066840	6.25950	–72.20878	18.04	17.50	5780	4.10	–14.2	...	0.51 ±0.10
00067280	6.02708	–72.20253	17.97	17.43	5808	4.07	–8.2	...	0.35 ±0.10
00069585	6.29904	–72.17517	17.95	17.39	5888	4.08	–13.3	...	0.31 ±0.10
00070686	6.22921	–72.16494	17.93	17.37	5808	4.05	–8.3	0.50 ±0.06	0.46 ±0.10
00070910	6.27663	–72.16297	17.94	17.40	5797	4.06	–7.3	...	0.30 ±0.10
00071404	6.29454	–72.15886	17.97	17.40	5787	4.06	–20.1	0.55 ±0.06	...
00072011	6.11733	–72.15458	18.02	17.44	5702	4.05	–12.4	...	...
00096225	6.27933	–72.02936	17.89	17.33	5805	4.04	–32.0	...	0.23 ±0.10
00097156	6.36075	–72.02406	17.93	17.36	5750	4.03	–15.7	0.53 ±0.06	...
00099636	6.26008	–72.00881	17.94	17.40	5799	4.06	–20.2	0.53 ±0.06	0.26 ±0.10
00100325	6.35675	–72.00369	17.93	17.37	5794	4.05	–18.1	...	0.42 ±0.10
00102294	6.06792	–71.98808	17.88	17.31	5772	4.01	–23.0	0.40 ±0.06	0.48 ±0.10
00102307	6.21471	–71.98781	17.93	17.38	5835	4.07	–25.2	0.33 ±0.06	0.44 ±0.10
00103067	5.94763	–71.98056	17.87	17.31	5665	3.98	–17.7	...	...
00103709	6.02521	–71.97353	17.89	17.31	5806	4.02	–22.6	...	...
00104049	6.17200	–71.96964	17.89	17.32	5768	4.02	–24.2	0.65 ±0.06	0.62 ±0.10
00106794	6.47321	–72.18328	18.01	17.45	5789	4.08	–13.7	0.64 ±0.06	0.48 ±0.10
00107260	6.45896	–72.17064	17.92	17.37	5829	4.06	–15.7	...	0.40 ±0.10
00107528	6.57650	–72.16361	17.98	17.44	5923	4.11	–10.0	...	...
00107618	6.59092	–72.16119	17.92	17.37	5831	4.06	–24.4	0.34 ±0.06	...
00107866	6.56246	–72.15469	18.00	17.46	5727	4.06	–9.1	...	...

Star ID	RA (2000)	Dec. (2000)	B mag	I mag	$T_{\rm eff}$ K	$\log g$ [cgs]	$v_{\rm rad}$ km/s	[Mg/Fe] 1D NLTE	[K/Fe] 1D NLTE
00108171	6.40738	–72.14778	17.93	17.38	5812	4.06	–9.1	...	0.34 ±0.10
00108389	6.58104	–72.14253	17.93	17.38	5808	4.05	–18.2	...	0.47 ±0.10
00109441	6.53275	–72.11814	17.91	17.36	5875	4.07	–21.8	...	...
00109777	6.50933	–72.11058	17.95	17.41	5873	4.09	–19.8	...	0.50 ±0.10
00110197	6.60008	–72.10139	17.97	17.42	5824	4.08	–16.6	...	...
00111136	6.48775	–72.08114	17.92	17.36	5908	4.08	–29.9	...	0.35 ±0.10
00111231	6.52613	–72.07919	17.94	17.37	5732	4.03	–11.5	...	...
00112473	6.59492	–72.05506	17.90	17.35	5840	4.05	–17.3	0.40 ±0.06	0.21 ±0.10
00112684	6.46096	–72.05136	17.89	17.33	5780	4.03	–29.1	...	0.44 ±0.10
00113090	6.47025	–72.04353	17.95	17.39	5794	4.05	–15.4	...	0.44 ±0.10
00113841	6.55175	–72.02800	17.95	17.39	5854	4.07	–23.5	...	0.36 ±0.10
00113959	6.49396	–72.02594	17.93	17.38	5968	4.10	–27.4	...	0.49 ±0.10
00115880	6.51471	–71.98331	17.94	17.37	5845	4.06	–13.7	...	0.36 ±0.10
10000002	5.43304	–72.05411	17.96	17.40	5894	4.09	–6.8	...	0.31 ±0.10
10000004	5.62229	–72.10428	17.94	17.39	5934	4.10	–22.7	0.36 ±0.06	0.28 ±0.10
10000008	5.70025	–72.15828	18.05	17.49	5905	4.13	–17.9	...	0.34 ±0.10
10000009	5.70075	–72.09483	18.03	17.48	5792	4.09	–7.2	...	...
10000012	5.70475	–72.08533	17.85	17.29	5836	4.03	–19.0	...	...
10000015	5.72129	–72.07636	17.91	17.33	5754	4.02	–8.1	...	...
10000016	5.72533	–72.02817	17.87	17.28	5724	3.98	–6.7	...	...
10000020	5.75263	–72.06483	18.00	17.46	5834	4.10	–21.9	0.36 ±0.06	0.23 ±0.10
10000022	5.76167	–72.04869	17.85	17.27	5749	3.99	–17.5	0.63 ±0.06	...
10000026	5.77117	–72.12517	17.97	17.41	5784	4.06	–9.8	0.52 ±0.06	0.20 ±0.10
10000027	5.77721	–72.12919	18.00	17.44	5829	4.08	–20.4	0.40 ±0.06	...
10000036	5.84604	–72.00550	17.90	17.33	5706	4.00	–25.4	...	...
10000038	5.86846	–72.19789	17.83	17.25	5810	4.00	–5.1	0.36 ±0.06	0.35 ±0.10
10000041	5.90950	–71.93806	17.93	17.37	5889	4.08	–27.4	...	...
10000043	5.94513	–72.17733	17.95	17.37	5883	4.05	–20.9	0.73 ±0.06	0.54 ±0.10
10000048	5.99058	–71.98381	17.93	17.36	5832	4.05	–22.2	...	0.45 ±0.10
10000049	6.00479	–72.18656	18.03	17.49	5935	4.14	–15.5	0.31 ±0.06	...
10000053	6.04242	–72.20942	17.93	17.38	5881	4.08	–20.0	0.41 ±0.06	0.47 ±0.10
10000057	6.08746	–71.93789	18.02	17.47	5846	4.10	–18.2	0.36 ±0.06	0.45 ±0.10
10000062	6.12154	–71.97469	17.98	17.43	5891	4.10	–13.3	...	0.49 ±0.10
10000068	6.15775	–71.95836	17.95	17.38	5923	4.09	–21.8	0.28 ±0.06	0.49 ±0.10
10000072	6.19088	–71.97972	18.01	17.46	5829	4.09	–17.1	0.50 ±0.06	0.37 ±0.10

Star ID	RA (2000)	Dec. (2000)	B mag	I mag	$T_{\rm eff}$ K	$\log g$ [cgs]	$v_{\rm rad}$ km/s	[Mg/Fe] 1D NLTE	[K/Fe] 1D NLTE
10000073	6.21196	–72.00553	17.85	17.29	5855	4.03	–24.5	...	...
10000075	6.24354	–71.96136	17.95	17.38	5882	4.08	–23.4	0.31 ±0.06	0.47 ±0.10
10000079	6.27275	–72.12033	18.03	17.50	5750	4.09	–29.6	...	0.41 ±0.10
10000086	6.30192	–72.05958	17.86	17.29	5708	3.99	–7.4	0.26 ±0.06	0.30 ±0.10
10000088	6.31217	–72.03944	18.00	17.45	5771	4.07	–16.0	0.43 ±0.06	0.30 ±0.10
10000090	6.34033	–71.96881	17.92	17.36	5921	4.08	–15.3	0.53 ±0.06	0.34 ±0.10
10000094	6.42554	–72.07425	18.01	17.46	5869	4.10	–20.8	0.37 ±0.06	0.30 ±0.10
Average								0.47	0.39
SD								0.12	0.09

VILNIAUS UNIVERSITETAS
FIZINIŲ IR TECHNOLOGIJOS MOKSLŲ CENTRAS

Algimantas
ČERNIAUSKAS

Galaktikos kamuolinio žvaigždžių spiečiaus Tukano 47 cheminės ir kinematinės savybės

DAKTARO DISERTACIJOS SANTRAUKA

Fiziniai mokslai,
fizika (02 P)

VILNIUS 2018

Tyrimo motyvacija

Mūsų Galaktikos kamuoliniai žvaigždžių spiečiai (GKŽS) yra masyvios (10^4-$10^6\,M_\odot$) ir kompaktiškos (pusės-šviesio spindulys 1-17 pc) žvaigždžių sistemos (van den Bergh 2010). Galaktikoje yra žinoma ∼150 kamuolinių žvaigždžių spiečių (Harris 1996), bet tikėtina, kad dalis jų dar neatrasta (Ivanov ir Borissova 2002). Nors individualių spiečių metalingumai apima platų intervalą ($-2,37 \leq$ [Fe/H] $\leq 0,00$, Harris 1996), iki šiol manyta, kad konkretaus spiečiaus žvaigždėms turėtų būti būdinga vienoda cheminė sudėtis, atitinkanti tarpžvaigždinio debesies, iš kurio formavosi šio spiečiaus žvaigždės, sudėtį (Elmegreen ir Efremov 1997). Pastarųjų dviejų dešimtmečių tyrimai parodė, kad praktiškai visiems iki šiol tirtiems spiečiams būdingi jas sudarančių žvaigždžių cheminės sudėties ir, galbūt, amžiaus skirtumai (platesnė apžvalga pateikiama Gratton ir kt. 2012; Bastian ir Lardo 2017).

Pirmosios prielaidos, kad GKŽS yra gerokai sudėtingesnės žvaigždžių sistemos nei manyta anksčiau, rėmėsi lengvųjų cheminių elementų (C, N, O) gausų tyrimais pavienių žvaigždžių, priklausiančių skirtingiems spiečiams, atmosferose (Bell ir Dickens 1980; Kraft 1994). Šie tyrimai parodė, kad kamuoliniams spiečiams būdinga didelė (iki 1 dex) CNO elementų gausų sklaida. Išsamūs pastarojo dešimtmečio spektriniai darbai atskleidė, kad GKŽS būdingi ir kitų lengvųjų cheminių elementų (Li, Na, Mg, Al) gausų skirtumai (Gratton ir kt. 2004, 2012), be to, pastebimos gan aiškios šių elementų gausų koreliacijos (Na–Al, Carretta ir kt. 2011) bei antikoreliacijos (O–Na, Carretta ir kt. 2009a). Taip pat nustatyta, kad skirtinga chemine sudėtimi charakterizuojamos spiečių žvaigždės skiriasi ir savo kinematinėmis savybėmis, pvz., spiečiaus žvaigždėms, kurios turi didžiausią Na ir mažiausią O gausą, būdinga koncentracija centrinėje dalyje bei didesnė radialinio greičio dispersija (Lardo ir kt. 2011; Bellazzini ir kt. 2012; Kučinskas ir kt. 2014). Fotometriniai GKŽS tyrimai taip pat parodė, kad praktiškai visiems spiečiams būdingos išplitusios pagrindinės sekos spalvos-ryškio diagramose, o kai kuriais atvejais jos netgi suskyla į kelias, aiškiai išskiriamas sekas (Hartwick ir McClure 1972; Lardo ir kt. 2011; Piotto ir kt. 2015). Šiuo metu manoma, kad tai lemia helio gausos skirtumai skirtingų to paties spiečiaus žvaigždžių (nuo TO iki RGB) atmosferose (Salaris ir kt. 2006).

Iki šiol buvo pasiūlyti keli GKŽS raidos scenarijai, remiantis kuriais bandyta paaiškinti aukščiau minėtas spiečių cheminės sudėties ir juos sudarančių žvaigždžių kinematinių savybių anomalijas. Kadangi šios anomalijos būdingos praktiškai visiems GKŽS, teoriniai spiečių raidos scenarijai turi būti pakankamai universalūs, t. y., paaiškinti lengvųjų elementų sklaidos ir šių elementų gausų koreliacijų egzistavimą spiečiuose, kurių masės ir

metalingumai kinta plačiuose intervaluose. Vienas iš tokių scenarijų, kartais vadinamas asimptotinės milžinių sekos (angl. *asymptotic giant branch*, AGB) scenarijumi, teigia, kad anksčiausiai susiformavę, t. y., masyviausios (7-9 $M_{\odot}$), spiečiaus AGB žvaigždės praranda dalį savo medžiagos, kuri lėtai pasklinda spiečiaus viduje. Ši medžiaga spiečiaus tarpžvaigždinėje erdvėje gali išlikti pakankamai ilgai, todėl iš jos palaipsniui pradeda formuotis naujos (antros) kartos žvaigždės, kurių atmosferos yra praturtintos cheminiais elementais, susintetintais pirmosios kartos žvaigždėse (Renzini 2008; Bekki 2010). Kitame scenarijuje, kuriame taip pat prognozuojamas antros kartos žvaigždžių formavimasis, svarbiausią vaidmenį atlieka masyvios, greitai besisukančios žvaigždės (FRMS scenarijus). Pasiūlyta ir daugiau scenarijų, kuriuos bandyta taikyti interpretuojant stebimas spiečių savybes, pvz., praturtinimo cheminiais elementais dvinarių žvaigždžių sistemose scenarijus (de Mink ir kt. 2009), ankstyvojo disko akrecijos scenarijus (Bastian ir kt. 2013).

Nepaisant to, nei vienas iki šiol pasiūlytų GKŽS raidos modelių negali pilnai paaiškinti visų aukščiau minėtų lengvųjų cheminių elementų gausų anomalijų, stebimų kamuoliniuose spiečiuose. Daugelyje iki šiol atliktų tyrimų buvo apsiribojama vien cheminių elementų gausų analize, tačiau nebuvo detaliau nagrinėjamos skirtinga lengvųjų cheminių elementų gausa pasižyminčių žvaigždžių kinematinės savybės. Galiausiai, kadangi bent keli scenarijai gan sėkmingai paaiškina stebimas lengvųjų cheminių elementų anomalijas, žinios, kurios apima informaciją tik apie šių elementų gausas, neleidžia identifikuoti būtent kuris iš šių scenarijų (ar kokiomis proporcijomis) lėmė kamuolinių spiečių evoliuciją.

Siekiant geriau suprasti GKŽS raidos ypatumus, disertacijoje buvo atliktas Na, Mg bei iki šiol mažai spiečių raidos kontekste tyrinėtų K ir Zn gausų tyrimas Galaktikos kamuolinio spiečiaus 47 Tucanae (47 Tuc) pagrindinės sekos posūkio taško (angl. *main sequence turn-off point*, TO) ir raudonųjų milžinių sekos (angl. *red giant branch*, RGB) žvaigždžių atmosferose. Šį pasirinkimą lėmė keletas priežasčių:

1. Fotometriniai ir spektriniai 47 Tuc tyrimai parodė, kad šiame spiečiuje egzistuoja kelios žvaigždžių populiacijos, kurioms būdinga skirtinga lengvųjų cheminių elementų bei helio gausa (žr., pvz., Milone ir kt. 2012; Carretta ir kt. 2009a). Atlikus pirmuosius sąsajų tarp cheminės ir kinematinės 47 Tuc žvaigždžių raidos tyrimus nustatyta, kad šio spiečiaus žvaigždėms, charakterizuojamoms skirtinga lengvųjų cheminių elementų gausa, būdingos ir skirtingos kinematinės savybės (Bellazzini ir kt. 2012; Kučinskas ir kt. 2014);

2. 47 Tuc yra vienas artimiausių kamuolinių spiečių ($d = 4,5$ kpc, McDonald ir kt. 2011), todėl tai vienas iš nedaugelio spiečių, kuriuose galima atlikti ne tik RGB, bet ir TO žvaigždžių spektrinius tyrimus bei, panaudojant šių žvaigždžių aukštos skyros spektrus, nustatyti tikslias cheminių elementų gausas jų atmosferose. Šiame kontekste itin

svarbi TO žvaigždžių tyrimo galimybė, kadangi jų atmosferos nėra praturtintos cheminiais elementais, kurie patenka į atmosferą iš gilesnių žvaigždės sluoksnių maišymosi procesų metu (kaip, pvz., RGB žvaigždėse pirmojo susimaišymo, ang. *first dredge - up*, metu), todėl TO žvaigždžių cheminė sudėtis turėtų atitikti medžiagos, iš kurios šios žvaigždės formavosi, cheminę sudėtį;

3. 47 Tuc yra vienas masyviausių mūsų Galaktikos spiečių ($7 \times 10^5\,M_\odot$, Baumgardt 2017), be to, jam būdingas gan ilgas relaksacijos charakteringas laikas, $t_{\rm rh}$= 3,0 mlrd. m. (Harris 1996). Tikėtina, kad dėl šios priežasties skirtinga chemine sudėtimi pasižyminčios šio spiečiaus žvaigždės gali būti nepilnai susimaišiusios kinematiniu požiūriu (žr., pvz., Vesperini ir kt. 2013), todėl šiame spiečiuje dar galima tikėtis aptikti sąsajas tarp spiečiaus žvaigždžių cheminės sudėties bei šių žvaigždžių kinematinių savybių;

4. Tyrimo metu buvo siekiama nustatyti ne tik Na ir Mg, bet ir K gausą šio spiečiaus TO ir RGB žvaigždžių atmosferose, bei Zn gausą RGB žvaigždėse. Pastarųjų dviejų cheminių elementų branduolinė sintezė vyksta skirtingų tipų žvaigždėse, todėl nauji faktai apie galimas jų gausų koreliacijas su lengvųjų elementų gausomis gali suteikti papildomos informacijos apie žvaigždes-teršėjas, kurių branduolinės sintezės produktais buvo praturtintos antrosios kartos žvaigždžių atmosferos.

Siekiant atlikti homogenišką cheminių elementų gausų analizę Na, Mg, K ir Zn gausa 47 Tuc žvaigždžių atmosferose buvo nustatyta naudojant tuos pačius analizės metodus, taikant vienmačius (1D) hidrostatinius žvaigždžių atmosferų modelius bei 1D LTE (angl. *local thermodynamic equilibrium*, LTE) ir 1D NLTE (angl. *non-local thermodynamic equilibrium*, NLTE) gausų analizės priemones. Šioje santraukoje pateikiami pagrindiniai tyrimo tikslai ir uždaviniai, bei apibendrinami tyrimo metu gauti rezultatai.

Tyrimo tikslas

Nustatyti Na, Mg, K ir Zn gausą Galaktikos kamuoliniame žvaigždžių spiečiuje 47 Tuc, atlikti spiečiaus žvaigždžių cheminių ir kinematinių savybių bei sąsajų tarp jų analizę.

Uždaviniai

1. Panaudojant 1D/3D hidrostatinius/hidrodinaminius žvaigždžių atmosferos modelius bei 1D NLTE/LTE teorinio spektro skaičiavimo metodiką, nustatyti Na, Mg, K ir Zn gausą Galaktikos kamuolinio spiečiaus 47 Tuc pagrindinės sekos posūkio taško (TO) ir raudonųjų milžinių sekos (RGB) žvaigždžių atmosferose.

2. Nustatyti kosminės sklaidos (angl. *intrinsic spread*) vertes šiems cheminiams elementams: Mg ir K - TO žvaigždėse, Na, Mg, K ir Zn - RGB žvaigždėse.

3. Apskaičiuoti 1D NLTE–LTE gausos pataisas Na, Mg ir K ir ištirti NLTE efektų įtaką Na I, Mg I ir K I spektro linijų formavimuisi 47 Tuc TO ir RGB žvaigždžių atmosferose.

4. Ištirti galimas sąsajas tarp Na, Mg, K ir Zn gausų 47 Tuc žvaigždėse, atlikti sąsajų tarp šių elementų gausų ir žvaigždžių kinematinių savybių analizę.

Ginami teiginiai

1. Nustatyta 1D NLTE Na, Mg ir K, bei 1D LTE Zn gausa 47 Tuc RGB žvaigždžių atmosferose, vidutinės tirtų cheminių elementų ir geležies gausos santykių vertės yra: $[\mathrm{Na/Fe}] = 0,42 \pm 0,13$ (imties dydis - 30 žvaigždžių), $[\mathrm{Mg/Fe}] = 0,41 \pm 0,11$ (25 žvaigždės), $[\mathrm{K/Fe}] = 0,05 \pm 0,14$ (28 žvaigždės) ir $[\mathrm{Zn/Fe}] = 0,11 \pm 0,09$ (27 žvaigždės).

2. Nustatyta 1D NLTE Mg ir K gausa 47 Tuc TO žvaigždžių atmosferose, vidutinės šių cheminių elementų ir geležies gausos santykių vertės yra: $[\mathrm{Mg/Fe}] = 0,47 \pm 0,12$ (53 žvaigždės) ir $[\mathrm{K/Fe}] = 0,39 \pm 0,09$ (75 žvaigždės).

3. 1D NLTE–LTE gausos pataisų, vertės Na I ($\lambda = 568,26$ nm ir $\lambda = 568,82$ nm), Mg I ($\lambda = 769,16$ nm) ir K I ($\lambda = 769,89$ nm) spektro linijoms yra neigiamos ir mažėja didėjant šiame darbe tirtų RGB žvaigždžių T_{eff} ir $\log g$. Pataisos, kai $T_{\mathrm{eff}} = 4390$ K, $\log g = 1,6$ [cgs], yra: $-0,28$ dex (Na), $-0,08$ dex (Mg), $-0,55$ dex (K), o $T_{\mathrm{eff}} = 4720$ K, $\log g = 2,3$ [cgs] atveju pataisos: $-0,19$ dex (Na), $-0,01$ dex (Mg), $-0,40$ dex (K).

4. 1D NLTE–LTE gausos pataisų vertės Mg I ($\lambda = 769,16$ nm) ir K I ($\lambda = 769,89$ nm) linijoms išlieka pastovios šiame darbe tirtų 47 Tuc TO žvaigždžių atmosferos parametrų

intervale. Pataisų vertės, kaip $T_{\rm eff} = 5690\,{\rm K}$, $\log g = 4,0$ [cgs], yra $-0,03$ dex (Mg), -0.48 dex (K), o kai $T_{\rm eff} = 5940\,{\rm K}$, $\log g = 4,1$ [cgs], pataisų vertės yra $-0,02$ dex (Mg), -0.50 dex (K).

5. 47 Tuc RGB žvaigždėse Mg kosminės sklaidos vertė yra $\sigma^{\rm int}([{\rm Mg/Fe}]) = 0,08 \pm 0,02$ dex (įskaičius matavimų paklaidas). K gausos ateju kosminės sklaidos nėra, $\sigma^{\rm int}([{\rm K/Fe}]) = 0,00 \pm 0,05$ dex, todėl visos registruojamos sklaidos priežastis - gausos matavimo paklaidos.

6. 47 Tuc TO žvaigždėse Mg gausos atveju kosminės sklaidos vertė yra $\sigma^{\rm int}([{\rm Mg/Fe}]) = 0,09 \pm 0,01$ dex (įskaičius matavimų paklaidas). K gausos atveju kosminės sklaidos nėra, $\sigma^{\rm int}([{\rm K/Fe}]) = 0,00 \pm 0,03$ dex, o visa registruota sklaida atsiranda dėl gausos nustatymo paklaidų.

7. Vidutinė [Zn/Fe] gausos santykio vertė 47 Tuc RGB žvaigždžių atmosferose, $\langle[{\rm Zn/Fe}]\rangle^{\rm 1D\ LTE} = 0,11 \pm 0,09$ (27 objektai), statistiškai nesiskiria nuo vidutinės [Zn/Fe] vertės, nustatytos to paties metalingumo Galaktikos lauko žvaigždėse, $\langle[{\rm Zn/Fe}]\rangle^{\rm 1D\ LTE} = 0,15 \pm 0,14$ (19 objektų).

Publikacijos disertacijos tema Clarivate Analytics WoS žurnaluose

1. **Černiauskas, A.**, Kučinskas, A., Klevas, J., Prakapavičius, D., Korotin, S. A., Bonifacio, P., Ludwig, H.-G., Caffau, E., Steffen, M. 2017, *Abundances of Na, Mg, and K in the atmospheres of red giant branch stars of Galactic globular cluster 47 Tucanae* // Astronomy and Astrophysics, 604, A35.

2. **Černiauskas, A.**, Kučinskas, A., Klevas, J., Dobrovolskas, V., Korotin, S. A., Bonifacio, P., Ludwig, H.-G., Caffau, E., Steffen, M. 2018, *Abundances of Mg and K in the atmospheres of turn-off stars in Galactic globular cluster 47 Tucanae* // Astronomy and Astrophysics, spaudoje (DOI: https://doi.org/10.1051/0004-6361/201731659).

3. **Černiauskas, A.**, Kučinskas, A., Klevas, J., Bonifacio, P., Ludwig, H.-G., Caffau, E., Steffen, M. 2018, *Abundance of Zinc in the atmospheres of red giant branch stars of Galactic globular cluster 47 Tucanae* // Astronomy and Astrophysics, spaudoje (DOI: https://doi.org/10.1051/0004-6361/201833255).

Kitos publikacijos Clarivate Analytics WoS žurnaluose

1. Kučinskas, A., Dobrovolskas, V., **Černiauskas, A.**, Tanabé, T. 2008, *Properties of Red Giant Branches of Star Clusters in the Magellanic Clouds and Their Relation with Cluster Metallicity* // Baltic Astronomy, 17, 363–372.

Pranešimai konferencijose disertacijos tema

1. **Černiauskas, A.**, Kučinskas, A., Klevas, J., Prakapavičius, D., Korotin, S. A., Bonifacio, P., Ludwig, H.-G., Caffau, E., Steffen, M. 2018, *Abundance of K in the Galactic globular cluster 47 Tuc: current status and future challenges* // COST ChETEC WG3 workshop, Vilnius, Kovo 14–16, 2018 (žodinis pranešimas).

2. **Černiauskas**, A. and Kučinskas, A., Bonifacio, P., Andrievsky, S. M., Korotin, S. A., Dobrovolskas, V. 2014 *Light element abundances in the Galactic globular cluster 47 Tuc* // International conference "Metal Production and Distribution in a Hierarchical Universe", Spalio 21-25, 2013, Paryžius (Prancūzija). MmSAI, 85, 291 (stendinis paranešimas).

3. **Černiauskas, A.**, Kučinskas, A., Bonifacio, P., Andrievsky, S., Korotin, S., Dobrovolskas, V., 2013 *Chemical evolution of light elements in the Galactic globular cluster 47 Tuc* // "40th Lithuanian National Physics Conference", birželio 10–12, 2013, Vilnius, (stendinis paranešimas; programa ir pranešimų tezės, Vilniaus universitetas, psl. 226).

Mokslinis naujumas

Disertacijoje pateiktų rezultatų naujumą sudaro:

1. Panaudojant 1D NLTE metodologiją, atliktas sistemingas ir homogeniškas K ir Mg gausų tyrimas kol kas didžiausioje Galaktikos kamuolinio žvaigždžių spiečiaus 47 Tuc TO žvaigždžių imtyje.

2. Zn gausa nustatyta 27 RGB žvaigždžių atmosferose, tai kol kas didžiausia RGB žvaigždžių imtis priklausanti spiečiui 47 Tuc, kurioje nustatyta Zn gausa. Tyrimas parodė, kad Zn gausa 47 Tuc RGB žvaigždėse yra labai artima Galaktikos lauko žvaigždžių vidutinei vertei. Tai reiškia, kad šio elemento nukleosintezė šiame spiečiuje vyko tokio paties tipo žvaigždėse kaip ir Galaktikos lauko žvaigždžių populiacijose.

3. Pirmą kartą ištirtos cheminių elementų K ir Zn bei Na ir Mg gausos TO ir RGB žvaigždėse bei jų sąsajos su šių žvaigždžių kinematinėmis savybėmis. Remiantis atliktu tyrimu galima teigti, kad nėra statistiškai reikšmingo sąryšio tarp darbe nustatytų cheminių elementų gausos ir RGB bei TO žvaigždžių kinematinių savybių.

4. Suskaičiuotas naujas 1D NLTE–LTE kalio gausų pataisų tinklas RGB žvaigždėms, panaudojant atnaujintą kalio atomo modelį, ATLAS9 hidrostatinius žvaigždžių atmosferos modelius bei MULTI programų paketą.

Asmeninis indėlis

Autorius atliko archyvinių spektrų, gautų 2dF/HERMES spektrografu, pirminio apdorojimo darbus bei nustatė 32 RGB žvaigždžių atmosferų parametrus, atliko 1D hidrostatinių žvaigždžių atmosferos modelių bei 1D NLTE teorinio spektro skaičiavimus, nustatė Na, Mg ir K 1D NLTE gausą 47 Tuc RGB žvaigždžių atmosferose bei įvertino gausų matavimo paklaidas. Autorius taip pat atliko Mg I ir K I linijų 1D NLTE teorinio spektro skaičiavimus, nustatė Mg ir K gausą 75 TO žvaigždžių atmosferose bei įvertino gausų matavimo paklaidas. Kartu su bendraautoriais, atliko vidinės cheminių elementų gausų sklaidos TO ir RGB žvaigždžių atmosferose, bei galimų sąsajų tarp cheminių elementų gausų šių žvaigždžių atmosferose ir kinematinių žvaigždžių parametrų analizę (straipsnio bendraautoriai suformulavo tyrimo tikslus ir uždavinius, sukūrė tyrimo metu naudotas 1D NLTE gausų analizės bei vidinės gausų sklaidos skaičiavimo priemones, apskaičiavo 3D hidrodinaminius atmosferos modelius ir 3D–1D LTE gausos pataisas Na I, Mg I ir K I spektro linijoms). Šios tyrimo dalies rezultatai apibendrinti dviejuose moksliniuose straipsniuose, Černiauskas ir kt. (2017) ir Černiauskas ir kt. (2018a), atitinkamai pirmasis ir antrasis straipsniai publikacijų disertacijos tema Clarivate Analytics WoS žurnaluose sąraše). Autorius taip pat atliko

47 Tuc 32 žvaigždžių archyvinių spektrų, gautų 2dF/HERMES spektrografu, pirminio apdorojimo darbus bei nustatė šių žvaigždžių atmosferų parametrus, atliko 1D hidrostatinių žvaigždžių atmosferos modelių bei 1D NLTE teorinio spektro skaičiavimus, nustatė Zn 1D LTE gausą šių žvaigždžių atmosferose bei įvertino gausų matavimo paklaidas, kartu su bendraautoriais atliko vidinės cheminių elementų gausų sklaidos bei galimų sąsajų tarp Zn ir kitų cheminių elementų Na, Mg ir K gausų bei kinematinių žvaigždžių parametrų analizę (straipsnio bendraautoriai suformulavo tyrimo tikslus ir uždavinius, apskaičiavo 3D hidrodinaminius atmosferos modelius ir 3D–1D LTE gausos pataisas Na I, Mg I ir K I spektro linijoms). Šios tyrimo dalies rezultatai apibendrinami moksliniame straipsnyje Černiauskas ir kt. (2018b), trečiasis straipsnis publikacijų disertacijos tema Clarivate Analytics WoS žurnaluose sąraše.

Rengiant disertaciją, autorius sukūrė Python paprogrames, kurias taikant galima pusiau automatiniu būdu nustatyti žvaigždžių efektinę temperatūrą ir mikroturbulencijos greitį, panaudojant ATLAS9 ir SYNTHE programų paketus bei Fe I linijų ekvivalentinio pločio matavimų rezultatus. Autorius taip pat sukūrė Python paprogrames, kurios suteikia galimybę MULTI programų paketą naudoti pusiau automatiniu būdu, keičiant įvesties parametrus viename įvesties faile.

1 Cheminių elementų gausų analizės metodai ir programinė įranga

Disertacijoje naudoti archyviniai spektriniai 47 Tuc TO ir RGB žvaigždžių stebėjimai buvo gauti 2dF/HERMES (AAT teleskopas, Siding Spring observatorija, Australija) ir FLAMES/GIRAFFE (VLT-UT2 teleskopas, Europos pietinė observatorija, Čilė) spektrografais. Abu spektrografai yra šviesolaidiniai ir daugiaobjektiniai, o tai leidžia stebėti vienu metu daugiau kaip šimtą objektų. Šiame darbe cheminių elementų gausų nustatymui panaudoti 1D hidrostatiniai ATLAS9 atmosferų modeliai, teorinio spektro linijų skaičiavimai buvo atliekami naudojant SYNTHE (1D LTE) ir MULTI (1D NLTE) programų paketus. Konvekcijos įtakos tiriamų cheminių elementų spektro linijų formavimosi įvertinimui ir 3D–1D gausų pataisų įverčių skaičiavimui buvo naudojami 3D hidrodinaminiai CO^{5}BOLD ir 1D hidrostatiniai LHD atmosferų modeliai.

Spektriniai stebėjimai

Cheminių elementų Na, Mg ir K gausų spiečiaus 47 Tuc RGB žvaigždžių atmosferose tyrime (2 Santraukos skyrius) buvo naudojami archyviniai 2dF/HERMES (R = 28 000) spektriniai stebėjimai, gauti 2013 metais spalio 22 d. - gruodžio 19 d. (viso 32 žvaigždės). Na atveju, spektrai gauti 564,9 - 587,3 nm intervale (dvi Na I linijos), Mg ir K atveju - 758,5 - 788,7 nm intervale (po vieną Mg I ir K I linijas). Zn gausos tyrime, panaudotas 471,5 - 490,0 nm spektro intervalas. Visais atvejais ekspozicijos trukmė buvo 1200 s. Spektrų redukcija atlikta naudojant 2dfdr[1] programų paketą bei šių stebėjimų metu gautų 25 dangaus spektrų rinkinį.

Atliekant Mg ir K gausų tyrimą TO žvaigždžių atmosferose (3 Santraukos skyrius) panaudoti archyviniai FLAMES/GIRAFFE (R=5500-65 000) spektrografu gauti spektrai. Šiame tyrime nagrinėta ta pati žvaigždžių imtis kaip ir Dobrovolskas ir kt. (2014). Tiriamų cheminių elementų spektro linijos yra HR18 spektro intervale (746,8 - 788,9 nm), spektro skyra ties šio intervalo viduriu R = 18 000. Šios imties žvaigždžių spektrai ir 16 dangaus spektrų gauti 2008 rugpjūčio 18-20 (stebėjimų programos numeris: 081.D-0287(A)).

Žvaigždžių atmosferų parametrai

47 Tuc RGB žvaigždžių efektinė temperatūra nustatyta panaudojant fotometrinius stebėjimų duomenis iš Bergbusch ir Stetson (2009) katalogo ir $T_{\rm eff} - (V - I)$ kalibraciją iš Ramírez ir Meléndez (2005). Prieš taikant šią kalibraciją, fotometriniai žvaigždžių duomenys pakoreguoti dėl tarpžvaigždinio paraudonavimo, laikant, kad $E(B - V) = 0,04$, o spalvos ekscesų santykis $E(V - I)/E(B - V) = 1,33$ (Bergbusch ir Stetson 2009). Laisvojo kritimo pagreitis žvaigždžių paviršiuje buvo įvertintas pasinaudojant M, L ir $T_{\rm eff}$ sąryšiu.

[1] https://www.aao.gov.au/science/software/2dfdr

Žvaigždžių šviesis nustatytas panaudojant geriausiai derančią 12 mlrd. m., [Fe/H] = –0.5 izochroną (Yi ir kt. 2001), absoliutusis ryškis V apskaičiuotas laikant, kad atstumo modulis yra $V - M_V = 13,37$ (Harris 1996). Tyrime pasirinktų žvaigždžių masės kinta labai nedideliame intervale, $\Delta M \sim 0,01\,M_\odot$ (žr. Yi ir kt. 2001), todėl laikyta, kad visų pasirinktų žvaigždžių masė yra vienoda ir lygi 0,9 $M_\odot$. Dėl mažo Fe I linijų skaičiaus stebėtame spektro ruože, mikroturbulencijos greitis nebuvo nustatomas individualiai kiekvienai žvaigždei, o pasirinkta viena, visoms žvaigždėms vienoda vertė, 1,5 km/s. Šios vertės pasirinkimą lėmė tai, kad panašiame efektinės temperatūros intervale esančioms to paties spiečiaus RGB žvaigždėms kiti autoriai gauna labai panašias vidutinės mikroturbulencijos greičio vertes (žr., pvz., Carretta ir kt. 2009a; Cordero ir kt. 2014).

TO žvaigždžių efektinė temperatūra buvo paimta iš Dobrovolskas ir kt. (2014) darbo, kur ji nustatyta priderinant teorinį Hα linijos profilį prie šios linijos sparnų, stebimų tiriamų TO žvaigždžių spektruose. Laisvojo kritimo pagreičio logaritmo, $\log g$, vertė įvertinta 1.1 sąryšiu (disertacijos 1.3 skyrius), o nustatant cheminių elementų gausą buvo taikyta ta pat, fiksuota, mikroturbulencijos greičio vertė, $\xi_t = 1,0$ km/s, kuri buvo gauta Dobrovolskas ir kt. (2014).

Žvaigždžių atmosferų modeliai

Disertacijoje buvo naudojami tiek 3D hidrodinaminiai, tiek ir 1D hidrostatiniai žvaigždžių atmosferų modeliai, kurie buvo taikomi sprendžiant skirtingus uždavinius. Pvz., 1D žvaigždžių atmosferų modeliai ATLAS9 (Kurucz 1993) buvo naudojami nustatant cheminių elementų gausą 47 Tuc žvaigždžių atmosferose.

Kitas 1D hidrostatinių atmosferų modelių tipas, kuris buvo naudotas šiame darbe, yra LHD atmosferų modeliai (Caffau et al. 2008). Šiuos modelius charakterizuoja trys pagrindiniai parametrai: $T_{\rm eff}$, $\log g$bei cheminė sudėtis. Svarbu paminėti, kad skaičiuojant šiuos modelius naudojama ta pati būsenos lygtis bei neskaidrumų lentelės (angl. *opacity tables*) kaip ir 3D hidrodinaminių CO^{5}BOLD žvaigždžių atmosferų modelių skaičiavimuose (žr. žemiau), todėl taikant CO^{5}BOLD ir LHD atmosferų modelius galima atlikti diferencialinę spektro linijų formavimosi analizę, pvz., siekiant įvertinti konvekcijos įtaką žvaigždės atmosferos struktūrai ir stebimoms savybėms (Kučinskas ir kt. 2013).

3D hidrodinaminių žvaigždžių atmosferų modelių skaičiavimui buvo naudojamas CO^{5}BOLD programų paketas. Esminis skirtumas tarp 3D hidrodinaminių ir 1D hidrostatinių žvaigždžių atmosferų modelių yra tas, kad 3D modeliuose sprendžiamos hidrodinamikos ir spinduliuotės pernašos lygtys, kurių kintamieji priklauso nuo erdvinių ir laiko koordinačių, todėl tai gerokai prailgina vieno žvaigždės atmosferos modelio skaičiavimo laiką. Kitas svarbus aspektas yra tas, kad 3D modeliuose žvaigždės atmosferoje tiesiogiai modeliuojamas nelokalus procesas - konvekcija (t. y., ji nėra aprašoma parametrizuotai, kaip 1D hidrostatinių modelių atveju), kuri, savo ruožtu, daro įtaką žvaigždės spinduliuotės srautui ir spektro linijų formavimuisi.

Tiriant cheminių elementų gausą 47 Tuc RGB žvaigždžių atmosferose (2 ir 4 Santraukos skyriai), kiekvienai žvaigždei buvo skaičiuojamas konkrečių atmosferos parametrų ATLAS9 modelis

Linux aplinkai pritaikytu programų paketu (Sbordone ir kt. 2004). Modeliams skaičiuoti naudotos ODFNEW neskaidrumų lenteles (Castelli ir Kurucz 2003) su α–proceso metu sintetinamų cheminių elementų gausų santykiu [α/Fe] =+0,4. Tiriant Mg ir K gausas TO žvaigždžių imtyse buvo naudojami ATLAS9 žvaigždžių atmosferų modeliai (3 Santraukos skyrius). Skaičiuojant šiuos modelius buvo naudojamas tas pats globalių parametrų (metalingumas, α–elementų gausa ir t.t.) rinkinys kaip ir RGB žvaigždėse, tačiau buvo parenkamos konkrečios, kiekvieną individualią TO žvaigždę atitinkančios $T_{\rm eff}$ ir $\log g$ vertės.

Svarbu pabrėžti, kad LHD ir CO^{5}BOLD modeliai nebuvo skaičiuojami kiekvienai imties žvaigždei atskirai, tyrime buvo naudojami atmosferos parametrų erdvėje tiriamoms žvaigždėms artimiausi modeliai iš CIFIST modelių banko (Ludwig ir kt. 2009).

Teorinio spektro skaičiavimo programų paketai

1D LTE cheminių elementų gausos nustatymui buvo naudojamas SYNTHE programų paketas (Kurucz ir Furenlid 1979; Sbordone ir kt. 2004). Šis programų rinkinys skirtas skaičiuoti teoriniams žvaigždžių spektrams, panaudojant šiam tikslui 1D hidrostatinius žvaigždžių atmosferos modelius ATLAS9. Kitas šiame darbe naudotas teorinio spektro skaičiavimo paketas, Linfor3D, suderinamas tiek su LHD tiek su CO^{5}BOLD žvaigždžių atmosferų modeliais ir jį galima naudoti skaičiuojant tiek 3D/1D LTE, tiek ir 3D/1D NLTE spektro linijų profilius.

1D NLTE cheminių elementų gausų nustatymui buvo naudotas MULTI programų paketas, kuris pritaikytas darbui su 1D hidrostatiniais ATLAS9 žvaigždžių atmosferų modeliais. Atliekant šį tyrimą buvo naudojami keli skirtingi atomų modeliai: Na atomo modelį (Korotin et al. 1999) sudaro 20 Na I lygmenų ir pagrindinis Na II lygmuo, iš viso atsižvelgiama į tarp 46 lygmenų vykstančius spindulinius (angl. *radiative transitions*) šuolius. Mg atomo modelį sudaro 84 Mg I, 12 Mg II lygmenys bei pagrindinis Mg III lygmuo, atliekant atomo lygmenų užpildų (angl. *level population numbers*) skaičiavimus atsižvelgiama į 59 tarp lygmenų vykstančius šuolius. Išsamus šio atomo modelio aprašas bei testavimo rezultatai pateikiami Mishenina ir kt. (2004) darbe. K atomą sudaro 20 K I lygmenų ir pagrindinis K II lygmuo, iš viso įskaitomi 62 šuoliai tarp šių lygmenų; detaliau šis atomo modelis aptariamas Andrievsky ir kt. (2010).

Gausų matavimo paklaidos ir kosminė sklaida

Siekiant nustatyti disertacijoje tirtų cheminių elementų kosminę (angl. *intrinsic*) gausos sklaidą TO ir RGB žvaigždžių imtyse, buvo taikytas didžiausio tikėtinumo metodas (angl. *maximum–likelihood method*, ML metodas). Taikant ML metodą remtasi prielaida, kad cheminių elementų gausų skirstinys visoje žvaigždžių imtyje atitinka Gauso skirstinį. ML metodo pagalba buvo siekta įvertinti, ar stebimą tam tikro cheminio elemento gausos sklaidą lemia vien tik to cheminio elemento gausos paklaidos, ar, vis dėlto, egzistuoja ir kosminė šio elemento gausos sklaidos komponentė. Taikant šį metodą buvo naudojama tikėtinumo funkciją, kurios vertės buvo skaičiaujamos dvimačiame tinkle, apibrėžtame $\langle$[A/B]$\rangle$ ir $\sigma_{\rm int}$ parametrų parinkčių aibėmis. Vidutinė tiriamų

cheminių elementų gausų santykio bei gausų santykio kosminės sklaidos vertės buvo nustatomos ieškant maksimalios tikėtinumo funkcijos vertės šiame dvimačiame tinkle.

Darbo metu taip pat buvo įvertintos kiekvieno tirto cheminio elemento gausos paklaidų vertės, kurias lėmė žvaigždės atmosferos parametrų ($T_{\rm eff}$, $\log g$, ir $\xi_{\rm t}$) nustatymo ir kontinuumo padėties parinkimo paklaidos. RGB žvaigždėms buvo nustatytos tokios atmosferos parametrų paklaidų vertės: efektinės temperatūros $\sigma(T_{\rm eff}) = \pm 65$ K, paviršiaus pagreičio $\sigma(\log g) = \pm 0,1$ dex, mikroturbulencijos $\sigma(\xi_{\rm t}) = \pm 0,2$ km/s. TO žvaigždėms šios vertės atitinkamai buvo ± 100 K, $\pm 0,1$ dex, ir $\pm 0,15$ km/s. Cheminio elemento gausos paklaida dėl kontinuumo padėties netikslumo buvo vertinama atskirai kiekvienai spektro linijai.

2 Na, Mg ir K gausa 47 Tuc RGB žvaigždžių atmosferose

Neseniai atlikti Galaktikos kamuolinių žvaigždžių spiečių cheminės sudėties tyrimai parodė, kad Galaktikos kamuoliniuose spiečiuose NGC 2419 (Mucciarelli ir kt. 2012) ir NGC 2808 (Mucciarelli ir kt. 2015) gali egzistuoti Mg–K gausos antikoreliacija. Pastarųjų cheminių elementų tyrimai žvaigždžių spiečiuose leidžia plačiau pažvelgti į nukleosintezės procesus vykstančius šiose žvaigždėse, bei, lyginant stebėjimų rezultatus ir teorines prognozės, atrinkti labiausiai tikėtinus spiečių formavimosi ir raidos scenarijus. Šių darbų autoriai teigia, kad be jau minėtos Mg–K antikoreliacijos šiuose spiečiuose taip pat stebimos statistiškai reikšminga K–Na koreliacija bei Al–O antikoreliacija. Jei šios sąsajos tarp kalio ir Na, Mg gausų egzistuoja iš tikrųjų, tuomet būtų galima teigti, kad Na, Al ir K turėjo būti sintetinami tuose pačiuose objektuose, kurie galiausiai ir praturtino dalį spiečiaus žvaigždžių šiais cheminiais elementais. Tokia informacija būtų itin vertinga siekiant griežčiau apriboti galimus spiečių raidos scenarijus.

Vis dėlto, svarbu paminėti, kad NGC 2419 ir NGC 2808 spiečiuose žvaigždės yra gerokai praturtintos heliu: helio koncentracija spiečiuje NGC 2808 yra Y=0,34 (Marino ir kt. 2014), o NGC 2419 ši vertė lygi Y=0,42 (di Criscienzo ir kt. 2011). Tai gerokai didesnė helio gausa, nei stebima kituose Galaktikos spiečiuose (see, e.g., Milone ir kt. 2014). Be to, šie spiečiai yra vieni iš nedaugelio, kuriuose aptinkamos žvaigždės su santykinai dideliu Mg gausos trukumu, [Mg/Fe] $< -0,2$ (Mucciarelli ir kt. 2015). Siekiant geriau suprasti K raidos tendencijas kamuoliniuose spiečiuose, disertacijoje buvo atliktas kompleksinis Na, Mg ir K tyrimas Galaktikos kamuolinio spiečiaus 47 Tuc TO ir RGB žvaigždžių atmosferose.

Na, Mg ir K gausos tyrimas

Na, Mg ir K gausos tyrimas buvo atliktas panaudojant 32 RGB žvaigždžių archyvinius 2dF/HERMES spektrinių stebėjimų duomenis. Tipinis šių žvaigždžių signalo–triukšmo santykis tiriamoje spektro srityje (λ = 769,0-770,1 nm) yra $S/N \sim 50$. Žvaigždžių $T_{\rm eff}$ nustatyta taikant $T_{\rm eff} - (V-I)$ kalibraciją (Ramírez ir Meléndez 2005), fotometriniai tiriamų žvaigždžių duomenys buvo paimti iš Bergbusch ir Stetson (2009) katalogo, $\log g$ nustatytas pasinaudojant M, L ir $T_{\rm eff}$ sąryšiu. Visoms imties RGB žvaigždėms taikytos tos pačios metalingumo, $[{\rm Fe/H}]^{\rm 1D\ LTE} = -0,76$, vertės (Carretta ir kt. 2009a), ir mikroturbulencijos greičio, $\xi_{\rm mic} = 1,5\,{\rm km\ s^{-1}}$, vertė.

Šiame tyrime panaudoti ATLAS9 žvaigždžių atmosferų modeliai ir 1D NLTE MULTI teorinio spektro skaičiavimo programų paketas. Šio paketo pagalba buvo suskaičiuoti teoriniai kiekvienos spektro linijos profiliai skirtingoms cheminio elemento gausos bei makroturbulencijos greičio vertėms, ir, priderinant prie stebėto spektro linijos profilio, parinktas geriausiai stebėtą spektrą

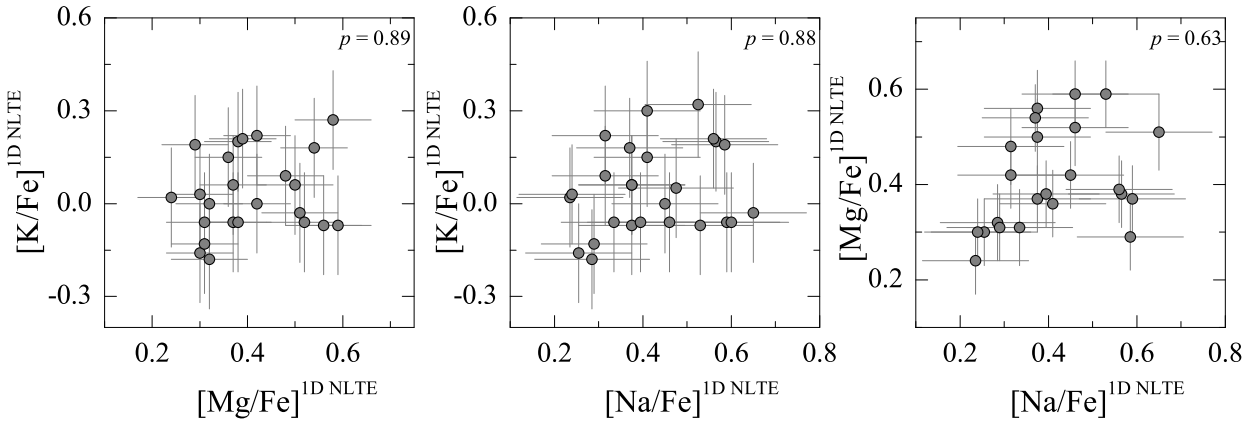

Fig. 1. Na, Mg, K ir geležies gausų santykiai 47 Tuc RGB žvaigždžių atmosferose. Atskirose paveikslo dalyse pateikiamos Student'o *t*-testo tikimybės *p* vertės, apskaičiuotos panaudojant Pearson' tiesinės koreliacijos koeficientą bei gausų paklaidas *x* ir *y* ašyse.

atitinkantis teorinis linijos profilis. Tyrimo metu nustatyti Na, Mg ir K geležies gausų santykiai pateikiami 1 pav.

Darbe tirtų cheminių elementų 3D–1D LTE gausų pataisos apskaičiuotos panaudojant 3D hidrodinaminius $\mathrm{CO^5BOLD}$ ir 1D hidrostatinius LHD žvaigždžių atmosferų modelius, o teorinio spektro linijų skaičiavimai atlikti naudojant $\mathrm{Linfor3D}$ programų paketą (1.5.3 disertacijos skyrius). Visų darbe naudotų spektro linijų 3D–1D LTE pataisos yra teigiamos ir neviršija +0,07 dex. Šie rezultatai rodo, kad konvekcijos įtaka darbe naudotų Na I, Mg I ir K I spektro linijų formavimuisi yra nedidelė. Kita vertus, NLTE efektų įtaka Na I ir K I spektro linijų formavimuisi gerokai didesnė: 1D NLTE–LTE gausos pataisos šiems elementams yra neigiamos ir gali siekti atitinkamai iki $-0,25$ ir $-0,55$ dex. Mg linijoms ši pataisa mažesnė ir neviršija $-0,08$ dex.

Rezultatai

Šiame darbe nustatytos vidutinės 1D NLTE Na, Mg ir K gausos 47 Tuc RGB žvaigždžių atmosferose, atitinkamai, yra $\langle$[Na/Fe]$\rangle = 0,42 \pm 0,13$, $\langle$[Mg/Fe]$\rangle = 0,41 \pm 0,11$ ir $\langle$[K/Fe]$\rangle = 0,05 \pm 0,14$ (skaičiai po ± ženklo atitinka visos žvaigždžių imties standartinio nuokrypio vertę). Šios vidutinės gausų vertės gerai dera su kitų autorių nustatytomis vertėmis (Carretta ir kt. 2013). Kita vertus, tyrimo metu nustatyta šiek tiek didesnė Mg gausos sklaida tiriamos imties žvaigždžių atmosferose, kurią galėjo lemti kiek didesnės sistematinės paklaidos nustatant šio elemento gausą, o pastarąsias, savo ruožtu, galėjo apspręsti kiek prastesnė spektrų kokybė.

ML testo rezultatai parodė, kad [Mg/Fe] santykio kosminė sklaida, lygi $0,08 \pm 0,02$ dex. Kalio gausai, vidinės sklaidos vertė yra lygi $0,00 \pm 0,05$ dex, todėl stebimą šio elemento sklaidą tiriamoje RGB žvaigždžių imtyje gali lemti vien gausų matavimų paklaidos.

Remiantis 1 pav. pateiktais rezultatais galima teigti, 47 Tuc RGB žvaigždėse nėra statistiškai reikšmingo sąryšio tarp [Na/Fe], [Mg/Fe] ir [K/Fe] gausų santykių. Tai rodo Student'o *t*-testo rezultatai, kuriuo buvo įvertinta tikimybė, *p*, kad Pearson'o koreliacijos koeficiento, *r*, vertė, apskaičiuota konkrečioje *x*-*y* koordinatėje, gali būti gaunama atsitiktinai. Visais atvejais, statistiškai

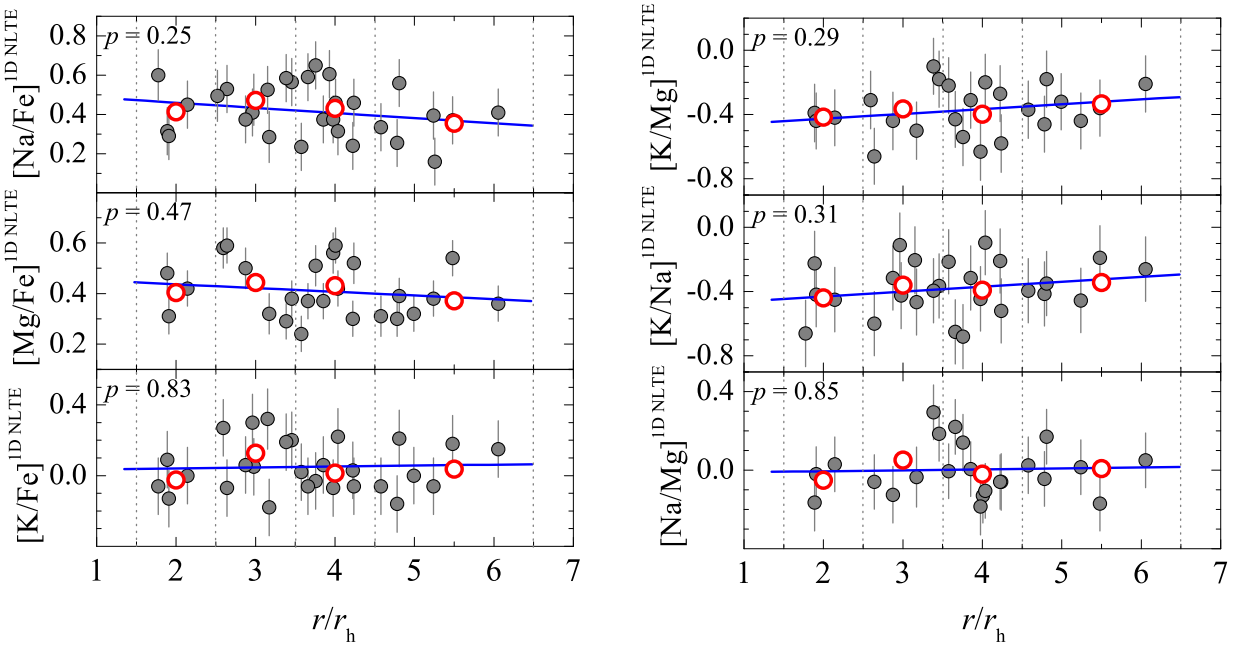

Fig. 2. Na, Mg, K ir geležies gausos santykiai (kairėje), bei lengvųjų elementų tarpusavio santykiai (dešinėje), pateikiami kaip atstumo nuo spiečiaus centro funkcija. Paveiksluose atstumas iki spiečiaus centro išreikštas $r/r_{\rm h}$ santykiniais vienetais, kur $r_{\rm h}$ yra 47 Tuc pusės masės spindulys ($r_{\rm h} = 174''$, Trager ir kt. 1993. Tuščiaviduriai simboliai žymi vidutines vertes, apskaičiuotas $\Delta r/r_{\rm h} = 1$ pločio nepersiklojančiuose intervaluose, paskutinis intervalas dvigubai didesnis. Mėlyna ištisinė linija - geriausiai deranti tiesė, priderinta panaudojant visus matavimus. Student'o t-testo tikimybės p vertės, apskaičiuotos panaudojant Pearson' tiesinės koreliacijos koeficientą, pateikiamos atskirai kiekvienoje paveikslo dalyje.

reikšmingos koreliacijos tarp Na ir Mg gausų neaptikta. Panaši tendencija stebima ir 2 pav., kuriame atvaizduota tiriamų cheminių elementų gausų santykių priklausomybė nuo atstumo iki spiečiaus centro. Verta pažymėti, kad toks rezultatas [Na/Fe] gausos santykiui gerai dera su Kučinskas ir kt. (2014) išvadomis, gautomis tiriant 102 47 Tuc TO žvaigždes, kai taip pat nebuvo aptikta statistiškai reikšmingos priklausomybės tarp [Na/Fe] gausos santykio ir atstumo iki spiečiaus centro.

Siekiant patikrinti, ar egzistuoja sąsajos tarp Na, Mg ir K gausos 47 Tuc žvaigždžių atmosferose ir šių žvaigždžių kinematinių savybių, buvo apskaičiuotas tiriamų RGB žvaigždžių absoliutusis radialinis greitis, $|\Delta v_{\rm r}| \equiv \left|v_{\rm rad} - \langle v_{\rm rad}\rangle^{\rm clust}\right|$, kur $v_{\rm rad}$ yra konkrečios žvaigždės radialinis greitis ir $\langle v_{\rm rad}\rangle^{\rm clust} = -18,6$ km/s yra vidutinė imties žvaigždžių radialinio greičio vertė (šios tyrimo dalies metodika pateikta Kučinskas ir kt. 2014). Gautos absoliučiojo radialinio greičio vertės atvaizduotos atžvilgiu Na, Mg ir K ir geležies gausos santykio bei Na, Mg ir K gausų tarpusavio santykio 3 pav. Nei vienu atveju sąsajų tarp cheminių ir kinematinių 47 Tuc RGB žvaigždžių savybių aptikta nebuvo.

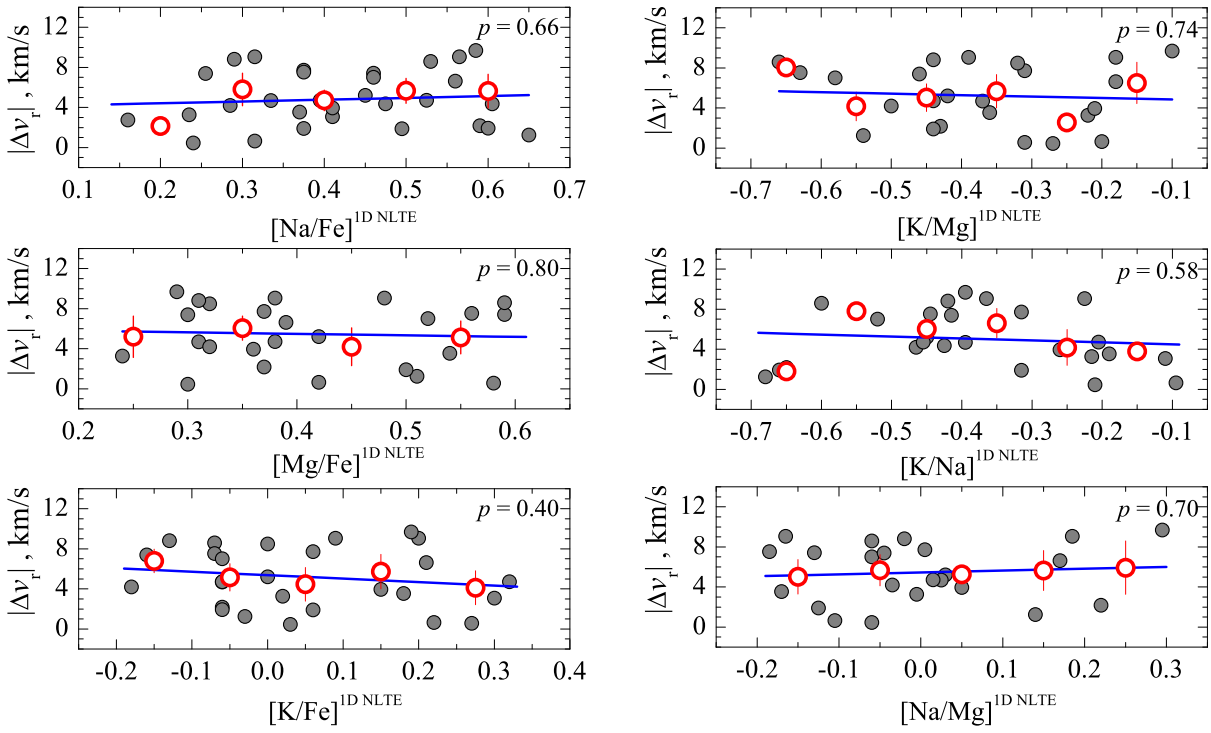

Fig. 3. 47 Tuc RGB žvaigždžių absoliučiojo radialinio greičio vertės kaip cheminių elementų gausų santykių funkcija. Individualių žvaigždžių matavimus žymi pilki pilnaviduriai apskritimai, vidutinės radialinio greičio vertės, apskaičiuotos 0,1 dex pločio gausų santykių intervaluose pavaizduotos raudonais apskritimais. Mėlyna ištisinė linija - geriausiai deranti tiesė, priderinta naudojant visus individualių žvaigždžių matavimus. Atskirose paveikslo dalyse pateikiamos Student'o *t*-testo tikimybės *p* vertės, apskaičiuotos panaudojant Pearson' tiesinės koreliacijos koeficientą.

3 Mg ir K gausa 47 Tuc TO žvaigždžių atmosferose

Iki šiol kalio gausa 47 Tuc buvo tirta tik 3 šio spiečiaus žvaigždėse (Carretta ir kt. 2013). Pagrindinės sekos žvaigždės itin įdomios spiečių raidos tyrimų kontekste, kadangi jų išorinėje dalyje esantis konvekcinis sluoksnis neprasiskverbia pakankamai giliai į žvaigždės vidinius sluoksnius, kuriuose vyksta protonų pagavos reakcijos, todėl šių žvaigždžių atmosferose esančių cheminių elementų gausa turėtų atitikti pirminio dujų ir dulkių debesies, iš kurio formavosi šios žvaigždės, cheminę sudėtį. Be abejo, ši prielaida negalioja jei šių žvaigždžių atmosferos buvo praturtintos cheminiais elementais, kurie buvo susintetinti kitose žvaigždėse. Būtent dėl šios priežasties TO žvaigždžių tyrimai gali suteikti vertingos informacijos apie spiečių cheminės raidos ypatumus. Siekiant nuodugniau ištirti cheminių elementų raidos tendencijas šiame spiečiuje, disertacijoje buvo atliktas Mg ir K gausos tyrimas atitinamai 53 ir 75 47 Tuc TO žvaigždžių atmosferose.

Mg ir K gausos tyrimas

Tiriant Mg ir K gausą 47 Tuc TO žvaigždžių atmosferose buvo panaudoti tie patys archyviniai spektriniai stebėjimai kaip ir D'Orazi ir kt. (2010) bei Dobrovolskas ir kt. (2014) darbuose. Svarbu paminėti, kad šiuose ankstesniuose darbuose Mg ir K gausa nebuvo nustatinėjama. Iš viso šios stebėjimų programos metu buvo gauta 116 žvaigždžių ir 16 dangaus fono spektrų. Mg ir K 1D NLTE gausos nustatytos panaudojant 1D hidrostatinius ATLAS9 atmosferų modelius bei MULTI teorinio spektro skaičiavimo programų paketą. Šių cheminių elementų 3D–1D LTE gausų pataisos apskaičiuotos panaudojant 3D hidrodinaminius CO^{5}BOLD bei 1D hidrostatinius LHD atmosferų modelius, o teorinių spektro linijų profilių skaičiavimai atlikti Linfor3D programų paketu.

Žvaigždžių atmosferų parametrai, $T_{\rm eff}$ ir $\log g$, paimti iš Dobrovolskas ir kt. (2014), tyrimo metu buvo naudojamos tos pačios Mg I ir K I spektro linijos kaip ir RGB žvaigždžių imtyje. Visoms imties žvaigždėms buvo laikoma, kad mikroturbulencijos greitis yra 1,0 km s^{-1} , o metalingumas, kaip ir RGB imtyje, $[{\rm Fe/H}]^{\rm 1D\ LTE} = -0,76$. K ir Mg 1D NLTE gausos TO žvaigždžių atmosferose nustatytos prie stebimo spektro linijos priderinant teorinį linijos profilį, kuris buvo apskaičiuotas panaudojant MULTI programų paketą. Siekiant išlaikyti gausų analizės TO ir RGB žvaigždžių imtyse homogeniškumą, MULTI pakete naudoti tie patys Mg ir K atomo modeliai.

Šioje tyrimo dalyje naudotų Mg I ir K I spektro linijų 3D–1D LTE pataisos Mg atveju yra teigiamos ir neviršija +0,05 dex, tuo tarpu K linijoms jos neigiamos ir gali siekti iki –0,09 dex. Gauti rezultatai rodo, kad konvekcijos įtaka tyrime naudotų Mg I ir K I spektro linijų formavimuisi nėra didelė. Kita vertus, NLTE efektų įtaką K I spektro linijų formavimuisi yra didelė: 1D NLTE–LTE gausos pataisa yra neigiama ir gali siekti iki $-0,5$ dex. Mg gausai, šių efektų svarba mažesnė: 1D NLTE–LTE gausos pataisos dydis Mg I linijoms neviršija 0,05 dex.

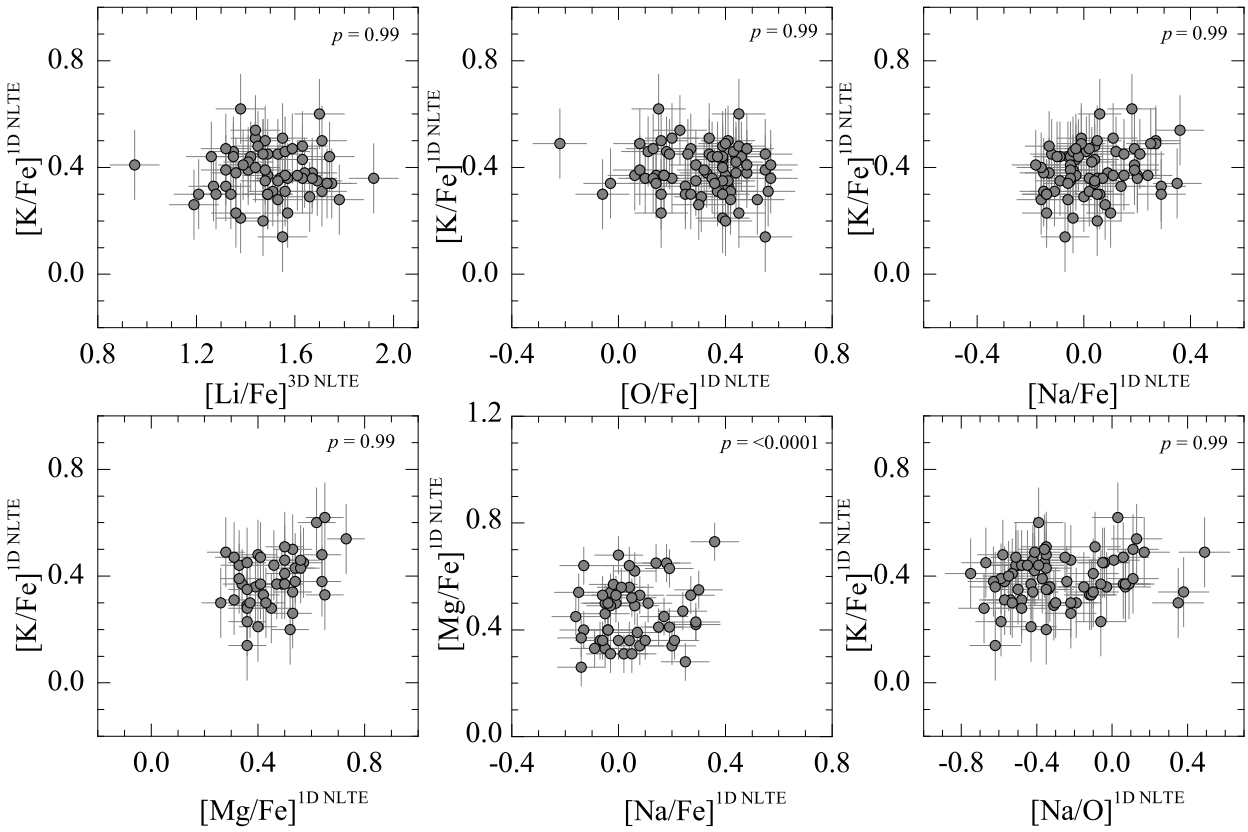

Fig. 4. Lengvųjų cheminių elementų gausų santykiai 47 Tuc TO žvaigždžių atmosferose. Kiekvienoje paveikslo dalyje pateikiamos Student'o *t*-testo tikimybės *p* vertės, apskaičiuotos panaudojant Pearson' tiesinės koreliacijos koeficientą bei gausų paklaidas *x* ir *y* ašyse.

Rezultatai

Atliekant šį tyrimą nustatyti vidutiniai 1D NLTE [Mg/Fe] ir [K/Fe] gausų santykiai Galaktikos kamuolinio žvaigždžių spiečiaus 47 Tuc TO žvaigždžių atmosferose yra, atitinkamai, [K/Fe] = $0,39 \pm 0,09$ ir [Mg/Fe] = $0,47 \pm 0,12$ (skaičiai po ± ženklo atitinka visos žvaigždžių imties standartinio nuokrypio vertę).

Disertacijoje nustatytos Mg ir K gausų kosminės sklaidos vertės sutampa su analogiškomis vertėmis RGB žvaigždių imtyje (2 Santraukos skyrius). Kaip ir RGB žvaigždžėse, K kosminės sklaidos neaptikta, mūsų gauta vertė, $\sigma^{\rm int}$([K/Fe]) = $0,00 \pm 0,02$, sutampa tiek su nustatyta TO žvaigždėms, $\sigma^{\rm int}$([K/Fe]) = $0,00 \pm 0,05$, tiek ir su verte, kurią gavo Mucciarelli ir kt. (2017), $\sigma^{\rm int}$([K/Fe]) = $0,00 \pm 0,02$. Mg atveju gautas rezultatas taip pat dera su šiame darbe RGB žvaigždėms nustatyta verte, $\sigma^{\rm int}$([Mg/Fe]) = $0,08 \pm 0,02$. Kita vertus, [Na/Fe] gausos santykiui TO žvaigždžių atmosferose buvo nustatyta didesnė nei RGB žvaigždžių gausos sklaida, $\sigma^{\rm int}$([Na/Fe]) = $0,12 \pm 0,01$ (plg., RGB žvaigždėms $\sigma^{\rm int}$([Na/Fe]) = $0,04 \pm 0,05$). Pastarąjį rezultatą galima paaiškinti tuo, kad RGB žvaigždžių spektrų kokybė yra prastesnė nei TO žvaigždžių, o tai, savo ruožtu, lemia didesnes RGB žvaigždžių gausos paklaidas ir mažesnę vidinę gausos sklaidą bei didesnę pastarosios paklaidos vertę.

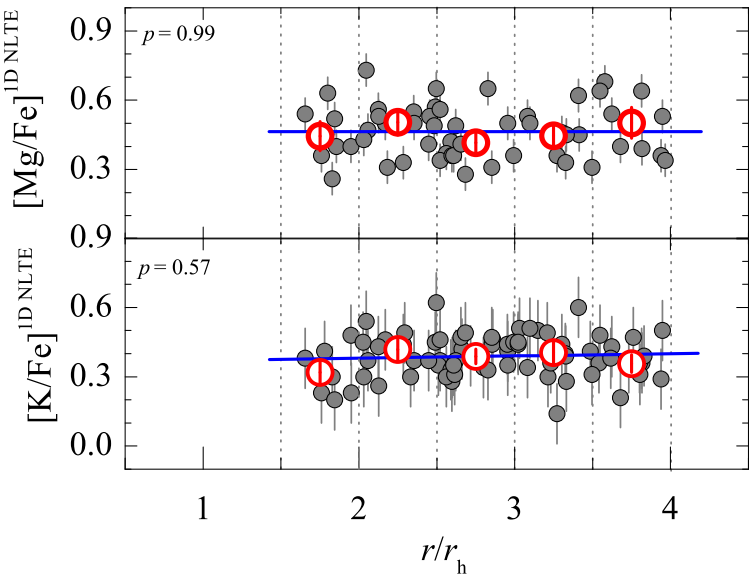

Fig. 5. [Mg/Fe] ir [K/Fe] gausų santykiai 47 Tuc TO žvaigždžių atmosferose kaip atstumo iki spiečiaus centro funkcija. Žvaigždės atstumas iki spiečiaus centro išreikštas $r/r_{\rm h}$ santykiniais vienetais, kur $r_{\rm h}$ yra 47 Tuc pusės masės spindulys, (Trager ir kt. 1993, $r_{\rm h} = 174''$). Tuščiaviduriai apskritimiai - lengvųjų cheminių elementų ir geležies santykio (kairėje) ir lengvųjų cheminių elemetų gausų tarpusavio santykio (dešinėje) vertės, apskaičiuotos $\Delta r/r_{\rm h} = 1$ pločio nepersiklojančiuose intervaluose. Mėlyna ištisinė linija - geriausiai deranti tiesė, priderinta panaudojant visus gausų santykių matavimus. Student'o t-testo tikimybės p vertės (pateiktos atskirai kiekvienoje šio paveikslo dalyje), apskaičiuotos panaudojant Pearson' tiesinės koreliacijos koeficientą.

Tikrinant ar egzistuoja sąsajos tarp skirtingų lengvųjų cheminių gausų, bei tarp cheminių elementų gausų ir spiečiaus žvaigždžių kinematinių savybių, buvo apskaičiuoti Pearson'o koreliacijos koeficientai. Siekiant įvertinti šių koeficientų statistinį reikšmingumą, taikant Student'o t-testą apskaičiuotos tikimybės, kad šios koeficientų vertės gali būti gautos atsitiktinai. Pirmiausia toks patikrinimas buvo atliktas naudojant duomenis, pavaizduotus 4 pav. Remiantis gautais rezultatais galima teigti, kad nėra statistiškai reikšmingo sąryšio K–Na koordinatėse. Statistiškai reikšmingos koreliacijos ar antikoreliacijos neaptiktos ir K–Mg koordinatėse.

5 pav. pateikta [Mg/Fe] ir [K/Fe] gausų santykių 47 Tuc TO žvaigždžių atmosferose kaip atstumo iki spiečiaus centro funkciją, kur $r/r_{\rm h}$ yra projekcinio atstumo iki spiečiaus centro, r, ir pusės masės spindulio, $r_{\rm h}$ (Trager ir kt. 1993, $r_{\rm h} = 174''$), santykis. Kaip ir anksteniame paveiksle, statistiškai reikšmingų sąryšių tarp cheminių elementų gausų santykių TO žvaigždžių atmosferose ir šių žvaigždžių projekcinio atstumo iki spiečiaus centro neaptikta.

Disertacijoje ištirtos galimos sąsajos tarp 47 Tuc TO žvaigždžių atmosferose nustatytų [Mg/Fe] ir [K/Fe] gausų santykių ir kinematinių šių žvaigždžių savybių, remiantis ankščiau RGB žvaigždėms taikyta metodika (Kučinskas ir kt. 2014, taip pat žr. šios santraukos 2 skyrių). Šiam tyrimui atlikti buvo naudojami TO žvaigždžių radialiniai greičiai, nustatyti Kučinskas ir kt. (2014) darbe, $|\Delta v_{\rm r}| \equiv \left|v_{\rm rad} - \langle v_{\rm rad}\rangle^{\rm clust}\right|$, kur $v_{\rm rad}$ individualių žvaigždžių radialinis greitis, o $\langle v_{\rm rad}\rangle^{\rm clust} = -18,6$ km/s žvaigždžių spiečiaus radialinis greitis. Student'o t-testo rezultatai rodo,

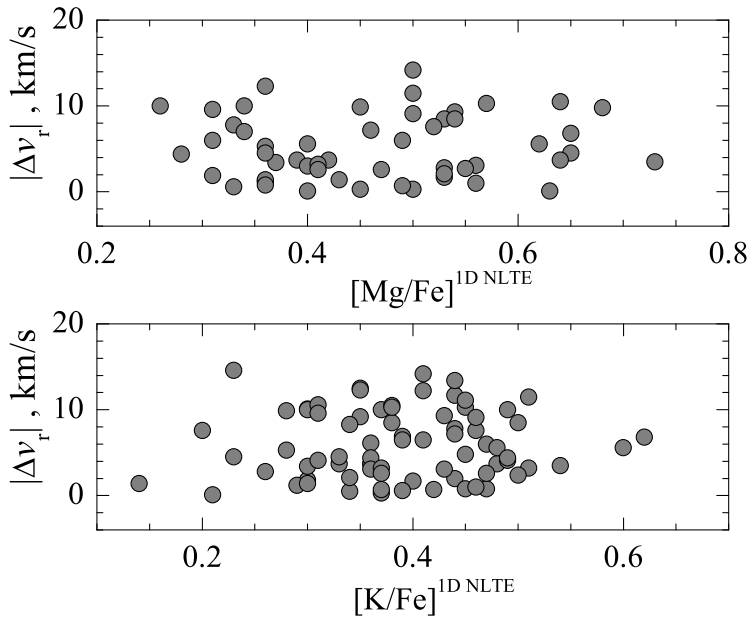

Fig. 6. Šiame darbe tirtų 47 Tuc TO žvaigždžių absoliutusis radialinis greitis kaip [Mg/Fe] (viršuje) ir [K/Fe] (apačioje) funkcija.

kad nėra statistiškai reikšmingo sąryšio tarp [Mg/Fe] bei [K/Fe] gausų santykio žvaigždės atmosferoje ir šios žvaigždės radialinio greičio.

Visais atvejais, išskyrus Mg–Na koordinates (4 pav.), *p*-reikšmės, apskaičiuotos naudojant Pearson'o koreliacijos koeficientus, yra labai panašios. Nepaisant to, pastarasis rezultatas nebūtinai reiškia tai, kad gali egzistuoti koreliacijos tarp šių elementų gausų santykių. Būtina pastebėti, kad K–Mg plokštumoje mažas *p* vertes lemia trys žvaigždės su didžiausia kalio gausa, tačiau jų gausų įverčiai nėra pakankamai patikimi, kadangi vienai iš jų K gausa, kitom dviem - Na - buvo nustatytos naudojant gan prastos kokybės spektro linijas. Pašalinus šias tris žvaigždes, gaunamos gerokai didesnės *p*–vertės. Analogiška situacija stebima ir K–Na plokštumoje, todėl, abiem atvejais, negalima tvirtai teigti, kad egzistuoja statistiškai reikšmingi sąryšiai tarp šių elementų gausų.

4 Cinko gausa 47 Tuc RGB žvaigždžių atmosferose

Astrofizikoje Zn tradiciškai traktuojamas kaip tarpinis elementas tarp geležies grupės ir lengvųjų *s*-proceso elementų. Zn gali būti sintetinamas vykstant įvairioms branduolinėms reakcijoms, pvz., II ir Ia tipo supernovose, vidutinės masės AGB žvaigždėse (*s*-procesas) ir masyvių, $M \geq 10$ $M_{\odot}$, žvaigždžių centrinėse dalyse (silpnasis *s*-procesas, angl. *weak s-process*; žr., pvz., Mishenina ir kt. 2002; Kobayashi ir kt. 2006).

Tai, kad Zn gali būti sintetinamas keliais skirtingais būdais ir skirtingų tipų objektuose, gali suteikti naujų galimybių tiriant Galaktikos kamuolinių spiečių cheminę raidą. Viename iš spiečių raidos scenarijų, kuris taikomas aiškinant kamuolinių spiečių žvaigždėse stebimas Na–O, Mg–Al antikoreliacijas, laikomasi prielaidos, kad antrosios kartos spiečiaus žvaigždės buvo užterštos cheminiais elementais, susintetintais pirmos kartos AGB žvaigždėse (Ventura ir kt. 2001). Kadangi Zn nukleosintezė gali vykti vidutinės masės (3–6 $M_{\odot}$) AGB žvaigždėse (Karakas ir kt. 2009), aptikus koreliacijas arba antikoreliacijas tarp Na, Mg, K ir Zn gausos būtų galima teigti, kad visi šie elementai buvo sintetinami tuose pačiuose objektuose, t. y., AGB žvaigždėse. Tokiu būdu, Zn gausos tyrimai kamuolinių spiečių žvaigždžių atmosferose galėtų suteikti papildomos informacijos apie žvaigždes, kurios branduolinės sintezės produktais buvo užterštos pirmosios kartos žvaigždžių.

Šiuo požiūriu, Galaktikos kamuolinis žvaigždžių spiečius 47 Tuc itin įdomus, kadangi jame ne tik stebimos įvairios koreliacijos ir/arba antikoreliacijos tarp lengvųjų cheminių elementų gausų (Carretta ir kt. 2009a; Dobrovolskas ir kt. 2014), bet jam būdingos ir sąsajos tarp šių elementų gausų spiečiaus žvaigždžių atmosferose bei šių žvaigždžių kinematinių savybių (Kučinskas ir kt. 2014). Nepaisant to, darbų, kuriuose buvo tiriama Zn gausa šio spiečiaus žvaigždėse, nėra daug, be to, šiuose tyrimuose naudotos palyginti nedidelės žvaigždžių imtys. Thygesen ir kt. (2014) nustatė Zn gausą 13 RGB žvaigždžių atmosferose, $[\mathrm{Zn/Fe}]^{\mathrm{1D\ LTE}} = 0,26 \pm 0,13$ (medianinė visos tirtų žvaigždžių imties vertė), ir nerado jokių šio cheminio elemento gausos astrofizikės sklaidos įrodymų. Duffau ir kt. (2017) nustatė Zn gausą 47 Tuc 19 RGB žvaigždžių atmosferose, gauta vidutinė gausos vertė yra $[\mathrm{Zn/Fe}]^{\mathrm{1D\ NLTE}} = 0,17 \pm 0,10$ (1D NLTE–LTE gausos pataisos Zn neviršija kelių šimtųjų dex). Zn gausos tyrimuose dažniausiai naudojamos dvi Zn I linijos, kurių centriniai bangos ilgiai yra 472,2 ir 481,0 nm. Šios linijos yra pakankamai stiprios didesnio metalingumo žvaigždžių spektruose ($W \approx 7$ - 8 pm Saulės spektre) ir labai nedaug blenduotos su silpnom linijom (Chen ir kt. 2004), todėl 47 Tuc RGB žvaigždėms jos gali būti sėkmingai naudojamos tiriant Zn gausą.

Zn gausos tyrimas

Zn gausos tyrimui panaudota ta pati 47 Tuc RGB žvaigždžių imtis kaip ir šios santraukos 2 skyriuje aprašytame Mg ir Na gausos tyrime. Šios žvaigždžių imties spektriniai stebėjimai gauti su

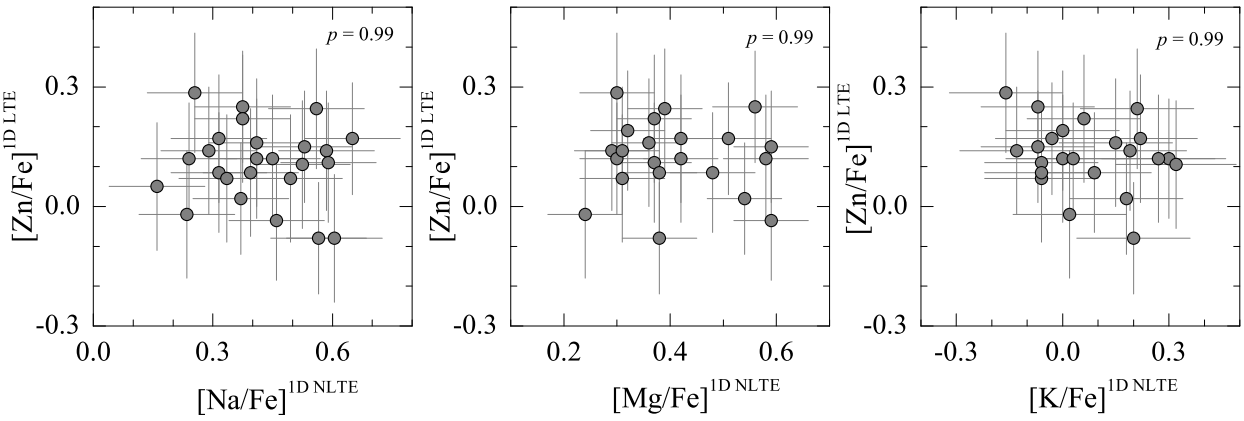

Fig. 7. Lengvųjų cheminių elementų [Na/Fe], [Mg/Fe] bei [K/Fe], [Zn/Fe] gausų santykiai 47 Tuc RGB žvaigždžių atmosferose. Skirtingose paveikslo dalyse pateikiamos Student'o *t*-testo tikimybės *p* vertės, apskaičiuotos panaudojant Pearson' tiesinės koreliacijos koeficientą.

2dF/HERMES spektrografu (AAT). Tiriamų žvaigždžių spektrai apima 471,5-490,0 nm bangos ilgių intervalą, spektrų $R \sim 28000$, ekspozicijos trukmė 1200 s. Tyrime naudotų RGB žvaigždžių atmosferos parametrų nustatymo procedūra aprašyta šios santraukos 2 skyriuje.

Zn gausa RGB žvaigždžių atmosferose nustatyta naudojant abi Zn I linijas, prie jų priderinant geriausiai stebėtus profilius atitinkantį teorinį žvaigždės spektrą. Atliekant Zn gausos matavimus, visoms imties žvaigždėms buvo taikomas fiksuotas 1,5 km s^{-1} mikroturbulencijos greitis bei metalingumas $[\mathrm{Fe/H}]^{\mathrm{1D\ LTE}} = -0,76$ (Carretta ir kt. 2009a). Šiame tyrime taip pat buvo naudojamos jau anksčiau disertacijoje nustatytos Na, Mg ir K 1D NLTE gausos. Nepaisant to, kad pastarųjų elementų gausos buvo nustatytos taikant 1D NLTE gausų analizės priemones, Zn 1D NLTE–LTE gausų pataisos, kaip jau buvo minėta, neviršija kelių šimtųjų dex (Duffau ir kt. 2017), todėl skaičiuojant cheminių elementų gausų santykius buvo naudotos Na, Mg ir K 1D NLTE gausos bei Zn 1D LTE gausa.

Zn gausos matavimų paklaidos buvo įvertintos panaudojant tą pačią paklaidų skaičiavimo metodiką, kuri taikyta ir kitų cheminių elementų (Na, Mg ir K) gausų paklaidų įvertinimui (1.7.1 disertacijos skyrius). Kadangi nustatant Zn gausą naudota ta pati žvaigždžių imtis, skaičiuojant Zn gausos paklaidą naudotos tos pačios atmosferos parametrų nustatymo paklaidos kaip ir šios santraukos 2 skyriuje aprašytame Na, Mg ir K gausos tyrime. Galutinė nustatyta Zn gausos paklaida 472,21 nm linijai yra 0,15 dex, o 481,05 nm linijai 0,14 dex.

Šioje tyrimo dalyje taip pat buvo ištirta, kokią įtaką Zn I spektro linijų formavimuisi daro konvekcija. Tai atlikta įvertinant šio elemento 3D–1D LTE gausos pataisą, $\Delta^{\mathrm{3D-1D\ LTE}}$, kurios skaičiavimo metodika smulkiau aprašyta santraukos 1 skyriuje. Nustatant gausos pataisas buvo naudojami 3D hidrodinaminiai CO^{5}BOLD ir 1D hidrostatiniai LHD žvaigždžių atmosferų modeliai, o skaičiuojant teorinius spektro linijų profilius panaudotas Linfor3D programų paketas. Abiems Zn linijoms šios pataisos yra teigiamos ir neviršija +0,05 dex, o tai rodo, kad konvekcijos įtaka šių linijų formavimuisi yra nedidelė.

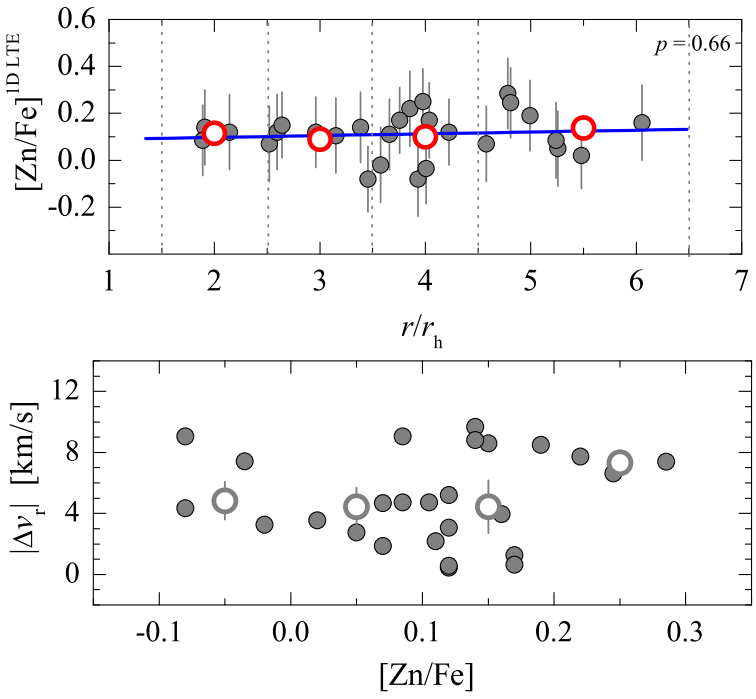

Fig. 8. [Zn/Fe] gausos santykis 47 Tuc RGB žvaigždžių atmosferose (27 objektai) kaip atstumo iki spiečiaus centro (viršuje) ir šių žvaigždžių absoliutus radialinis greičio (apačioje) funkcija.

Rezultatai

Disertacijoje nustatyta vidutinė 27 RGB žvaigždžių Zn–Fe santykio vertė yra $\langle[\mathrm{Zn/Fe}]\rangle^{\mathrm{1D\ LTE}} = 0,11 \pm 0,09$ (skaičiai po ± ženklo atitinka visos žvaigždžių imties standartinio nuokrypio vertę). Kadangi nustatyta gausos sklaidos vertė yra santykinai nemaža, buvo įvertinta kiek ją gali lemti kosminė Zn gausos sklaida. Taikant tą patį ML metodą kaip ir ankstesnėse tyrimo dalyse, nustatyta, kad kosminė Zn sklaidos vetė yra $\sigma^{\mathrm{int}}([\mathrm{Zn\ /Fe\ }]) = 0,00 \pm 0,04$, taigi, galima teigti, kad, paklaidų ribose, 47 Tuc RGB žvaigždėms būdinga ta pati Zn gausa, o nemažą Zn gausos sklaidą tirtoje žvaigždžių imtyje lemia šio elemento gausos matavimo paklaidos.

Kaip ir ankstesnėse tyrimo dalyse (2 ir 3 Santraukos skyriuose), taikant Student'o *t*-testą buvo ištirtos galimos sąsajos tarp Na, Mg, K ir Zn gausos įvairiose gausų santykių koordinatėse (7 pav). Statistiškai reikšmingų koreliacijų arba antikoreliacijų neaptikta. Analogiškai, tarp [Zn/Fe] verčių RGB žvaigždžių atmosferose ir šių žvaigždžių atstumo iki spiečiaus centro. Statistiškai reikšmingų sąsajų neaptikta ir $|\Delta v_{\mathrm{r}}|$–[Zn/Fe] koordinatėse.

Tyrimo metu nustatyta vidutinė Zn ir Fe gausos santykio 47 Tuc RGB žvaigždžių atmosferose vertė, $\langle[\mathrm{Zn/Fe}]\rangle^{\mathrm{1D\ LTE}} = 0,11 \pm 0,09$, gerai sutampa su ankstesniuose darbuose pateikiamomis vertėmis, gautomis tiriant mažesnes šio spiečiaus žvaigždžių imtis (plg., $[\mathrm{Zn/Fe}]^{\mathrm{1D\ LTE}} = 0,26 \pm 0,13$, Thygesen ir kt. 2014; $\langle[\mathrm{Zn/Fe}]\rangle^{\mathrm{1D\ NLTE}} = 0,17 \pm 0,10$, Duffau ir kt. 2017). Be to, disertacijoje nustatyta vidutinė Zn gausos vertė labai gerai dera su vidutine Zn gausos verte tokio paties metalingumo Galaktikos lauko žvaigždėse. Šis palyginimas buvo atliktas panaudojant [Zn/Fe] matavimus Galaktikos plonojo disko žvaigždžių atmosferose iš Allende Prieto ir kt.

(2004) (2 objektai), Bensby ir kt. (2014) (10 objektų) ir Mishenina et al. (2011) (7 objektai), atrenkant žvaigždes, kurių [Fe/H] vertės patenka į $\pm 3\sigma$ intervalą ($\pm 0,09$ dex) vidutinės [Fe/H] vertės 47 Tuc žvaigždžių atmosferose atžvilgiu, $\langle [\mathrm{Fe/H}] \rangle^{\mathrm{1D\ LTE}} = -0,76 \pm 0,03$ (Carretta ir kt. 2009a). Atrinktoje 19 Galaktikos lauko žvaigždžių imtyje nustatyta vidutinė Zn ir Fe santykio vertė, $\langle [\mathrm{Zn/Fe}] \rangle^{\mathrm{1D\ LTE}} = 0,15 \pm 0,14$, paklaidų ribose nesiskiria nuo disertacijoje gautos vidutinės vertės 47 Tuc RGB žvaigždžių atmosferose vertės, $\langle [\mathrm{Zn/Fe}] \rangle^{\mathrm{1D\ LTE}} = 0,11 \pm 0,09$. Taigi, apibendrinant, galima teigti, kad Zn nukleosintezė, 47 Tuc vyko tokio paties tipo objektuose kaip ir Galaktikos lauko žvaigždėse.

Pagrindiniai rezultatai ir išvados

Disertacijoje atliktas Na, Mg, K ir Zn gausos tyrimas Galaktikos kamuolinio žvaigždžių spiečiaus 47 Tuc TO ir RGB žvaigždžių atmosferose, nustatytos vidutinės šių cheminių elementų gausų vertės tiriamų žvaigždžių imtyse bei gausų kosminės sklaidos intervalai. Ištirti NLTE efektų bei konvekcijos įtaka tiriamų cheminių elementų spektro linijų formavimuisi, ištirtos sąsajos tarp skirtingų cheminių elementų gausų šio spiečiaus žvaigždžių atmosferose, atlikta sąsajų tarp cheminių elementų gausos bei šių žvaigždžių kinematinių savybių analizė. Tyrimas atliktas naudojant archyvinius spektrus, kurie gauti $2\mathrm{dF/HERMES}$ (AAT teleskopas, Australija) ir $\mathrm{FLAMES/GIRAFFE}$ (VLT teleskopas, Čilė) spektrografais. Nustatant cheminių elementų gausą bei atliekant konvekcijos ir NLTE efektų įtaką tiriamų cheminių elementų spektro linijų formavimuisi panaudoti klasikiniai vienmačiai (1D) hidrostatiniai ir trimačiai (3D) hidrodinaminiai žvaigždžių atmosferų modeliai. Teorinių spektrų linijų skaičiavimui 1D LTE atveju (Zn gausos nustatymui) panaudotas SYNTHE programų paketas, o 1D NLTE atveju (Na, Mg, K gausos nustatymui) - MULTI programų paketas.

Disertacijoje nustatytos vidutinės [Na/Fe], [Mg/Fe], [K/Fe] gausų santykių vertės 47 Tuc RGB žvaigždžių atmosferose atitinkamai yra $\langle[\mathrm{Na/Fe}]\rangle^{\mathrm{1D\ NLTE}} = 0,42 \pm 0,13$, $\langle[\mathrm{Mg/Fe}]\rangle^{\mathrm{1D\ NLTE}} = 0,41 \pm 0,11$, $\langle[\mathrm{K/Fe}]\rangle^{\mathrm{1D\ NLTE}} = 0,05 \pm 0,14$, $\langle[\mathrm{Zn/Fe}]\rangle^{\mathrm{1D\ LTE}} = 0,11 \pm 0,09$. Nustatyta tiriamų žvaigždžių atmosferose gali egzistuoti Mg gausos kosminė sklaida, kurios vertė lygi $\sigma^{\mathrm{int}}([\mathrm{Mg/Fe}]) = 0,08 \pm 0,02$ dex, tuo tarpu K šios sklaidos neaptika, $\sigma^{\mathrm{int}}([\mathrm{K/Fe}]) = 0,00 \pm 0,05$ dex. Disertacijoje alikto tyrimo rezultatai rodo, kad šio spiečiaus TO ir RGB imtyse nėra statistiškai reikšmingų sąryšių (t. y., koreliacijos arba antikoreliacijos) tarp [Na/Fe], [Mg/Fe] ir [K/Fe] gausų santykių. Tokių sąryšių neaptikta ir analizuojant sąsajas tarp šiame darbe nustatytų cheminių elementų gausų ir šių žvaigždžių atstumo iki spiečiaus centro bei jų kinematinių savybių.

Disertacijoje nustatytos [Mg/Fe] ir [K/Fe] gausų santykių vertės atitinkamai yra $\langle[\mathrm{Mg/Fe}]\rangle^{\mathrm{1D\ NLTE}} = 0,47 \pm 0,02$ (53 žvaigždės) ir $\langle[\mathrm{K/Fe}]\rangle^{\mathrm{1D\ NLTE}} = 0,39 \pm 0,09$ (75 žvaigždės). Mg atveju aptikta nedidelė šio elemento gausos kosminė sklaida, $\sigma^{\mathrm{int}}([\mathrm{Mg/Fe}]) = 0,08 \pm 0,02$, kurios vertė gerai dera su analogiška verte, nustatyta šiame darbe tiriant Mg gausą RGB žvaigždžių atmosferose. Kaip ir tirtose RGB žvaigždėse, K atveju kosminės sklaidos TO žvaigždžių imtyje neaptikta, $\sigma^{\mathrm{int}}([\mathrm{K/Fe}]) = 0,00 \pm 0,03$. Tyrimo metu nustatyta, kad TO žvaigždėse nėra statistiškai reikšmingų sąryšių tarp Na ir Mg gausų šių žvaigždžių atmosferose. Kaip ir RGB žvaigždėse, statistiškai reikšmingų sąryšių neaptikta ir tiriant sąsajas tarp šių elementų gausų TO žvaigždžių atmosferose iš šių žvaigždžių kinematinių savybių.

Zn gausos tyrime 47 Tuc RGB žvaigždžėse nustatyta vidutinė šio elemento ir geležies santykio vertė lygi $\langle[\mathrm{Zn/Fe}]\rangle^{\mathrm{1D\ LTE}} = 0,11 \pm 0,09$. Tyrimo metu gauta Zn gausos kosminė sklaidos vertė, $\sigma^{\mathrm{int}}([\mathrm{Zn/Fe}]) = 0,00 \pm 0,04$, rodo, kad, paklaidų ribose, tirtoms 47 Tuc RGB žvaigždėms būdinga ta pati Zn gausa. Analizuojant galimas Zn gausos sąsajas su Na, Mg ir K gausomis, statistiškai reikšmingų sąryšių neaptikta. Statistinės analizės rezultatai rodo, kad nėra ir statistiškai reikšmingų

sąsajų tarp Zn gausos šio spiečiaus RGB žvaigždžių atmosferose ir šių žvaigždžių kinematinių savybių.

Tyrimo metu atlikta NLTE efektų bei konvekcijos įtakos tirtų cheminių elementų spektro linijų formavimuisi 47 Tuc žvaigždžių atmosferose analizė parodė, kad Na ir K atvejais yra svarbūs NLTE efektai: 1D NLTE–LTE gausos pataisa K I linijai, stebimų TO žvaigždžių spektruose, gali siekti $-0,7$ dex tuo tarpu RGB žvaigždžių spektruose ši pataisa Mg I linijai yra $-0,25$, o K I linijai $-0,55$ dex. Analogiškos pataisos Mg atveju yra gerokai mažesnės ir neviršija 0,09 dex, tiek TO, tiek RGB žvaigždėms. Konvekcijos įtaka tirtų cheminių elementų linijoms taip pat nėra didelė: 3D–1D LTE gausos pataisos visiems trims elementams TO ir RGB žvaigždėse neviršija 0,1 dex.

Apibendrinant disertacijoje gautus rezultatus galima teigti, kad Na, Mg nukleosintezė 47 Tuc žvaigždėse nebuvo susijusi su K ir Zn nukleosintezė ir vyko skirtingų tipų žvaigždėse. Nustatytos vidutinės K ir Zn jų gausų vertės 47 Tuc žvaigždžių atmosferose, gerai dera su vertėmis, būdingomis to paties metalingumo Galaktikos lauko žvaigždėms, todėl tikėtina, kad šiame spiečiuje K ir Zn branduolinė sintezė vyko to paties tipo objektuose kaip ir Galaktikos lauko žvaigždėse.

Literatūra

Allende Prieto, C., Barklem, P. S., Lambert, D. L., ir Cunha, K. 2004, A&A, 420, 183

Andrievsky, S. M., Spite, M., Korotin, S. A., ir kt. 2010, A&A, 509, A88

Baumgardt, H. 2017, MNRAS, 464, 2174

Bastian, N., Lamers, H. J. G. L. M., de Mink, S. E., ir kt. 2013, MNRAS, 436, 2398

Bastian, N., ir Lardo, C. 2017, arXiv:1712.01286

Bensby, T., Feltzing, S., ir Oey, M. S. 2014, A&A, 562, A71

van den Bergh, S. 2010, AJ, 140, 1043

Bergbusch, P. A., ir Stetson, P. B. 2009, AJ, 138, 1455

Bell, R. A., ir Dickens, R. J. 1980, ApJ, 242, 657

Bellazzini, M., Bragaglia, A., Carretta, E., ir kt. 2012, A&A, 538, A18

Bekki, K. 2010, ApJ, 724, L99

Caffau, E., Ludwig, H.-G., Steffen, M., ir kt. 2008, A&A, 488, 1031

Carretta, E., Bragaglia, A., Gratton, R., ir kt. 2009a, A&A, 505, 117

Carretta, E., Lucatello, S., Gratton, R. G., ir kt. 2011, A&A, 533, A69

Carretta, E., Gratton, R., Bragaglia, A., ir kt. 2013, ApJ, 769, 40

Castelli, F., ir Kurucz, R. L. 2003, in Modeling of Stellar Atmospheres, eds. N. E. Piskunov, W. W. Weiss, ir D. F. Gray, Proc. IAU Symp. 210, poster, A20 (CD-ROM

Černiauskas, A., Kučinskas, A., Klevas, J., ir kt. 2017, A&A, 604, A35

Černiauskas, A., Kučinskas, A., Klevas, J., ir kt. 2018, spaudoje (https://doi.org/10.1051/0004-6361/201731659)

Černiauskas, A., Kučinskas, A., Klevas, J., ir kt. 2018, spaudoje (https://doi.org/10.1051/0004-6361/201833255)

Chen, Y. Q., Nissen, P. E., ir Zhao, G. 2004, A&A, 425, 697

Cordero, M. J., Pilachowski, C. A., Johnson, C. I., ir kt. 2014, ApJ, 780, 94

de Mink, S. E., Pols, O. R., Langer, N., ir Izzard, R. G. 2009, A&A, 507, L1

di Criscienzo, M., D'Antona, F., Milone, A. P., ir kt. 2011, MNRAS, 414, 3381

Dobrovolskas, V., Kučinskas, A., Bonifacio, P., ir kt. 2014, A&A, 565, A121

D'Orazi, V., Lucatello, S., Gratton, R., ir kt. 2010, ApJ, 713L, 1

Duffau, S., Caffau, E., Sbordone, L., ir kt. 2017, A&A, 604, 128

Elmegreen, B. G., ir Efremov, Y. N. 1997, ApJ, 480, 235

Gratton, R., Sneden, C., ir Carretta, E. 2004, ARA&A, 42, 385

Gratton, R. G., Villanova, S., Lucatello, S., ir kt. 2012, A&A, 544, A12

Harris, W. E. 1996, AJ, 112, 1487; internetinė versija:
http://physwww.mcmaster.ca/~harris/mwgc.dat

Hartwick, F. D. A., ir McClure, R. D. 1972, ApJ, 176, L57

Ivanov, V. D., ir Borissova, J. 2002, A&A, 390, 937

Karakas, A. I., van Raai, M. A., Lugaro, M., ir kt. 2009, ApJ, 690, 1130

Kobayashi, C., Umeda, H., Nomoto, K., ir kt. 2006, ApJ, 653, 1145

Korotin, S. A., Andrievsky, S. M., ir Luck, R. E. 1999, A&A, 351, 168

Kraft, R. P. 1994, PASP, 106, 553

Kučinskas, A., Steffen, M., Ludwig, H.-G., ir kt. 2013, A&A,, 549, A14

Kučinskas, A., Dobrovolskas, V., ir Bonifacio, P. 2014, A&A, 568, L4

Kurucz, R. L., ir Furenlid, I. 1979, SAO Special Report, 387

Kurucz, R. L. 1993, ATLAS9 Stellar Atmosphere Programs and 2 km s^{-1} Grid, CD-ROM No. 13 (Cambridge, Mass)

Lardo, C., Bellazzini, M., Pancino, E., ir kt. 2011, A&A, 525, A114

Ludwig, H.-G., Caffau, E., Steffen, M., ir kt. 2009, Memorie della Societa Astronomica Italiana, 80, 711

Marino, A. F., Milone, A. P., Przybilla, N., ir kt. 2014, MNRAS, 437, 1609

McDonald, I., Boyer, M. L., van Loon, J. T., ir kt. 2011, ApJS, 193, 23

Milone, A. P., Piotto, G., Bedin, L. R., ir kt. 2012, ApJ, 744, 58

Milone, A. P., Marino, A. F., Dotter, A., ir kt. 2014, ApJ, 785, 21

Mishenina, T. V., Kovtyukh, V. V., Soubiran, C., ir kt. 2002, A&A, 396, 189

Mishenina, T. V., Soubiran, C., Kovtyukh, V. V., ir kt. 2004, A&A, 418, 551

Mucciarelli, A., Bellazzini, M., Ibata, R., ir kt. 2012, MNRAS, 426, 2889

Mucciarelli, A., Bellazzini, M., Merle, T., ir kt. 2015, ApJ, 801, 68

Mucciarelli, A., Merle, T., ir Bellazzini, M. 2017, A&A, 600, 104

Piotto, G., Milone, A. P., Bedin, L. R., ir kt. 2015, AJ, 149, 91

Ramírez, I., Meléndez, J. 2005, ApJ, 626, 465

Renzini, A. 2008, MNRAS, 391, 354

Salaris, M., Weiss, A., Ferguson, J. W., ir kt. 2006, ApJ, 645, 1131

Sbordone, L., Bonifacio, P., Castelli, F., ir Kurucz, R. L. 2004, Memorie della Societa Astronomica Italiana Supplementi, 5, 93

Thygesen, A. O., Sbordone, L., Andrievsky, S., ir kt. 2014, A&A, 572, A108

Trager, S.C., Djorgovski, S.G., ir King, I.R. 1993, ASP Conf. Ser., 50, 347

Ventura, P., D'Antona, F., Mazzitelli, I., ir Gratton, R. 2001, ApJ, 550, L65

Vesperini, E., McMillan, S. L. W., D'Antona, F., ir D'Ercole, A. 2013, MNRAS, 429, 1913

Yi, S., Demarque, P., Kim, Y.-C., ir kt. 2001, ApJS, 136, 417

Acknowledgments

I am deeply grateful to my supervisor Arūnas Kučinskas, not just for his encouragement and guidance but also for being a great mentor. I am very grateful to Roma Lazauskaitė for a very important and as I see now correct e-mail in 2007. I would like to say thank you my foreign colleagues Piercarlo Bonifacio, Frederic Royer, Elisabetta Caffau, Matthias Steffen, Sergey Andrievsky, Sergey Korotin, Tamara Mishenina, Vadim Tsymbal. Special thanks should go to my local colleagues Vidas Dobrovolskas, Jonas Klevas, Dainius Prakapavičius, Mindaugas Macijauskas for our common dream of astronomy. I am looking forward to working with all of you in the future.

For sharing a good times in the office, I want to thank Šarūnas Mikolaitis, Augustinas Ivanauskas, and Gintaras Valiauga. Beside my colleagues at work, I have to express my gratitude to my gang: Audrius, Rasa, Rūta, Julius, Laima, Giedrius, Emilija, Ieva. I would like to acknowledge Vilnius University and Lithuania Research Council for financial support and opportunities to meet and work with my foreign colleagues. I am also grateful to the anonymous referees who greatly improved the quality of the papers.

I wish to thank to staff from Molėtai astronomical observatory, especially Saulius for sharing cosmic positive energy, and Valerija for help with accommodation during our group meetings. For a place of endless scientific discussions and wonderful pizzas and beer I would like to thank "Gintaras baras" bar owner Gintaras.

I am thankful to my wife Rūta, who supported me in any respect during not only my PhD studies but much before that. Your love has made this final sprint so much easier. I would like to thank my family, for his encouragement when I was young. Without them I would never have achieved my goals.

I dedicate this work to my son Rapolas.

List of publications and published papers

1. **Černiauskas, A.**, Kučinskas, A., Klevas, J., Prakapavičius, D., Korotin, S. A., Bonifacio, P., Ludwig, H.-G., Caffau, E., Steffen, M. 2017, *Abundances of Na, Mg, and K in the atmospheres of red giant branch stars of Galactic globular cluster 47 Tucanae* // Astronomy and Astrophysics, 604, A35.

2. **Černiauskas, A.**, Kučinskas, A., Klevas, J., Dobrovolskas, V., Korotin, S. A., Bonifacio, P., Ludwig, H.-G., Caffau, E., Steffen, M. 2018, *Abundances of Mg and K in the atmospheres of turn-off stars in Galactic globular cluster 47 Tucanae* // Astronomy and Astrophysics, in press (DOI: https://doi.org/10.1051/0004-6361/201731659).

3. **Černiauskas, A.**, Kučinskas, A., Klevas, J., Bonifacio, P., Ludwig, H.-G., Caffau, E., Steffen, M. 2018, *Abundance of Zinc in the atmospheres of red giant branch stars of Galactic globular cluster 47 Tucanae* // Astronomy and Astrophysics, in press (DOI: https://doi.org/10.1051/0004-6361/201833255).

I

Abundances of Na, Mg, and K in the atmospheres of red giant branch stars of Galactic globular cluster 47 Tucanae

A.Černiauskas, A.Kučinskas, J.Klevas, D. Prakapavičius, S.Korotin, P. Bonifacio, H.-G. Ludwig, E. Caffau, and M. Steffen

Astronomy and Astrophysics 2017, 604, 35

A&A 604, A35 (2017)
DOI: 10.1051/0004-6361/201630305

Astronomy & Astrophysics

Abundances of Na, Mg, and K in the atmospheres of red giant branch stars of Galactic globular cluster 47 Tucanae

A. Černiauskas[1], A. Kučinskas[1], J. Klevas[1], D. Prakapavičius[1], S. Korotin[2,3], P. Bonifacio[4], H.-G. Ludwig[5,4], E. Caffau[4], and M. Steffen[6]

[1] Institute of Theoretical Physics and Astronomy, Vilnius University, Saulėtekio al. 3, 10222 Vilnius, Lithuania
e-mail: algimantas.cerniauskas@tfai.vu.lt
[2] Department of Astronomy and Astronomical Observatory, Odessa National University and Isaac Newton Institute of Chile Odessa branch, Shevchenko Park, 65014 Odessa, Ukraine
[3] Crimean Astrophysical Observatory, 298409 Nauchny, Crimea
[4] GEPI, Observatoire de Paris, PSL Research University, CNRS, Place Jules Janssen, 92190 Meudon, France
[5] Zentrum für Astronomie der Universität Heidelberg, Landessternwarte, Königstuhl 12, 69117 Heidelberg, Germany
[6] Leibniz-Institut für Astrophysik Potsdam, An der Sternwarte 16, 14482 Potsdam, Germany

Received 21 December 2016 / Accepted 28 March 2017

ABSTRACT

Aims. We study the abundances of Na, Mg, and K in the atmospheres of 32 red giant branch (RGB) stars in the Galactic globular cluster (GGC) 47 Tuc, with the goal to investigate the possible existence of Na–K and Mg–K correlations/anti-correlations, similar to those that were recently discovered in two other GGCs, NGC 2419 and 2808.
Methods. The abundances of K, Na, and Mg were determined using high-resolution 2dF/HERMES spectra obtained with the Anglo-Australian Telescope (AAT). The one-dimensional (1D) NLTE abundance estimates were obtained using 1D hydrostatic ATLAS9 model atmospheres and spectral line profiles synthesized with the MULTI package. We also used three-dimensional (3D) hydrodynamical CO^{5}BOLD and 1D hydrostatic LHD model atmospheres to compute 3D–1D LTE abundance corrections, $\Delta_{\rm 3D-1D\ LTE}$, for the spectral lines of Na, Mg, and K used in our study. These abundance corrections were used to understand the role of convection in the formation of spectral lines, as well as to estimate the differences in the abundances obtained with the 3D hydrodynamical and 1D hydrostatic model atmospheres.
Results. The average element-to-iron abundance ratios and their RMS variations due to star-to-star abundance spreads determined in our sample of RGB stars were $\langle$[Na/Fe]$\rangle^{\rm 1D\ NLTE} = 0.42 \pm 0.13$, $\langle$[Mg/Fe]$\rangle^{\rm 1D\ NLTE} = 0.41 \pm 0.11$, and $\langle$[K/Fe]$\rangle^{\rm 1D\ NLTE} = 0.05 \pm 0.14$. We found no statistically significant relations between the abundances of the three elements studied here. Also, there were no abundance trends with the distance from the cluster center, nor any statistically significant relations between the abundance/abundance ratios and absolute radial velocities of individual stars. All these facts suggest the similarity of K abundance in stars that belong to different generations in 47 Tuc which, in turn, may hint that evolution of K in this particular cluster was unrelated to the nucleosynthesis of Na and/or Mg.

Key words. globular clusters: individual: NGC 104 – stars: late-type – stars: atmospheres – stars: abundances – techniques: spectroscopic – convection

1. Introduction

The current paradigm of Galactic globular cluster (GGC) evolution has changed dramatically with the discovery of significant star-to-star variation in the abundances of light elements (such as C, N, O, and Na), as well as correlations/anti-correlations between their abundances (see, e.g., Kraft 1994; Gratton et al. 2004, for a review). Photometric studies of numerous GGCs carried out during the past decade have revealed the existence of multiple sub-sequences on their main sequence (MS), subgiant (SGB), and red giant branches (RGB; Piotto et al. 2007; Milone et al. 2012). Further spectroscopic observations have confirmed that stars on these sub-sequences differ in their light element abundances (Carretta et al. 2009a; Marino et al. 2008; Gratton et al. 2012), while stars with different light element abundances tend to concentrate in different parts of the cluster (Bellazzini et al. 2012; Cordero et al. 2014). All these observational facts suggest that these stellar systems formed via two or more star formation episodes, thereby producing several generations of stars characterized by different light element abundances and, possibly, also by different kinematical properties (Richer et al. 2013; Kučinskas et al. 2014). This, clearly, contradicts the previously held notion that GGCs are perfect examples of simple stellar populations.

General consensus today is that during the early evolution of the GGCs, their first-generation (1G) stars somehow enriched second-generation (2G) stars with certain light elements (e.g., Na) and made them depleted in others (e.g., O). Such view is supported, for example, by the existence of various correlations/anti-correlations of light element abundances seen in the GGCs, such as Na–O anti-correlation (Carretta et al. 2006, 2009a; Marino et al. 2011), Mg–Al anti-correlation (Carretta et al. 2009a), Li–O correlation (Pasquini et al. 2005; Shen et al. 2010). Also, recent theoretical modeling predicts

that stars characterized by different light element abundances (i.e., those that belong to different stellar generations) should have different spatial distributions and dynamical properties that can still be detectable in some GGCs (Bekki 2011; Hénault-Brunet et al. 2015) – which is, again, in line with the observations. Although several competing scenarios have been proposed to explain these observed trends, none of them is able to meet *all* available constraints simultaneously yet (see, e.g., Bastian et al. 2013; Renzini et al. 2015).

In this context, the recently discovered Mg–K anti-correlation is especially interesting as it may help shed further light on nucleosynthetic networks that have taken place in stars belonging to the GGCs and, ultimately, may help to discriminate between the different suggested evolutionary scenarios. So far, Mg–K anti-correlation has been observed in two clusters, NGC 2419 (Mucciarelli et al. 2012) and NGC 2808 (Mucciarelli et al. 2015). Besides the Mg–K anti-correlation, the authors found statistically significant correlations of [K/Fe] with [Na/Fe] and [Al/Fe], and anti–correlation with [O/Fe] abundance ratios. Also, both clusters have extreme He enrichment: NGC 2808 $Y = 0.34$ (Marino et al. 2014), NGC 2419 $Y = 0.42$ (di Criscienzo et al. 2011). These values are much higher than what has been determined in other globular clusters (see, e.g., Milone et al. 2014). The simultaneous existence of all these trends may suggest that the same self-enrichment mechanisms that produced correlations/anti-correlations between the abundances of other light elements, such as O, Na, Mg, Al, were also responsible for producing the observed spread in K abundance. The question is, of course, whether such correlations/anti-correlations between the abundances K and other light elements can be found in other GGCs. Indeed, it is possible that NGC 2419 and 2808 are not typical examples of genuine GGCs: NGC 2419 may be a remnant of an accreted dwarf galaxy (Mackey & van den Berg 2005), while NGC 2808 shows a very extended O–Na anti-correlation (e.g., Carretta et al. 2009a) and harbors four Mg-poor ([Mg/Fe] < 0) stars (e.g., Carretta et al. 2009b; Carretta 2014) – the properties that are rare amongst other GGCs. In addition, a study of K abundance using small samples of stars in seven "classical" GGCs carried out by Carretta et al. (2013) has revealed no intrinsic scatter in K abundances. Therefore, it is unclear how widespread Mg–K anti-correlation may be amongst the GGCs in general. To answer this question, analysis based on larger stellar samples in other clusters is needed.

In this work we therefore study abundances of Na, Mg, and K in a sample of 32 RGB stars in 47 Tuc with the aim to search for the possible existence of Mg–K anti-correlation and Na–K correlation. This cluster shows interesting connections between chemical abundances and kinematical properties of stars belonging to different generations (e.g., Richer et al. 2013; Kučinskas et al. 2014). Such connections have not been observed in other GGCs yet. This offers a possibility not only to search for possible connections between the abundance of K and those of Na and/or Mg but to also investigate whether or not stars characterized with different K abundance do also differ in their kinematical properties.

The paper is structured as follows. In Sect. 2 we present photometric and spectroscopic data used in our study and outline the procedures used to determine 1D non-local thermodynamical equilibrium (NLTE) abundances of Na, Mg, and K, as well as the corresponding 3D–1D abundance corrections. Analysis and discussion of the obtained results is presented in Sect. 3, while the main findings of this paper and final conclusions are outlined in Sect. 4.

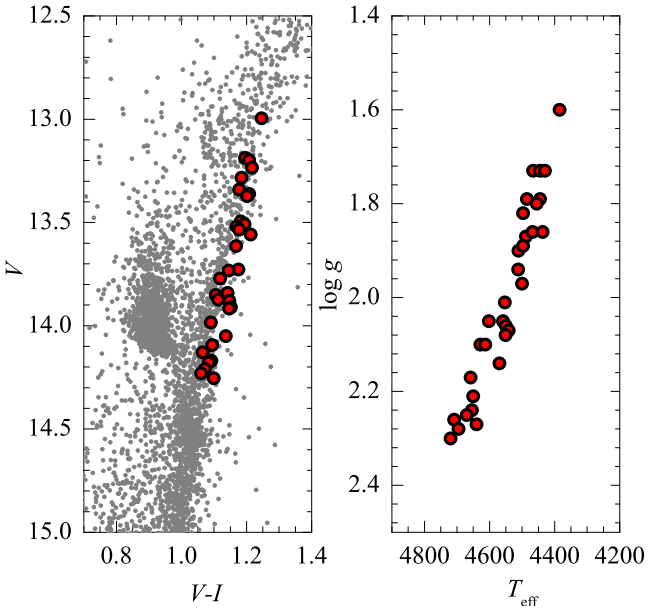

Fig. 1. *Left*: part of $V - (V - I)$ color-magnitude diagram of 47 Tuc from Bergbusch & Stetson (2009). Stars used in this study are marked as filled red circles. *Right*: a sample of RGB stars used in this work plotted in the $T_{\rm eff} - \log g$ plane.

2. Methodology

Abundance analysis of Na, Mg, and K was performed in two steps. First, we determined 1D NLTE abundances using 1D hydrostatic ATLAS9 model atmospheres and 1D non-local thermodynamical equilibrium (NLTE) abundance analysis methodology. Then, 3D hydrodynamical CO^{5}BOLD and 1D hydrostatic LHD model atmospheres were used to compute the 3D–1D abundance corrections (see Sect. 2.4) and to evaluate the influence of convection on the formation of spectral lines used in our study.

2.1. Spectroscopic data

In this study we used a sample of 32 RGB stars in 47 Tuc which were observed with the 2dF optical fibre positioner and HERMES spectrograph mounted on the Anglo-Australian Telescope (AAT). The raw spectra were obtained during the science verification phase of GALAH survey (De Silva et al. 2015), and were downloaded from the AAT data archive[1]. We used 2dF/HERMES spectra obtained in two wavelength regions, 564.9–587.3 nm (GREEN) and 758.5–788.7 (IR), using the spectral resolution of $R \sim 28\,000$ and exposure time of 1200 s. The observations were carried out during the period of Oct. 22 – Dec. 20, 2013 (see Table 1 for details).

The raw spectra were reduced using 2dfdr data reduction software (version 6.28)[2]. Sky subtraction was carried out using data obtained with 25 sky fibres during each observing night. Continuum normalization was done using the IRAF (Tody 1986) *continuum* task. Radial velocities of individual stars were measured using the IRAF *fxcorr* task, to make sure that all stars are cluster members. The typical signal–to–noise ratio (per pixel) in the vicinity of Na, Mg, and K lines was $S/N \approx 50$.

[1] http://site.aao.gov.au/arc-bin/wdb/aat_database/observation_log/make
[2] https://www.aao.gov.au/get/document/2dF-AAOmega-obs-manual-71-90.pdf

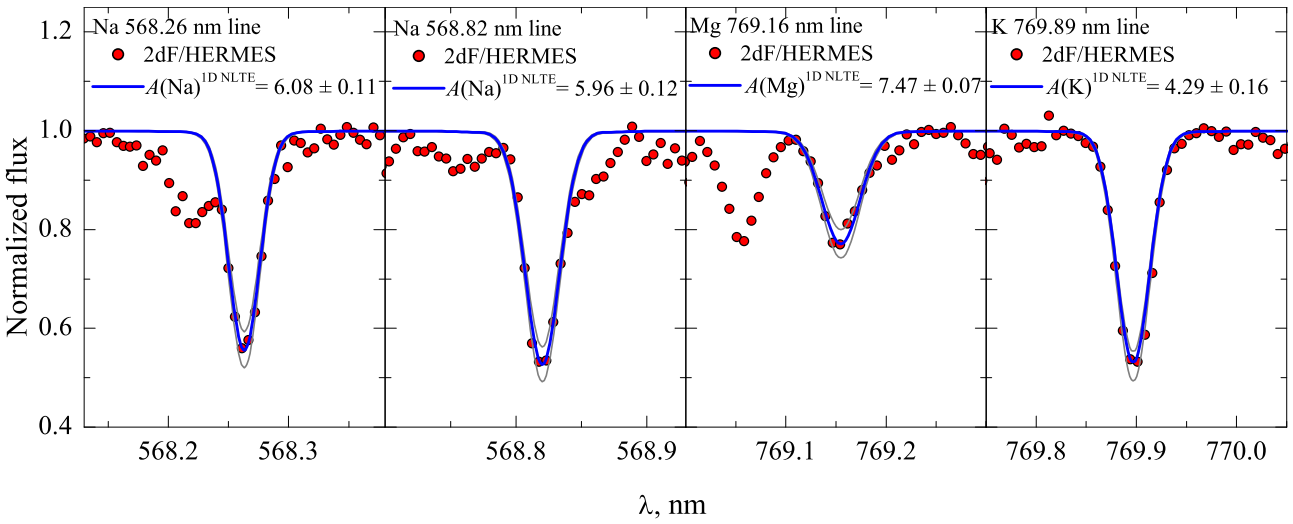

Fig. 2. Typical fits of the synthetic Na, Mg, and K line profiles (solid blue lines) to those in the observed 2dF/HERMES spectrum (filled red circles) of the target RGB star 47TucS2220 ($T_{\rm eff}$ = 4490 K, $\log g$ = 1.8). We also indicate the abundances determined from each observed line, A(X), together with their errors (see Sect. 2.3). Thin gray lines show synthetic profiles computed with the abundances altered by ±0.2 dex.

The color-magnitude diagram of 47 Tuc with the target RGB stars marked is shown in Fig. 1.

2.2. Atmospheric parameters of the target stars

Effective temperatures of the sample stars were determined using photometric data from Bergbusch & Stetson (2009) and $T_{\rm eff}-(V-I)$ calibration of Ramírez & Meléndez (2005). Prior to the effective temperature determination, photometric data were de-reddened assuming $E(B-V)$ = 0.04 and the color excess ratio $E(V-I)/E(B-V)$ = 1.33 (Bergbusch & Stetson 2009). Surface gravities were estimated using the classical relation between the surface gravity, mass, effective temperature, and luminosity. Luminosities of individual stars were determined using 12 Gyr Yonsei-Yale isochrones (Yi et al. 2001) and absolute V magnitudes obtained assuming the distance modulus $V-M_{\rm V}$ = 13.37 (Harris 1996). The same set of isochrones was used to estimate masses of the sample stars. Because of a very small mass range occupied by the sample RGB stars (~0.01 $M_{\odot}$), identical mass of 0.9 $M_{\odot}$ was adopted for all investigated stars.

2.3. 1D NLTE abundances of Na, Mg, and K

Two lines of the same Na doublet transition were used in the determination of Na abundances, 568.26 and 568.82 nm (HERMES/GREEN). In the case of Mg, we used one line located at 769.16 nm (HERMES/IR). Two lines of K resonance doublet located at 766.49 nm and 769.89 nm were available in the 2dF/HERMES spectra (IR region) of the sample RGB stars. Unfortunately, the weaker line (λ = 766.49 nm) was strongly blended with telluric O_2 feature which rendered this K line unusable. For K abundance determination we therefore used the remaining clean line located at 769.89 nm. The two lines of Na and the line of Mg were not affected by telluric lines.

Atomic data were taken from the VALD-3 database (Piskunov et al. 1995; Kupka et al. 2011) for the spectral lines of Na and Mg. In case of K, we used oscillator strengths from Morton (1991) and the line broadening constants from the VALD-3 database. All atomic data are provided in Table 2 where the line wavelengths, excitation potentials, and oscillator strengths are given in Cols. 2–4, and the line broadening constants (natural, Stark, and van der Waals) are listed in Cols. 5–7.

Table 1. Spectroscopic 2dF/HERMES observations of the target RGB stars in 47 Tuc.

Date	N stars	Exp. time s
2013-10-22	1	1200
2013-11-20	1	1200
2013-12-12	28	1200
2013-12-19	2	1200

Table 2. Atomic parameters of Na, Mg, and K lines used in the abundance determinations.

Element	λ, nm	χ, eV	$\log gf$	$\log\gamma_{\rm rad}$	$\log\frac{\gamma_4}{N_{\rm e}}$	$\log\frac{\gamma_6}{N_{\rm H}}$
Na I	568.26	2.102	−0.70	7.84	−4.22	−6.85
Na I	568.82	2.104	−0.45	7.84	−4.22	−6.85
Mg I	769.16	5.753	−0.78	7.57	−3.25	−6.83
K I	769.89	0.000	−0.17	7.56	−5.44	−7.45

In our 1D NLTE analysis, we used 1D hydrostatic ATLAS9 model atmospheres (Kurucz 1993), which were computed using the Linux port of the ATLAS9 code (Sbordone et al. 2004; Sbordone 2005). The model atmospheres were calculated using ODFNEW opacity tables (Castelli & Kurucz 2003), with the α−element enhancement of $[\alpha/{\rm Fe}]$ = +0.4. The mixing length parameter was set to $\alpha_{\rm MLT}$ = 1.25 and the overshooting was switched off.

The 1D NLTE abundances of all three elements were determined using the synthetic spectrum fitting technique. Since the atmospheric parameters of our sample stars were very similar, we used identical microturbulence velocity for all stars, $\xi_{\rm mic}$ = 1.5 km s^{-1}. This value was chosen based on the mean microturbulence velocity that was determined in a sample of 139 RGB stars in 47 Tuc, which was constructed by adding together the samples analyzed spectroscopically by Carretta et al. (2009a, 58 objects) and Cordero et al. (2014, 81 objects); we refer to Appendix B.1 for details. For all sample stars, we also assumed identical rotational velocity of 2 km s^{-1} but determined

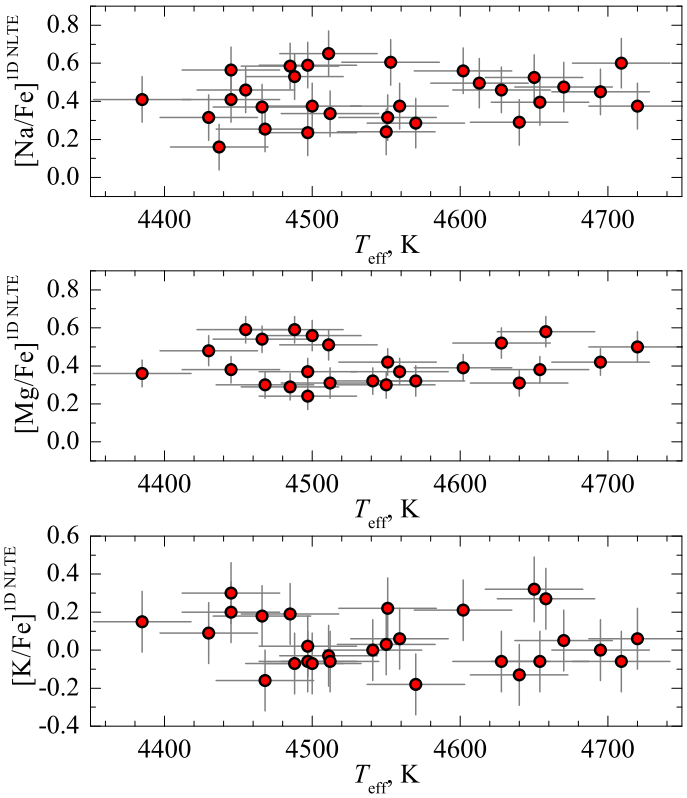

Fig. 3. [Na/Fe] (*top*), [Mg/Fe] (*middle*), and [K/Fe] (*bottom*) abundance ratios determined in the sample of 32 RGB stars in 47 Tuc and plotted versus the effective temperature of individual stars.

macrotubulence velocities, $\xi_{\rm mac}$ using each individual spectral line. Typical $\xi_{\rm mac}$ values obtained for Na, Mg, and K lines were 3–5 km s^{-1}. A fixed value of $[{\rm Fe/H}]^{\rm 1D\,LTE} = -0.76$ (Carretta et al. 2009a) was used throughout this study.

The 1D NLTE abundances of Na, Mg, and K were determined using synthetic line profiles computed with the MULTI code (Carlsson 1986) modified by Korotin et al. (1999). The model atom of Na that we used to compute level departure coefficients was presented and thoroughly tested in Dobrovolskas et al. (2014). It consisted of 20 levels of Na I and the ground level of Na II. In total, 46 bound-bound radiative transitions were taken into account when computing level population numbers. Collisional cross-sections obtained using quantum mechanical computations (Barklem et al. 2010) were used for the 9 lowest levels. For other levels, the classical formula of Drawin was utilized in the form suggested by Steenbock & Holweger (1984), with the correction factor $S_{\rm H} = 1/3$. In the case of Mg, we used the model atom from Mishenina et al. (2004). It consisted of 84 levels of Mg I, 12 levels of Mg II, and a ground state of Mg III. In the computation of departure coefficients, radiative transitions between the first 59 levels of Mg I and ground level of Mg II were taken into account. For the 7 lowest levels we used collisional cross-sections obtained using quantum mechanical computations by Barklem et al. (2012), while for other levels we applied the formula of Steenbock & Holweger (1984) with the correction factor $S_{\rm H} = 0.15$. The model atom of K was taken from Andrievsky et al. (2010) and consisted of 20 levels of K I and the ground level of K II. In addition, another 15 levels of K I and 7 levels of K II were used to ensure particle number conservation. The total number of bound-bound radiative transitions taken into account was 62 (see Andrievsky et al. 2010, for further details). Collisions with neutral H for all levels were taken into account using the formula of Steenbock & Holweger (1984), with the correction factor $S_{\rm H} = 0.05$ (Andrievsky et al. 2010).

Table 3. 1D NLTE–LTE abundance corrections, $\Delta_{\rm 1D\,NLTE-LTE}$, for the spectral lines of Na, Mg, and K used in this work (see text for details).

Element	Line	$T_{\rm eff} = 4385$, $\log g = 1.6$		$T_{\rm eff} = 4720$, $\log g = 2.3$	
	λ, nm	W, pm	$\Delta_{\rm 1D\,NLTE-LTE}$	W, pm	$\Delta_{\rm 1D\,NLTE-LTE}$
Na I	568.26	12.3	−0.25	10.6	−0.19
		16.4	−0.28	15.1	−0.23
Na I	568.82	13.3	−0.26	11.7	−0.20
		16.7	−0.26	15.5	−0.22
Mg I	769.16	8.5	−0.05	7.6	−0.01
		11.0	−0.08	10.1	−0.01
K I	769.89	19.8	−0.48	17.3	−0.55
		24.0	−0.40	21.6	−0.49

Typical fits of the synthetic 1D NLTE line profiles to those observed in the 2dF/HERMES spectrum are shown in Fig. 2 while the determined abundances of all three elements are given in Table A.1. We verified that for all elements studied there is no dependence of the determined abundances on the effective temperature (Fig. 3).

Although we directly determined 1D NLTE abundances of all elements studied here, that is, without measuring their 1D LTE abundances, we also computed 1D NLTE–LTE abundance corrections for the spectral lines used in our work. The corrections were calculated using two ATLAS9 model atmospheres with the effective temperatures and gravities similar to those of stars at the extreme ends of our RGB star sample, for two line equivalent widths for each spectral line used (the W values used represent the minimum and maximum values measured in the RGB star spectra). The obtained abundance corrections are provided in Table 3. Clearly, they are large for the lines of Na and K which demonstrates that NLTE effects play an important role in their formation and that NLTE analysis is necessary in order to obtain reliable abundances using these spectral lines. Indeed, this is in line with the findings of earlier studies (e.g., Takeda et al. (2009), Lind et al. (2011).

The total errors in the determined abundances of Na, Mg, and K, as well as individual contributions to the total error entering during different steps of the abundance analysis, are given in Table B.1 (the total error, $\sigma(A)_{\rm tot}$, is a sum of individual contributions in quadratures). The detailed description of how the individual contributions towards the total error were estimated is provided in Appendix B.

2.4. 3D+NLTE abundances of Na, Mg, and K

To study the influence of convection on the formation of Na I, Mg I, and K I lines in the atmospheres of the target RGB stars, we used 3D hydrodynamical CO^{5}BOLD and 1D hydrostatic LHD model atmospheres (see Freytag et al. 2012; Caffau et al. 2008, respectively). Because the range spanned by the atmospheric parameters of the sample stars was relatively small ($\Delta T \approx 300$ K, $\Delta \log g \approx 0.3$), we used 3D hydrodynamical and 1D hydrostatic model atmospheres with the atmospheric parameters similar to those of the median object in our RGB star sample (median star: $T_{\rm eff} \approx 4545$ K and $\log g = 2.02$; model: $T_{\rm eff} \approx 4490$ K and $\log g = 2.0$). Since we did not have models at the metallicity of 47 Tuc, we used those computed at [M/H] = −1.0. We expect however that the difference between the model and target metallicities should have minor influence on the 3D–1D abundance

corrections (see below) because they change little in the interval between [M/H] = $-0.7 \cdots -1.0$ (cf. Dobrovolskas et al. 2013).

The 3D hydrodynamical CO^{5}BOLD model atmosphere was calculated using MARCS opacities (Gustafsson et al. 2008) grouped into six opacity bins (see, e.g., Ludwig 1992; Ludwig et al. 1994). We utilized the solar-scaled abundance table from Grevesse & Sauval (1998), with CNO abundances set to A(C) = 8.39, A(N) = 7.80, A(O) = 8.66, and the enhancement in α-element abundances to [α/Fe] = +0.4. The CO^{5}BOLD model atmosphere was computed using a "box-in-a-star" setup, on a Cartesian grid of $180 \times 180 \times 145$ points corresponding to the physical dimensions of $1.65 \times 1.65 \times 0.78$ Gm in two horizontal ($x \times y$) and the vertical (z) directions, respectively. Radiative opacities and source function were computed under the assumption of LTE. The entire CO^{5}BOLD simulation sequence covered the interval of ≈ 10 convective turnover times, as measured by the Brunt-Vaiasälä timescale (see Ludwig & Kučinskas 2012, for details). The 1D hydrostatic LHD model atmosphere was computed using atmospheric parameters, chemical composition, opacities, and equation of state identical to those used in the CO^{5}BOLD simulation. This choice made it possible to make a strictly differential comparison between the spectral line strengths computed with the two types of model atmospheres.

In order to reduce computational load, spectral line synthesis with the 3D hydrodynamical CO^{5}BOLD model atmospheres was done using a subset of twenty 3D hydrodynamical model structures computed at different time instants (snapshots) and spaced over the entire span of the model simulation run (see Kučinskas et al. 2013, for details on snapshot selection procedure). Spectral line synthesis computations were carried out with the Linfor3D spectral synthesis package[3].

The influence of convection on the line strengths was assessed using 3D–1D LTE abundance corrections, $\Delta_{\mathrm{3D-1D\ LTE}}$. The abundance correction measures the difference in the abundance of a given chemical element that would be obtained using 3D hydrodynamical and 1D hydrostatic model atmospheres from the same observed spectral line (e.g., Kučinskas et al. 2013; Dobrovolskas et al. 2013). To compute abundance corrections, for each spectral line used in this work we calculated synthetic curves of growth using CO^{5}BOLD and LHD model atmospheres. Then, for a set of line equivalent widths, W, bracketing the values determined for that particular line from the 2dF/HERMES spectra of different sample stars, we measured the difference in the abundance between the 3D and 1D curves of growth, $\Delta_{\mathrm{3D-1D\ LTE}}$. Using this procedure we obtained 3D–1D LTE abundance corrections at several values of W, for each spectral line used in this study (see below). For computing abundance corrections, instead of using microturbulence velocity utilized in the 1D NLTE abundance analysis we used ξ_{mic} determined from the 3D hydrodynamical model atmosphere (Steffen et al. 2013). As argued in Prakapavičius et al. (2017), such an approach allows to diminish the influence of shortcomings in the 3D hydrodynamical model atmospheres on the resulting abundance corrections. Microturbulence velocity in the 3D model atmosphere was determined using Method 1 described in Steffen et al. (2013). In this approach, the original velocity field of the 3D hydrodynamical model atmosphere was switched off and the profiles of Na I, Mg I, and K I lines were computed using a set of different depth-independent microturbulence velocities. We then interpolated between the equivalent widths of the obtained line profiles to determine ξ_{mic} at which the equivalent width of the line profile obtained using 3D model and depth independent ξ_{mic} was equal to that computed using full 3D hydrodynamical model atmosphere (i.e., with hydrodynamical velocity field switched on; we note that microturbulence velocities, ξ_{mic}, obtained in this way were slightly different for different lines, see Table 4). The obtained value of ξ_{mic} was then used to compute spectral line profiles which were used for constructing 1D LTE curves-of-growth. These curves-of-growth, together with those computed using full 3D hydrodynamical model atmosphere, were used to calculate 3D–1D LTE abundance corrections, $\Delta_{\mathrm{3D-1D\ LTE}}$.

[3] http://www.aip.de/Members/msteffen/linfor3d

Table 4. 3D–1D abundance corrections, $\Delta_{\mathrm{3D-1D\ LTE}}$, for the different strengths of spectral lines of Na I, Mg I, and K I used in this work (see text or details).

Element	$\lambda_{\mathrm{central}}$ nm	ξ_{micro} km s^{-1}	$\Delta_{\mathrm{3D-1D\ LTE}}$, dex weak	strong
Na I	568.3 nm	1.11 ± 0.02	+0.05	+0.06
Na I	568.8 nm	1.11 ± 0.02	+0.06	+0.07
Mg I	769.2 nm	1.03 ± 0.01	+0.06	+0.07
K I	769.9 nm	1.06 ± 0.002	+0.05	+0.05

The obtained 3D–1D LTE abundance corrections are provided in Table 4 for all lines of Na, Mg, and K used in this study. Since the abundance corrections showed little variation with the line strength, in the case of each element they are provided for two values of W (corresponding to "weak" and "strong" spectral lines) that bracket the range of equivalent widths measured in the observed spectra of the sample RGB stars. The following line strengths were used: for the weakest lines 8.5, 5, and 20 pm, and for the strongest lines 14, 9, and 22 pm, in case of Na, Mg, and K, respectively. We also provide microturbulence velocities determined for each spectral line using 3D hydrodynamical CO^{5}BOLD model atmosphere, as described above, as well as the range in ξ_{mic} computed at the extreme values of W (Table 4, Col. 3). For all lines, the abundance corrections were small and did not exceed $\approx$0.07 dex.

Based on the small size of the abundance corrections, we therefore conclude that convection plays a minor role in the formation of these particular spectral lines in the atmospheres of RGB stars in 47 Tuc. This is in line with our earlier findings which have shown that at the metallicity of 47 Tuc the $\Delta_{\mathrm{3D-1D\ LTE}}$ corrections expected for lines of Na I, Mg I, and K I should be small, typically, <0.10 dex (Dobrovolskas et al. 2013; see also Collet et al. 2007). Obviously, NLTE effects may play their part in, for example, changing the concentration of neutral atoms in the red giant atmospheres due to overionization. This may have an impact on the line strengths and, thus, the abundance corrections. At the moment, however, we are not able to evaluate the size of these effects for Na, Mg, and K in 3D NLTE. Nevertheless, in the case of Li I, which has an atomic structure similar to that of Na I and K I, these effects are typically small, with the resulting influence on the abundance corrections of <0.1 dex (Klevas et al. 2016).

One may therefore conclude that $\Delta_{\mathrm{3D-1D\ LTE}}$ abundance corrections were found to be small and it is likely that they will not be dramatically different if obtained in 3D NLTE. Nevertheless, we refrain from adding the obtained 3D–1D LTE corrections to our 1D NLTE abundances. As it was shown in Klevas et al. (2016) that such procedure is generally incorrect since it may predict abundances that are different from those that would be obtained using the full 3D NLTE approach, especially at subsolar metallicities. In any case, given their size, the 3D–1D abundance corrections are not very important in the context of the

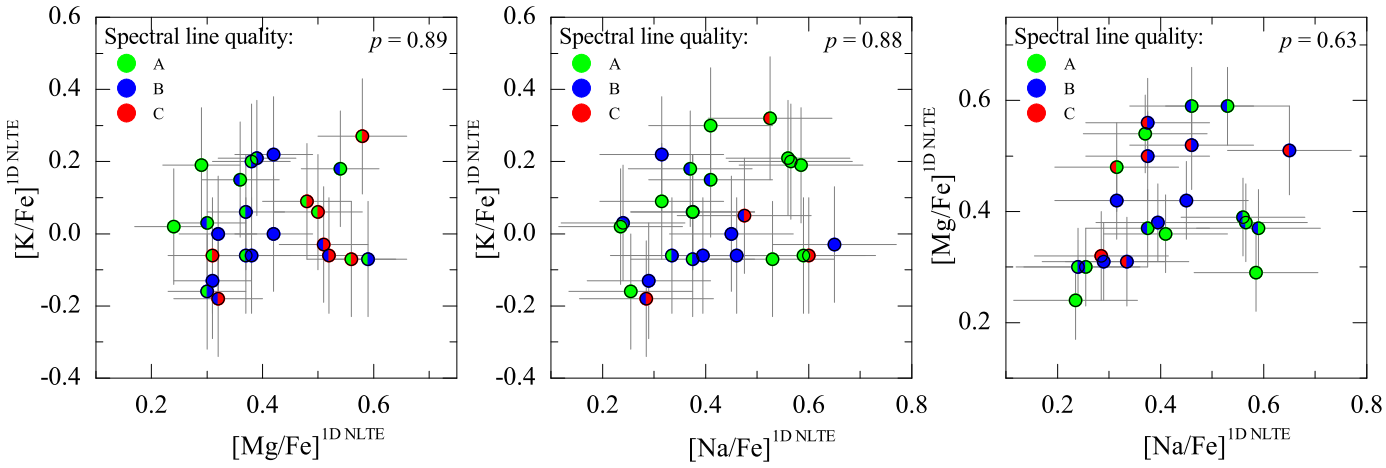

Fig. 4. Abundances of Na, Mg, and K determined in the sample of RGB stars and shown in various abundance-abundance planes. Colors on the left and right sides of the symbols correspond to the quality (class) of lines used to determine abundances plotted on the y and x axes, respectively (see Appendix B.2 for details). The two-tailed probability p-values are marked in the corresponding panels.

present study as applying them would only result in a small uniform shift of the abundance zero-points.

3. Results and discussion

Abundances of potassium in 47 Tuc were investigated by Carretta et al. (2013). The authors used three turn–off (TO) and nine SGB stars and obtained the average 1D NLTE element-to-iron abundance ratios $\langle[K/Fe]\rangle_{TO} = 0.19 \pm 0.07$ and $\langle[K/Fe]\rangle_{SGB} = 0.12 \pm 0.12$, respectively (the error here is RMS deviation due to star–to–star abundance variation; for simplicity, we henceforth refer to the element-to-iron abundance ratio as "abundance" because, for computing these ratios, we used a fixed iron abundance, $[Fe/H]^{1D\ LTE} = -0.76$ (see Sect. 2.3) and thus the star-to-star variation in, for example, the [K/Fe] abundance ratio is caused solely by the variation in K abundance). These values are comparable with the average K abundances obtained in this work using RGB stars, $\langle[K/Fe]\rangle^{1D\ NLTE} = 0.05 \pm 0.14$, although the star-to-star variation is slightly larger in our case. In case of Na and Mg, the average values obtained by us are $\langle[Na/Fe]\rangle^{1D\ NLTE} = 0.42 \pm 0.13$ and $\langle[Mg/Fe]\rangle^{1D\ NLTE} = 0.41 \pm 0.11$, respectively. Again, these abundances are comparable with those obtained in 1D NLTE by Carretta et al. (2009b), $\langle[Na/Fe]\rangle = 0.53 \pm 0.15$ and $\langle[Mg/Fe]\rangle = 0.52 \pm 0.03$ though scatter in the case of Mg is significantly larger in our case (also see below).

Recently, a study of potassium abundance in 47 Tuc was presented in Mucciarelli et al. (2017). Authors derived 1D NLTE abundance of potassium in 144 RGB stars and obtained the average element-to-iron abundance ratio $\langle[K/Fe]\rangle_{RGB} = -0.12 \pm 0.01$. This value is 0.17 dex lower than the one obtained in our study. Nevertheless, the difference between the two abundance estimates is not very large and can be explained by differences in the analysis techniques, for example, different approaches with treating microturbulence velocities in the two studies (a more exhaustive comparison with these results will be presented in our forthcoming paper on K abundance in 47 Tuc). It is important to stress, however, that, just as in our study, Mucciarelli et al. (2017) find no intrinsic spread of potassium abundance in 47 Tuc.

The 1D NLTE abundances of Na, Mg, and K obtained in our study are plotted in Fig. 4 (the abundances shown in this plot were computed using a fixed value of $[Fe/H]^{1D\ LTE} = -0.76$, see Sect. 2.3). One may notice a significant star-to-star variation in the case of all three elements. In order to investigate whether or not this variation may be caused by intrinsic spread in the elemental abundances, we used the maximum-likelihood (ML) technique identical to the one applied by Mucciarelli et al. (2012, 2015) to study K abundance spreads in NGC 2419 and NGC 2808 (see Appendix C for details). The results of the ML test suggest that there may exist small intrinsic abundance spreads in the case of Na and Mg; 0.04 dex and 0.08 dex, respectively (Table C.1). In fact, in the case of Mg the abundance determination errors may be larger than those provided in Table B.1 (see Sect. B). This may be also indirectly supported by the larger total star-to-star root mean square (RMS) abundance variation seen in our sample, for example, in comparison to that determined in other studies (e.g., Carretta et al. 2009b). Therefore, the existence of intrinsic abundance spread in the case of Mg still needs to be confirmed. However, we detected no intrinsic spread in the abundance of K.

We find no statistically significant correlations in different abundance-abundance planes shown in Fig. 4. For this, we verified whether or not the null hypothesis (i.e., that the slope in the given plane is zero) can be rejected based on the two-tailed probability p that was determined from our data using Student's t-test (with smaller p meaning higher evidence against the null hypothesis). In all planes the obtained p values were $p \geq 63\%$, thus rendering the rejection of the null hypothesis unwarranted. Similarly, no statistically significant relations were found between either the abundance or different abundance-abundance ratios of light elements measured in the atmosphere of a given star and the star's distance from the cluster center (the data is shown in Fig. 5): in all planes we obtained $p \geq 25\%$. In the case of the [Na/Fe] ratio, non-detection agrees with our earlier result obtained using 102 TO stars in 47 Tuc where no correlation between Na abundance and distance from the cluster center was found (cf. Kučinskas et al. 2014).

Following Kučinskas et al. (2014), we also computed absolute radial velocities of the target RGB stars, $|\Delta v_r| \equiv \left|v_{rad} - \langle v_{rad}\rangle^{clust}\right|$, where v_{rad} is radial velocity of the individual star and $\langle v_{rad}\rangle^{clust} = -18.6\,km\,s^{-1}$ is the mean radial velocity of the sample. The obtained absolute radial velocities of individual stars are plotted versus abundance and different abundance-abundance ratios in Fig. 6 (we also show the average

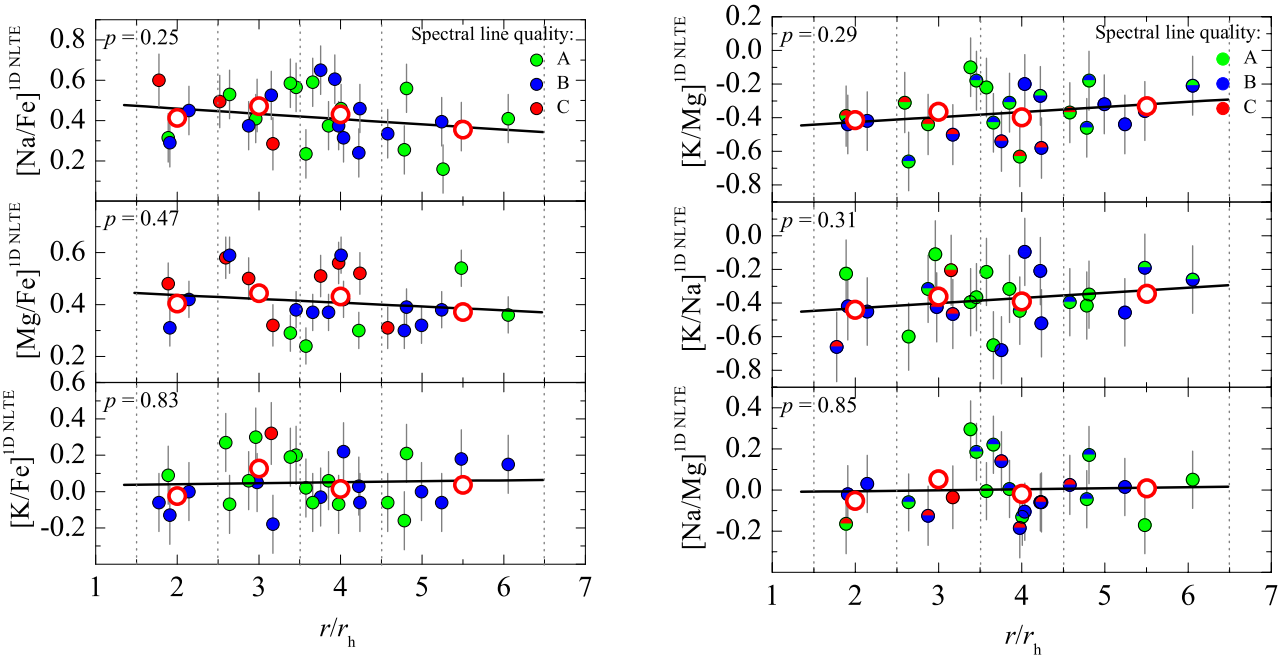

Fig. 5. Abundances of Na, Mg, and K (*left*) and abundance-abundance ratios (*right*) plotted versus the distance from the cluster center, $r/r_{\rm h}$ (small filled circles; $r_{\rm h}$ is a half-mass radius of 47 Tuc, $r_{\rm h} = 174''$, taken from Trager et al. 1993). Symbol color denotes quality (class) of the spectral lines from which the abundance was determined (see Fig. 4). Large open circles are average abundances/abundance ratios computed in non-overlapping $\Delta r/r_{\rm h} = 1$ wide distance bins (marked by the vertical dashed lines; note that the outermost bin is wider; error bars measure the RMS scatter of abundances/abundance ratios in a given bin). Black solid lines are linear fits to the data of individual stars, with the p-values (see text) marked in the corresponding panels.

absolute velocities which were computed in 0.1 dex-wide abundance bins). For all elements, the obtained p-values were $p \geq 40\%$ thereby rendering the rejection of the null hypothesis unwarranted.

Taken together, these results suggest that stars belonging to different stellar generations in 47 Tuc (as judged, e.g., by their Na abundance) do not show statistically significant differences in the abundances of Mg and/or K. The obtained results also suggest that different stellar generations do not differ in their mean absolute radial velocities. The latter finding contradicts our results obtained using 102 TO stars in 47 Tuc which suggested that kinematical properties of stars in primordial (1G) and extreme generations (3G) may be different (Kučinskas et al. 2014). It is important to note though that the sample of RGB stars used in this study is kinematically cooler than that of TO stars used in our previous study. For example, the fraction of stars with $|\Delta v_{\rm r}| \leq 8.0\,{\rm km\,s^{-1}}$ is larger in our sample than that in the sample of TO stars, ≈83% versus ≈70%, respectively. Also, in our sample there are no stars with $|\Delta v_{\rm r}| > 10.0\,{\rm km\,s^{-1}}$ while the fraction of such objects in the TO sample is ≈18%. Therefore, it is possible that this disagreement between the findings of the two studies may be due to the fact that in our sample we miss part of the primordial generation (1G) stars characterized by the largest absolute radial velocities.

4. Conclusions

We studied abundances of Na, Mg, and K in the atmospheres of 32 RGB stars that are members of Galactic globular cluster 47 Tuc. The abundances were determined using archival 2dF/HERMES spectra that were obtained with the Anglo-Australian Telescope in two wavelength regions, 564.9–587.3 nm (GREEN) and 758.5–788.7 (IR). The spectroscopic data were analyzed using 1D ATLAS9 model atmospheres and 1D NLTE abundance analysis methodology. In the case of all three elements, 1D NLTE spectral line synthesis was performed with the MULTI package, using up-to-date model atoms of Na, Mg, and K. We also used 3D hydrodynamical CO^{5}BOLD and 1D hydrostatic LHD model atmospheres to compute 3D–1D abundance corrections for the spectral lines of all three elements utilized in this study (3D–1D abundance correction is a difference in the abundance of a given element that would be obtained from the same spectral line with the 3D hydrodynamical and 1D hydrostatic model atmospheres). The obtained abundance corrections were small, in all cases ≤0.07 dex, indicating that the influence of convection on the formation of these spectral lines in the atmospheres of RGB stars in 47 Tuc is minor.

The obtained sample-averaged abundances were $\langle[{\rm Na/Fe}]\rangle^{\rm 1D\ NLTE} = 0.42 \pm 0.13$, $\langle[{\rm Mg/Fe}]\rangle^{\rm 1D\ NLTE} = 0.41 \pm 0.11$, and $\langle[{\rm K/Fe}]\rangle^{\rm 1D\ NLTE} = 0.05 \pm 0.14$ (numbers after the ± sign are RMS abundance variations due to star-to-star scatter). These numbers agree well with the average abundances obtained earlier by other authors (e.g., Carretta et al. 2009b, 2013). However, we detected somewhat larger star-to-star variation in the case of Mg which may be due to larger systematical uncertainties in its abundance determination.

We found no statistically significant relations between the abundances of Na, Mg, and K (we note that we actually compared element-to-iron abundance ratios though in all cases we used identical fixed iron abundance). We also detected no significant correlations/anti-correlations between the abundance/abundance-abundance ratios and distance from the cluster center. Finally, there were no relations between the absolute radial velocities of individual stars and abundances of the light elements in their atmospheres. These results may suggest that production of Na and K, and that of Mg and K has evolved via different and, possibly, unrelated pathways in 47 Tuc. Nevertheless, we stress that RGB stars studied in this work are

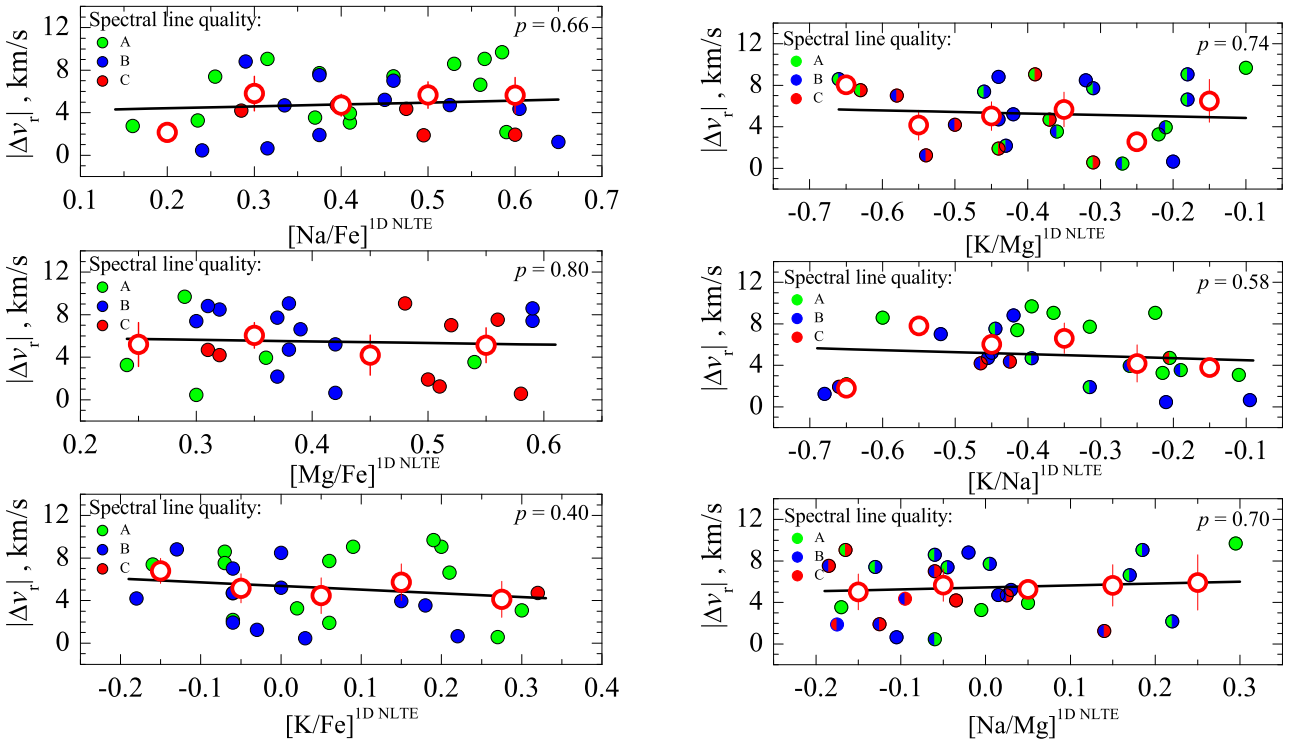

Fig. 6. Absolute radial velocities of RGB stars in 47 Tuc, $|\Delta v_r|$, plotted versus the abundance (*left*) and abundance-abundance ratios (*right*) of Na, Mg, and K. Measurements of individual stars are shown as small filled circles while the absolute radial velocities averaged in 0.1 dex-wide non-overlapping abundance bins are plotted as large open circles (error bars in the latter case measure RMS scatter of $|\Delta v_r|$ in a given abundance bin). Symbol color denotes quality (class) of the spectral lines from which the abundance was determined (see Fig. 4). Solid lines are linear fits to the data of individual stars, with the *p*-values (see text) marked in the corresponding panels.

slightly cooler kinematically than TO stars used in our earlier study where we detected differences in the absolute kinematical velocities of stars in different generations (Kučinskas et al. 2014). As a consequence, some stars with the largest absolute radial velocities, which according to Kučinskas et al. (2014) should be predominantly those that belong to primordial generation (1G), may be missing in our sample of RGB stars. Therefore, while our present results suggest that the origin of K in 47 Tuc has not been directly related to the nucleosynthesis of Na and Mg, it still needs to be verified whether this conclusion may also hold true in the case of stars characterized by the largest absolute radial velocities.

Acknowledgements. Based on data acquired through the Australian Astronomical Observatory, under program 2013B/13. This work was supported by a grant from the Research Council of Lithuania (MIP-089/2015). H.G.L. acknowledges financial support by Sonderforschungsbereich SFB 881 "The Milky Way System" (subproject A4) of the German Research Foundation (DFG). A.C. is grateful to V. Dobrovolskas for his help with the technical issues of the manuscript preparation. We also thank the anonymous referee for her/his constructive comments and suggestions that have helped to improve the paper.

References

Andrievsky, S. M., Spite, M., Korotin, S. A., et al. 2010, A&A, 509, A88
Barklem, P. S., Belyaev, A. K., Dickinson, A. S., & Gadéa, F. X. 2010, A&A, 519, A20
Barklem, P. S., Belyaev, A. K., Spielfiedel, A., Guitou, M., & Feautrier, N. 2012, A&A, 541, A80
Bastian, N., Lamers, H. J. G. L. M., de Mink, S. E., et al. 2013, MNRAS, 436, 2398
Bekki, K. 2011, MNRAS, 412, 2241
Bellazzini, M., Bragaglia, A., Carretta, E., et al. 2012, A&A, 538, A18
Bergbusch, P. A., & Stetson, P. B. 2009, AJ, 138, 1455
Caffau, E., Ludwig, H.-G., Steffen, M., et al. 2008, A&A, 488, 1031
Carlsson, M. 1986, Uppsala Astron. Obs. Rep., 33
Carretta, E. 2014, ApJ, 795, L28
Carretta, E., Bragaglia, A., Gratton, R. G., et al. 2006, A&A, 450, 523
Carretta, E., Bragaglia, A., Gratton, R., et al. 2009a, A&A, 505, 117
Carretta, E., Bragaglia, A., Gratton, R., et al. 2009b, A&A, 505, 139
Carretta, E., Gratton, R., Bragaglia, A., et al. 2013, ApJ, 769, 40
Castelli, F., & Kurucz, R. L. 2003, in Modeling of Stellar Atmospheres, eds. N. E. Piskunov, W. W. Weiss, & D. F. Gray, Proc. IAU Symp., 210, A20
Collet, R., Asplund, M., & Trampedach, R. 2007, A&A, 469, 687
Cordero, M. J., Pilachowski, C. A., Johnson, C. I., et al. 2014, ApJ, 780, 94
De Silva, G.M., Freeman, K. C., Bland-Hawthorn, J., et al. 2015, MNRAS, 449, 2604
di Criscienzo, M., D'Antona, F., Milone, A. P., et al. 2011, MNRAS, 414, 3381
Dobrovolskas, V., Kučinskas, A., Steffen, M., et al. 2013, A&A, 559, A102
Dobrovolskas, V., Kučinskas, A., Bonifacio, P., et al. 2014, A&A, 565, A121
Freytag, B., Steffen, M., Ludwig, H.-G., et al. 2012, J. Comp. Phys., 231, 919
Gratton, R., Sneden, C., & Carretta, E. 2004, ARA&A, 42, 385
Gratton, R. G., Villanova, S., Lucatello, S., et al. 2012, A&A, 544, A12
Grevesse, N., & Sauval, A. J. 1998, Space Sci. Rev., 85, 161
Gustafsson, B., Edvardsson, B., Eriksson, K., et al. 2008, A&A, 486, 951
Harris, W. E. 1996, AJ, 112, 1487; version: http://www.physics.mcmaster.ca/~harris/mwgc.dat (December 2010 revision)
Hénault-Brunet, V., Gieles, M., Agertz, O., & Read, J. I. 2015, MNRAS, 450, 1164
Iliadis, C., Karakas, A. I., Prantzos, N., et al. 2016, ApJ, 818, 98
Kirby, E. N., Guhathakurta, P., Bolte, M., Sneden, C., & Geha, M. C. 2009, ApJ, 705, 328
Klevas, J., Kučinskas, A., Steffen, M. et al. 2016, A&A, 586, A156
Korotin, S. A., Andrievsky, S. M., & Luck, R. E. 1999, A&A, 351, 168
Kraft, R. P. 1994, PASP, 106, 553
Kučinskas, A., Steffen, M., Ludwig, H.-G., et al. 2013, A&A, 549, A14
Kučinskas, A., Dobrovolskas, V., & Bonifacio, P. 2014, A&A, 568, L4
Kupka, F., Dubernet, M.-L., & VAMDC Collaboration 2011, Balt. Astron., 20, 503

Kurucz, R. L. 1993, ATLAS9 Stellar Atmosphere Programs and 2 km s^{-1} Grid, CD-ROM No. 13 (Cambridge, Mass.)
Lind, K., Asplund, M., Barklem, P. S., & Belyaev, A. K. 2011, A&A, 528, A103
Ludwig, H. G. 1992, Ph.D. Thesis, Univ. Kiel
Ludwig, H.-G., & Kučinskas, A. 2012, A&A, 547, A118
Ludwig, H.-G., Jordan, S., & Steffen, M. 1994, A&A, 284, 105
Mackey, A.D., & van den Berg, S. 2005, MNRAS, 360, 631
Marino, A. F., Villanova, S., Piotto, G., et al. 2008, A&A, 490, 625
Marino, A. F., Villanova, S., Milone, A. P., et al. 2011, ApJ, 730, L16
Marino, A. F., Milone, A. P., Przybilla, N., et al. 2014, MNRAS, 437, 1609
Milone, A. P., Piotto, G., Bedin, L. R., et al. 2012, ApJ, 744, 58
Milone, A. P., Marino, A. F., Dotter, A., et al. 2014, ApJ, 785, 21
Mishenina, T. V., Soubiran, C., Kovtyukh, V. V., & Korotin, S. A. 2004, A&A, 418, 551
Morton, D.C. 1991, ApJS, 77, 119
Mucciarelli, A., Bellazzini, M., Ibata, R., et al. 2012, MNRAS, 426, 2889
Mucciarelli, A., Bellazzini, M., Merle, T., et al. 2015, ApJ, 801, 68
Mucciarelli, A., Merle, T., & Bellazzini, M. 2017, A&A, 600, A104
Pasquini, L., Bonifacio, P., Molaro, P., et al. 2005, A&A, 441, 549
Piotto, G., Bedin, L. R., Anderson, J., et al. 2007, ApJ, 661, 53
Piskunov, N. E., Kupka, F., Ryabchikova, T. A., Weiss, W. W., & Jeffery, C. S. 1995, A&AS, 112, 525
Prakapavičius, D., Kučinskas, A., Dobrovolskas, V., et al. 2017, A&A, 599, A128
Pryor, C., & Meylan, G. 1993, ASP Conf. Ser., 50, 357
Ramírez, I., & Meléndez, J. 2005, ApJ, 626, 465
Renzini, A., D'Antona, F., Cassisi, S., et al. 2015, MNRAS, 454, 4197
Richer, H. B., Heyl, J., Anderson, J., et al. 2013, ApJ, 771, L15
Sbordone, L. 2005, Mem. Soc. Astron. It., 8, 61
Sbordone, L., Bonifacio, P., Castelli, F., & Kurucz, R. L. 2004, Mem. Soc. Astron. It., 5, 93
Shen, Z.-X., Bonifacio, P., Pasquini, L., & Zaggia, S. 2010, A&A, 524, L2
Steenbock, W., & Holweger, H. 1984, A&A, 130, 319
Steffen, M., Caffau, E., & Ludwig, H.-G. 2013, Mem. Soc. Astron. It. Suppl., 24, 37
Takeda, Y., Kaneko, H., Matsumoto, N., et al. 2009, PASJ, 61, 563
Trager, S. C., Djorgovski, S. G., & King, I. R. 1993, ASP Conf. Ser., 50, 347
Tody, D. 1986, Proc. SPIE, 627, 733
Yi, S., Demarque, P., Kim, Y.-C., et al. 2001, ApJS, 136, 417

Appendix A: Abundances of Na, Mg, and K determined in the sample of RGB stars in 47 Tuc

Table A.1. Target RGB stars in 47 Tuc, their atmospheric parameters, and determined abundances of Na, Mg and K.

Star	RA	Dec	V	I	$T_{\rm eff}$	$\log g$	$v_{\rm rad}$	[Na/Fe]	[Mg/Fe]	[K/Fe]
name	(2000)	(2000)	mag	mag	K	[cgs]	km s^{-1}	1D NLTE	1D NLTE	1D NLTE
N104-S1667	6.40433	–72.20061	13.19	11.99	4450	1.73	–9.5	0.56 ± 0.12	0.38 ± 0.07	0.20 ± 0.16
N104-S2214	6.31979	–72.07552	13.23	12.01	4430	1.73	–27.6	0.31 ± 0.12	0.48 ± 0.08	0.09 ± 0.16
N104-S1213	5.79479	–71.93364	13.28	12.09	4490	1.79	–8.9	0.58 ± 0.12	0.29 ± 0.07	0.19 ± 0.16
N104-S1430	5.98271	–71.90491	13.34	12.16	4500	1.82	–16.4	0.59 ± 0.12	0.37 ± 0.07	–0.06 ± 0.16
N104-S1625	6.35437	–71.98103	13.36	12.15	4450	1.79	–21.6	0.41 ± 0.12	...	0.30 ± 0.16
N104-S2499	6.64554	–72.11236	13.37	12.17	4460	1.80	–11.2	0.46 ± 0.12	0.59 ± 0.07	...
N104-S2220	6.36883	–72.01095	13.49	12.31	4490	1.87	–27.2	0.53 ± 0.12	0.59 ± 0.07	–0.07 ± 0.16
N104-S1800	6.55300	–72.00191	13.52	12.35	4510	1.90	–17.3	0.65 ± 0.12	0.51 ± 0.08	–0.03 ± 0.16
N104-S1481	6.09350	–72.25283	13.53	12.35	4500	1.89	–21.8	0.23 ± 0.12	0.24 ± 0.07	0.02 ± 0.16
N104-S1849	6.60921	–72.01517	13.72	12.55	4500	1.97	–26.1	0.38 ± 0.12	0.56 ± 0.08	–0.07 ± 0.16
N104-S1779	6.53142	–71.97400	13.73	12.58	4550	2.01	–22.9	0.61 ± 0.12	...	...
N104-S1490	6.13163	–72.26456	13.84	12.69	4560	2.05	–10.8	0.38 ± 0.12	0.37 ± 0.07	0.06 ± 0.16
N104-S2328	5.39333	–72.14819	13.85	12.74	4630	2.10	–11.5	0.46 ± 0.12	0.52 ± 0.08	–0.06 ± 0.16
N104-S1636	6.36917	–72.02222	13.87	12.76	4610	2.10	–16.7	0.49 ± 0.13	...	...
N104-S1751	6.51550	–72.20506	13.91	12.77	4550	2.08	–19.2	0.31 ± 0.12	0.42 ± 0.07	0.22 ± 0.16
N104-S1657	6.39483	–72.13347	13.98	12.89	4660	2.17	–18.0	...	0.58 ± 0.08	0.27 ± 0.16
N104-S1750	6.51125	–72.05508	14.09	13.00	4650	2.21	–23.3	0.53 ± 0.12	...	0.32 ± 0.17
N104-S1543	6.23467	–72.13755	14.12	13.06	4710	2.26	–16.6	0.60 ± 0.13	...	–0.06 ± 0.16
N104-S1732	6.49112	–72.08711	14.17	13.09	4670	2.25	–22.9	0.47 ± 0.13	...	0.05 ± 0.16
N104-S1563	6.27129	–72.15166	14.21	13.13	4700	2.28	–13.4	0.45 ± 0.12	0.42 ± 0.07	0.00 ± 0.16
N104-S167	5.09500	–72.02045	12.99	11.75	4390	1.60	–22.5	0.41 ± 0.12	0.36 ± 0.07	0.15 ± 0.16
N104-S292	5.17163	–72.04539	13.18	11.99	4470	1.73	–15.0	0.37 ± 0.12	0.54 ± 0.07	0.18 ± 0.16
N104-S1084	5.60667	–71.88953	13.50	12.31	4470	1.86	–11.2	0.25 ± 0.12	0.30 ± 0.07	–0.16 ± 0.16
N104-S2474	6.47350	–71.86870	13.55	12.34	4440	1.86	–15.8	0.16 ± 0.12	...	...
N104-S1844	6.60458	–71.95181	13.61	12.44	4510	1.94	–23.2	0.33 ± 0.12	0.31 ± 0.08	–0.06 ± 0.16
N104-S2333	5.40721	–72.21652	13.77	12.65	4600	2.05	–25.2	0.56 ± 0.12	0.39 ± 0.07	0.21 ± 0.16
N104-S1070	5.58192	–72.23414	13.87	12.73	4550	2.06	–18.1	0.24 ± 0.12	0.30 ± 0.07	0.03 ± 0.16
N104-S2494	6.62525	–72.23708	13.91	12.75	4540	2.07	–10.1	...	0.32 ± 0.07	0.00 ± 0.16
N104-S1692	6.43354	–71.99447	14.05	12.91	4570	2.14	–22.8	0.29 ± 0.13	0.32 ± 0.08	–0.18 ± 0.16
N104-S2439	6.24533	–71.83745	14.17	13.07	4650	2.24	–23.3	0.39 ± 0.12	0.38 ± 0.07	–0.06 ± 0.16
N104-S1524	6.19971	–72.20933	14.23	13.17	4720	2.30	–16.7	0.38 ± 0.12	0.50 ± 0.08	0.06 ± 0.16
N104-S2176	6.21292	–72.00975	14.25	13.15	4640	2.27	–27.4	0.29 ± 0.12	0.31 ± 0.07	–0.13 ± 0.16
mean								0.42	0.41	0.05
σ								0.13	0.11	0.14

Notes. Column 1: object name; Col. 2: right ascension; Col. 3: declination; Col. 4: V magnitude; Col. 5: I magnitude; Col. 6: effective temperature; Col. 7: surface gravity; Col. 8: radial velocity; Col. 9: 1D NLTE sodium abundance and its error; Col. 10: 1D NLTE magnesium abundance and its error; Col. 11: 1D NLTE potassium abundance and its error.

In this section we provide a list of target RGB stars (32 objects), their atmospheric parameters (determined in Sect. 2.2), and abundances of Na, Mg, and K (Sects. 2.3 and 2.4). This information is summarized in Table A.1.

Table B.1. Errors in the determined abundances of Na, Mg, and K.

Element	Line wavelength, nm	Line quality	$\sigma(T_{\rm eff})$ dex	$\sigma(\log g)$ dex	$\sigma(\xi_{\rm t})$ dex	σ(cont) dex	σ(fit) dex	$\sigma(A)_{\rm tot}$ dex
Na I	568.26	A	±0.07	∓0.01	∓0.08	0.03	0.03	0.11
		B	±0.07	∓0.01	∓0.08	0.03	0.04	0.12
		C	±0.07	∓0.01	∓0.08	0.03	0.04	0.12
Na I	568.82	A	±0.07	∓0.01	∓0.08	0.04	0.02	0.12
		B	±0.07	∓0.01	∓0.08	0.04	0.03	0.12
		C	±0.07	∓0.01	∓0.08	0.04	0.06	0.13
Mg I	769.16	A	±0.03	∓0.01	∓0.05	0.03	0.02	0.07
		B	±0.03	∓0.01	∓0.05	0.03	0.03	0.07
		C	±0.03	∓0.01	∓0.05	0.03	0.04	0.08
K I	769.89	A	±0.07	∓0.00	∓0.14	0.04	0.02	0.16
		B	±0.07	∓0.00	∓0.14	0.04	0.03	0.16
		C	±0.07	∓0.00	∓0.14	0.04	0.05	0.17

Notes. The sign ± or ∓ reflects the change in the elemental abundance which occurs due to increase (top sign) or decrease (bottom sign) in a given atmospheric parameter. For example, increase in the effective temperature leads to an increase in the abundance (±) while increasing microturbulence velocity results in decreasing abundance (∓).

Appendix B: Errors in the abundances of Na, Mg, and K

In this study we applied a maximum-likelihood technique in order to estimate the extent of possible intrinsic star-to-star variation in the abundances of Na, Mg, and K. For this, we needed realistic estimates of the abundance errors. The procedures used in their derivation are briefly summarized below. Note that in all cases these errors represent the lower limits since they do not account for various possible systematic errors.

B.1. Errors due to uncertainties in the atmospheric parameters

The error in the determination of effective temperature, was estimated by computing effective temperatures using $V - I$ color indices that were increased/decreased by the amount given by their observational errors. For the latter, we used a conservative estimate of $\sigma(V) = \sigma(I) = 0.03$ mag. The obtained error in the effective temperature, ±65 K, was used to evaluate the influence of the uncertainty in $T_{\rm eff}$ on the determined abundances of Na, Mg, and K using the usual procedure adopted for this. The obtained errors, $\sigma(T_{\rm eff})$, are provided for all three elements in Col. 4, Table B.1.

The error in the effective temperature, along with those in luminosity (±0.03 $L_{\odot}$, estimated from photometric error in $M_{\rm V}$) and stellar mass (±0.01 $M_{\odot}$, obtained from the isochrones), were used to obtain the error in $\log g$, ±0.04 dex. Although we used the slightly higher (and, in our view, more realistic) value of ±0.1 dex when estimating the resulting errors in the elemental abundances, $\sigma(\log g)$, we stress that these errors are very small and thus their contribution to the final abundance error is essentially negligible (Table B.1, Col. 5).

To estimate the error arising due to uncertainty in the microturbulence velocity, we utlized a sample of RGB stars in 47 Tuc for which $\xi_{\rm t}$ was determined spectroscopically in earlier studies using Fe I lines. For this, we used 58 RGB stars from Carretta et al. (2009a) and 81 RGB stars from Cordero et al. (2014) which were selected to match the same range in effective temperature as stars used in our sample. We then computed the mean microturbulence and its RMS variation, $\xi_{\rm t} = 1.48 \pm 0.18\,{\rm km\,s^{-1}}$ which agrees well with $\xi_{\rm t} = 1.5\,{\rm km\,s^{-1}}$ used in our study. The obtained RMS variation of microturbulence velocity was used as a representative uncertainty in $\xi_{\rm t}$ to estimate the resulting errors in the abundances of Na, Mg, and K, $\sigma(\xi_{\rm t})$ (Table B.1, Col. 6).

B.2. Errors due to uncertainties in the continuum determination and line profile fitting

All spectral lines used in this study were carefully inspected for blends and/or possible contamination with telluric lines. Nevertheless, even the lines that were deemed to be the cleanest and thus suitable for the abundance analysis differed in their quality significantly. In order to take this into account, we grouped spectral lines of Na, Mg, and K into three classes according to their quality:

- A-class: strong or moderately strong lines with well-resolved line profiles;
- B-class: moderately blended lines, or lines that were insufficiently resolved in the line wings;
- C-class: weak, poorly resolved, or significantly blended lines.

We then selected several representative spectra with lines of each class and identified wavelength intervals in the vicinity of Na, Mg, and K lines that were clean from spectral lines, either stellar or telluric (in fact, these intervals were used to determine continuum level for the abundance analysis). We further assumed that intensity variation in these intervals was caused entirely by the noise in the spectra. The error in the continuum determination was then computed as:

$$err(\text{cont}) = \frac{\sigma_{\rm cont}}{\sqrt{N}}, \tag{B.1}$$

where $\sigma_{\rm cont}$ is dispersion in the continuum variation obtained using all wavelength intervals available for the continuum determination in case of a given spectral line, and N is the total number of wavelength points in these wavelength intervals. The resulting errors were used to estimate their impact on the abundance determination, that is, line profile fitting was done again with the continuum level shifted up and down by *err*(cont), to obtain errors in the abundances of Na, Mg, and K. The resulting abundance errors are listed in Col. 7 of Table B.1.

Table C.1. Results of the maximum-likelihood (ML) testing of the intrinsic spread in the abundances of Na, Mg, and K.

Element X_i	$\langle[X_i/\mathrm{Fe}]\rangle$, likelihood value dex	$\sigma[X_i/\mathrm{Fe}]$ dex	$\sigma_{\mathrm{int}}[X_i/\mathrm{Fe}]$ dex
Na	0.49 ± 0.02	0.13	0.04 ± 0.05
Mg	0.48 ± 0.02	0.11	0.08 ± 0.02
K	0.10 ± 0.03	0.14	0.00 ± 0.05

To estimate the errors in the line profile fitting, we used the representative spectra selected in the previous step, as well as synthetic line profiles that were obtained during the abundance analysis as best-fits to these particular observed lines of Na, Mg, and K. We then computed RMS deviations between the observed and synthetic line profiles which were further converted into the uncertainties in the line equivalent width, and, finally, the resulting errors in the determined abundances, σ_{fit} (listed in Col. 8 of Table B.1).

B.3. Total error in the abundances of Na, Mg, and K

The individual contributions to the total error due to uncertainties in the atmospheric parameters, continuum determination, and spectral line profile fitting were added in quadratures to obtain the total error in the abundances of Na, Mg, and K. These errors are provided in the last column of Table B.1. We stress that they provide a lower limit for the uncertainties in the determined abundances of Na, Mg, and K since they do not account for various systematic uncertainties that are unavoidable in the abundance analysis procedure.

Appendix C: Maximum-likelihood testing of the intrinsic spread in elemental abundances

In order to estimate the size of the possible intrinsic spread in the abundances of Na, Mg, and K, we followed the procedure described in Mucciarelli et al. (2012, 2015) which was used by these authors to study K abundance spreads in NGC 2419 and NGC 2808. For this, maximum-likelihood (ML) technique was utilized to evaluate the mean abundance ratio, $\langle[\mathrm{A/B}]\rangle$, of elements A and B, as well as its intrinsic spread, σ_{int}[4]. We defined the likelihood as

$$L(\langle[\mathrm{A/B}]\rangle, \sigma_{\mathrm{int}}) = \prod_{\mathrm{i}=1}^{N} p_i(\langle[\mathrm{A/B}]\rangle, \sigma_{\mathrm{int}}), \tag{C.1}$$

where the multiplication was done using quantities computed for each star in a sample of N stars. In the equation above, p_i is a Gaussian probability function defined as

$$p_i(\langle[\mathrm{A/B}]\rangle, \sigma_{\mathrm{int}}) = \frac{1}{\sqrt{\sigma_{\mathrm{int}}^2+\sigma_i^2}} \exp\left[-\frac{1}{2}\left(\frac{\langle[\mathrm{A/B}]\rangle - \langle[\mathrm{A/B}]\rangle_i}{\sqrt{\sigma_{\mathrm{int}}^2+\sigma_{\mathrm{i}}^2}}\right)^2\right] \tag{C.2}$$

where $\langle[\mathrm{A/B}]\rangle_i$ and σ_i is the abundance ratio and its error for the ith star in the sample taken from Table A.1.

We computed likelihood values for a 2D grid that was defined by various combinations of parameters ($\langle[\mathrm{A/B}]\rangle$, σ_{int}). The mean abundance and its internal spread was determined by maximizing likelihood values in the computed 2D grid. We also computed errors in the derived quantities according to the prescription given in Pryor & Meylan (1993, see their Eqs. (5)–(10)).

The obtained mean abundance ratio, $\langle[X_i/\mathrm{Fe}]\rangle$, and its uncertainty, as well as the total variation, $\sigma[X_i/\mathrm{Fe}]$ ($\equiv\sqrt{\sigma_{\mathrm{int}}^2+\sigma_i^2}$), and the determined intrinsic variation, $\sigma_{\mathrm{int}}[X_i/\mathrm{Fe}]$, in the abundance of element X_i are provided in Table C.1. Although our test results suggest the existence of small intrinsic spread of similar size in case of Na and Mg, we note that for Mg the real spread may in fact be significantly smaller (we note that although we used abundance-to-iron ratios, iron abundance was assumed to be fixed and thus it had no effect on the spread of individual abundance-to-iron ratios). The reason for this is that the spectral lines of Mg I used in our work were relatively poorly resolved in the 2dF/HERMES spectra which in many cases meant that only part of the observed line profile could be fitted with the synthetic profile. This made the total error of the line profile fitting smaller which, in turn, may have lead to an overestimated intrinsic abundance variation. Therefore, existence of the intrinsic spread in the case of Mg needs to be verified using higher quality spectroscopic data.

[4] In this study [Na/Fe], [Mg/Fe], and [K/Fe] abundance ratios were used.

II

Abundances of Mg and K in the atmospheres of turn-off stars in Galactic globular cluster 47 Tucanae

A.Černiauskas, A.Kučinskas, J.Klevas, V. Dobrovolskas, S.Korotin, P. Bonifacio, H.-G. Ludwig, E. Caffau, and M. Steffen

Astronomy and Astrophysics 2018, doi:10.1051/0004-6361/201731659

Astronomy & Astrophysics manuscript no. 47Tuc_TO_Mg-K
July 12, 2018

Abundances of Mg and K in the atmospheres of turn-off stars in Galactic globular cluster 47 Tucanae⋆

A. Černiauskas[1], A. Kučinskas[1], J. Klevas[1], V. Dobrovolskas[1], S. Korotin[2,3], P. Bonifacio[4], H.-G. Ludwig[5,4], E. Caffau[4], and M. Steffen[6]

[1] Institute of Theoretical Physics and Astronomy, Vilnius University, Saulėtekio al. 3, Vilnius LT-10222, Lithuania
e-mail: algimantas.cerniauskas@tfai.vu.lt
[2] Department of Astronomy and Astronomical Observatory, Odessa National University and Isaac Newton Institute of Chile Odessa branch, Shevchenko Park, 65014 Odessa, Ukraine
[3] Crimean Astrophysical Observatory, Nauchny 298409, Crimea
[4] GEPI, Observatoire de Paris, PSL Research University, CNRS, Place Jules Janssen, 92190 Meudon, France
[5] Zentrum für Astronomie der Universität Heidelberg, Landessternwarte, Königstuhl 12, 69117 Heidelberg, Germany
[6] Leibniz-Institut für Astrophysik Potsdam, An der Sternwarte 16, D-14482 Potsdam, Germany

Received 27 July 2017 / Accepted 6 April 2018

ABSTRACT

Aims. We determined abundances of Mg and K in the atmospheres of 53 (Mg) and 75 (K) turn-off (TO) stars of the Galactic globular cluster 47 Tuc. The obtained abundances, together with those of Li, O, and Na that we had earlier determined for the same sample of stars, were used to search for possible relations between the abundances of K and other light elements, Li, O, Na, and Mg, as well as the connections between the chemical composition of TO stars and their kinematical properties.
Methods. Abundances of Mg and K were determined using archival high resolution VLT FLAMES/GIRAFFE spectra, in combination with the one-dimensional (1D) non-local thermodynamic equilibrium (NLTE) spectral synthesis methodology. Spectral line profiles were computed with the MULTI code, using 1D hydrostatic ATLAS9 stellar model atmospheres. We also utilized three-dimensional (3D) hydrodynamical CO^{5}BOLD and 1D hydrostatic LHD model atmospheres for computing 3D–1D LTE abundance corrections for the spectral lines of Mg and K, in order to assess the influence of convection on their formation in the atmospheres of TO stars.
Results. The determined average abundance-to-iron ratios and their root mean square (RMS) variations due to star-to-star abundance spreads were $\langle$[Mg/Fe]$\rangle^{\rm 1D\ NLTE} = 0.47 \pm 0.12$, and $\langle$[K/Fe]$\rangle^{\rm 1D\ NLTE} = 0.39 \pm 0.09$. Although the data suggest the possible existence of a weak correlation in the [K/Fe]–[Na/Fe] plane, its statistical significance is low. No statistically significant relations between the abundance of K and other light elements were detected. Also, we did not find any significant correlations or anti-correlations between the [Mg/Fe] and [K/Fe] ratios and projected distance from the cluster center. Similarly, no relations between the absolute radial velocities of individual stars and abundances of Mg and K in their atmospheres were detected. The 3D–1D abundance corrections were found to be small (≤ 0.1 dex) for the lines of Mg and K used in this study, thus indicating that the influence of convection on their formation is small.

Key words. Globular clusters: individual: NGC 104 – Stars: late type – Stars: atmospheres – Stars: abundances – Techniques: spectroscopic – Convection

1. Introduction

During the last decade studies of Galactic globular clusters (GGCs) opened a new chapter when it was discovered that GGCs may consist of multiple stellar generations. The first strong evidence in favor of this paradigm came from spectroscopic observations, which lead to the discovery of large star-to-star variation in the light element abundances within a given GGC (Kraft 1994; Gratton et al. 2004), and, then, to the detection of various (anti-)correlations between the abundances of these elements, such as Na–O (Carretta et al. 2009a) and Li–O (Pasquini et al. 2005; Shen et al. 2010) correlations, and Na–Li (Bonifacio et al. 2007) and Mg–Al (Carretta et al. 2009a) anti-correlations. It is worth mentioning that these abundance trends are not seen in Galactic halo field stars. Further photometric observations have revealed the existence of multiple subsequences in the cluster color-magnitude diagrams (CMDs), all the way from the main sequence (MS) and up to the tip of the red giant branch (RGB) (Piotto et al. 2007; Milone et al. 2012). All these findings suggest that stars in the GGCs may have formed during two or more star formation episodes (see, e.g., Gratton et al. 2012), thus contradicting the earlier notion that GGCs are perfect examples of simple stellar populations.

The most popular theories are that either massive asymptotic giant branch (AGB) stars (e.g., Ventura et al. 2001) or fast-rotating massive stars (e.g., Decressin et al. 2007) could have enriched the second-generation stars in Na and Al, and depleted them in O and Mg. Other scenarios, such as enrichment by binary stars (de Mink et al. 2009) and early disk accretion (Bastian et al. 2013) have been discussed, too. However, none of them can explain, for example, all observed abundance (anti-)correlations simultaneously (see discussion in, e.g., Bastian et al. 2015). From the theoretical point of view, new ideas regarding the possible polluters are needed. From the ob-

⋆ Based on data obtained with the Very Large Telescope at the European Southern Observatory, programme ID: 081.D-0287(A).

servational side, it would be desirable to identify new chemical elements that would allow us to discern between the different already proposed self-enrichment scenarios of the GGCs or, possibly, help to suggest new ones.

Potentially, new clues in this context may come from the investigations of potassium abundance. Since K is synthesized mainly via oxygen burning in high-mass stars, it is unlikely that the atmospheric K abundance would undergo any appreciable changes during the course of the stellar evolution of the low-mass stars in the GGCs. Mucciarelli et al. (2012) presented an analysis of RGB stars in NGC 2419 ([Fe/H] = −2.09) in which the first hints of K–Mg anti-correlation and bimodal distribution of [Mg/Fe] ratio were detected. The authors also confirmed an unusually large (≈ 2 dex) spread and depletion (to ≈ −1 dex) in the magnesium abundance. A more recent study of NGC 2808 ([Fe/H] = −1.1) by Mucciarelli et al. (2015) has revealed the existence of statistically significant correlations of the [K/Fe] abundance ratio with [Na/Fe] and [Al/Fe], and anti–correlations with [O/Fe] and [Mg/Fe]. A fraction of the stars in both clusters is strongly enhanced in helium, with $Y = 0.34$ in NGC 2808 (Marino et al. 2014) and $Y = 0.42$ in NGC 2419 (di Criscienzo et al. 2011). These values are much higher than those observed in other GGCs (Milone et al. 2014). Mucciarelli et al. (2015) suggested a self-enrichment model proposed by D'Ercole et al. (2012) as one of the possible explanations of [K/Fe] – [Mg/Fe] anti-correlation. In this scenario, Mg-poor/K-rich (extreme population) stars formed from the ejecta of AGB and super-AGB stars. However, this scenario still requires some fine tuning in the nuclear reaction cross-sections and burning temperatures to explain the observed trends satisfactorily.

In their recent study of 144 RGB stars in 47 Tuc, Mucciarelli et al. (2017) claimed a detection of a mild [K/Fe] – [Na/Fe] correlation and [K/Fe] – [O/Fe] anti-correlation. This is in contrast with the results of our recent study of Na, Mg, and K abundances in the atmospheres of RGB stars in 47 Tuc, where we found no statistically significant relations between either the abundances of different elements, or the abundances and kinematical properties of the cluster stars (Černiauskas et al. 2017, hereafter Paper I). It is conceivable, however, that non-detection in our case could be due to a smaller sample of RGB stars studied: 32 in our work versus 144 in the study of Mucciarelli et al. (2017). Apart from these two studies, the only other investigation of K abundances in 47 Tuc was done by Carretta et al. (2013) who determined K abundances in three turn-off (TO) and nine subgiant branch (SGB) stars. Obviously, the sample size used in the latter study was too small to search for possible relations between the elemental abundances among little-evolved stars.

Given this somewhat ambiguous situation, investigation of K abundances in the atmospheres of TO stars in 47 Tuc could be very interesting, especially if based on a larger sample of stars than that used by Carretta et al. (2013). It is well know that the cores of unevolved low-mass stars do not reach temperatures high enough for Ne−Na and/or Mg−Al cycles to operate. Moreover, their convective envelopes are not deep enough to bring up to the surface the products of proton-capture reactions. Therefore, the atmospheres of these stars should have retained their primordial chemical composition, unless their atmospheres have been contaminated by accreted chemical elements synthesized in other stars. In the present study we therefore determine abundances of Mg and K in the atmospheres of 53 and 75 (TO) stars in 47 Tuc, respectively (abundances of both elements were obtained in 44 stars). We then use this data to search for possible relations between the abundances of K and Mg, and those of other light elements, Li, O, and Na (with their abundances taken from Dobrovolskas et al. 2014), as well as relations between the elemental abundances and kinematical properties of TO stars.

The paper is structured as follows. In Sect. 2 we present spectroscopic data used in our study and outline the procedures used to determine abundances of Mg and K using one-dimensional (1D) non-local thermodynamic equilibrium (NLTE) methodology. Analysis and discussion of the obtained results is presented in Sect. 3, while the main findings of this paper and final conclusions are outlined in Sect. 4.

2. Methodology

Abundances of Mg and K were determined using 1D hydrostatic ATLAS9 model atmospheres and 1D NLTE abundance analysis methodology. Additionally, we also utilized three-dimensional (3D) hydrodynamical CO^{5}BOLD and 1D hydrostatic LHD model atmospheres to compute the 3D–1D abundance corrections using the assumption of local thermodynamic equilibrium (LTE; see Sect. 2.3.3 for details). This was done in order to study the importance of convection in the formation of the spectral lines of Mg I and K I used in this study, though the obtained corrections were not applied to determine 3D-corrected elemental abundances (see Sect. 2.3.3 for details). A brief description of all steps involved in the abundance analysis is provided below.

2.1. Spectroscopic data

In this work we used the same sample of TO stars of 47 Tuc as in D'Orazi et al. (2010) and Dobrovolskas et al. (2014). We note that in the two previous studies abundances of Mg and K in the atmospheres of these stars were not determined.

In the abundance analysis we utilized high-resolution archival VLT FLAMES/GIRAFFE spectra of TO stars that were reduced by and used in Dobrovolskas et al. (2014, programme ID: 081.D-0287(A), PI: Shen). The spectra were obtained in Medusa mode using HR 18 setup (746.8 – 788.9 nm, R=18400). In total, 116 fibers were dedicated to target stars and 16 were used for sky spectra. The continuum normalization procedure was completed using IRAF (Tody 1986) *continuum* task (see Dobrovolskas et al. 2014, for details).

Effective temperatures and surface gravities of the sample TO stars were taken from Dobrovolskas et al. (2014). The former were determined by fitting the wings of Hα line profiles, while the latter were obtained using the classical relation between the surface gravity, mass, effective temperature, and luminosity.

2.2. Model atmospheres

We used two types of 1D hydrostatic model atmospheres, ATLAS9 and LHD, and 3D hydrodynamical CO^{5}BOLD model atmospheres:

– ATLAS9: for the atmospheric parameters of each individual sample star we computed a 1D hydrostatic model atmosphere using the ATLAS9 code (Kurucz 1993; Sbordone 2005). The model atmospheres were calculated using ODFNEW [M/H] = −1.0 opacity tables (Castelli & Kurucz 2003), with the α−element enhancement of [α/Fe] = +0.4. The mixing length parameter was set to $\alpha_{\rm MLT} = 1.25$ and the overshooting was switched off. These model atmospheres were used in the 1D NLTE abundance analysis of Mg and

Table 1. Parameters of the 3D hydrodynamical CO5BOLD model atmospheres used in this work.

$T_{\rm eff}$, K	$\log g$	[M/H]	Grid dimension, Mm x × y × z	Grid resolution x × y × z
5470	4.0	0.0	20.3 × 20.3 × 10.6	140 × 140 × 150
5530	4.0	-1.0	19.9 × 19.9 × 10.6	140 × 140 × 150
5930	4.0	0.0	25.8 × 25.8 × 12.5	140 × 140 × 150
5850	4.0	-1.0	25.8 × 25.8 × 12.5	140 × 140 × 150

K for synthesizing spectral line profiles with the MULTI code (see Sect. 2.3);

– LHD: the 1D hydrostatic LHD models were computed using the LHD model atmospheres code (Caffau et al. 2008), which utilises chemical composition, equation of state, and opacities identical to those used in the 3D hydrodynamical CO5BOLD model atmospheres (see below). In order to compute the 3D–1D abundance corrections for magnesium and potassium (see Sect. 2.3.3), atmospheric parameters of the LHD models were matched to those of the CO5BOLD model atmospheres;
– CO5BOLD: the 3D hydrodynamical CO5BOLD model atmosphere code solves time-dependent equations of hydrodynamics and radiation transfer on a Cartesian grid (Freytag et al. 2012). We used four 3D hydrodynamical model atmospheres from the CIFIST grid (Ludwig et al. 2009), which we utilised for computing the 3D–1D abundance corrections. Atmospheric parameters of the CO5BOLD models are provided in Table 1. The CO5BOLD and LHD models were computed using an identical chemical composition, equation of state, opacities, and radiative transfer scheme.

Table 2. Atomic parameters of the spectral lines used in the abundance determinations of Mg and K. Natural ($\gamma_{\rm rad}$), Stark ($\frac{\gamma_4}{N_e}$), and van der Waals ($\frac{\gamma_6}{N_{\rm H}}$) broadening constants computed using classical prescription are provided in the last three columns.

Element	λ, nm	χ, eV	$\log gf$	$\log\gamma_{\rm rad}$	$\log\frac{\gamma_4}{N_e}$	$\log\frac{\gamma_6}{N_{\rm H}}$
Mg I	769.16	5.753	−0.78	7.57	−3.25	−6.83
K I	769.89	0.000	−0.17	7.56	−5.44	−7.45

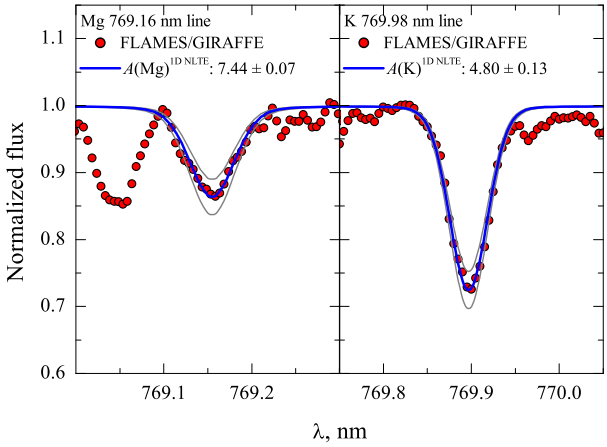

Fig. 1. Typical fits of synthetic Mg and K line profiles (solid blue lines) to those in the observed GIRAFFE spectrum (filled red circles) of the target TO star 47Tuc45982 ($T_{\rm eff}$ = 5707 K, $\log g$ = 4.00). We also provide the abundances determined from each observed line, A(X), together with their errors (see Sec. 2.3.4). Thin gray lines show synthetic line profiles computed with the abundances altered by ±0.2 dex.

2.3. Determination of 1D NLTE abundances of Mg and K

The 1D NLTE abundances of Mg and K were determined using the MULTI code (Carlsson 1986) modified by Korotin et al. (1999). The code computes theoretical line profiles using 1D ATLAS9 model atmospheres and a model atom of a given chemical element (Sect. 2.3.1). Atomic parameters of the spectral lines that were used in our study are provided in Table 2. In the case of Mg, line parameters were taken from the Vienna atomic line database (VALD-3) database (Piskunov et al. 1995; Kupka et al. 2011). For K, $\log gf$ value was taken from Morton (1991) while the line broadening constants are from VALD-3. We stress that in the case of K, the NLTE approach in the abundance analysis is critical since for this element 1D NLTE–LTE abundance corrections are typically very large, reaching from −0.5 to −0.7 dex (Takeda et al. 2002). Besides, they tend to be larger for the late-type stars and increase with decreasing metallicity (Andrievsky et al. 2010).

Abundances of each element were determined by fitting theoretical line profiles to those observed in a given TO star. A typical example of the obtained best fit is shown in Fig. 1. During the fitting procedure, we used a fixed microturbulence velocity of 1.0 km s^{-1} for all sample stars, while the macroturbulence velocity was varied during each iteration as a free parameter to obtain the best match to the observed line profile. The macroturbulence velocities of stars in our sample were in the range of 1 to 5 km s^{-1}. A fixed value of [Fe/H]$^{\rm 1D\ LTE}$ = −0.76 from Carretta et al. (2009a) was used throughout this study. We verified that the determined abundances show no dependence on the effective temperature (Fig. 2).

2.3.1. Model atoms of Mg and K

The model atoms of Mg and K that were used in our study are briefly described below; for more details see Paper I and references therein. In the case of Mg, we used the model atom from Mishenina et al. (2004). It consisted of 84 levels of Mg I, 12 levels of Mg II, and the ground state of Mg III. In the computation of departure coefficients, radiative transitions between the first 59 levels of Mg I and ground level of Mg II were taken into account.

The model atom of K was taken from Andrievsky et al. (2010) and consisted of 20 levels of K I and the ground level of K II. In addition, another 15 levels of K I and seven levels of K II were used to ensure particle number conservation. The total number of bound-bound radiative transitions taken into account was 62 (see Andrievsky et al. 2010, for further details).

2.3.2. 1D NLTE abundances of Mg and K in the atmospheres of TO stars in 47 Tuc

Before the determination of Mg and K abundances, Mg I and K I lines in the spectra of all stars studied were carefully inspected for blends and/or possible contamination by telluric lines (to remind, we had only one spectral line per element available for the abundance determination in the spectrum of each TO star). This inspection revealed significant star-to-star variation in terms of the line quality. In order to take this into account, we grouped Mg I and K I lines into three classes according to their quality, the latter determined by visual inspection using the following criteria:

– A-class: strong or moderately strong lines with well-resolved line profiles;
– B-class: lines that are moderately blended with telluric lines, or lines that were insufficiently resolved in the line wings;
– C-class: lines with weak and/or poorly defined profiles, or significantly blended lines.

These quality flags are marked by different colors in Fig. 3. The line of Mg I and the line of K I in the spectrum of each star were always assigned to their individual quality classes. As a consequence, even in the spectrum of the same star, Mg I and K I lines could belong to different quality classes, for example, Mg line to A-class, K line to C-class. This explains why both Mg and K could not be determined in all the stars, because for some stars only one of the two lines was suitable for abundance determination.

To verify that the spectral lines used in our study are not seriously affected by telluric lines, such as telluric A band in the vicinity of the K I 769.89 nm line, we used (a) telluric lines identified in the spectrum of fast-rotating O6.5 III spectral type star HD94963, which was taken from the UVES POP spectral library (Bagnulo et al. 2003); and (b) a synthetic spectrum of the atmospheric transmission computed with the TAPAS tool (Bertaux et al. 2014) for the dates when the observations were done.

The 1D NLTE abundances of Mg and K were then determined by fitting synthetic spectral line profiles to those observed in the spectra of TO stars.

The iron abundance among the stars in 47 Tuc is very homogeneous: from 147 stars observed with GIRAFFE Carretta et al. (2009a) found [Fe/H] = −0.743 ± 0.003 (stat) ± 0.026 (syst) and from 11 stars observed with UVES, Carretta et al. (2009b) determined [Fe/H] = −0.768 ± 0.016 (stat) ± 0.031 (syst), in both cases with the assumed iron abundance A(Fe) = 7.54 from Gratton et al. (2003). In our GIRAFFE spectra we can measure about 20 Fe I lines, which are of poor quality, due to the low signal-to-noise ratios, S/N, of the spectra and contamination from telluric lines. As a consequence, the line to line scatter is 0.2 dex or larger for our stars. We therefore consider it more robust to assume for each star the mean Fe abundance of the cluster that we take as the average of the measurements from the UVES spectra by Carretta et al. (2009b) and the GIRAFFE spectra by Carretta et al. (2009a): [Fe/H] = −0.76. Solar Mg and K abundances, $A(\mathrm{Mg})_{\odot}^{\mathrm{1D\ NLTE}} = 7.64 \pm 0.05$ and $A(\mathrm{K})_{\odot}^{\mathrm{1D\ NLTE}} = 5.10 \pm 0.07$, were determined in this work (see Appendix A). The 1D NLTE abundance ratios of [Li/Fe], [O/Fe], and [Na/Fe] were taken from Dobrovolskas et al. (2014) where authors determined them using the same [Fe/H] value as utilized in the present study. More information about the procedure of Li, O, and Na abundance determination see Sect. 5.2.2, 5.2.3, and 5.3 in Dobrovolskas et al. (2014).

The determined average element-to-iron abundance ratios in the sample of TO stars are $\langle[\mathrm{Mg/Fe}]\rangle^{\mathrm{1D\ NLTE}} = 0.47 \pm 0.12$ (53 objects) and $\langle[\mathrm{K/Fe}]\rangle^{\mathrm{1D\ NLTE}} = 0.39 \pm 0.09$ (75 objects; numbers after the ± sign are RMS abundance variations due to star-to-star scatter). In Fig. 3 we show [K/Fe], [Mg/Fe], [Na/Fe], [O/Fe], and [Li/Fe] abundance ratios plotted in various abundance-abundance planes.

2.3.3. 3D–1D abundance corrections for Mg and K

To assess the role of convection in the formation of Mg and K lines in the atmospheres of TO stars, we used 3D hydrodynamical CO^{5}BOLD and 1D hydrostatic LHD model atmospheres (Sect. 2.2). The two types of model atmospheres were used to compute 3D–1D LTE abundance corrections for the spectral lines of Mg I and K I utilized in our study (corrections for the lines of O I and Na I were computed earlier in Dobrovolskas et al. 2014). Spectral line synthesis computations were carried out with the Linfor3D spectral synthesis package.[1]

The procedure used to compute the 3D–1D LTE abundance corrections, $\Delta_{\mathrm{3D-1D\ LTE}}$, was identical to that utilized in Paper I. Since the abundance corrections of Mg and K showed little variation with the spectral line strength, in case of each element they were computed for two values of line equivalent width, W (corresponding to "weak" and "strong" spectral lines) that bracketed the range measured in the observed spectra of the sample TO stars. Equivalent widths used for the weakest lines were 4 pm and 15 pm, while for the strongest lines we used 7 pm and 18 pm, in the case of Mg, and K, respectively. Microturbulence velocity in the 3D model atmosphere was determined by applying Method 1 described in Steffen et al. (2013) and was subsequently used in the spectral line synthesis with the LHD model atmospheres (see Paper I for details).

The obtained 3D–1D LTE abundance corrections, $\Delta_{\mathrm{3D-1D\ LTE}}$, are provided in Table 3. For both lines, they do not exceed 0.09 dex, which allows us to conclude that the influence of convection on the formation of Mg I and K I lines in the atmospheres of TO stars is minor.

We note that the obtained abundance corrections were not used for obtaining 3D-corrected abundances which, in principle, could be done by adding the 3D–1D LTE corrections to the determined 1D NLTE abundances of Mg and K. Such a procedure

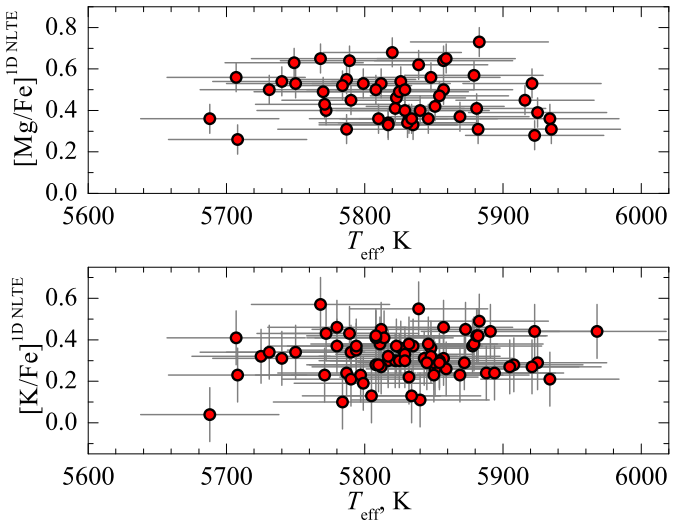

Fig. 2. [Mg/Fe] (top) and [K/Fe] (bottom) abundance ratios determined in the sample of TO stars in 47 Tuc and plotted versus the effective temperature of individual stars. Error bars show uncertainties that were computed as described in Sect.2.3.4.

Table 3. ~~Obtained~~ 3D–1D abundance corrections, $\Delta_{\mathrm{3D-1D\ LTE}}$, computed for different strengths of Mg I and K I lines used in this work (see text for details).

Element	$\lambda_{\mathrm{central}}$	$\Delta_{\mathrm{3D-1D\ LTE}}$, dex	
	nm	weak	strong
Mg I	769.16 nm	+0.04	+0.05
K I	769.89 nm	−0.09	−0.03

[1] http://www.aip.de/Members/msteffen/linfor3d.

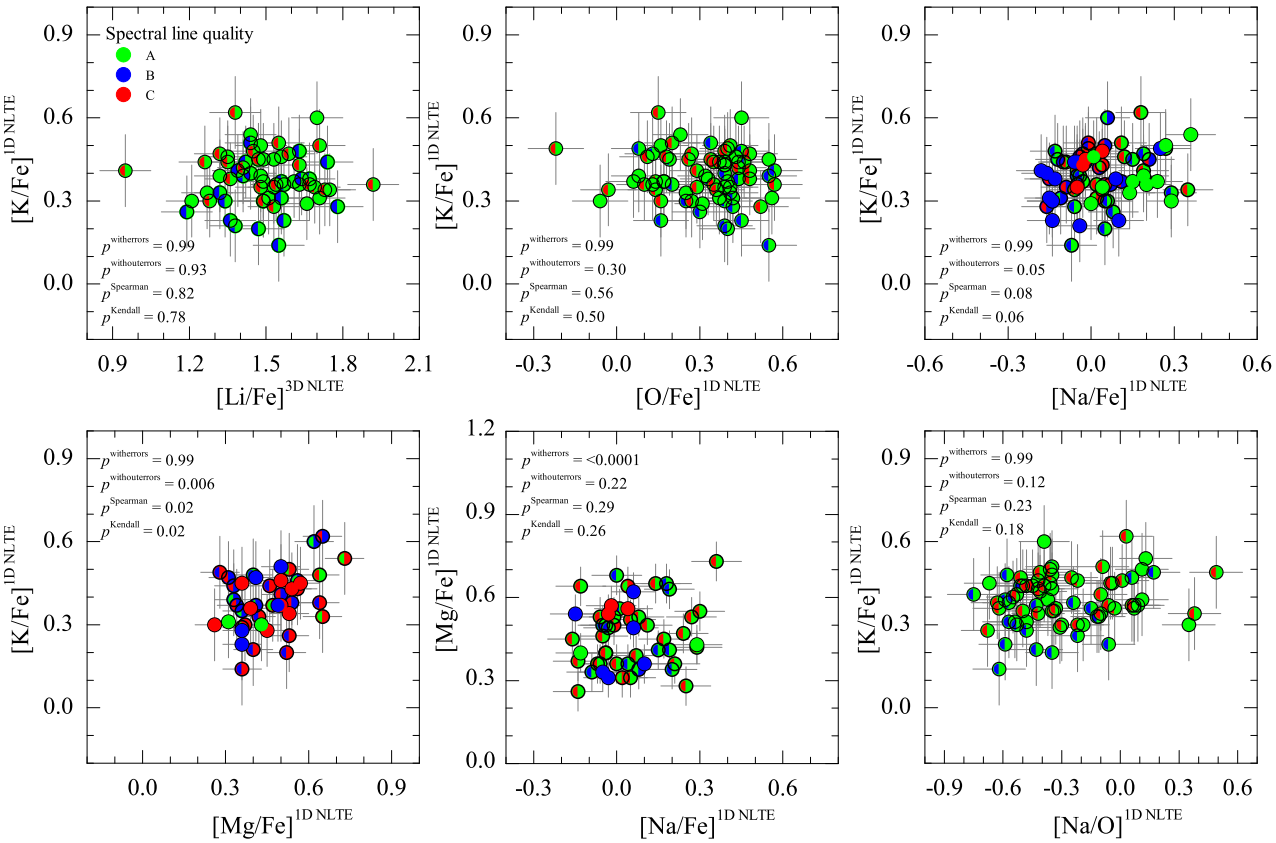

Fig. 3. Abundance-to-iron ratios of Li, O, Na, Mg, and K in the sample of TO stars, shown in various abundance-abundance planes. Colors on the left and right sides of the symbols correspond to the quality (symbols denoting different quality classes are shown in the top-left panel) of spectral lines used to determine abundances of the light elements in a given star plotted on the y and x axes, respectively (see Sect. 2.3.2 for details). The values of two-tailed probabilities, p, computed using Pearson's parametric correlation coefficients (with and without abundance errors, $p^{\rm witherrors}$ and $p^{\rm withouterrors}$, respectively), Spearman's, and Kendall's non-parametric rank-order correlation coefficients are given in the corresponding panels (see Sect. 3.2).

was avoided for two reasons. First, abundances obtained in this way would be generally different from those that would be obtained using the full 3D NLTE approach (see, e.g., Klevas et al. 2016). Second, the determined 3D–1D abundance corrections are small, therefore applying them would result in a small and nearly uniform shift of the abundances determined in all our sample stars. In fact, only in the case of K is the difference in the 3D–1D abundance corrections obtained for weak and strong lines somewhat larger, 0.06 dex, while for Mg this difference is only 0.01 dex. Our tests have shown that if these (small) 3D–1D abundance corrections are taken into account, our conclusions regarding the intrinsic abundance spreads and possible existence of different relations between, for example, the abundance of K and those of other light elements, remain unaltered (see Sect. 3).

2.3.4. Uncertainties in the determined abundances of Li, O, Na, Mg, and K

The uncertainties in the determined abundances occur for two main reasons: (i) inaccurate determination of atmospheric parameters (effective temperature, surface gravity, and microturbulence velocity); and (ii) uncertainties in the spectral line profile fitting (due to the choice of continuum level and inaccurate spectral line profile fit). Individual contributions to the total uncertainty in the determined abundances of O, Na, Mg, and K arising from the different error sources were estimated in the following way:[2]

- $\sigma(T_{\rm eff})$ (Table 4, col. 4): effective temperatures that were used in our study were obtained in Dobrovolskas et al. (2014) using the Hα line profile fitting. The authors estimated that the uncertainty in their determined effective temperatures was ±100 K . We used this value to evaluate the influence of the uncertainty in $T_{\rm eff}$ on the determined elemental abundances, $\sigma(T_{\rm eff})$;
- $\sigma(\log g)$ (Table 4, col. 5): the error in the surface gravity, $\log g$, ±0.04 dex, was obtained from the individual components: error in the effective temperature (±100 K), error in luminosity (±0.03 $L_\odot$), estimated from the photometric error in $M_{\rm V}$, and stellar mass (±0.01 $M_\odot$, obtained from the isochrones). However, the error in surface gravity obtained in this way was, in our view, unrealistically low. Therefore, to estimate the resulting errors in the determined abundances, $\sigma(\log g)$, a more conservative error of ±0.1 dex was used;
- $\sigma(\xi_{\rm t})$ (Table 4, col. 6): the error in the microturbulence velocity was estimated by evaluating the slope uncertainty in

[2] An identical error determination procedure was also used in Paper I. In this procedure errors due to uncertainties in the atomic line parameters, as well as various systematic errors, were ignored. Apart from the uncertainties for Mg and K, for consistency we also re-derived the errors for Li, O, and Na, which had their abundances determined in Dobrovolskas et al. (2014).

Table 4. Errors in the abundances of Li, O, Na, Mg, and K determined in TO stars of 47 Tuc. The sign ± or ∓ reflects the change in the elemental abundance, which occurs due to the increase (top sign) or decrease (bottom sign) by the value of typical uncertainty (Sect. 2.3.4) in $T_{\rm eff}$, $\log g$, $\xi_{\rm t}$, continuum placement, and the line profile fit (cols. 4–8). For example, an increase in the effective temperature leads to increasing abundance (±), while increasing microturbulence velocity results in decreasing abundance (∓). The total estimated uncertainty is provided in col. 9.

Element	Line λ, nm	Line quality	$\sigma(T_{\rm eff})$ dex	$\sigma(\log g)$ dex	$\sigma(\xi_{\rm t})$ dex	σ(cont) dex	σ(fit) dex	$\sigma(A)_{\rm tot}$ dex
Li I	670.80	A	±0.09	∓0.01	∓0.01	0.03	0.01	0.10
		B	±0.09	∓0.01	∓0.01	0.03	0.02	0.10
		C	±0.09	∓0.01	∓0.01	0.03	0.03	0.10
O I	777.19	A	±0.09	∓0.03	∓0.02	0.02	0.01	0.10
		B	±0.09	∓0.03	∓0.02	0.02	0.02	0.10
		C	±0.09	∓0.03	∓0.02	0.02	0.03	0.10
O I	777.53	A	±0.09	∓0.03	∓0.02	0.02	0.01	0.10
		B	±0.09	∓0.03	∓0.02	0.02	0.03	0.10
		C	±0.09	∓0.03	∓0.02	0.02	0.04	0.11
Na I	818.32	A	±0.06	∓0.02	∓0.06	0.02	0.01	0.09
		B	±0.06	∓0.02	∓0.06	0.02	0.02	0.09
		C	±0.06	∓0.02	∓0.06	0.02	0.03	0.09
Na I	819.48	A	±0.06	∓0.02	∓0.06	0.03	0.01	0.09
		B	±0.06	∓0.02	∓0.06	0.03	0.02	0.09
		C	±0.06	∓0.02	∓0.06	0.03	0.03	0.10
Mg I	769.16	A	±0.04	∓0.03	∓0.04	0.03	0.01	0.07
		B	±0.04	∓0.03	∓0.04	0.03	0.01	0.07
		C	±0.04	∓0.03	∓0.04	0.03	0.02	0.07
K I	769.89	A	±0.08	∓0.02	∓0.10	0.02	0.01	0.13
		B	±0.08	∓0.02	∓0.10	0.02	0.02	0.13
		C	±0.08	∓0.02	∓0.10	0.02	0.03	0.13

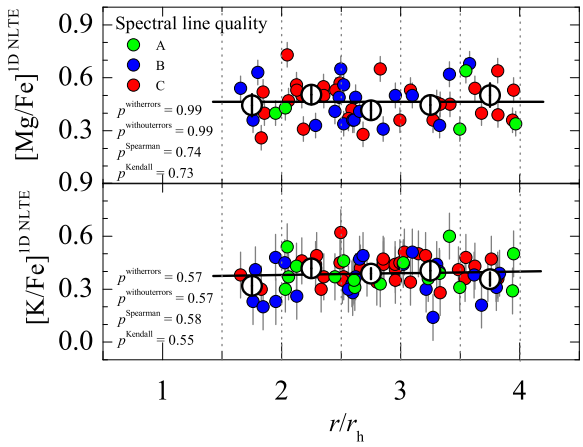

Fig. 4. Abundance-to-iron ratios of Mg and K plotted versus the projected distance from the cluster center, $r/r_{\rm h}$ (small filled circles; $r_{\rm h}$ is a half-mass radius of 47 Tuc, $r_{\rm h} = 174''$, taken from Trager et al. 1993). Symbol color denotes quality (class) of the spectral lines from which the abundance was determined. Large open circles are average abundance ratios computed in non-overlapping $\Delta r/r_{\rm h} = 1$ wide distance bins (marked by the vertical dashed lines; RMS scatter of the abundance ratios in a given bin is shown by the black vertical error bars). Black solid lines are linear fits to the data of individual stars, with the p-values obtained using different tests (see text) marked in the corresponding panels.

the [Fe/H] – W plane (W is line equivalent width). In this procedure we used six TO stars for which we were able to determine Fe abundance using individual Fe I lines. The average slope error determined in this way was ±0.001 dex/pm, which corresponds to the error in $\xi_{\rm t}$ of ±0.29 km/s. This value was used as a representative uncertainty in $\xi_{\rm t}$ to estimate the resulting abundance errors, $\sigma(\xi_{\rm t})$;

– σ(cont) (Table 4, col. 7): the error in continuum determination was estimated in the same way as in Paper I, by measuring the dispersion at the continuum level in the spectral windows expected to be free of spectral lines, both of stellar and telluric origin (see Paper I for details). The continuum was then shifted by the amount of this uncertainty to obtain the resulting error in the determined abundance, σ(cont);

– σ(fit) (Table 4, col. 8): to estimate the errors in the line profile fitting, we computed RMS deviation between the observed and synthetic line profiles, which were converted into the uncertainties in the line equivalent width, W, and, finally, into the errors in the determined abundances, σ(fit) (see Paper I for details).

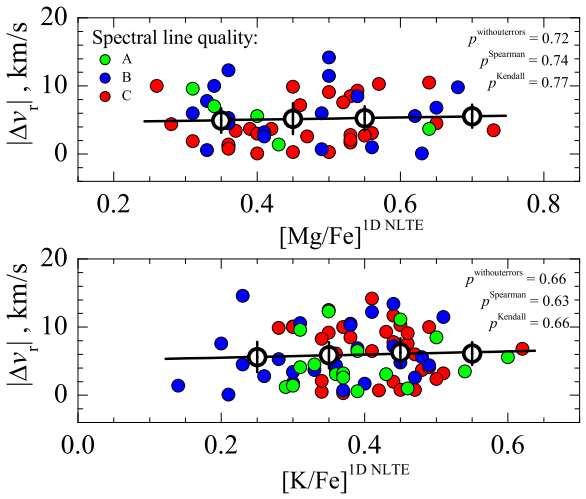

Fig. 5. Absolute radial velocities of TO stars in 47 Tuc, $|\Delta v_{\rm r}|$, plotted versus [Mg/Fe] and [K/Fe] abundance ratios measured in their atmospheres. Other symbols and notations are as in Fig. 4.

Individual errors were added in quadratures to obtain the total error in the determined abundances of O, Na, Mg, and K (col. 9 in Table 4). The obtained total errors were further used in Sect 2.3.5 to estimate the possible intrinsic spreads in the obtained elemental abundances (see Sect. 2.3.5 for details). We stress that they only provide a lower limit for the uncertainties in the determined abundances since they do not account for various systematic uncertainties that are unavoidable in the abundance analysis procedure.

In the case of Li, the procedure was similar except for the following two points:

– Li abundances in Dobrovolskas et al. (2014) were determined by using the A(Li)–W interpolation formula from Sbordone et al. (2010) and W was determined by fitting synthetic line profiles. Therefore, the line profile fitting errors were estimated by measuring RMS deviation between the observed and best-fit Gaussian profiles;

– an error in the determined Li abundance stemming from the use of the interpolation formula was taken into account by using an estimated uncertainty of ±0.01 dex (Sbordone et al. 2010).

The determined uncertainties are provided in Table 4.

2.3.5. Maximum-likelihood testing of the intrinsic spread in elemental abundances

In order to estimate the size of the possible intrinsic spread in the 1D NLTE abundances of Li, O, Na, Mg, and K, we followed the procedure used in Paper I, which is based on the prescription of Mucciarelli et al. (2012, 2015) that the authors applied

Table 5. Results of the maximum-likelihood testing of the intrinsic spread in the abundances of Li, O, Na, Mg, and K.

Element, X_i	$\langle[X_i/Fe]\rangle$	$\sigma^{[X_i/Fe]}$	$\sigma_{int}^{[X_i/Fe]}$
	dex	dex	dex
Li	1.49 ± 0.02	0.18	0.15 ± 0.02
O	0.33 ± 0.01	0.16	0.12 ± 0.01
Na	0.03 ± 0.01	0.14	0.11 ± 0.01
Mg	0.47 ± 0.02	0.12	0.09 ± 0.01
K	0.39 ± 0.02	0.09	0.00 ± 0.02

to study the K abundance spreads in NGC 2419 and NGC 2808, and, later, also in 47 Tuc (Mucciarelli et al. 2017). In the present work, the maximum-likelihood (ML) technique was utilized to evaluate the mean abundance ratio, $\langle[A/B]\rangle$, of elements A and B, as well as intrinsic spread, σ_{int}, in the determined [A/B] abundance ratio. Here, we used [Li/Fe], [O/Fe], [Na/Fe], [Mg/Fe], and [K/Fe] abundance ratios in the TO stars, with the former three taken from Dobrovolskas et al. (2014) and the latter two determined in this study. The obtained mean abundance ratio, $\langle[X_i/Fe]\rangle$, and its uncertainty, as well as the total dispersion due to star-to-star abundance spread, $\sigma^{[X_i/Fe]}$, and the determined intrinsic abundance variation, $\sigma_{int}^{[X_i/Fe]}$, in the abundance of element X_i are provided in Table 5.

3. Results and discussion

3.1. Average abundances and intrinsic abundance spreads in 47 Tuc

To our knowledge, the only studies of K abundance in 47 Tuc that have been carried out until now are those by Carretta et al. (2013) and Mucciarelli et al. (2017). The average 1D NLTE potassium-to-iron abundance ratios obtained by Carretta et al. (2013) in three TO and nine SGB stars were $\langle[K/Fe]\rangle_{TO} = 0.19 \pm 0.07$ and $\langle[K/Fe]\rangle_{SGB} = 0.12 \pm 0.12$, respectively (the error is RMS deviation due to star-to-star abundance variation). These values are compatible with the average 1D NLTE abundance ratios obtained using RGB stars in Paper I, $\langle[K/Fe]\rangle_{RGB} = 0.05 \pm 0.13$. However, the average potassium-to-iron abundance ratio determined using TO stars in the present study, $\langle[K/Fe]\rangle_{TO} = 0.39 \pm 0.09$, is 0.2 dex higher than that obtained using three TO stars by Carretta et al. (2013). We found that two stars are common to both samples. For them, the average abundance ratios obtained by Carretta et al. (2013) and determined in our study are $\langle[K/Fe]\rangle_{TO} = 0.18$ and $\langle[K/Fe]\rangle_{TO} = 0.32$ (the 1D NLTE–LTE abundance corrections and microturbulence velocities used for these stars in the two studies are nearly identical). When corrected for the difference in iron abundance used by Carretta et al. (2013, [Fe/H] = −0.65) and us (–0.76), the two values become nearly identical, with our [K/Fe] ratio being only 0.03 dex higher. We therefore conclude that the difference in [K/Fe] ratios obtained in the TO samples by Carretta et al. (2013) and us is mostly due to the different [Fe/H] values used to compute [K/Fe] ratios. In addition, a substantial difference in the sample sizes may also lead to slightly different average [K/Fe] ratios.

The sample-averaged K abundance obtained in the study of 144 RGB stars in 47 Tuc by Mucciarelli et al. (2017), $\langle[K/Fe]\rangle^{1D\ NLTE} = -0.12 \pm 0.08$, is somewhat lower than that determined in Paper I, $\langle[K/Fe]\rangle_{RGB} = 0.05 \pm 0.13$. This difference may be a result of the different microturbulent velocties used in the two studies: the sample-averaged value in Mucciarelli et al. (2017) is $\xi_t = 1.66$ km/s while in our analysis we used 1.5 km/s. Our tests show that the difference of 0.16 km/s in ξ_t would lead to an ∼ 0.13 dex decrease in the average [K/Fe] ratio determined in Paper I using RGB stars. With this taken into account, abundances obtained in the two studies would become very similar.

The origin of the significant difference between the average [K/Fe] ratios obtained by us in the TO and RGB stars, 0.34 dex, is not entirely clear, however. One possibility is that the value of microturbulent velocity used in our analysis of TO stars was in fact too low. We checked this using the six TO stars mentioned in Sect. 2.3.4 where we determined their iron abundances and microturbulence velocities using individual Fe I lines. The average microturbulence velocity obtained in this way for the six stars was $\xi_t = 1.22 \pm 0.07$ km/s, where error is RMS star-to-star variation. This value is significantly higher than the one used in the present study, 1.0 km/s. With the higher value of ξ_t, the average abundance obtained in our sample of TO stars would become ≈ 0.1 dex lower. Still, this would still leave a difference of ≈ 0.25 dex between the values obtained using TO and RGB stars. On the other hand, it may also be that the microturbulence velocity used in our analysis of RGB stars, 1.5 km/s, was slightly too low. For example, the $\xi_t - \log g$ calibration of Kirby et al. (2009) that was also used in Mucciarelli et al. (2017) would predict the average microturbulence velocity of 1.66 km/s for the gravity range of our RGB stars. Unfortunately, we could not obtain a reliable constraint on ξ_t in our RGB stars using spectroscopic means, due to an insufficient number of iron lines available in their spectra (see Černiauskas et al. 2017). Nevertheless, the increase in ξ_t in both TO and RGB star samples would reduce the average abundance but the difference between two samples would remain almost the same.

Nevertheless, analysis of the six TO stars mentioned above revealed that star-to-star scatter in the determined microturbulence velocities was ≈ ±0.07 km/s. In terms of the determined K abundances, this would lead to a scatter of ≈ 0.03 dex. Such star-to-star variation should have no detectable effect on various possible (anti-)correlations between the light element abundances. Therefore, our conclusions obtained in Sect. 3.2 below should remain unaffected.

The intrinsic abundance spreads of Li, O, Na, Mg, and K determined in our analysis are provided in Table 5. In the case of K, we find zero intrinsic spread, $\sigma_{int}^{[K/Fe]} = 0.00 \pm 0.03$, identical to what was determined in Paper I using RGB stars, $\sigma_{int}^{[K/Fe]} = 0.00 \pm 0.05$, and obtained by Mucciarelli et al. (2017), $\sigma_{int}^{[K/Fe]} = 0.00 \pm 0.02$. While the intrinsic spread of [Mg/Fe] in TO stars is similar to that determined by us in RGB stars, $\sigma_{int}^{[Mg/Fe]} = 0.08 \pm 0.02$ (Paper I), in the present work we obtain considerably larger intrinsic spread in [Na/Fe], $\sigma_{int}^{[Na/Fe]} = 0.12 \pm 0.01$ (TO) versus $\sigma_{int}^{[Na/Fe]} = 0.04 \pm 0.05$ (RGB, Paper I). The latter difference may be due to the lower quality of the RGB spectra, which led to larger abundance errors obtained using RGB stars and, thus, smaller intrinsic abundance spread. An intrinsic scatter of similar size was obtained in the case of Li and O for TO stars, $\sigma_{int}^{[Li/Fe]} = 0.14 \pm 0.02$ and $\sigma_{int}^{[O/Fe]} = 0.10 \pm 0.02$.

3.2. Relations between the abundances of light elements and evolutionary properties of TO stars in 47 Tuc

As in our previous study, Paper I, we used Student's *t*-test to verify the validity of the null hypothesis, that is, that the Pearson's correlation coefficient is equal to zero and, thus, there is no correlation in the abundance–iron and/or abundance–abundance

planes (for simplicity, hereafter we will refer to the abundance ratios as abundances; we note that all abundance-to-iron ratios were obtained by scaling abundances of individual elements by the same constant value of [Fe/H]). For this, using each $x - y$ dataset shown in the panels of Fig. 3, we computed the two-tailed probability, p, that the t-value in the given dataset could be equal or higher than its attained value when there is no correlation in the given $x-y$ plane. In all panels Pearson's correlation coefficients were computed by taking errors on both x and y axes into account. The obtained p-values are listed in Table 6.

Our results suggest that there is no statistically significant relations in the [K/Fe]–[O/Fe] ($p = 0.99$) and [K/Fe]–[Na/Fe] ($p = 0.99$) planes. Similarly, we find no evidence for statistically significant relations in the [K/Fe]–[Li/Fe] ($p = 0.99$), [K/Fe]–[Mg/Fe] ($p = 0.99$), and [K/Fe]–[Na/O] ($p = 0.99$) planes. We only found statistically significant relation in the [Mg/Fe]–[Na/Fe] plane ($p < 0.0001$), which may suggest that the null hypothesis can be formally rejected on a high significance level (see below, however).[3]

In Fig. 4 we show the determined [Mg/Fe] and [K/Fe] abundance ratios plotted versus the normalized distance from the cluster center, $r/r_{\rm h}$, were r is the projected distance from the cluster center and $r_{\rm h}$ is the half-light radius of 47 Tuc taken from Trager et al. (1993, $r_{\rm h} = 174''$). In both planes the obtained probabilities are $p \geq 0.55$ indicating that there are no statistically significant relations between the two abundance ratios and the projected distance from the cluster center.

Following Kučinskas et al. (2014) and Paper I, we also investigated whether there are any significant relations between the kinematical properties of TO stars and the abundances of Mg and K in their atmospheres. For this we used absolute radial velocities of TO stars computed in Kučinskas et al. (2014), $|\Delta v_{\rm r}| \equiv \left|v_{\rm rad} - \langle v_{\rm rad}\rangle^{\rm clust}\right|$, where $v_{\rm rad}$ is the radial velocity of the individual star and $\langle v_{\rm rad}\rangle^{\rm clust} = -18.6$ km/s is the mean radial velocity of the sample. As the p -values of the t-test indicate (see Table 6), there are no statistically significant relations between the abundances of Mg and K and radial velocities.

These findings support our earlier results obtained in the analysis of Na, Mg, and K abundances in 32 RGB stars in Paper I, where we found no statistically significant relations in the abundance-abundance, abundance-distance, and abundance-absolute radial velocity planes. On the other hand, a study of 144 RGB stars in 47 Tuc by Mucciarelli et al. (2017) revealed statistically significant [K/Fe] − [Na/Fe] correlation and [K/Fe] − [O/Fe] anti-correlation (in the same study, such correlations were also detected in the globular cluster NGC 6752). In their analysis, Mucciarelli et al. (2017) used Spearman's non-parametric rank-order correlation coefficients, $r_{\rm s}$, and computed the two-tailed probability, p, that in a given dataset $r_{\rm s}$ could attain a value that is equal to or larger than its measured value.

We therefore also performed non-parametric Spearman's and Kendall's τ rank-correlation tests using the data in our Figs. 3-5. We also computed p-values using Pearson's correlation coefficients calculated without taking abundance errors into account. The p-values determined in all tests are provided in Table 6 and in the corresponding panels of Figs. 3-5.

[3] To test whether adding 3D–1D abundance corrections may change our conclusions regarding the possible relations in different abundance-abundance planes, we also computed Student's t-values using 3D+NLTE abundances instead of those determined in 1D NLTE. In all planes involving different abundance ratios, the obtained p-values were only slightly different from those determined earlier, thereby confirming the findings obtained in the 1D NLTE case.

Table 6. Pearson's, Spearman's, and Kendall's two-tailed p-values for various abundance-abundance, abundance-$r/r_{\rm h}$, and $|\Delta v_{\rm r}|$-abundance velocity planes.

Plane	Pearson p-value[1]	Pearson p-value[2]	Spearman p-value	Kendall p-value
[K/Fe] – [Li/Fe]	0.999	0.929	0.824	0.781
[K/Fe] – [O/Fe]	0.999	0.296	0.557	0.500
[K/Fe] – [Na/Fe]	0.999	0.050	0.076	0.060
[K/Fe] – [Mg/Fe]	0.995	0.006	0.024	0.022
[Mg/Fe] – [Na/Fe]	<0.0001	0.220	0.288	0.258
[K/Fe] – [Na/O]	0.999	0.115	0.231	0.175
[Mg/Fe] – $r/r_{\rm h}$		0.995	0.741	0.729
[K/Fe] – $r/r_{\rm h}$		0.567	0.578	0.545
$\lvert\Delta v_{\rm r}\rvert$ – [Mg/Fe]		0.722	0.743	0.770
$\lvert\Delta v_{\rm r}\rvert$ – [K/Fe]		0.655	0.626	0.657

Notes. [(1)] Taking into account errors on both $x-y$ axes. [(2)] Without $x-y$ errors.

Except for the [Mg/Fe]–[Na/Fe] plane, the p-values computed using the Pearson's, Spearman's, and Kendall's correlation coefficients are all very similar but, at the same time, are significantly smaller than the p-values obtained using Pearson's coefficients computed with errors. In two planes, [K/Fe]–[Mg/Fe] and [K/Fe]–[Na/Fe], the obtained p-values are now sufficiently small to indicate the possible existence of weak correlations. In the [K/Fe]–[Mg/Fe] plane, however, the result may be influenced by the three stars with highest K abundances (for one of them K abundance and for two of them Na abundances were poorly determined as they were obtained from lines of quality classes B-C). When these points were removed from the analysis, Spearman's and Kendall's p-values became significantly larger, $p = 0.22$ and 0.21, respectively. Therefore, despite the relatively small p-values obtained in this plane using all data, we cannot reject with certainty the possibility that these small values are in fact a spurious result. In the [Mg/Fe]–[Na/Fe] plane, the p-values obtained in all three additional tests are significantly larger than the one determined by taking abundance errors into account. This may indicate that the very small p-value obtained by us in the analysis, when errors on both the x and y axes were taken into account, was spurious. Therefore, we conclude that also in this case the null hypothesis cannot be rejected. Finally, no statistically significant relations were detected between abundances (see Figs. 4-5).

The possible existence of the weak correlation in the [K/Fe]–[Na/Fe] plane may be seen as being compatible with the result obtained by Mucciarelli et al. (2017) who detected a correlation in the [K/Fe]–[Na/Fe] plane with Spearman's $p = 0.017$. Although our Spearman's and Kendall's p-values are larger than those computed by Mucciarelli et al. (2017), the difference at least in part may be due to different sample sizes used in the two studies. Nevertheless, the null hypothesis, that there is no correlation between the two abundance ratios, cannot be rejected with confidence based alone on the p-values obtained in our Spearman and Kendall tests. We note that the analysis performed on subsamples of stars selected according to the quality class of spectral lines did not reveal any significant relations in any of the data planes studied above.

4. Conclusions

We performed abundance analyses of Mg and K in the turn-off stars of the Galactic globular cluster 47 Tuc. Abundances were determined using archival VLT FLAMES/GIRAFFE spectra that were obtained in HR 18 setup (746.8 − 788.9 nm, R = 18 400). Spectroscopic data were analyzed using 1D ATLAS9 model atmospheres and 1D NLTE abundance analysis methodology. One-dimensional NLTE spectral line synthesis was performed with the MULTI package, using up-to-date model atoms of Mg and K. We also used 3D hydrodynamical CO^{5}BOLD and 1D hydrostatic LHD model atmospheres to compute 3D–1D abundance corrections for the spectral lines of Mg I and K I utilized in this study. The obtained abundance corrections were small, in all cases < 0.1 dex, indicating that the influence of convection on the formation of these spectral lines in the atmospheres of TO stars in 47 Tuc should be minor.

The determined sample-averaged abundance ratios are $\langle$[Mg/Fe]$\rangle^{\rm 1D\ NLTE} = 0.47 \pm 0.12$ and $\langle$[K/Fe]$\rangle^{\rm 1D\ NLTE} = 0.39 \pm 0.09$ (numbers after the ± sign are RMS abundance variations due to star-to-star scatter). In the case of Mg we find small but significant intrinsic star-to-star scatter in the [Mg/Fe] abundance ratio, $\sigma_{\rm int}^{\rm [Mg/Fe]} = 0.10 \pm 0.01$. No intrinsic scatter was found for K. Both results are in line with our earlier findings obtained using RGB stars in 47 Tuc (Paper I). Abundances of another three light elements, Li, O, and Na, that were determined in our sample stars earlier by Dobrovolskas et al. (2014), also show intrinsic scatter on levels similar to that of Mg, $\sigma_{\rm int}^{\rm [Li,O,Na/Fe]} = 0.10$ to 0.12 dex.

Although our data suggest the existence of a weak correlation in the [K/Fe]–[Na/Fe] plane, its statistical significance is not high enough to claim its existence with confidence. We also detected no statistically significant correlations or anti-correlations between [Mg/Fe] and [K/Fe] abundance ratios and projected distance from the cluster center. Finally, we found no relations between the absolute radial velocities of individual stars and abundances of Mg and K in their atmospheres.

The absence of statistically significant relations between abundances of different light elements, as well as those between their abundances and the kinematical properties of the host stars, is in good agreement with the results obtained in our previous analysis of RGB stars in 47 Tuc (Paper I). The results of the present analysis may be seen to support the existence of a possible relation in the [K/Fe]–[Na/Fe] plane, as found in Mucciarelli et al. 2017, albeit at a lower level of significance. However, we find no statistically significant relation in the [K/Fe]–[O/Fe] plane. Differences in the statistical significance levels obtained in the two studies may in part be due to the factor of two difference in the sample sizes used. Therefore, further homogeneous analyses of larger stellar samples using higher quality spectroscopic data may be needed to shed further light on this controversial issue.

Acknowledgements. We would like to thank the anonymous referee for constructive comments and suggestions that have helped to improve the paper. This work was supported by grants from the Research Council of Lithuania (MIP-089/2015, TAP LZ 06/2013). The study was based on observations made with the European Southern Observatory telescopes obtained from the ESO/ST-ECF Science Archive Facility.

References

Andreasen, D.T., Sousa, S.G., Delgado Mena, E. et al. 2016, A&A, 585, A143
Andrievsky, S. M., Spite, M., Korotin, S. A., et al. 2010, A&A, 509, A88
Bagnulo, S., Jehin, E., Ledoux, C., et al. 2003, The Messenger, 114, 10
Bastian, N., Lamers, H. J. G. L. M., de Mink, S. E., et al. 2013, MNRAS, 436, 2398
Bastian, N., Cabrera-Ziri, I., & Salaris, M. 2015, MNRAS, 449, 3333
Bertaux, J.L., Lallement, R., Ferron, S. et al. 2014, A&A, 564, A46
Bonifacio, P., Pasquini, L., Molaro, P., et al. 2007, A&A, 470, 153
Caffau, E., Ludwig, H.-G., Steffen, M., Ayres, T. R., Bonifacio, P., Cayrel, R., Freytag, B., & Plez, B. 2008, A&A, 488, 1031
Carlsson, M. 1986, UppOR, 33
Carretta, E., Bragaglia, A., Gratton, R., et al. 2009a, A&A, 505, 117
Carretta, E., Bragaglia, A., Gratton, R., & Lucatello, S. 2009b, A&A, 505, 139
Carretta, E., Gratton, R., Bragaglia, A., et al. 2013, ApJ, 769, 40
Castelli, F., & Kurucz, R. L. 2003, in Modeling of Stellar Atmospheres, eds. N. E. Piskunov, W. W. Weiss, & D. F. Gray, Proc. IAU Symp. 210, poster, A20 (CD-ROM)
Černiauskas, A., Kučinskas, A., Klevas, J., et al. 2017, A&A, 604, A35
de Mink, S. E., Pols, O. R., Langer, N., & Izzard, R. G. 2009, A&A, 507, L1
Decressin, T., Meynet, G., Charbonnel, C., Prantzos, N., & Ekström, S. 2007, A&A, 464, 1029
D'Ercole, A., D'Antona, F., Carini, R., Vesperini, E., & Ventura, P. 2012, MNRAS, 423, 1521
di Criscienzo, M., D'Antona, F., Milone, A. P., et al. 2011, MNRAS, 414, 3381
Dobrovolskas, V., Kučinskas, A., Bonifacio, P., et al. 2014, A&A, 565, A121
D'Orazi, V., Lucatello, S., Gratton, R., Bragaglia, A., Carretta, E., et al. 2010, ApJ, 713L, 1
Freytag, B., Steffen, M., Ludwig, H.-G., et al. 2012, J. Comp. Phys., 231, 919
Gratton, R. G., Carretta, E., Claudi, R., Lucatello, S., & Barbieri, M. 2003, A&A, 404, 187
Gratton, R., Sneden, C., & Carretta, E. 2004, ARA&A, 42, 385
Gratton, R. G., Villanova, S., Lucatello, S., et al. 2012, A&A, 544, A12
Hinkle, K., Wallace, L., Valenti, J., & Harmer, D. 2000, Visible and Near Infrared Atlas of the Arcturus Spectrum 3727-9300 A ed. Kenneth Hinkle, Lloyd Wallace, Jeff Valenti, and Dianne Harmer. (San Francisco: ASP) ISBN: 1-58381-037-4, 2000.
Jofré, P. Heiter, U, Soubiran, C. et al. 2015, A&A, 582, A81
Kirby, E. N., Guhathakurta, P., Bolte, M. et al. 2009, ApJ, 705, 328
Klevas, J., Kučinskas, A., Steffen, M. et al. 2016, A&A, 586, A156
Korotin, S. A., Andrievsky, S. M., & Luck, R. E. 1999, A&A, 351, 168
Kraft, R. P. 1994, PASP, 106, 55
Kučinskas, A., Dobrovolskas, V., & Bonifacio, P. 2014, A&A, 568, L4
Kupka, F., Dubernet, M.-L., & VAMDC Collaboration 2011, Baltic Astronomy, 20, 503
Kurucz, R. L. 1993, ATLAS9 Stellar Atmosphere Programs and 2 km s^{-1} Grid, CD-ROM No. 13 (Cambridge, Mass)
Kurucz, R. L. 2006, arXiv:astro-ph/0605029
Ludwig, H.-G., Caffau, E., Steffen, M., Freytag, B., Bonifacio, P., & Kučinskas, A. 2009, Mem. Soc. Astron. Italiana, 80, 711
Marino, A. F., Milone, A. P., Przybilla, N., et al. 2014, MNRAS, 437, 1609
Milone, A. P., Piotto, G., Bedin, L. R., et al. 2012, ApJ, 744, 58
Milone, A. P., Marino, A. F., Dotter, A., et al. 2014, ApJ, 785, 21
Mishenina, T. V., Soubiran, C., Kovtyukh, V. V., & Korotin, S. A. 2004, A&A, 418, 551
Morton, D.C. 1991, ApJS, 77, 119
Mucciarelli, A., Bellazzini, M., Ibata, R., et al. 2012, MNRAS, 426, 2889
Mucciarelli, A., Bellazzini, M., Merle, T., et al. 2015, ApJ, 801, 68
Mucciarelli, A., Merle, T., & Bellazzini, M. 2017, A&A, 600, A104
Pasquini, L., Bonifacio, P., Molaro, P., et al. 2005, A&A, 441, 549
Piotto, G., Bedin, L. R., Anderson, J., et al. 2007, ApJ, 661, 53
Piskunov, N. E., Kupka, F., Ryabchikova, T. A., Weiss, W. W., & Jeffery, C. S. 1995, A&AS, 112, 525
Ramírez, I., & Allende Prieto, C. 2011, ApJ, 743, 135
Sbordone, L. 2005, Mem. Soc. Astron. Italiana, 8, 61
Sbordone, L., Bonifacio, P., Caffau, E., et al. 2010, A&A, 522, A26
Shen, Z.-X., Bonifacio, P., Pasquini, L., & Zaggia, S. 2010, A&A, 524, L2
Steffen, M., Caffau, E., & Ludwig, H.-G. 2013, Memorie della Societa Astronomica Italiana Supplementi, 24, 37
Takeda, Y., Zhao, G., Chen, Y.-Q., Qiu, H.-M., & Takada-Hidai, M. 2002, PASJ, 54, 275
Tody, D. 1986, Proc. SPIE, 627, 733
Trager, S.C., Djorgovski, S.G., & King, I.R. 1993, ASP Conf. Ser., 50, 347
Ventura, P., D'Antona, F., Mazzitelli, I., & Gratton, R. 2001, ApJ, 550, L65

Table A.1. Errors in the determined abundances of Mg and K in the atmospheres of the Sun and Arcturus, $\sigma(A)_{\rm tot}$, obtained by changing various atmospheric parameters by their errors. The sign ± or ∓ reflects the change in the elemental abundance, which occurs due to an increase (top sign) or decrease (bottom sign) in a given atmospheric parameter.

Element	Line	$\sigma(T_{\rm eff})$	$\sigma(\log g)$	$\sigma(\xi_{\rm t})$	σ(cont)	σ(fit)	$\sigma(A)_{\rm tot}$
	λ, nm	dex	dex	dex	dex	dex	dex
Sun							
Mg I	769.16	±0.004	∓0.001	∓0.001	±0.009	±0.025	0.026
K I	769.16	±0.009	∓0.005	∓0.009	±0.008	±0.055	0.057
Arcturus							
Mg I	769.16	±0.009	∓0.012	∓0.015	±0.022	±0.045	0.054
K I	769.89	±0.033	∓0.001	∓0.088	±0.028	±0.059	0.114

Appendix A: Determination of Mg and K abundances in the Sun and Arcturus

To verify the adopted model atoms and atomic parameters of Mg I and K I lines that were used in our study of TO stars in 47 Tuc, we used the MULTI code to compute their synthetic 1D NLTE line profiles and determined abundances of these elements in the Sun and Arcturus. The obtained solar abundances were also used to compute element-to-iron abundance ratios in the sample of TO stars (Sect. 2.3.2.

Appendix A.1: Observed spectra and abundance determination

For Mg and K 1D NLTE abundance determination in the Sun, we used the re-reduced Kitt Peak Solar Flux atlas from Kurucz (2006). The spectrum covers a range of 300–1000 nm, with $R = 523\,000$, and $S/N \sim 4000$ in the infrared part of the spectrum. A solar model atmosphere computed with the ATLAS9 code was used in the abundance determination. The model atmosphere was computed using $T_{\rm eff} = 5777 \pm 10$ K and $\log g = 4.43 \pm 0.02$ (Andreasen et al. 2015). The value of solar microturbulence velocity used in the abundance determination, $\xi_{\rm t} = 1.01 \pm 0.06$ km/s, was also taken from Andreasen et al. (2015).

In the case of Arcturus, we used a spectral atlas from Hinkle et al. (2000). The spectrum covers a wavelength range of 372.7–930.0 nm, has a resolution of $R = 150\,000$, and $S/N \sim 1000$ in the near-infrared part of the spectrum. For the abundance determination we computed an ATLAS9 model atmosphere using the atmospheric parameters from Ramírez & Allende Prieto (2011): $T_{\rm eff} = 4286 \pm 30$ K, $\log g = 1.66 \pm 0.05$, and [Fe/H] $= -0.52 \pm 0.04$. The value of microturbulent velocity, $\xi_{\rm t} = 1.58 \pm 0.12$ km/s, was taken from Jofré et al. (2015). The fits of Mg and K line profiles in the spectra of the Sun and Arcturus are shown in Figs. A.1 and A.2.

Appendix A.2: Errors in the determined abundances of Mg and K

To estimate errors in the determined K and Mg abundances in the Sun and Arcturus, we used the same methodology that was employed to obtain abundance determination errors for TO stars (Sect. 2.3.4). The determined individual errors arising due to inaccuracies in the determined effective temperature, gravity, microturbulence velocity, continuum placement, and the line profile fit, as well as the total error in the determined abundance, are provided in columns 3-8 of Table A.1.

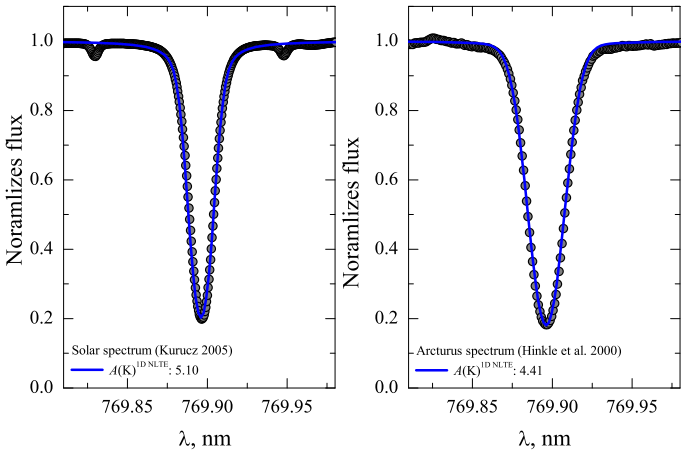

Fig. A.1. Potassium line profiles in the spectra of the Sun and Arcturus. Gray dots show the observed spectra and the blue solid lines are theoretical 1D NLTE line profiles computed using the MULTI code.

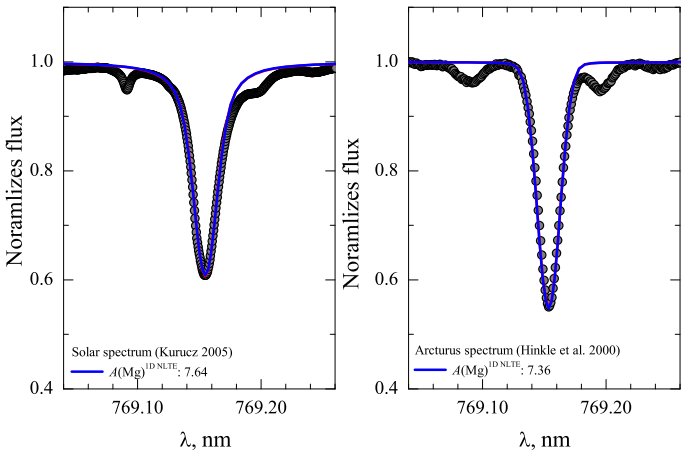

Fig. A.2. Magnesium line profiles in the spectra of the Sun and Arcturus. Gray dots show the observed spectra and the blue solid lines are theoretical 1D NLTE line profiles computed using the MULTI code.

Appendix A.3: Abundances of Mg and K in the Sun and Arcturus

The determined solar 1D NLTE abundance of potassium is $A({\rm K})_\odot^{\rm 1D\ NLTE} = 5.10 \pm 0.06$. The obtained 1D LTE potassium abundance is $A({\rm K})_\odot^{\rm 1D\ LTE} = 5.20 \pm 0.06$, which is slightly lower than $A({\rm K})_\odot^{\rm 1D\ LTE} = 5.31 \pm 0.02$ obtained by Ramírez & Allende Prieto (2011). In the case of magnesium, we determined $A({\rm Mg})_\odot^{\rm 1D\ NLTE} = 7.64 \pm 0.03$ and $A({\rm Mg})_\odot^{\rm 1D\ LTE} = 7.67 \pm 0.03$. The latter value is slightly larger than $A({\rm K})_\odot^{\rm 1D\ LTE} = 7.59 \pm 0.02$ determined by Ramírez & Allende Prieto (2011).

For Arcturus, we determined $A({\rm K})^{\rm 1D\ NLTE} = 4.41 \pm 0.11$. The 1D LTE potassium abundance, $A({\rm K})^{\rm 1D\ LTE} = 5.01 \pm 0.11$, agrees very well with $A({\rm K})^{\rm 1D\ LTE} = 4.99 \pm 0.07$ obtained by Ramírez & Allende Prieto (2011). For magnesium, we obtained $A({\rm Mg})^{\rm 1D\ NLTE} = 7.36 \pm 0.05$. In the case of 1D LTE abundances, again, we obtained a good agreement between our 1D LTE abundance, $A({\rm Mg})^{\rm 1D\ LTE} = 7.46 \pm 0.05$, and $A({\rm Mg}) = 7.47 \pm 0.03$ from Ramírez & Allende Prieto (2011).

Appendix B: Abundances of Mg and K in the atmospheres of TO stars of 47 Tuc

The 1D NLTE [Mg/Fe] and [K/Fe] abundance ratios determined in the sample of TO stars in 47 Tuc are provided in Table B.1. A detailed description of the methodology used to determine elemental abundances is given in Sect. 2.3. The contents of Table B.1 are:

- column 1: object identification (ID);
- column 2: right ascension;
- column 3: declination;
- column 4: effective temperature;
- column 5: surface gravity;
- column 6: radial velocity;
- column 7: 1D NLTE magnesium abundance and its error;
- column 8: 1D NLTE potassium abundance and its error.

The sample-averaged values of the determined abundance ratios and their RMS values are provided in the last two lines of Table B.1.

Table B.1. Target TO stars in 47 Tuc, their atmospheric parameters, and determined [Mg/Fe] and [K/Fe] abundance ratios.

Star ID	RA (2000)	Dec. (2000)	$T_{\rm eff}$ K	$\log g$ [cgs]	$v_{\rm rad}$ km/s	[Mg/Fe] 1D NLTE	[K/Fe] 1D NLTE
00006129	6.15846	–71.96322	5851	4.06	–21.1	0.42 ±0.07	0.33 ±0.13
00006340	5.96746	–71.96075	5817	4.02	–7.4	0.34 ±0.07	0.37 ±0.13
00007619	6.33533	–71.94289	5790	4.05	–10.9	...	0.41 ±0.13
00007969	6.11763	–71.93814	5811	4.06	–28.5	...	0.45 ±0.13
00008359	6.24488	–71.93133	5839	4.06	–23.0	0.62 ±0.07	0.60 ±0.13
00008881	6.16508	–71.92217	5916	4.10	–17.1	0.45 ±0.07	...
00009191	6.21133	–71.91592	5826	4.07	–26.7	0.54 ±0.07	0.43 ±0.13
00009243	6.27892	–71.91464	5857	4.08	–27.9	0.64 ±0.07	0.38 ±0.13
00009434	6.24204	–71.91056	5872	4.08	–21.8	...	0.36 ±0.13
00009540	6.11050	–71.90853	5843	4.06	–7.1	...	0.38 ±0.13
00014912	5.80258	–71.96294	5859	4.08	–12.9	0.65 ±0.07	0.33 ±0.13
00015086	5.76054	–71.96000	5878	4.07	–30.8	...	0.44 ±0.13
00015174	5.82779	–71.95847	5788	4.04	–24.3	...	...
00015346	5.58437	–71.95531	5725	4.03	–10.5	...	0.39 ±0.13
00016131	5.77725	–71.94094	5823	4.07	–10.2	0.46 ±0.07	0.44 ±0.13
00016631	5.75729	–71.92917	5820	4.08	–27.2	0.68 ±0.07	...
00017628	5.87896	–71.90236	5925	4.11	–21.1	0.39 ±0.07	0.36 ±0.13
00017767	5.84779	–71.89828	5812	4.06	–25.9	0.53 ±0.07	0.50 ±0.13
00031830	5.41504	–72.04769	5832	4.05	–18.6	0.36 ±0.07	0.29 ±0.13
00036086	5.70875	–72.20400	5850	4.05	–14.3	...	0.36 ±0.13
00036747	5.77333	–72.19608	5814	4.09	–9.8	...	0.46 ±0.13
00038656	5.62004	–72.17497	5850	4.08	–19.2	...	0.30 ±0.13
00040049	5.74092	–72.16181	5822	4.07	–14.2	0.41 ±0.07	0.37 ±0.13
00040087	5.53888	–72.16119	5787	4.03	–27.0	0.31 ±0.07	0.31 ±0.13
00040355	5.72492	–72.15906	5879	4.06	–7.1	0.57 ±0.07	0.45 ±0.13
00043095	5.67775	–72.13700	5770	4.05	–23.4	0.49 ±0.07	...
00043108	5.57883	–72.13678	5797	4.03	–19.5	...	...
00044983	5.71950	–72.12375	5848	4.04	–14.3	0.56 ±0.07	0.43 ±0.13
00045982	5.64500	–72.11706	5707	4.00	–16.4	0.56 ±0.07	0.46 ±0.13
00046498	5.51050	–72.11339	5790	4.04	–7.5	0.45 ±0.07	0.28 ±0.13
00049829	5.76571	–72.09175	5740	3.99	–25.9	0.54 ±0.07	0.38 ±0.13
00051341	5.55921	–72.08197	5731	4.01	–3.2	0.50 ±0.07	0.41 ±0.13
00051740	5.53704	–72.07939	5857	4.07	–28.9	0.50 ±0.07	0.51 ±0.13
00052108	5.50988	–72.07694	5688	3.99	–16.0	0.36 ±0.07	0.14 ±0.13
00054596	5.61767	–72.06100	5825	4.05	–16.7	0.49 ±0.07	0.37 ±0.13
00058492	5.68208	–72.03306	5728	4.02	–11.1	...	...
00059579	5.66825	–72.02414	5660	3.98	–7.9	...	...
00061639	5.69313	–72.00528	5779	4.03	–20.0	...	...
00062314	5.56467	–71.99794	5740	4.03	1.3	...	...
00062737	5.58004	–71.99319	5691	4.01	–20.4	...	...
00062773	5.87338	–71.99317	5854	4.05	–20.0	0.47 ±0.07	0.37 ±0.13
00063201	5.60025	–71.98767	5759	4.02	–13.8	...	...
00063954	5.77167	–71.97908	5801	4.02	–13.2	...	...
00063973	5.70850	–71.97875	5780	4.02	–8.1	...	...
00065981	6.05225	–72.22219	5814	4.07	–26.2	...	...
00066603	6.05375	–72.21225	5848	4.08	–10.9	...	0.39 ±0.13
00066813	6.34237	–72.20903	5817	4.07	–16.8	0.33 ±0.07	0.39 ±0.13
00066840	6.25950	–72.20878	5780	4.10	–14.2	...	0.51 ±0.13
00067280	6.02708	–72.20253	5808	4.07	–8.2	...	0.35 ±0.13
00069585	6.29904	–72.17517	5888	4.08	–13.3	...	0.31 ±0.13
00070686	6.22921	–72.16494	5808	4.05	–8.3	0.50 ±0.07	0.46 ±0.13
00070910	6.27663	–72.16297	5797	4.06	–7.3	...	0.30 ±0.13
00071404	6.29454	–72.15886	5787	4.06	–20.1	0.55 ±0.07	...
00072011	6.11733	–72.15458	5702	4.05	–12.4	...	...
00096225	6.27933	–72.02936	5805	4.04	–32.0	...	0.23 ±0.13
00097156	6.36075	–72.02406	5750	4.03	–15.7	0.53 ±0.07	...
00099636	6.26008	–72.00881	5799	4.06	–20.2	0.53 ±0.07	0.26 ±0.13
00100325	6.35675	–72.00369	5794	4.05	–18.1	...	0.42 ±0.13

00102294	6.06792	–71.98808	5772	4.01	–23.0	0.40 ±0.07	0.48 ±0.13
00102307	6.21471	–71.98781	5835	4.07	–25.2	0.33 ±0.07	0.44 ±0.13
00103067	5.94763	–71.98056	5665	3.98	–17.7	...	...
00103709	6.02521	–71.97353	5806	4.02	–22.6	...	...
00104049	6.17200	–71.96964	5768	4.02	–24.2	0.65 ±0.07	0.62 ±0.13
00106794	6.47321	–72.18328	5789	4.08	–13.7	0.64 ±0.07	0.48 ±0.13
00107260	6.45896	–72.17064	5829	4.06	–15.7	...	0.40 ±0.13
00107528	6.57650	–72.16361	5923	4.11	–10.0	...	...
00107618	6.59092	–72.16119	5831	4.06	–24.4	0.34 ±0.07	...
00107866	6.56246	–72.15469	5727	4.06	–9.1	...	...
00108171	6.40738	–72.14778	5812	4.06	–9.1	...	0.34 ±0.13
00108389	6.58104	–72.14253	5808	4.05	–18.2	...	0.47 ±0.13
00109441	6.53275	–72.11814	5875	4.07	–21.8	...	...
00109777	6.50933	–72.11058	5873	4.09	–19.8	...	0.50 ±0.13
00110197	6.60008	–72.10139	5824	4.08	–16.6	...	...
00111136	6.48775	–72.08114	5908	4.08	–29.9	...	0.35 ±0.13
00111231	6.52613	–72.07919	5732	4.03	–11.5	...	...
00112473	6.59492	–72.05506	5840	4.05	–17.3	0.40 ±0.07	0.21 ±0.13
00112684	6.46096	–72.05136	5780	4.03	–29.1	...	0.44 ±0.13
00113090	6.47025	–72.04353	5794	4.05	–15.4	...	0.44 ±0.13
00113841	6.55175	–72.02800	5854	4.07	–23.5	...	0.36 ±0.13
00113959	6.49396	–72.02594	5968	4.10	–27.4	...	0.49 ±0.13
00115880	6.51471	–71.98331	5845	4.06	–13.7	...	0.36 ±0.13
10000002	5.43304	–72.05411	5894	4.09	–6.8	...	0.31 ±0.13
10000004	5.62229	–72.10428	5934	4.10	–22.7	0.36 ±0.07	0.28 ±0.13
10000008	5.70025	–72.15828	5905	4.13	–17.9	...	0.34 ±0.13
10000009	5.70075	–72.09483	5792	4.09	–7.2	...	...
10000012	5.70475	–72.08533	5836	4.03	–19.0	...	...
10000015	5.72129	–72.07636	5754	4.02	–8.1	...	...
10000016	5.72533	–72.02817	5724	3.98	–6.7	...	...
10000020	5.75263	–72.06483	5834	4.10	–21.9	0.36 ±0.07	0.23 ±0.13
10000022	5.76167	–72.04869	5749	3.99	–17.5	0.63 ±0.07	...
10000026	5.77117	–72.12517	5784	4.06	–9.8	0.52 ±0.07	0.20 ±0.13
10000027	5.77721	–72.12919	5829	4.08	–20.4	0.40 ±0.07	...
10000036	5.84604	–72.00550	5706	4.00	–25.4	...	...
10000038	5.86846	–72.19789	5810	4.00	–5.1	0.36 ±0.07	0.35 ±0.13
10000041	5.90950	–71.93806	5889	4.08	–27.4	...	...
10000043	5.94513	–72.17733	5883	4.05	–20.9	0.73 ±0.07	0.54 ±0.13
10000048	5.99058	–71.98381	5832	4.05	–22.2	...	0.45 ±0.13
10000049	6.00479	–72.18656	5935	4.14	–15.5	0.31 ±0.07	...
10000053	6.04242	–72.20942	5881	4.08	–20.0	0.41 ±0.07	0.47 ±0.13
10000057	6.08746	–71.93789	5846	4.10	–18.2	0.36 ±0.07	0.45 ±0.13
10000062	6.12154	–71.97469	5891	4.10	–13.3	...	0.49 ±0.13
10000068	6.15775	–71.95836	5923	4.09	–21.8	0.28 ±0.07	0.49 ±0.13
10000072	6.19088	–71.97972	5829	4.09	–17.1	0.50 ±0.07	0.37 ±0.13
10000073	6.21196	–72.00553	5855	4.03	–24.5	...	...
10000075	6.24354	–71.96136	5882	4.08	–23.4	0.31 ±0.07	0.47 ±0.13
10000079	6.27275	–72.12033	5750	4.09	–29.6	...	0.41 ±0.13
10000086	6.30192	–72.05958	5708	3.99	–7.4	0.26 ±0.07	0.30 ±0.13
10000088	6.31217	–72.03944	5771	4.07	–16.0	0.43 ±0.07	0.30 ±0.13
10000090	6.34033	–71.96881	5921	4.08	–15.3	0.53 ±0.07	0.34 ±0.13
10000094	6.42554	–72.07425	5869	4.10	–20.8	0.37 ±0.07	0.30 ±0.13
Sample-average						0.47	0.39
RMS						0.12	0.09

III

Abundance of zinc in the red giants of Galactic globular cluster 47 Tucanae

A.Černiauskas, A.Kučinskas, J.Klevas, P. Bonifacio, H.-G. Ludwig, E. Caffau, and M. Steffen

Astronomy and Astrophysics 2018, doi:10.1051/0004-6361/201833255

Astronomy & Astrophysics manuscript no. 47Tuc_RGB_Zn
June 12, 2018

Abundance of zinc in the red giants of Galactic globular cluster 47 Tucanae

A. Černiauskas[1], A. Kučinskas[1], J. Klevas[1], P. Bonifacio[2], H.-G. Ludwig[3,2], E. Caffau[2], and M. Steffen[4]

[1] Astronomical Observatory of Vilnius University, Saulėtekio al. 3, Vilnius LT-10257, Lithuania
e-mail: algimantas.cerniauskas@tfai.vu.lt
[2] GEPI, Observatoire de Paris, Université PSL, CNRS, 5 Place Jules Janssen, 92190 Meudon, France
[3] Zentrum für Astronomie der Universität Heidelberg, Landessternwarte, Königstuhl 12, 69117 Heidelberg, Germany
[4] Leibniz-Institut für Astrophysik Potsdam, An der Sternwarte 16, D-14482 Potsdam, Germany

Received 18 April 2018; accepted 30 May 2018

ABSTRACT

Aims. We investigate possible relations between the abundances of zinc and the light elements sodium, magnesium, and potassium in the atmospheres ofred giant branch (RGB) stars of the Galactic globular cluster 47 Tuc and study connections between the chemical composition and dynamical properties of the cluster RGB stars.
Methods. The abundance of zinc was determined in 27 RGB stars of 47 Tuc using 1D local thermal equilibrium (LTE) synthetic line profile fitting to the high-resolution 2dF/HERMES spectra obtained with the Anglo-Australian Telescope (AAT). Synthetic spectra used in the fitting procedure were computed with the SYNTHE code and 1D ATLAS9 stellar model atmospheres.
Results. The average 1D LTE zinc-to-iron abundance ratio and its RMS variations due to star-to-star abundance spread determined in the sample of 27 RGB stars is $\langle$[Zn/Fe]$\rangle^{\rm 1D\ LTE} = 0.11 \pm 0.09$. We did not detect any statistically significant relations between the abundances of zinc and those of light elements. Neither did we find any significant correlation or anticorrelation between the zinc abundance in individual stars and their projected distance from the cluster center. Finally, no statistically significant relation between the absolute radial velocities of individual stars and the abundance of zinc in their atmospheres was detected. The determined average [Zn/Fe] $^{\rm 1DLTE}$ ratio agrees well with those determined in this cluster in earlier studies and nearly coincides with that of Galactic field stars at this metallicity. All these results suggest that nucleosynthesis of zinc and light elements proceeded in separate, unrelated pathways in 47 Tuc.

Key words. Globular clusters: individual: NGC 104 – Stars: late type – Stars: atmospheres – Stars: abundances – Techniques: spectroscopic – Convection

1. Introduction

Zinc has traditionally been considered as a transition element between the Fe-peak and light *s*-process species. It is thought that zinc is produced through a variety of channels: explosive nucleosynthesis in type II supernovae (SNe II) and type Ia SNe (SNe Ia), hypernovae, the main and the weak components of the *s*-process (see, e.g., Sneden et al. 1991; Matteucci et al. 1993; Mishenina et al. 2002; Kobayashi et al. 2006).

Observational and theoretical studies of the Galactic evolution of zinc performed during the past decade have confirmed that zinc is synthesized through multiple channels in stars that belong to different Galactic populations. These investigations have shown that the [Zn/Fe] ratio reaches up to $\approx +0.5$ in halo stars with [Fe/H] < -3.0 (Cayrel et al. 2004). In the thin and thick disks, however, its value decreases with increasing metallicity and becomes sub-solar at [Fe/H] ≈ 0.0, with significant scatter in [Zn/Fe] ratios at this metallicity in giant stars that most likely belong to the thin disk (e.g., Duffau et al. 2017). Nissen & Schuster (2011) have found that solar neighborhood stars with low and high α-element abundances were characterized with correspondingly low and high [Zn/Fe] ratios. More recently, Duffau et al. (2017) have shown that stars located at galactocentric distances < 7 kpc seem be to be depleted in zinc, down to [Zn/Fe] ≈ -0.3, which agrees with the values found in the Galactic bulge stars (Barbuy et al. 2015; da Silveira et al. 2018). These and other observations suggest a related origin of zinc and α-elements (e.g., da Silveira et al. 2018). However, [Zn/Fe] trends at low metallicity point to a production of zinc in high-energy core-collapse supernovae, that is, hypernovae (Kobayashi et al. 2006). The significant scatter observed in [Zn/Fe] ratios at solar metallicity is somewhat more difficult to explain and may require a dilution with essentially zinc-free type SN Ia ejecta (see Duffau et al. 2017, for adiscussion).

That zinc may be produced through several channels makes it a potentially interesting tracer in the context of Galactic globular cluster (GGCs) evolution. One of the scenarios that was suggested to explain relations between the abundances of light elements observed in GGCs (such as the Na–O, Mg–Al anticorrelation; see, e.g., Carretta et al. 2009) assumes that atmospheres of the second-generation stars could have been polluted with elements synthesized in asymptotic giant branch (AGB) stars (Ventura et al. 2001). Since zinc may be produced during the *s*-process nucleosynthesis that takes place in intermediate-mass AGB stars (3-6 $M_\odot$, e.g., Karakas et al. 2009), relations between its abundance and those of light elements (e.g., sodium) may point to AGB stars as possible polluters. Therefore, a study of the zinc abundance in the atmospheres of GGC stars characterized by different sodium abundances may reveal additional clues about the possible polluters of second-generation stars in the GGCs. As far as individual GGCs are concerned, one poten-

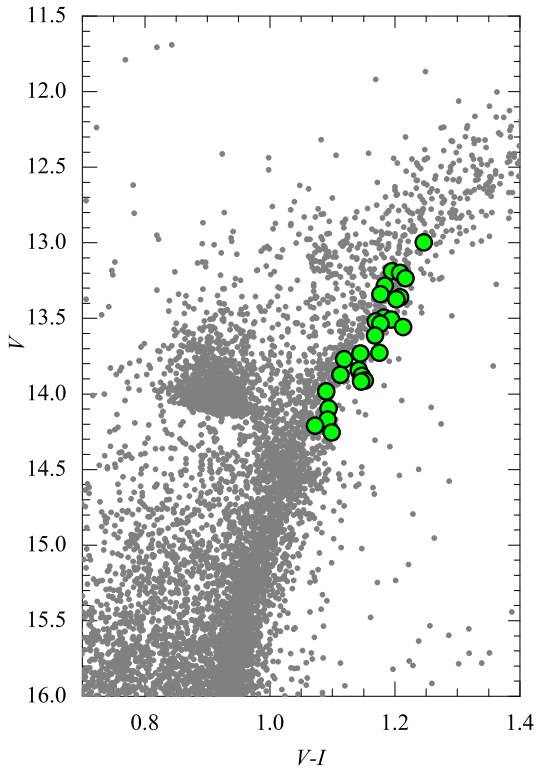

Fig. 1. Upper part of the color-magnitude diagram of 47 Tuc constructed using VI photometry from Bergbusch & Stetson (2009). RGB stars used in this study are marked as filled green circles.

tially interesting target is 47 Tuc, which not only exhibits various correlations and anticorrelations between the abundances of light elements, such as Li, O, Na, Mg, and Al (Carretta et al. 2009; D'Orazi et al. 2010; Dobrovolskas et al. 2014), but also shows indications for connections between their abundances in the atmospheres of individual cluster stars and kinematical properties of these stars (see, e.g., Kučinskas et al. 2014).

Only a few determinations of zinc abundances in 47 Tuc are available, and they are typically based on relatively small samples of stars. For example, Thygesen et al. (2014) determined the zinc-to-iron ratio in 13 RGB stars of this cluster, with a median value of $[\mathrm{Zn/Fe}]^{\mathrm{1D\ LTE}} = 0.26 \pm 0.13$ and no evidence for an intrinsic zinc abundance spread. More recently, based on the study of 19 RGB stars in 47 Tuc, Duffau et al. (2017) obtained a mean value of $\langle[\mathrm{Zn/Fe}]\rangle^{\mathrm{1D\ NLTE}} = 0.17 \pm 0.10$ (1D NLTE–LTE abundance corrections for zinc are small, < 0.1 dex, see Sect. 2.2; thus, we directly compared LTE and NLTE estimates here). This relatively limited information about the zinc abundance in 47 Tuc is rather unfortunate, especially because at the metallicity of 47 Tuc, $[\mathrm{Fe/H}]^{\mathrm{1D\ LTE}} = -0.76$ (Carretta et al. 2009), Zn I lines located at 472.2 nm and 481.0 nm are quite strong in the spectra of its RGB stars (7–10 pm) and are only weakly blended in their wings, which makes them good targets for investigating the zinc abundance.

The main goal of this study was therefore to determine the zinc abundance in a larger sample of RGB stars in 47 Tuc and to search for possible relations between the zinc abundance and those of light elements, primarily sodium and magnesium (but also potassium, see Sect. 3 for a discussion). In addition, we also aimed to study possible connections between the kinematical properties of RGB stars and the zinc abundance in their atmospheres.

Table 1. Atomic parameters of Zn I lines that were used in this study. Natural (γ_{rad}), Stark ($\frac{\gamma_4}{N_{\mathrm{e}}}$), and van der Waals ($\frac{\gamma_6}{N_{\mathrm{H}}}$) broadening constants computed using classical prescription are provided in the last three columns.

Element	λ, nm	χ, eV	$\log gf$	$\log\gamma_{\mathrm{rad}}$	$\log\frac{\gamma_4}{N_{\mathrm{e}}}$	$\log\frac{\gamma_6}{N_{\mathrm{H}}}$
Zn I	472.21	4.02	−0.33	7.99	-6.21	-7.87
Zn I	481.05	4.07	−0.13	7.98	-6.19	-7.87

The paper is structured as follows: spectroscopic data and the determination of the atmospheric parameters of the target stars are presented in Sect. 2.1, while the method we used to determine the zinc abundance and its uncertainties is described in Sect. 2.2. The influence of convection on the Zn I line formation in red giant atmospheres is investigated in Sect 2.3. The determined zinc abundances, as well as their possible relations with those of light elements and kinematical properties of RGB stars, are discussed in Sect. 3. Finally, the main results obtained in this work are summarized in Sect. 4.

2. Methodology

The abundance of zinc was determined using 1D hydrostatic `ATLAS9` model atmospheres and a 1D LTE abundance analysis methodology. A brief description of all steps involved in the abundance analysis is provided below.

2.1. Spectroscopic data and atmospheric parameters of the sample stars

We used the same sample of RGB stars of 47 Tuc as in Černiauskas et al. (2017, hereafter Paper I), as well as the same set of archival high-resolution `2dF/HERMES` spectra obtained with the Anglo-Australian Telescope (AAT)[1]. The spectra were acquired during the science verification phase of the GALAH survey (De Silva et al. 2015) in the wavelength range of 471.5 − 490.0 nm (`HERMES/BLUE`) using a spectral resolution of $R \sim 28000$ and exposure time of 1200 s. The typical signal–to–noise ratio (per pixel) in this wavelength range was $S/N \approx 50$. Further details regarding the reduction and continuum normalization of the observed spectra are provided in Paper I.

The final sample of RGB stars for which zinc abundances were determined contained 27 stars (see Fig. 1). Their effective temperatures and surface gravities were taken from Paper I: the former were determined using photometric data from Bergbusch & Stetson (2009) and $T_{\mathrm{eff}} - (V - I)$ calibration of Ramírez & Meléndez (2005), while the latter were estimated using the classical relation between the surface gravity, mass, effective temperature, and luminosity.

2.2. Determination of the 1D LTE zinc abundance in the atmospheres of RGB stars in 47 Tuc

Zinc abundances in individual RGB stars were determined using two Zn I lines located at 472.21 nm and 481.05 nm. Excitation potentials and oscillator strengths of these spectral lines

[1] The raw spectra were downloaded from the AAT data archive `http://site.aao.gov.au/arc-bin/wdb/aat_database/observation_log/make`.

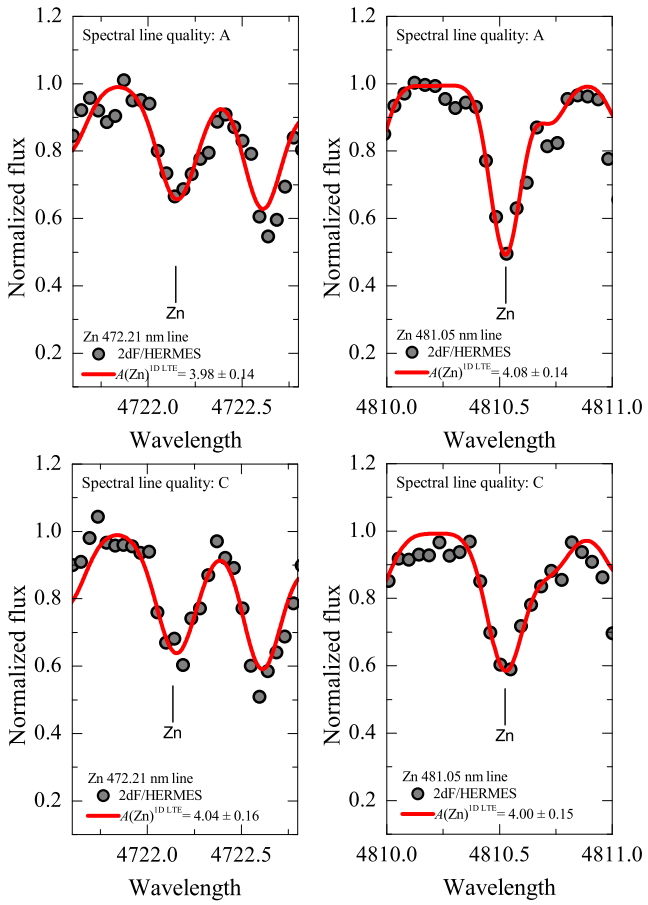

Fig. 2. Typical fits of synthetic spectra (red solid lines) to the observed Zn I line profiles (marked by vertical ticks) in the 2dF/HERMES spectra (filled gray circles) of the target RGB stars S1800 (top row; $T_{\rm eff}$ = 4510 K, $\log g$ = 1.90) and S167 (bottom row; $T_{\rm eff}$ = 4390 K, $\log g$ = 1.60). We also indicate zinc abundances A(Zn) determined from each spectral line, together with their errors (Sect. 2.2). The quality class of the Zn I line is indicated at the top of each panel (see Sect. 2.2 for the line class definition).

were taken from the VALD-3 database (Piskunov et al. 1995; Kupka et al. 2011). Broadening constants were computed using the classical prescription from Castelli (2005). All atomic line parameters are provided in Table 1.

The spectra of all RGB stars used in this study were carefully inspected for blends and/or possible contamination of Zn I lines with telluric lines. We verified that Zn I lines were not affected by telluric lines, therefore we did not correct the spectra for telluric absorption. Since Zn I lines were of different quality in the spectra of different stars, the lines were grouped into three classes according to their quality, which was determined by visual inspection:

- A-class: strong or moderately strong lines with well-resolved line profiles;
- B-class: lines that were moderately blended or insufficiently resolved in the line wings;
- C-class: weak, poorly resolved, or significantly blended lines.

Zinc abundances were determined using synthetic 1D LTE spectra that were computed using the SYNTHE package and 1D hydrostatic ATLAS9 model atmospheres (Kurucz 1993), with both SYNTHE and ATLAS9 packages used in the form of the

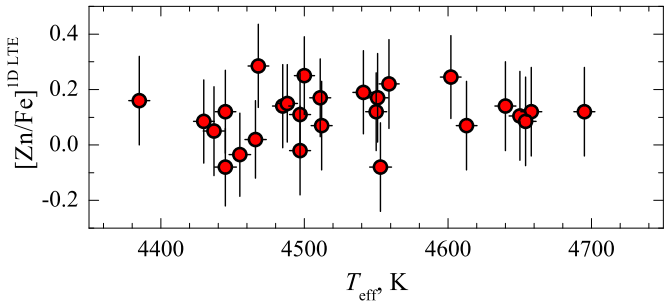

Fig. 3. [Zn/Fe] abundance ratios determined in the sample of 27 RGB stars in 47 Tuc and plotted vs. the effective temperature of individual stars.

Table 2. The 3D–1D abundance corrections, $\Delta_{\rm 3D-1D\ LTE}$, computed for different strengths of Zn I lines used in this work (see text for details).

Element	$\lambda_{\rm central}$	$\Delta_{\rm 3D-1D\ LTE}$, dex	
	nm	weak	strong
Zn I	472.21	0.039	0.047
Zn I	481.05	0.039	0.052

Linux port by Sbordone et al. (2004) and Sbordone (2005). Several typical examples of synthetic spectra fits are provided in Fig. 2. As in Paper I, a fixed value of microturbulence velocity, ξ = 1.5 km/s, was used to compute all synthetic spectra. The macroturbulence velocity was varied as a free fitting parameter to obtain the best match to the observed Zn I lines, with its value changing in the range from 1 to 6 km s^{-1} in different stars of our sample. We verified that there is no dependence of the determined zinc abundances on the effective temperature (Fig. 3).

The solar zinc abundance used in our analysis was $A(\mathrm{Zn})_{\odot}^{\rm 1D\ LTE}$ = 4.62 ± 0.04. As described in Appendix A, this value was obtained from the same spectral lines that were used in the analysis of zinc abundance in 47 Tuc (Table 1). The obtained value agrees well with the previous determinations of the solar zinc abundance, for example, $A(\mathrm{Zn})_{\odot}^{\rm 1D\ LTE}$ = 4.58 obtained using the same Zn I lines by Takeda et al. (2005).

As discussed in Paper I, we did not determine the iron abundance in individual RGB stars because the number of available Fe I lines was small and the quality of the spectra did not allow obtaining reliable estimates of the iron abundance. Instead, the fixed value of $[\mathrm{Fe/H}]^{\rm 1D\ LTE}$ = −0.76 taken from Carretta et al. (2009) was used for all stars in this study. To check the validity of this assumption, we determined the iron abundance for three stars with the best-quality spectra in our sample, S167, S1490, and S1563 ($T_{\rm eff}$ = 4385, 4560, 4695 K and $\log g$ = 1.60, 2.05, 2.30, respectively). In each case, we could identify six Fe I lines suitable for the abundance analysis. The iron-to-hydrogen ratios determined in these stars were $[\mathrm{Fe/H}]^{\rm 1D\ LTE}$ = −0.77, −0.73, and −0.76, respectively, with the mean value, $\langle[\mathrm{Fe/H}]^{\rm 1D\ LTE}\rangle$ = −0.75, nearly identical to $[\mathrm{Fe/H}]^{\rm 1D\ LTE}$ = −0.76 used in this work. As explained above, however, determination of iron abundances for all stars in our sample was not feasible.

We did not correct the obtained zinc abundances for NLTE effects. To our knowledge, the only available source of published 1D NLTE–LTE abundance corrections for the two Zn I lines used in our study is Takeda et al. (2005). However, the authors do not provide corrections at the effective temperatures and gravities bracketing those of our sample stars because of numerical problems in their NLTE computations at these atmospheric pa-

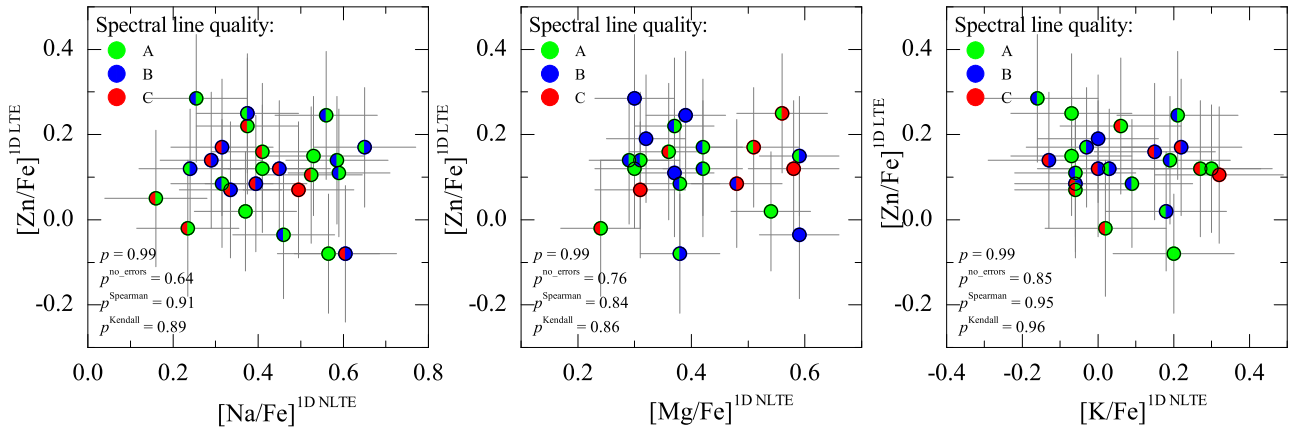

Fig. 4. [Zn/Fe] abundance ratios determined in the sample of 27 RGB stars in 47 Tuc and plotted versus [Na/Fe], [Mg/Fe], and [K/Fe] ratios obtained in the same stars in Paper I. The color on the left and right sides of the symbols denote quality class of the spectral lines used to determined abundance ratios on the y and x axes, respectively (see Sect. 2.2). We also list the values of two-tailed probabilities, p, computed using Pearson's parametric correlation coefficients (with and without abundance errors, p and $p^{\rm no\_errors}$, respectively), as well as Spearman's ($p^{\rm Spearman}$) and Kendall's ($p^{\rm Kendall}$) non-parametric rank-order correlation coefficients (see Sect. 3).

rameters. Nevertheless, by extrapolating their available data, we estimated that abundance corrections for our sample stars will be on the order of $\Delta_{\rm 1D\ NLTE-LTE} \approx -0.05$ dex and are therefore of little significance in the context of present study.

Uncertainties in the determined zinc abundances were evaluated using the same methodology as in Paper I, which is described in Appendix B. Our basic assumption was that these uncertainties were governed by the errors in the determined stellar atmospheric parameters and uncertainties in the line profile fitting. We stress that we did not take into account errors due to uncertainties in the atomic line parameters. Therefore, the obtained error estimates (Table A.2) only provide a lower limit for the uncertainties in the zinc abundances determined from individual Zn I lines because they do not account for other possible sources of systematic errors. Moreover, the individual errors are considered to be uncorrelated.

2.3. 3D–1D LTE zinc abundance corrections

The influence of 3D hydrodynamical effects on the formation of Zn I lines has so far been investigated only for dwarf and subgiant stars (Nissen et al. 2004). The authors have found that the role of these effects was very small, with the resulting 3D–1D LTE abundance corrections significantly below 0.1 dex.

To investigate the 3D effects of the formation of Zn I lines in the atmospheres of RGB stars in 47 Tuc, we used 3D hydrodynamical CO^{5}BOLD (Freytag et al. 2012) and 1D hydrostatic LHD (Caffau et al. 2008) model atmospheres. For this, we used models with atmospheric parameters similar to those of the median object in our RGB star sample, $T_{\rm eff} \approx 4490$ K, $\log g = 2.0$, and [M/H] $= -1.0$. This choice is justified because the range covered by the atmospheric parameters of the sample stars is small ($\Delta T_{\rm eff} \approx 300$ K, $\Delta \log g \approx 0.3$), which means that the obtained corrections should be applicable to all RGB stars in our sample. In addition to the atmospheric parameters, the CO^{5}BOLD and LHD models share identical chemical composition, opacities, and equation of state (see Paper I for details). Spectral line synthesis computations were carried out with the Linfor3D spectral synthesis package[2].

The 3D–1D LTE abundance corrections, $\Delta_{\rm 3D-1D\ LTE}$, were computed for two values of the line equivalent width, W (corresponding to "weak" and "strong" spectral lines) that bracketed the range measured in the observed spectra of the sample RGB stars. Equivalent widths used for the weakest lines were 8.5 pm and 8 pm, while for the strongest lines we used 10.5 pm and 10 pm for Zn 472.21 and Zn 481.05, respectively. The microturbulence velocity in the 3D model atmosphere was determined by applying Method 1 [3] described in Steffen et al. (2013) and was subsequently used in the spectral line synthesis with the LHD model atmospheres (see Paper I).

The obtained 3D–1D LTE abundance corrections are provided in Table 2. For both lines, they do not exceed 0.05 dex and show little dependence on the line strength, which allows us to conclude that the influence of convection on the formation of Zn I lines in the atmospheres of RGB stars is minor. The value of the 3D–1D LTE abundance correction for Zn I line at 481.05 nm is indeed very similar to that obtained using the same CO^{5}BOLD and LHD models by Duffau et al. (2017).

We note that the computed abundance corrections were not used to obtain the 3D-corrected abundances by adding the 3D–1D LTE corrections to the determined 1D LTE abundances of zinc. The main reason for this was that the obtained $\Delta_{\rm 3D-1D\ LTE}$ corrections were small. Therefore, if applied, they result in a very small and nearly uniform shift of abundances determined in all RGB stars, with no effect on the intrinsic abundance spread of zinc and/or various possible relations in the [Zn/Fe] – [Na/Fe] and [Zn/Fe] – [Mg/Fe] planes.

3. Results and discussion

The mean value of the zinc-to-iron abundance ratio we obtained in the sample of 27 RGB stars is $\langle$[Zn/Fe]$\rangle^{\rm 1D\ LTE} = 0.11 \pm 0.09$, where the number after the ± sign is the RMS abundance variation due to the star-to-star scatter. Since this variation is not insignificant, the question arises whether it might be a result of intrinsic scatter in the zinc abundance. To answer this question,

[2] http://www.aip.de/Members/msteffen/linfor3d

[3] The microturbulence velocity shows very little variation (< 0.01 km/s) within the range of line strengths ~~we~~ used to calculate the 3D–1D abundance corrections.

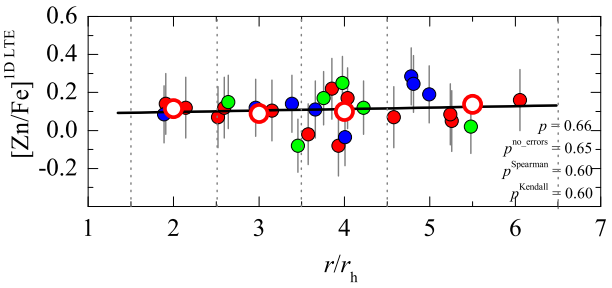

Fig. 5. [Zn/Fe]$^{1D\ LTE}$ abundance ratios determined in the sample of 27 RGB stars in 47 Tuc and plotted vs. the projected radial distance of individual stars (small filled symbols). The symbol colors are identical to those shown in Fig 4. Large open circles are averages obtained in non-overlapping $\Delta r/r_h = 1$ bins.

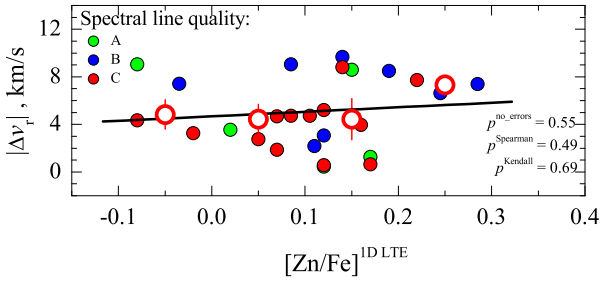

Fig. 6. Absolute radial velocities determined for the sample of 27 RGB stars in 47 Tuc and plotted vs. [Zn/Fe]$^{1D\ LTE}$ ratios of individual stars (small filled symbols). The symbol colors are identical to those shown in Fig 4. Large open circles are averages obtained in non-overlapping Δ[Zn/Fe]$^{1D\ LTE} = 0.1$ bins.

we applied the maximum-likelihood (ML) technique to evaluate the mean zinc-to-iron abundance ratio, $\langle$[Zn/Fe]$\rangle$, as well as its intrinsic spread, $\sigma_{\rm int}^{\rm [Zn/Fe]}$, in our sample of RGB stars. For this, we followed the procedure used in Paper I, which was based on the prescription of Mucciarelli et al. (2012, 2015). The average zinc-to-iron ratio obtained in the ML test is $\langle$[Zn/Fe]$\rangle = 0.11$ and its uncertainty is ± 0.03. We note that the latter value is the error of the mean and therefore is smaller than the RMS variation due to the star-to-star abundance scatter. The determined intrinsic abundance variation is $\sigma_{\rm int}^{\rm [Zn/Fe]} = 0.00 \pm 0.04$, thus there is no intrinsic variation intrinsic variation in the zinc abundance in the RGB stars of 47 Tuc. We stress, however, that this non-detection may be at least partly due to significant uncertainties of the zinc abundance measurements in individual stars, which in turn were caused by the relatively low S/N in the observed spectra.

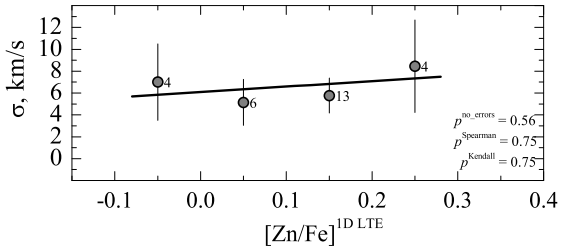

Fig. 7. Radial velocity dispersion of RGB stars in 47 Tuc plotted versus the [Zn/Fe]$^{1D\ LTE}$ ratio (both quantities were computed in non-overlapping Δ[Zn/Fe]$^{1D\ LTE} = 0.1$ bins). The black solid line shows a linear fit to the data.

To investigate possible relations between the abundance of zinc and those of other light elements, we used the abundances of Na, Mg, and K determined in our sample RGB stars in Paper I (all abundances of light elements were determined using the 1D NLTE methodology). It is well established that the sodium abundance shows a significant intrinsic star-to-star variation and is anticorrelated with that of oxygen in the vast majority of GGCs studied so far. Therefore, the relation between abundances of Na and Zn would indicate that the two elements were synthesized by the same polluters. In some GGCs, the Mg–Al correlation is observed and points to the Mg–Al cycle, which occurs at higher temperatures than the synthesis of Na. Thus, in a similar way, the relation between Zn and Mg abundances may indicate that the nucleosynthesis of the two elements is connected. The case with potassium is less clear. Recently, Mucciarelli et al. (2017) claimed a detection of a K–Na correlation and K–O anticorrelation in a sample of 144 RGB stars in 47 Tuc. However, our own study of the K abundance in RGB and TO stars in 47 Tuc (32 and 75 objects, respectively) does not support this claim (Paper I and Černiauskas et al. (2018), hereafter Paper II; we note that our data may suggest a weak K–Na anticorrelation in TO stars, but its statistical significance is low). It is worthwhile noting that, if confirmed, relations between the abundance of K and other light elements would be very difficult to explain from the theoretical point of view because K is synthesized at temperatures $\approx 2 \times 10^8$ K, at which all sodium should be destroyed (e.g., Prantzos et al. 2017). Despite this, we wished to verify whether a relation between the abundance of zinc and potassium in the sample of our RGB stars existed, which in case of a positive detection would add another piece of information that would need to be explained by the chemical evolution models of the GGCs. The yields from AGBs depend on the stellar mass, thus in order to reproduce general trends of the light chemical elements (O, Na, Mg, and Al) seen in different globular clusters, the mass range of AGB stars should be in the range of 5-9 $M_\odot$ (D'Ercole et al. 2010; Ventura et al. 2012). Zinc may be synthesized in slightly less massive AGB stars, 3-6 $M_\odot$ (Karakas et al. 2009), thus there may be a slight overlap in stellar masses in which both zinc and light elements could synthesized in AGB stars. In such a situation, relations between the abundances of zinc and those of light elements would be expected.

The determined [Zn/Fe] ratios are plotted versus various light element element-to-iron ratios in Fig. 4. Similar to Paper I, we used Student's t-test to verify the validity of the null hypothesis, meaning that there is no correlation in the different panels of Fig. 4. For this, using each $x - y$ dataset shown in the three panels of Fig. 4, we computed the two-tailed probability, p, that the t-value in the given dataset could attain the value we obtained when there is no correlation in the given $x-y$ plane. In all panels of Fig. 4, Pearson's correlation coefficients were computed by taking errors on both x and y axes into account (they are marked as p in Fig. 4). In addition, we also carried out non-parametric Spearman's and Kendall's τ rank-correlation tests, in this case without accounting for errors in the determined abundances. Finally, we also computed p-values using Pearson's correlation coefficients obtained without taking abundance errors into account (marked as $p^{\rm no\_errors}$ in Fig. 4). These tests were also performed using the data shown in Fig. 5–7 (see discussion below). The p-

values determined in all tests are provided in the corresponding panels of Fig. 4–7.

The results of these tests do not show any indications of statistically significant relations between the abundances of zinc and the other light elements shown in Fig. 4: in all cases, the p-values are ≥ 0.64. Similarly, there is no statistically significant relation between the determined [Zn/Fe] ratios and the normalized distance from the cluster center, $r/r_{\rm h}$ (Fig. 5): all p-values are ≥ 0.60 (here, r is the projected distance from the cluster center and $r_{\rm h}$ is the half-light radius of 47 Tuc taken from Trager et al. 1993, $r_{\rm h} = 174''$). Neither do we find a statistically significant relation between the [Zn/Fe] ratios and absolute radial velocities of RGB stars, $|\Delta v_{\rm r}| \equiv \left| v_{\rm rad} - \langle v_{\rm rad} \rangle^{\rm clust} \right|$, where $v_{\rm rad}$ is radial velocity of the individual star and $\langle v_{\rm rad} \rangle^{\rm clust} = -18.6$ km/s is the mean radial velocity of the sample (Fig. 6). In this test, the absolute radial velocities were taken from Paper I, while the obtained p-values are all ≥ 0.49. Finally, we tested whether there may be a relation between the radial velocity dispersion of individual stars (computed in non-overlapping 0.1 dex wide bins of [Zn/Fe] ratios) and their average [Zn/Fe] values (Fig.7). Again, we find no statistically significant relation, with p-values for all tests ≥ 0.33.

We also performed all statistical tests mentioned above using the three sub-samples of zinc abundances sorted according to the quality class of Zn I lines from which the abundances were determined. For none of the three subsamples (A-C, marked with different symbols in Figs.4-6) did we find statistically significant relations in any of the planes shown in Figs.4-6.

Our results therefore indicate that there is no relation between the nucleosynthesis of zinc and that of light elements in 47 Tuc. The sample-averaged zinc-to-iron abundance ratio determined in this study, $\langle$[Zn/Fe]$\rangle^{\rm 1D\ LTE} = 0.11 \pm 0.09$, agrees to within less than one sigma to those obtained by Thygesen et al. (2014), [Zn/Fe]$^{\rm 1D\ LTE} = 0.26 \pm 0.13$ (13 RGB stars), and Duffau et al. (2017), $\langle$[Zn/Fe]$\rangle^{\rm 1D\ NLTE} = 0.17 \pm 0.10$ (19 RGB stars). Our value is nearly identical to the average [Zn/Fe] ratio typical to Galactic field stars at the metallicity of 47 Tuc (e.g., Mishenina et al. 2002; Barbuy et al. 2015; Duffau et al. 2017; da Silveira et al. 2018). It also agrees well with the [Zn/Fe] ratio determined at this galactocentric distance for the Galactic red giants of similar metallicity (Duffau et al. 2017; Ernandes et al. 2018). All this evidence suggests that the production of zinc in 47 Tuc most likely followed the same pathways as in Galactic field stars of the same metallicity, and it most likely occurred through α-element nucleosynthesis. We find no evidence that zinc could have been synthesized in 47 Tuc during the s-process nucleosynthesis.

4. Conclusions

We determined the abundance of zinc in the atmospheres of 27 RGB stars in the Galactic globular cluster 47 Tuc. The abundances were obtained using archival `2dF/HERMES` spectra (471.5 − 490.0 nm, $R = 28\,000$, $S/N \approx 50$) that were obtained with the Anglo-Australian Telescope. Spectroscopic data were analyzed using 1D `ATLAS9` model atmospheres and the 1D LTE abundance analysis methodology. The 1D LTE spectral line synthesis was performed with the `SYNTHE` package. The obtained sample-averaged zinc-to-iron abundance ratio is $\langle$[Zn/Fe]$\rangle^{\rm 1D\ LTE} = 0.11 \pm 0.09$, here the value following the ± sign is RMS abundance variation due to star-to-star scatter. We also used 3D hydrodynamical `CO`^{5}`BOLD` and 1D hydrostatic `LHD` model atmospheres to compute the 3D–1D LTE abundance corrections for Zn I lines. The obtained 3D–1D LTE abundance corrections are always positive and are in the range 0.04 to 0.05 dex, indicating that the influence of convection on the formation of Zn I lines in the atmospheres of RGB stars in 47 Tuc is minor. Applying these corrections would lead to a 3D-corrected estimate of the average zinc-to-iron abundance ratio of $\langle$[Zn/Fe]$\rangle^{\rm 1D\ LTE} = 0.16 \pm 0.09$.

The averaged $\langle$[Zn/Fe]$\rangle^{\rm 1D\ LTE} = 0.11 \pm 0.09$ ratio derived in this study agrees well with the mean [Zn/Fe] ratios in 47 Tuc determined in the previous studies that were based on smaller samples of stars, [Zn/Fe]$^{\rm 1D\ LTE} = 0.26 \pm 0.13$ (Thygesen et al. 2014, 13 RGB stars) and $\langle$[Zn/Fe]$\rangle^{\rm 1D\ NLTE} = 0.17 \pm 0.10$, Duffau et al. (2017, 19 RGB stars). Our results show no statistically significant relations between the [Zn/Fe]$^{\rm 1D\ LTE}$ ratio and abundances of light elements (Na, Mg, K), as well as between the [Zn/Fe]$^{\rm 1D\ LTE}$ ratio and kinematic properties of the RGB stars. The sample-averaged [Zn/Fe]$^{\rm 1D\ LTE}$ ratio coincides with the mean [Zn/Fe] ratio obtained in Galactic field stars at the metallicity of 47 Tuc. All these facts indicate that the nucleosynthesis of zinc and that of light elements, such as Na and Mg, has proceeded separately in 47 Tuc. The obtained average [Zn/Fe]$^{\rm 1D\ LTE}$ ratio suggests that in 47 Tuc zinc is slightly enhanced at this metallicity and most likely originated during the α-element nucleosynthesis.

Acknowledgements. Based on data acquired through the Australian Astronomical Observatory, under program 2013B/13. This work was supported by grants from the Research Council of Lithuania (MIP-089/2015, TAP LZ 06/2013). H.G.L. acknowledges financial support by the Sonderforschungsbereich SFB 881 "The Milky Way System" (subprojects A4) of the German Research Foundation (DFG).

References

Andreasen, D.T., Sousa, S.G., Delgado Mena, E. et al. 2016, A&A, 585, A143
Asplund, M., Grevesse, N., Sauval, A. J., et al. 2009, ARA&A, 47, 481
Barbuy, B., Friaça, A. C. S., da Silveira, C. R., et al. 2015, A&A, 580, A40
Bergbusch, P. A., & Stetson, P. B. 2009, AJ, 138, 1455
Caffau, E., Ludwig, H.-G., Steffen, M., Ayres, T. R., Bonifacio, P., Cayrel, R., Freytag, B., & Plez, B. 2008, A&A, 488, 1031
Carretta, E., Bragaglia, A., Gratton, R., et al. 2009, A&A, 505, 117
Castelli, F. 2005, Mem. Soc. Astron. Italiana, 8, 44
Cayrel, R., Depagne, E., Spite, M., et al. 2004, A&A, 416, 1117
Černiauskas, A., Kučinskas, A., Klevas, J., et al. 2017, A&A, 604, A35 (Paper I)
Černiauskas, A., Kučinskas, A., Klevas, J., et al. 2018, A&A, arXiv:1804.10033 (Paper II)
Cordero, M. J., Pilachowski, C. A., Johnson, C. I., et al. 2014, ApJ, 780, 94
da Silveira, C. R., Barbuy, B., Friaça, A. C. S., et al. 2018, A&A, in press (arXiv:1803.09942)
D'Ercole, A., D'Antona, F., Ventura, P., Vesperini, E., & McMillan, S. L. W. 2010, MNRAS, 407, 854
De Silva, G. M., Freeman, K. C., Bland-Hawthorn, J., et al. 2015, MNRAS, 449, 2604
Dobrovolskas, V., Kučinskas, A., Bonifacio, P., et al. 2014, A&A, 565, A121
D'Orazi, V., Lucatello, S., Gratton, R., Bragaglia, A., Carretta, E., et al. 2010, ApJ, 713L, 1
Duffau, S., Caffau, E., Sbordone, L., et al. 2017, arXiv:1704.02981
Ernandes, H., Barbuy, B., Alves-Brito, A., et al. 2018, arXiv:1801.06157
Freytag, B., Steffen, M., Ludwig, H.-G., et al. 2012, J. Comp. Phys., 231, 919
Karakas, A. I., van Raai, M. A., Lugaro, M., Sterling, N. C., & Dinerstein, H. L. 2009, ApJ, 690, 1130
Kobayashi, C., Umeda, H., Nomoto, K., et al. 2006, ApJ, 653, 1145
Kučinskas, A., Dobrovolskas, V., & Bonifacio, P. 2014, A&A, 568, L4
Kupka, F., Dubernet, M.-L., & VAMDC Collaboration 2011, Baltic Astronomy, 20, 503
Kurucz, R. L. 1993, ATLAS9 Stellar Atmosphere Programs and 2 km s^{-1} Grid, CD-ROM No. 13 (Cambridge, Mass)
Kurucz, R. L. 2006, arXiv:astro-ph/0605029
Lodders, K., Palme, H., & Gail, H.-P. 2009, Abundances of the elements in the solar system. In Landolt Börnstein, New Series, Vol. VI/4B, Chap. 4.4, J.E. Trümper (ed.), Berlin, Heidelberg, New York: Springer-Verlag, p. 560-630.
Matteucci, F., Raiteri, C. M., Busso, M., et al. 1993, A&A, 272, 421

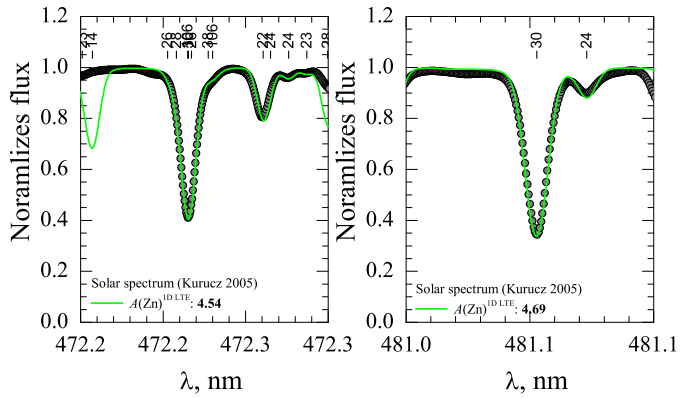

Fig. A.1. Zn I lines (filled gray circles) observed at 472.2 nm and 481.0 nm in the solar spectrum. The synthetic solar spectrum is shown as a green solid line. Numbers above the spectrum correspond to the atomic numbers of the line-producing chemical element.

Mishenina, T. V., Kovtyukh, V. V., Soubiran, C., Travaglio, C., & Busso, M. 2002, A&A, 396, 189
Mucciarelli, A., Bellazzini, M., Ibata, R., et al. 2012, MNRAS, 426, 2889
Mucciarelli, A., Bellazzini, M., Merle, T., et al. 2015, ApJ, 801, 68
Mucciarelli, A., Merle, T., & Bellazzini, M. 2017, A&A, 600, A104
Nissen, P. E., Chen, Y. Q., Asplund, M., & Pettini, M. 2004, A&A, 415, 993
Nissen, P. E., & Schuster, W. J. 2011, A&A, 530, A15
Piskunov, N. E., Kupka, F., Ryabchikova, T. A., Weiss, W. W., & Jeffery, C. S. 1995, A&AS, 112, 525
Prantzos, N., Charbonnel, C., & Iliadis, C. 2017, A&A, 608, A28
Ramírez, I., Meléndez, J. 2005, ApJ, 626, 465
Sbordone, L. 2005, Mem. Soc. Astron. Italiana, 8, 61
Sbordone, L., Bonifacio, P., Castelli, F., & Kurucz, R. L. 2004, Mem. Soc. Astron. Italiana, 5, 93
Sneden, C., Gratton, R. G., & Crocker, D. A. 1991, A&A, 246, 354
Steffen, M., Caffau, E., & Ludwig, H.-G. 2013, Memorie della Societa Astronomica Italiana Supplementi, 24, 37
Takeda, Y., Hashimoto, O., Taguchi, H., et al. 2005, PASJ, 57, 751
Thygesen, A. O., Sbordone, L., Andrievsky, S., et al. 2014, A&A, 572, A108
Trager, S.C., Djorgovski, S.G., & King, I.R. 1993, ASP Conf. Ser., 50, 347
Ventura, P., D'Antona, F., Mazzitelli, I., & Gratton, R. 2001, ApJ, 550, L65
Ventura, P., D'Antona, F., Di Criscienzo, M., et al. 2012, ApJ, 761, L30

Appendix A: Zinc abundance in the Sun

We determined the solar zinc abundance using the same Zn I lines and their atomic parameters (Table 1) as used by us in the analysis of the zinc abundance in RGB stars in 47 Tuc. Synthetic Zn I line profiles were computed using the SYNTHE spectral synthesis package and 1D hydrostatic ATLAS9 model atmospheres (see Sect. 2.2). Atomic line parameters were taken from the VALD-3 atomic database (Piskunov et al. 1995; Kupka et al. 2011).

To determine the solar zinc abundance, we used the re-reduced Kitt Peak Solar Flux atlas of Kurucz (2006). The solar spectrum covers a wavelength range of 300–1000 nm, with $R = 523\,000$, and $S/N \approx 3500$ in the wavelength range around Zn I lines. The solar 1D LTE zinc abundance was determined using the spectral lines located at 472.2 nm and 481.0 nm, with the microturbulence velocity set to 1.0 km/s. Each line was fit independently with the synthetic spectrum (Fig. A.1) that was computed using an ATLAS9 model atmosphere of the Sun ($T_{\rm eff} = 5777$ K and $\log g = 4.43$, as recommended by Andreasen et al. 2015). The solar abundances of zinc obtained from the 472.2 nm and 481.0 nm Zn I lines were $A(\mathrm{Zn})_{\odot}^{\rm 1D\ LTE} = 4.54$ and $A(\mathrm{Zn})_{\odot}^{\rm 1D\ LTE} = 4.69$, respectively, with a mean value of $A(\mathrm{Zn})_{\odot}^{\rm 1D\ LTE} = 4.62 \pm 0.08$ (the value after the "±" sign is the RMS variation). This agrees well with those determined in the earlier studies, for example, $A(\mathrm{Zn})_{\odot}^{\rm 1D\ LTE} = 4.58$ obtained using the same Zn I lines by Takeda et al. (2005), $A(\mathrm{Zn})_{\odot}^{\rm 1D\ LTE} = 4.62$ derived by Lodders et al. (2009), and $A(\mathrm{Zn})_{\odot}^{\rm 1D\ LTE} = 4.56 \pm 0.05$ recommended by Asplund et al. (2009).

We further estimated the uncertainty of the solar zinc abundance determination using the same procedure and uncertainties in the atmospheric parameters of the Sun and spectral line fitting procedure as described in Paper II. Errors from the individual uncertainties are provided in Table A.1. The final value of the solar zinc abundance obtained from the two Zn I lines is $A(\mathrm{Zn})_{\odot}^{\rm 1D\ LTE} = 4.62 \pm 0.04$.

Table A.1. Total error in the abundance of zinc determined from the Zn I lines in the atmosphere of the Sun, $\sigma(A)_{\rm tot}$,. The sign ± or ∓ reflects the change in the elemental abundance that occurs due to the increase (top sign) or decrease (bottom sign) in the uncertainty from a given error source (as indicated in column header; see Paper II for details).

Element	λ	$\sigma(T_{\rm eff})$	$\sigma(\log g)$	$\sigma(\xi_{\rm t})$	σ(cont)	σ(fit)	$\sigma(A)_{\rm tot}$
	nm	±10 K,	±0.02	±0.06 km/s			
Sun							
Zn I	472.21	±0.005	∓0.001	∓0.023	±0.015	±0.017	0.032
Zn I	481.05	±0.011	∓0.005	∓0.032	±0.016	±0.019	0.042

Table A.2. Errors in the abundance of zinc determined from the two Zn I lines used in this study and different spectral line quality (A–C, see Sect. 3). The ± or ∓ sign reflects the change in elemental abundance that occurs due to increase (top sign) or decrease (bottom sign) in a given atmospheric parameter. For example, an increase in the effective temperature leads to an increase in the abundance of zinc (±), while increasing microturbulence velocity results in a decreasing zinc abundance (∓).

Element	Line	Line	$\sigma(T_{\rm eff})$	$\sigma(\log g)$	$\sigma(\xi_{\rm t})$	σ(cont)	σ(fit)	$\sigma(A)_{\rm tot}$
	λ, nm	quality	dex	dex	dex	dex	dex	dex
Zn I	472.21	A	±0.03	∓0.04	∓0.11	0.04	0.06	0.14
		B	±0.03	∓0.04	∓0.11	0.04	0.08	0.15
		C	±0.03	∓0.04	∓0.11	0.04	0.09	0.16
Zn I	481.05	A	±0.03	∓0.03	∓0.11	0.05	0.05	0.14
		B	±0.03	∓0.03	∓0.11	0.05	0.06	0.14
		C	±0.03	∓0.03	∓0.11	0.05	0.08	0.15

Appendix B: Uncertainties in zinc abundances determined in the RGB stars in 47 Tuc

The uncertainty in the determined zinc abundances was estimated following the same procedure as in Paper I. For this, we assumed that the error in the determined abundances occurs due to an inaccurate determination of the atmospheric parameters ($T_{\rm eff}$, $\log g$, $\xi_{\rm t}$) and the spectral line profile fitting, with the additional assumption that the latter depends on the goodness of line profile fit and the placement of continuum level. These uncertainties were estimated in the following way:

– Errors in the determination of atmospheric parameters: Following Paper I, we assumed that the error in the determination of the effective temperature of the RGB stars was ±65 K. The errors in the determined zinc abundance resulting from this uncertainty, $\sigma(T_{\rm eff})$, are provided in Table A.2, Col. 4, for both Zn I lines. For the uncertainty in surface gravity, we adopted a conservative (and, in our view, more realistic) value ±0.1 dex; the resulting errors in the zinc abundances, $\sigma(\log g)$, are listed in Table A.2, Col. 5. Since we did not derive individual values of the microturbulence velocity for individual RGB stars, we adopted an uncertainty in the microturbulence velocity of ±0.15 km/s. This value is based on

the RMS variation of microturbulence velocity determined in RGB stars in 47 Tuc by Carretta et al. (2009, 58 objects) and Cordero et al. (2014, 81 objects), with stars occupying the same range in the effective temperature as those used in our sample. The obtained abundance uncertainties that occur due to errors in microturbulence velocity, $\sigma(\xi_t)$, are listed in Table A.2, Col. 6.

– Errors in the spectral line profile fitting: The error in continuum determination was estimated in the same way as in Paper I, that is, by measuring the dispersion at the continuum level (inverse signal-to-noise ratio) in the spectral regions deemed to be free of spectral lines (see Appendix B in Paper I for details). The errors in the line profile fitting were computed individually for each line quality class (see Sect. 2.2) using RMS values as a measure of differences between the observed and best-fit synthetic line profiles. These RMS values were used to compute the change in the determined abundance of zinc. The final errors due to continuum determination and spectral line profile fitting are shown in Table A.2, Cols. 7 and 8, respectively.

The errors in the determined zinc abundances resulting from various uncertainty sources are listed in Table A.2. The total uncertainties in zinc abundance (obtained by adding individual components in quadratures, Col. 9 in Table A.2) are shown in Fig.3, 4, and 5. These errors were also used in the ML analysis aimed to determine the average value of the zinc abundance and its intrinsic spread in the sample of RGB stars (see Sect. 3).

We stress that in this procedure, errors resulting from uncertainties in the atomic line parameters were ignored. Therefore, the total abundance uncertainties listed in Table A.2 are only lower limit estimates because they do not account for the various systematic uncertainties that are unavoidable in the abundance analysis procedure.